Final Report on the 2019 Airborne Electromagnetic Survey of Selected Areas Within the Marina Coast Water District

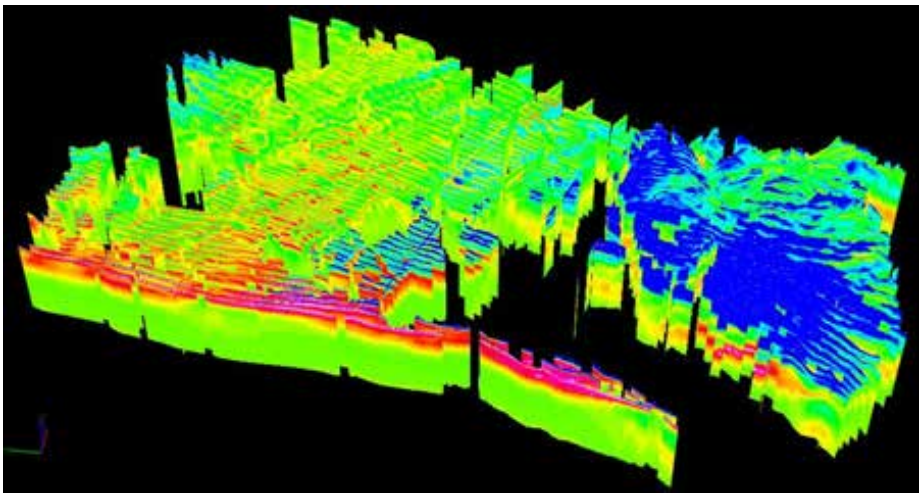

Theodore H. Asch, CA GP#1038
Principle Geophysicist
(720) 415-7312

Jared Dale Abraham, CA GP#1089
Principle Geophysicist
(303) 905-6240

Aqua Geo Frameworks, LLC
130360 County Road D
Mitchell, NE 69357

Disclaimer:
AGF conducted this project using the current standards of the geophysical industry and used in-house quality control standards to produce this geophysical survey and products. The geophysical methods and procedures described in this report are applicable to the particular project objectives, and these methods have been successfully applied by AGF to investigations and projects of similar size and nature. However, field or subsurface conditions may differ from those anticipated, and the resultant data may not achieve the project objectives. AGF's services were performed consistent with the professional skill and care ordinarily provided by professional geophysicists under the same or similar circumstances. No other warranty or representation, either expressed or implied, is made by AGF in connection with its services unless in writing and signed by an authorized representative of AGF

Executive Summary

Aqua Geo Frameworks, LLC. (AGF) is pleased to submit this report titled *"Final Report on the 2019 Airborne Electromagnetic Survey of Selected Areas Within the Marina Coast Water District*. An understanding of the hydrogeological framework in the survey area is desired to assist in resource management. AGF entered into an agreement with the Marina Coast Water District (MCWD) to collect, process, and interpret airborne electromagnetic (AEM) data, in conjunction with other available background information (the 2017 AEM investigation), to develop a 3D hydrogeologic framework of the Marina Coast Water District project area, and to recommend future work to enhance groundwater management activities.

The scope of work for this project was as follows:

1. SCOPE OF WORK

1.1 An AEM survey utilizing the SkyTEM312 system was flown over the MCWD project area. These flights have been provided as preliminary AEM inversions and the final AEM data and inversions are included as a product attached to this data report.

1.2 AGF began project planning upon signing of the project between AGF and the MCWD. This work included flight plans, database development, and review of hydrogeologic and geologic work for the area.

1.3 Upon conclusion of the design process, the MCWD AEM investigation utilized the SkyTEM312 system to fly the same flight lines as were flown in 2017 (with the hope to image deeper where possible) plus an extension of the flight area to the south onto the former Fort Ord. The purpose of the extension was to characterize the influx of groundwater from the highlands of former Fort Ord into the Salinas River Valley. The MCWD SkyTEM312 flight lines had a maximum length of approximately 15 miles (24 km) in the primary north-south direction, separated by approximately 650 feet (about 180-220 m), and a maximum of about 7 miles (11 km) along the east-west tie-lines.

1.4 AGF acquired AEM data over the MCWD, commencing 24 April 2019 and finishing on 26 April 2019, to support development of the hydrogeological framework. Approximately 543.9 line-miles (881.1 line-kilometers) were acquired over the MCWD AEM survey area. Status reports of the flying were provided to the MCWD daily, including the areas flown, production rates, and flight plan for the following day.

1.5 AGF processed and conducted quality assurance and quality control (QA/QC) procedures on all data collected from the acquisition system. AGF delivered a letter report on the QA/QC performed on the acquired data plus the inversions as 2D profiles and 3D fence diagrams on May 10, 2019. The analysis continued with further processing, editing, and then Spatially-Constrained inversions. Approximately 455.3-line-miles (737.6-line kilometers) were retained for inversion amounting to a retention rate of 83.7%. This high rate is the result of careful flight line planning and design given the infrastructure that was encountered during the acquisition.

1.6 AGF inverted the AEM data. These final inverted georeferenced data are delivered to the LCNRD with this report. After inversion, AGF derived 2D sections, 3D electrical models, and interpreted geologic and hydrogeologic surfaces of the surveyed area.

1.7 AGF is providing a hydrogeologic framework report that includes maps of aquifer materials, estimated chloride concentrations, and a comparison between the 2017 and 2019 inverted AEM earth models. This report, as mentioned above, also includes all data (acquired, processed, developed) files. The report is delivered in PDF digital format and the data in ASCII and native formats.

2. KEY FINDINGS AND RECOMMENDATIONS

2.1 2019 AEM Investigation - The MCWD 2019 AEM investigation successfully, and accurately per borehole correlations, mapped the subsurface resistivity distribution and provided an estimation of the chloride concentration within the AEM survey boundary. Besides mapping the known locations of fresher water, additional fresher water is indicated under the hills south of the Salinas River on Fort Ord of which some is likely flowing downhill towards the Salinas Valley. Below this zone of fresher water on Fort Ord is a clear very conductive zone that is likely more saline water.

2.2 Comparison of MCWD 2017 and 2019 AEM Investigations - A comparison between the MCWD AEM investigations from May 2017 and April 2019 has been conducted via 2D profiles and 3D voxels. The main differences between the two survey periods is that the 2019 electrical resistivity at a depth near the coast, primarily north of the Salinas River, and continuing inland, that is likely the 400-Foot Aquifer, does not indicate the very low resistivities observed in the 2017 AEM investigation that are interpreted to be saline water, likely sea water. While there are some local variations, the resistivity mapping of the 180-Foot Aquifer generally does not show much difference between 2017 and 2019. If MCWD believes that there have been substantial changes in the subsurface over the 2019 investigation area due to variations in local environmental conditions, then it is recommended that MCWD consider an additional AEM mapping campaign or part or all of the 2019 AEM survey area.

2.3 Need Additional Water Table and Water Quality Data Across the Salinas River Valley - It was observed during analysis of the AEM inversion results when applying the available water table elevation and water quality data, that there isn't a lot of this information publicly available. The only available water quality information was from the MPWSP monitoring well reports and those were not consistent in their reporting or possibly accuracy and calibration. Additional compilation and integration of water level measurement locations and accurate water quality data would improve local water table and water quality maps and help in the analysis and interpretation of the previously acquired, and any future, AEM data.

3. DELIVERABLES

- Raw EM Mag data as ASCII *.xyz
- SCI inversion as ASCII *.xyz
- Utilized borehole databases as ASCII *.xyz
- Interpretations as ASCII *.xyz
- Raw Data Files - SkyTEM files *.gex, *skb, *.lin
- Resistivity and Estimated Chloride Concentration Voxel Grids as ASCII *.xyz
- 2D Profiles and 3D fence diagrams of the AEM survey lines
- Google Earth KMZs for AsFlown, Retained

Table of Contents

List of Figures

List of Tables

List of Abbreviations

1D	One-dimensional
2D	Two-dimensional
3D	Three-dimensional
A*m^2	Ampere meter squared
AEM	Airborne Electromagnetic
AGF	Aqua Geo Frameworks, LLC
ASCII	American Standard Code for Information Interchange
Bgl/Bgs	Below Ground Level/Below Ground Surface
CA-DWR	California Department of Water Resources
dB/dt	Change in amplitude of magnetic field with time
DEM	Digital Elevation Model
DOI	Depth of Investigation
DGPS	Differential global positioning system
em, EM	Electromagnetic
EPA	U.S. Environmental Protection Agency
ft	Feet
Fm, FM	Formation
GIS	Geographic Information System
gpm	Gallons per minute
gr	granitic rocks
Hz	Hertz (cycles per second)
IGRF	International Geomagnetic Reference Field
Km/km	Kilometers
KMZ/kmz	Keyhole Markup language Zipped file
m	Meters
MPWSP	Monterey Peninsula Water Supply Program
MAG	Magnetic (data); Magnetometer (instrument)
MCG	Minimum curvature gridding
md	Meters per day
mg/L	Milligrams per liter
NAD83	North American Datum of 1983
NAVD88	North American Vertical Datum of 1988
NWIS	National Water Information System
OM	Geosoft Oasis montaj
Ohm-m	Ohm per meter
PDF	Portable Document Format
PFC	Primary Field Compensation
PLNI	Power Line Noise Intensity
PLSS	Public Land Survey System
QA/QC	Quality Assurance and Quality Control
Rx	Receiver

SCI	Spatially-Constrained Inversion
STD	Standard Deviation
TEM	Transient Electromagnetic
TDEM	Time-Domain Electromagnetic
TDS	Total dissolved solids
Tx	Transmitter
USGS	United States Geological Survey
UTM	Universal Transverse Mercator
V/m^2	Volts per meter squared

1 Introduction

The Marina Coast Water District (MCWD) required a detailed hydrogeological framework of the area around Marina, California in order to implement ground water management plans. MCWD contracted Aqua Geo Frameworks, LLC (AGF) who sub-contracted with SkyTEM Canada (SkyTEM) to implement an Airborne Electromagnetic (AEM) survey of selected areas within the MCWD that had been surveyed previously in May of 2017 (Gottschalk et al., 2018). Specifically, MCWD would like to gain knowledge of the distribution of aquifer materials and their relations to high Total Dissolved Solids (T.D.S.) waters present in the area and compare the 2019 AEM survey results to the 2017 AEM survey results. The 2019 AEM data acquisition plan is presented in Figure 1-1. The 2017 "as-flown" AEM flight lines overlie the 2019 planned AEM flight lines in Figure 1-2. The difference between the two sets of flight lines is that the 2019 AEM flight lines extend further south over the former Fort Ord, down towards California State Highway 218.

Figure 1-1. Planned 2019 AEM acquisition (blue lines) within the MCWD.

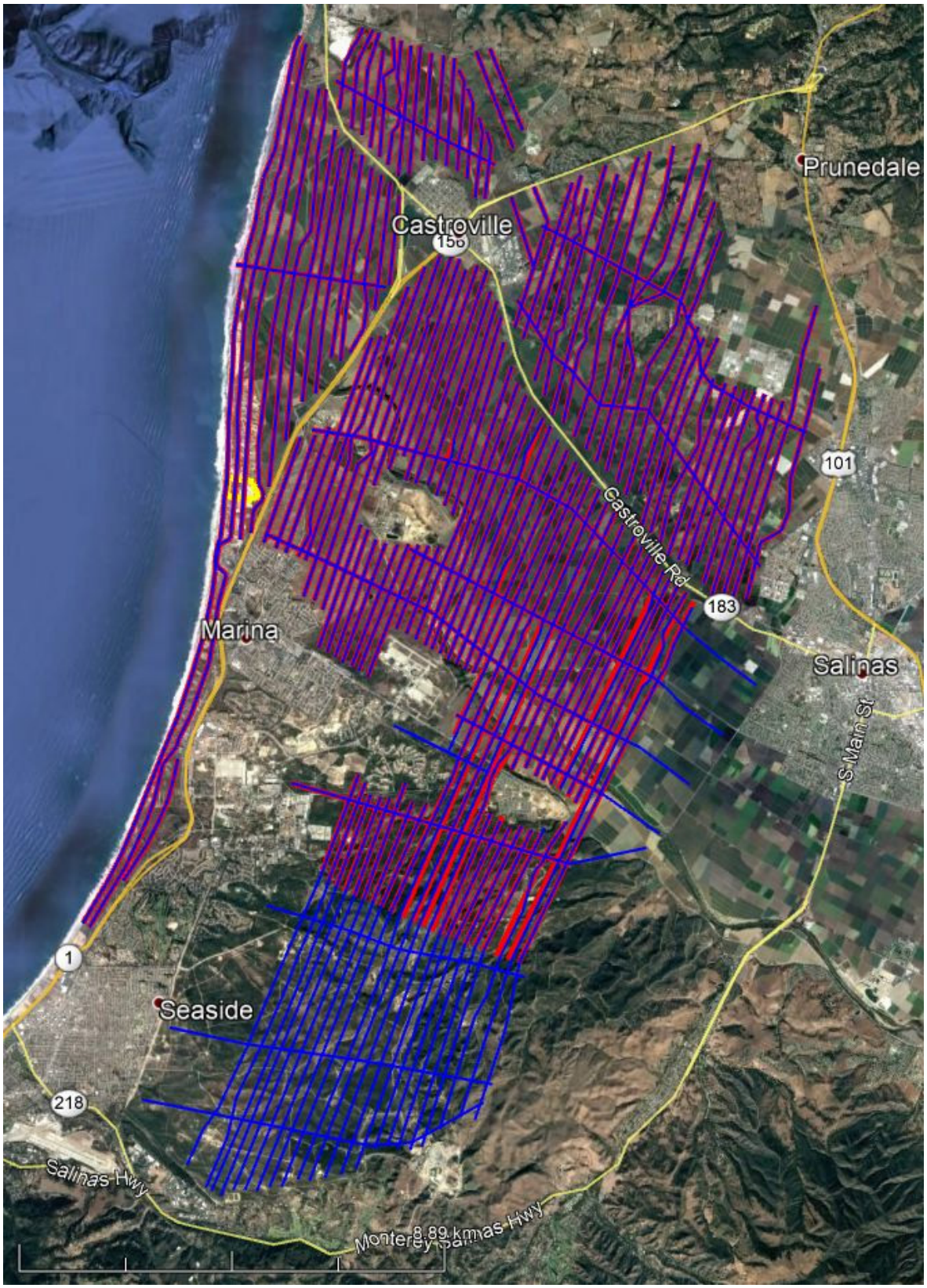

Figure 1-2. Planned 2019 AEM acquisition (blue lines) within the MCWD and the 2017 AEM flight lines (red lines).

2 Borehole Lithology and Geophysical Log Data

Borehole data for this project consisted of a combination of lithologic and downhole geophysical logs. Some of the borehole information utilized in Gottschalk et al. (2018) was also utilized in the current analysis including 186 lithology logs (red circles in Figure 2-1) and 36 geophysical logs (green circles in Figure 2-1) that were directly in the vicinity of the acquired AEM flight lines.

In addition, the U.S. Army Corps or Engineers at Fort Ord provided an additional 84 borehole logs in the vicinity of the AEM flight lines (USACE, 2019).

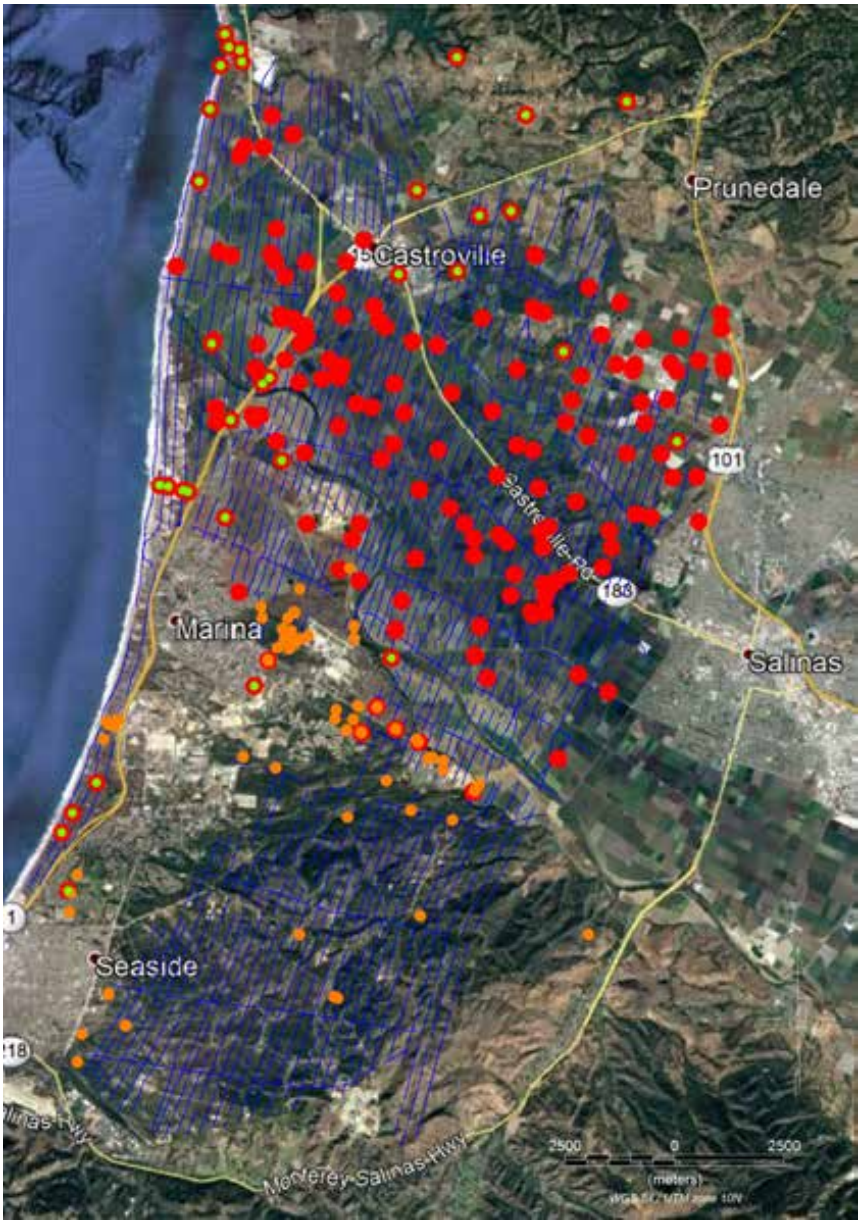

Figure 2-1. Locations of boreholes used for interpretation in the MCWD 2019 survey area. Lithology logs – red circles; Lithology logs received from Fort Ord – orange circles; Geophysical logs – green circles, sometimes overlaying red lithology circles.

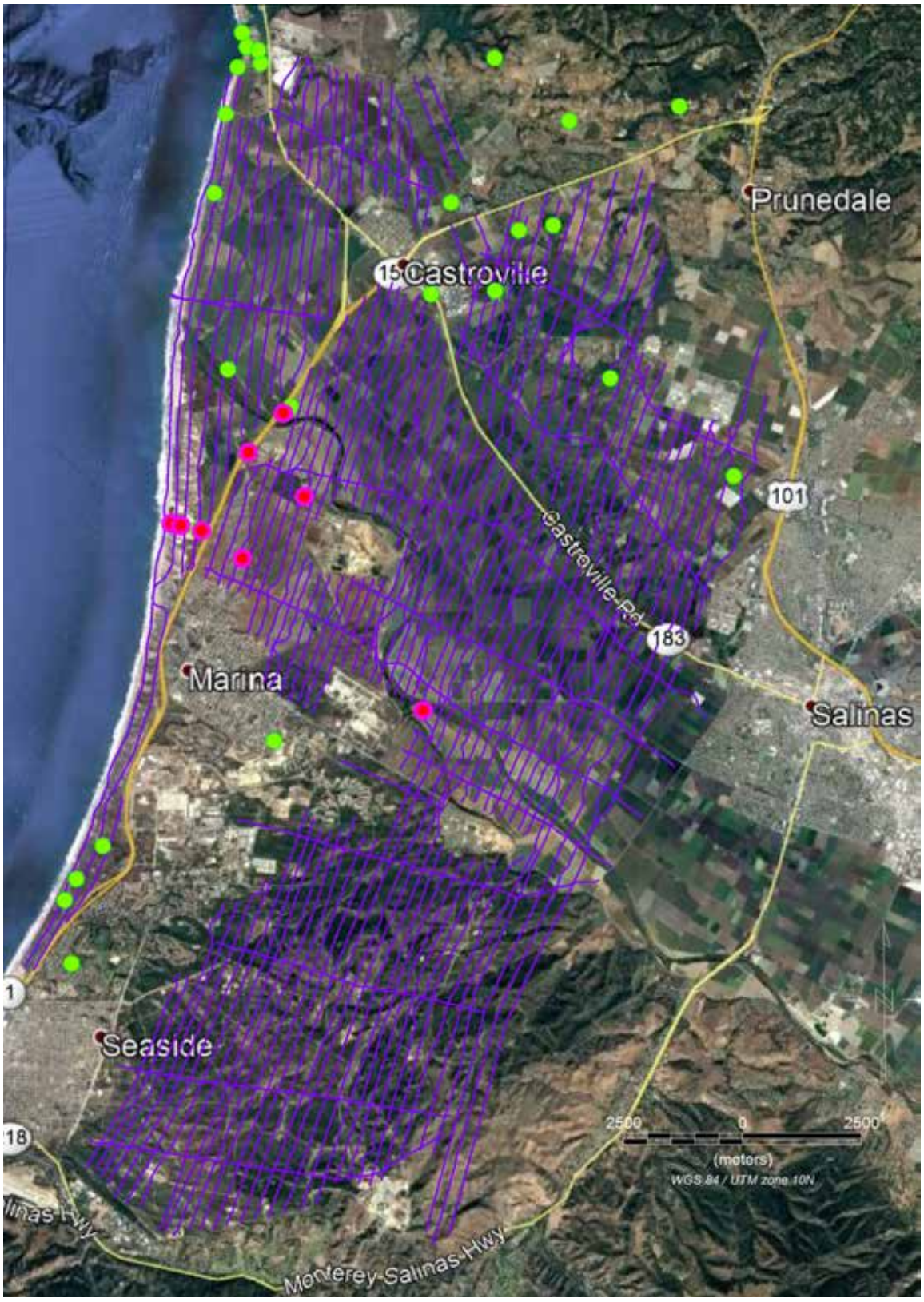

Figure 2-2. Geophysical logs used in MCWD 2019 AEM to E-Logs comparison. Green circles – 35 geophysical logs of which the MW wells (Red circles) are part.

3 Geophysical Methodology, Acquisition and Processing

3.1 Geophysical Methodology

Airborne Transient Electromagnetic (TEM) or airborne Time-Domain Electromagnetic (TDEM), or generally AEM, investigations provide characterization of electrical properties of earth materials from the land surface downward using electromagnetic induction. Figure 3-1 gives a conceptual illustration of the airborne TEM method.

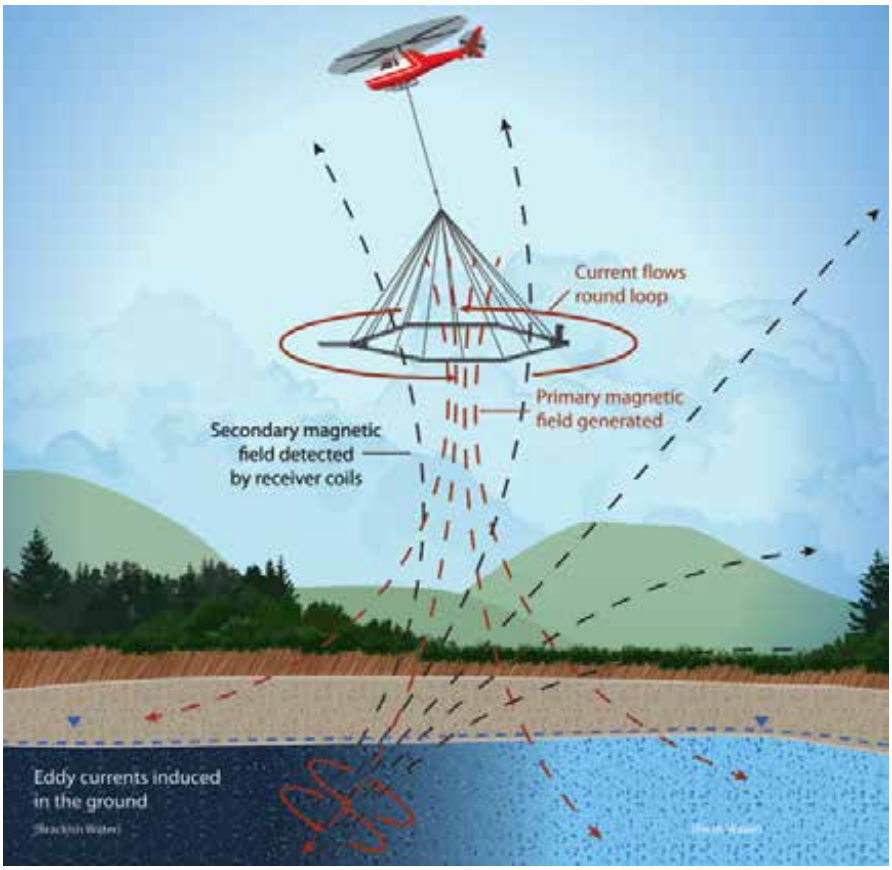

Figure 3-1: Schematic of an airborne electromagnetic survey, modified from Carney et al. (2015).

To collect TEM data, an electrical current is sent through a large loop of wire consisting of multiple turns which generates an electromagnetic (EM) field. This is called the transmitter (Tx) coil. After the EM field produced by the Tx coil is stable, it is switched off as abruptly as possible. The EM field dissipates and decays with time, traveling deeper and spreading wider into the subsurface. The rate of dissipation is dependent on the electrical properties of the subsurface (controlled by the material composition of the geology including the amount of mineralogical clay, the water content, the presence of dissolved solids, the metallic mineralization, and the percentage of void space). At the moment of turnoff, a secondary EM field, which also begins to decay, is generated within the subsurface. The decaying secondary EM field generates a current in a receiver (Rx) coil, per Ampere's Law. This current is measured at several different moments in time (each moment being within a time band called a "gate"). From the induced current, the time rate of decay of the magnetic field, B, is determined (dB/dt). When compiled in time,

these measurements constitute a “sounding” at that location. Each TEM measurement produces an EM sounding at one point on the surface.

The sounding curves are numerically inverted to produce a model of subsurface resistivity as a function of depth. Inversion relates the measured geophysical data to probable physical earth properties. Figure 3-2 shows an example of a dual-moment TEM dB/dt sounding curve and the corresponding inverted electrical resistivity model.

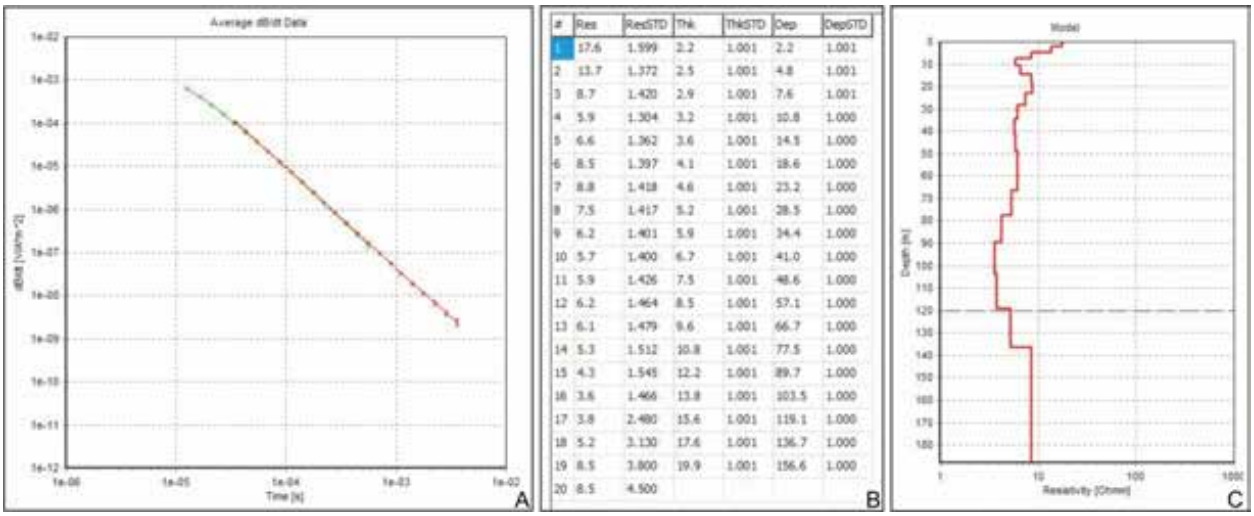

#	Res	ResSTD	Thk	ThkSTD	Dep	DepSTD
1	17.6	1.599	2.2	1.001	2.2	1.001
2	13.7	1.372	2.5	1.001	4.8	1.001
3	8.7	1.420	2.9	1.001	7.6	1.001
4	5.9	1.304	3.2	1.001	10.8	1.000
5	6.6	1.362	3.6	1.001	14.5	1.000
6	8.5	1.397	4.1	1.001	18.6	1.000
7	8.8	1.418	4.6	1.001	23.2	1.000
8	7.5	1.417	5.2	1.001	28.5	1.000
9	6.2	1.401	5.9	1.001	34.4	1.000
10	5.7	1.400	6.7	1.001	41.0	1.000
11	5.9	1.426	7.5	1.001	48.6	1.000
12	6.2	1.464	8.5	1.001	57.1	1.000
13	6.1	1.479	9.6	1.001	66.7	1.000
14	5.3	1.512	10.8	1.001	77.5	1.000
15	4.3	1.545	12.2	1.001	89.7	1.000
16	3.6	1.466	13.8	1.001	103.5	1.000
17	3.8	2.480	15.6	1.001	119.1	1.000
18	5.2	3.130	17.6	1.001	136.7	1.000
19	8.5	3.800	19.9	1.001	156.6	1.000
20	8.5	4.500				

Figure 3-2: A) Example of a dB/dt sounding curve. B) Corresponding inverted model values. C) Corresponding resistivity earth model.

3.2 Flight Planning/Utility Mapping

The primary source of noise in geophysical electromagnetic surveys are other electromagnetic devices that are part of typical municipal utility infrastructure. These include, for example, power lines, railroads, pipelines, and water pumps. Prior to AEM data acquisition in the MCWD, utilities (roads, pipelines, railroads, and power lines) were located by inspection from Google Earth imagery.

The locations of the flight lines were converted from a regularly spaced grid to one with flight lines optimized to avoid electromagnetic coupling with the previously mentioned utilities. This was done by moving along each flight line in Google Earth to inspect the path for visible power lines, radio towers, railroads, highways and roads, confined feeding operations and buildings, and any other obstructions that needed to be avoided during flight.

Upon conclusion of the design process, the MCWD AEM investigation utilized the SkyTEM312 system to fly the same flight lines as were flown in 2017 (with the hope to image deeper where possible) plus an extension of the flight area to the south onto the former Fort Ord. The purpose of the extension was to characterize the influx of groundwater from the highlands of former Fort Ord into the Salinas River Valley. The MCWD SkyTEM312 flight lines had a maximum length of approximately 15 miles (24 km) in the primary north-south direction, separated by approximately 650 feet (about 180-220 m), and a maximum of about 7 miles (11 km) along the east-west tie-lines.

3.3 AEM Survey Instrumentation

AEM data were acquired using the SkyTEM312 (312) airborne electromagnetic system (SkyTEM Airborne Surveys Worldwide, 2019). This is a different system than was used for the 2017 MCWD AEM survey. The SkyTEM312 can image somewhat deeper than the SkyTEM304M, depending on the geology being imaged. The 312 is a rigid frame, dual-magnetic moment (Low and High) TEM system. The area of the 312 Tx coil is 342 m^2. A peak current of six (6) amps is passed through two (2) turns of wire in the Tx for Low Moment measurements and a peak current of 110 amps is passed through twelve (12) turns of wire for High Moment measurements. This results in peak Tx Low and High magnetic moments of ~4,100 Ampere-meter-squared ($A*m^2$) and ~450,000 $A*m^2$, respectively.

The SkyTEM 312 system utilizes an offset receiver (Rx) positioned slightly behind the Tx coil resulting in a 'null' position which is a location where the intensity of the primary field from the system transmitter is minimized. This is desirable as to minimize the amplitude of the primary field at the Rx to maximize the sensitivity of the Rx to the secondary fields. The 312 multi-turn Rx vertical (Z) coil has an effective area of 105 m^2. In addition to the Tx and Rx that constitute the TEM instrument, the 312 is also equipped with a Total Field magnetometer (MAG) and data acquisition systems for both instruments. The 312 also includes two each of laser altimeters, inclinometers/tilt meters, and differential global positioning system (DGPS) receivers. Positional data from the frame mounted DGPS receivers are recorded by the AEM data acquisition system. The magnetometer includes a third DGPS receiver whose positional data is recorded by the magnetometer data acquisition system. Figure 3-3 gives a simple illustration of the 312 frame and instrument locations. The image is viewed along the +z axis looking at the horizontal x-y plane. The axes for the image are labeled with distance in meters. The magnetometer is located on a boom off the front of the frame (right side of image). The Tx coil is located around the octagonal frame and the Rx Coil is located at the back of the frame (left side of image). Some images of the SkyTEM system in the air are presented in Figure 3-4.

The coordinate system used by the 312 defines the +x direction as the direction of flight, the +y direction is defined 90 degrees to the right and the +z direction is downward. The center of the transmitter loop, mounted to the octagonal SkyTEM frame is used as the origin in reference to instrumentation positions. Table 3-1 lists the positions of the instruments and Table 3-2 lists the corners of the transmitter loop.

The DGPS and magnetometer mounted on the frame of the 312 require the use of base stations, which are located on the ground and are positioned in an area with low cultural noise. In this case these instruments were located at the Marina Airport. Data from the magnetometer and DGPS base stations were downloaded each day after the end of the day's AEM flights. The DGPS and magnetometer base stations were placed at the Universal Transverse Mercator (UTM) coordinate system Zone 10 North (Table 3-3). The horizontal geodetic reference used is North American Datum of 1983 (NAD83 in meters). All elevations are from USGS's National Elevation Dataset, referenced to the North American Vertical Datum of 1988; with meters as the unit of measurement.

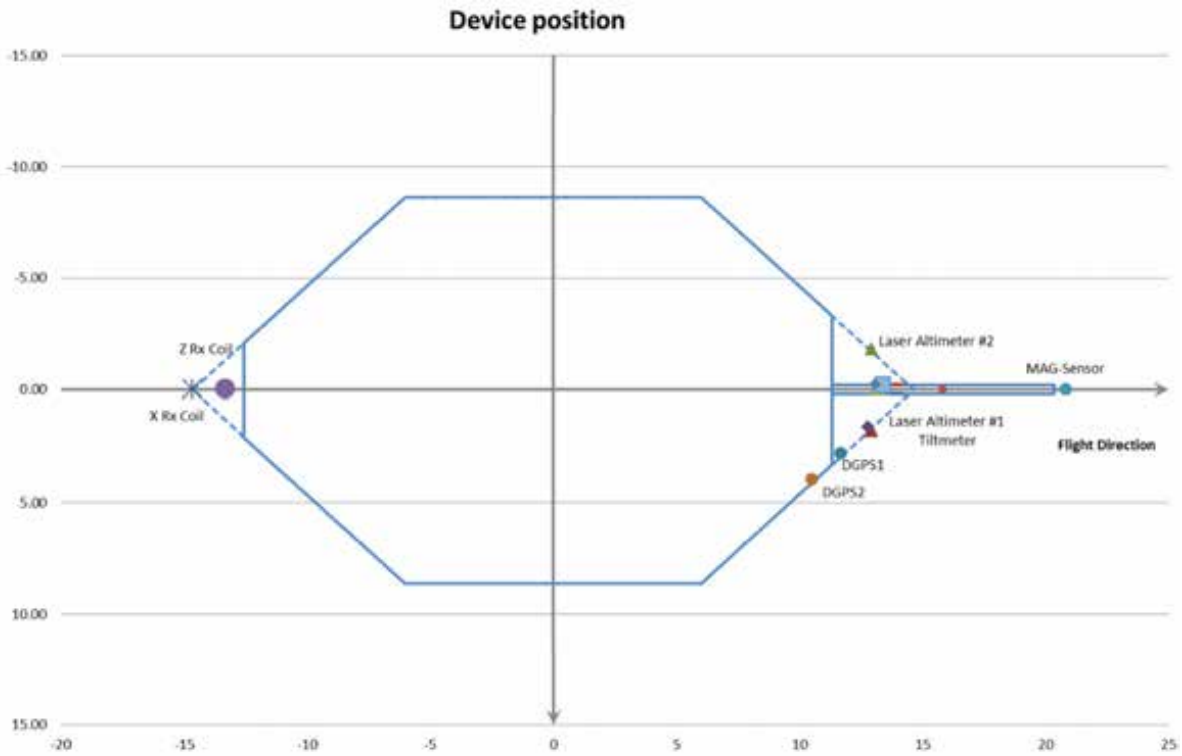

Figure 3-3: SkyTEM304M/312 frame, including instrumentation locations and X and Y axes. Distances are in meters. Instrumentation locations listed in Table 3-1.

Figure 3-4: Photos of the SkyTEM312 system in suspension beneath the helicopter.

Table 3-1: Positions of instruments on the SkyTEM312 frame, using the center of the frame as the origin, in feet.

	DGPS 1	DGPS 2	Inclinometer 1	Inclinometer 2	Altimeter 1	Altimeter 2	Magnetic Sensor	Rx Coil
X	38.31	34.47	41.95	41.95	42.44	42.44	67.24	-43.46
Y	9.15	12.96	5.38	-5.38	5.87	-5.87	0.00	0.00
Z	-0.52	-0.52	-0.39	-0.39	-0.39	-0.39	-1.71	-6.56

Table 3-2: Positions of corners of the SkyTEM312 transmitter coil, using the center of the frame as the origin, in feet.

Tx Corners	1	2	3	4	5	6	7	8
X	-41.16	-19.78	18.83	37.19	39.19	18.83	-19.78	-41.16
Y	-6.89	-27.98	-28.18	-10.85	10.85	28.18	27.98	6.89

Table 3-3: Location of DGPS and magnetic field base station instruments at the Marina Municipal Airport.

Instrument	Easting (m)	Northing (m)	UTM Zone
Magnetometer Base Station	611145	4059781	10 N
DGPS Base Station	611136	4059778	10 N

3.4 Data Acquisition

All SkyTEM systems are calibrated to a ground test site in Lyngby, Denmark prior to being used for production work (HydroGeophysics Group Aarhus University, 2010; HydroGeophysics Group Aarhus University, 2011; Foged et al., 2013). The calibration process involves acquiring data with the system hovering at different altitudes, from 5 m to 50 m (16 ft to 164 ft), over the Lyngby site. Acquired data are processed and a scale factor (time and amplitude) is applied so that the inversion process produces the model that approximates the known geology at Lyngby.

The SkyTEM 312 system was assembled April 20-22, 2019 at the Sinton Helicopters office in Paso Robles, CA and ground tests and airborne tests were conducted. SkyTEM mobilized to Marina Municipal Airport on April 23, 2019, where additional refinements and high-altitude airborne tests were conducted. Production began on April 24 and continued through April 26, 2019. The system was then parked at the Marina Municipal Airport at the completion of data acquisition to await data approval.

Ground tests included checking for system operation including the following sub-systems: 1) transmitter (Tx) current amplitude and stability including waveform recording of both high moment (HM) and low moment (LM); 2) receiver (Rx) functionality for both Z and X-components, 3) laser altimeter operation; 4) GPS operation; 5) tilt meter/attitude sensor operation and calibration; 6) navigation and wireless communication; 7) airborne magnetometer operation; 8) base station magnetometer stability and field strength stability; and 9) DGPS base station operation.

Airborne tests are conducted to establish and confirm the minimum primary field signal level, otherwise known as the “null” position, of both the Z and X Receiver (Rx) components. This is done by mechanically moving the Rx’s to locate the best null position by multiple flights. At the time of the

establishment of the nulls the system is flown to a high level to eliminate the earth response. At that altitude, typically 1,000 meters above ground level (AGL), only the background noise of the system and the helicopter is received. That is checked against the designed system noise level and used as a calibration point. In addition to the calibrations and the nulls, the system is operated to ensure the mechanical stability of the system and that all acquisition systems are functional. Additional overflight passes are performed in order to adjust the length of the supporting tow ropes to control the angle of the system at acquisition production speeds.

All MCWD 2019 AEM airborne operations were based out of the Marina Municipal Airport and were carried out by Sinton Helicopters under contract to SkyTEM, Inc. The production flights took place from April 24-26, 2019. Two production flights were flown each day. Line-km (and miles) totals from each flight are provided in Table 3-4. Figure 3-5 is an "as-flown" map view of the timing and spatial orientation of the flight lines grouped by date. In some locations, the as-flown lines deviate from the planned lines due to infrastructure and safety as determined by the pilot.

Table 3-4. Flight line production by flight.

Date	Flight	Line-km Total	Line-miles Total
24-April-2019	1	152.9	94.4
	2	172.4	106.4
25-April-2019	1	154.8	95.6
	2	161.6	99.8
26-April-2019	1	166.2	102.6
	2	73.2	45.2
Total		881.1	544.0

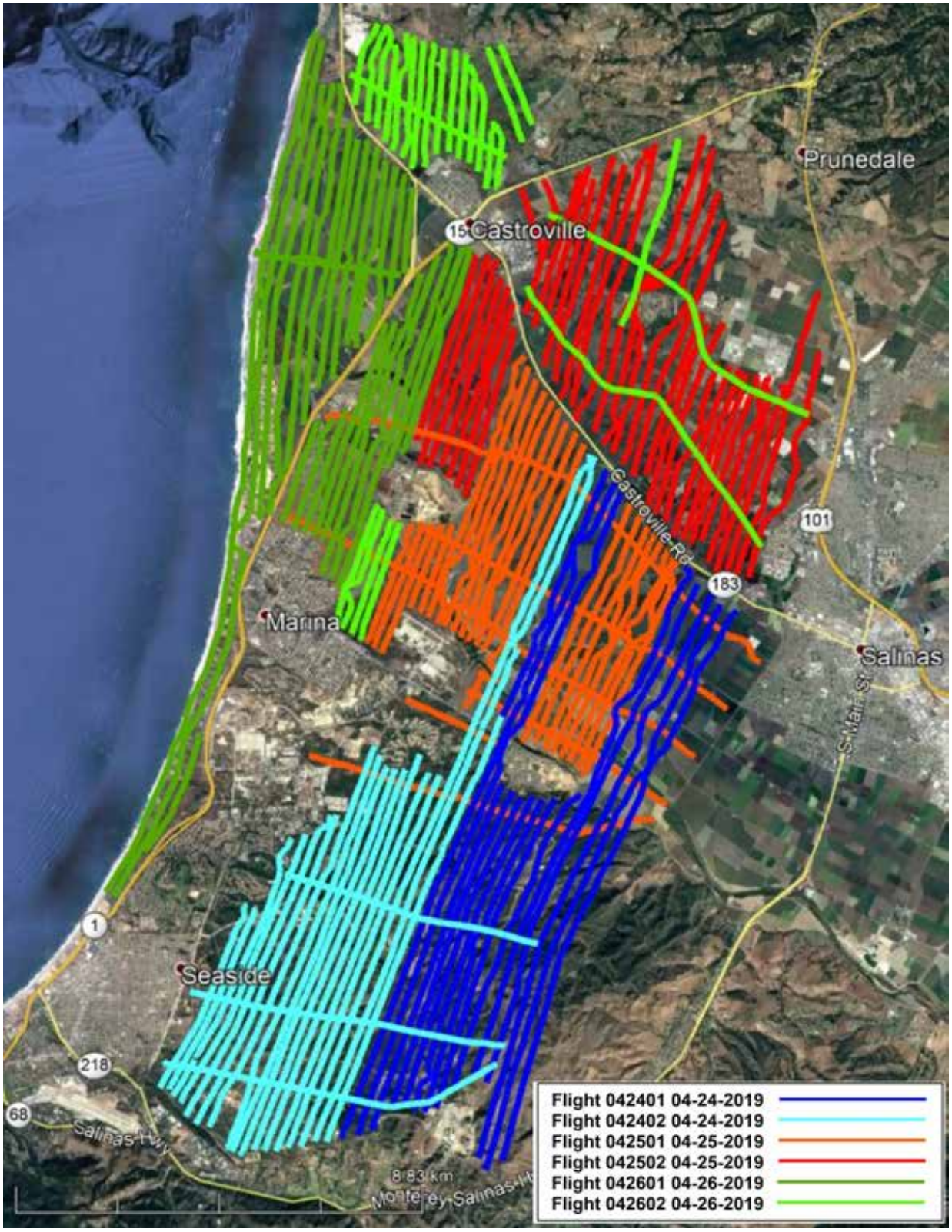

Figure 3-5: As-Flown map showing timing of the MCWD 2019 AEM survey data acquisition.

3.4.1 System Flight Parameters

3.4.1.1 Flight Height

The system height was specified at 30 meters; however, due to safety and other judgments by the pilot the flight heights will deviate. The goal is to maintain a height as low as possible in the window from 25 to 50 m AGL. In the MCWD 2019 data set the average height was 42.7 m with a minimum of 20.0 m and a maximum of 192.9 m. The maximum flight heights were encountered over large powerlines. Those data were removed from the dataset before inversion due to EM coupling and did not impact the final product. A map of the flight height throughout the survey area is presented in Figure 3-6.

3.4.1.2 Flight Speed

Speed determines the distance between ground samples. However, there is a tradeoff between the cost of the survey and the speed of the system related to the foot print of the system. In many surveys, the specified speed is 100 km/hr. The critical factor in the flight speed is to maintain a speed where the system is as level as possible. This may require that the pilot speed up in the downwind direction or slowdown in the up-wind direction. The pilot uses the readout display of the system tilt angles to help maintain this speed. For the MCWD 2019 survey the ropes suspending the system beneath the helicopter needed to be adjusted due to the slower speeds that were required to maintain a safe operation in the MCWD area allowing the pilot to avoid infrastructure and obstacles. A map of the flight speeds of the MCWD survey is presented in Figure 3-7. The average ground speed of the survey was 87.5 km/hr with a minimum ground speed of 0.6 km/hr and a maximum ground speed of 118.4 km/hr.

3.4.1.3 System Angles

System angles are critical to ensure that quality data are submitted to the inversion. The system's Tx initial current at time-off of 0.0 sec is the image of the size of the loop on the surface. If the system is tilted, that image will be less than the original size of the TX. Inversion algorithms can account for ±10 degrees of angle in calculating the effective Tx size. To this end, it is important to keep the Tx frame within ±10 degrees. The position of the Rx is also impacted by the angle of the system and any deviation from perpendicular has an impact by including off perpendicular components. As noted, algorithms can account for ±10 degrees in the Rx angle. Both the X-Angle (in the direction of flight) and the Y-Angle (perpendicular to the direction of flight) were checked for the MCWD 2019 survey. When the system is flown over obstacles or while turning around at the end of a line, the angles can be higher than the ±10 degrees. These flight line edges are typically cut out of the survey data set prior to inversion. Figure 3-8 and Figure 3-9 are plots of the X-angle and the Y-angle tils, respectively. During the MCWD survey, both angles were within acceptable ranges. The X-angle averaged approximately -1.10 degrees with a minimum of -18.50 degrees and a maximum of 26.29 degrees. The Y-angle tilt averaged about 2.80 degrees with a minimum of -21.97 degrees and a maximum of 30.11 degrees.

3.4.1.4 Transmitter Current

The SkyTEM 312 system utilizes a dual-moment system (High (HM) and Low (LM)) and two different Tx current and waveforms. These waveforms are recorded before and after the survey to ensure that that no changes have occurred during the survey. Figure 3-10 and Figure 3-11 are plots of the recorded low moment (LM) and the high moment (HM) Tx waveforms, respectively. The LM Tx source is used to highlight the very near surface geology and the HM current source is used to get more electromagnetic power at depth in order to characterize the deeper geologic units.

The current should be stable throughout the survey, but changes in the temperature can impact the resistance of the Tx wire and circuit by either increasing or lowering the peak current output. The peak current is recorded during acquisition of each sounding and is used to adjust the Tx waveform in the inversion. For the MCWD 2019 survey the LM current mean was 5.97 amp with a minimum current of 5.94 amp and a maximum current of 5.98 amp. For the HM, mean was 112.26 amp with a minimum current of 108.60 amp and a maximum current of 114.97 amp. Both of the moments show stability in the current and will provide no problems in the inversion.

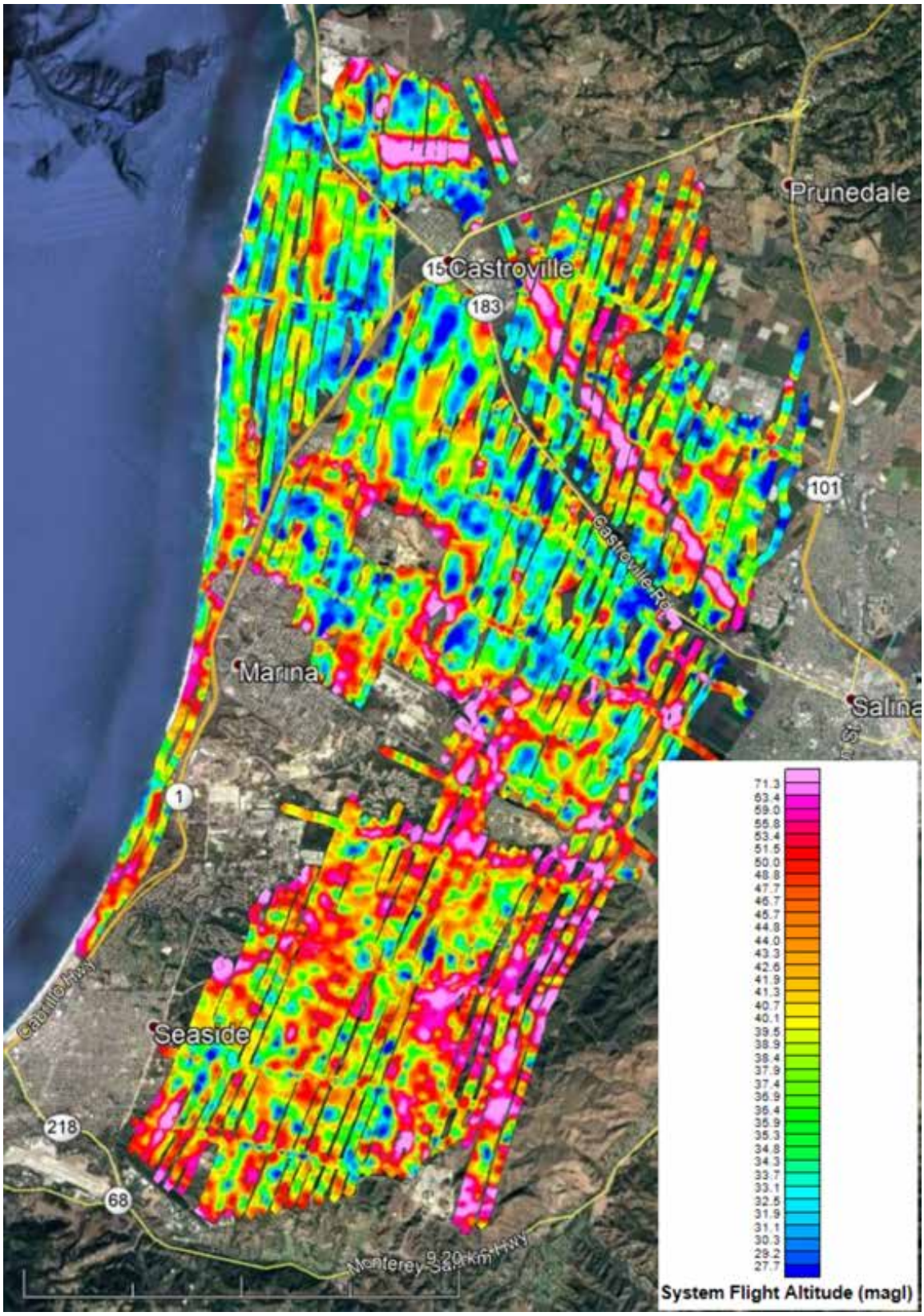

Figure 3-6. Map of the system height (in meters above ground level) recorded during the MCWD 2019 survey, as-flown flight lines are indicated as black lines.

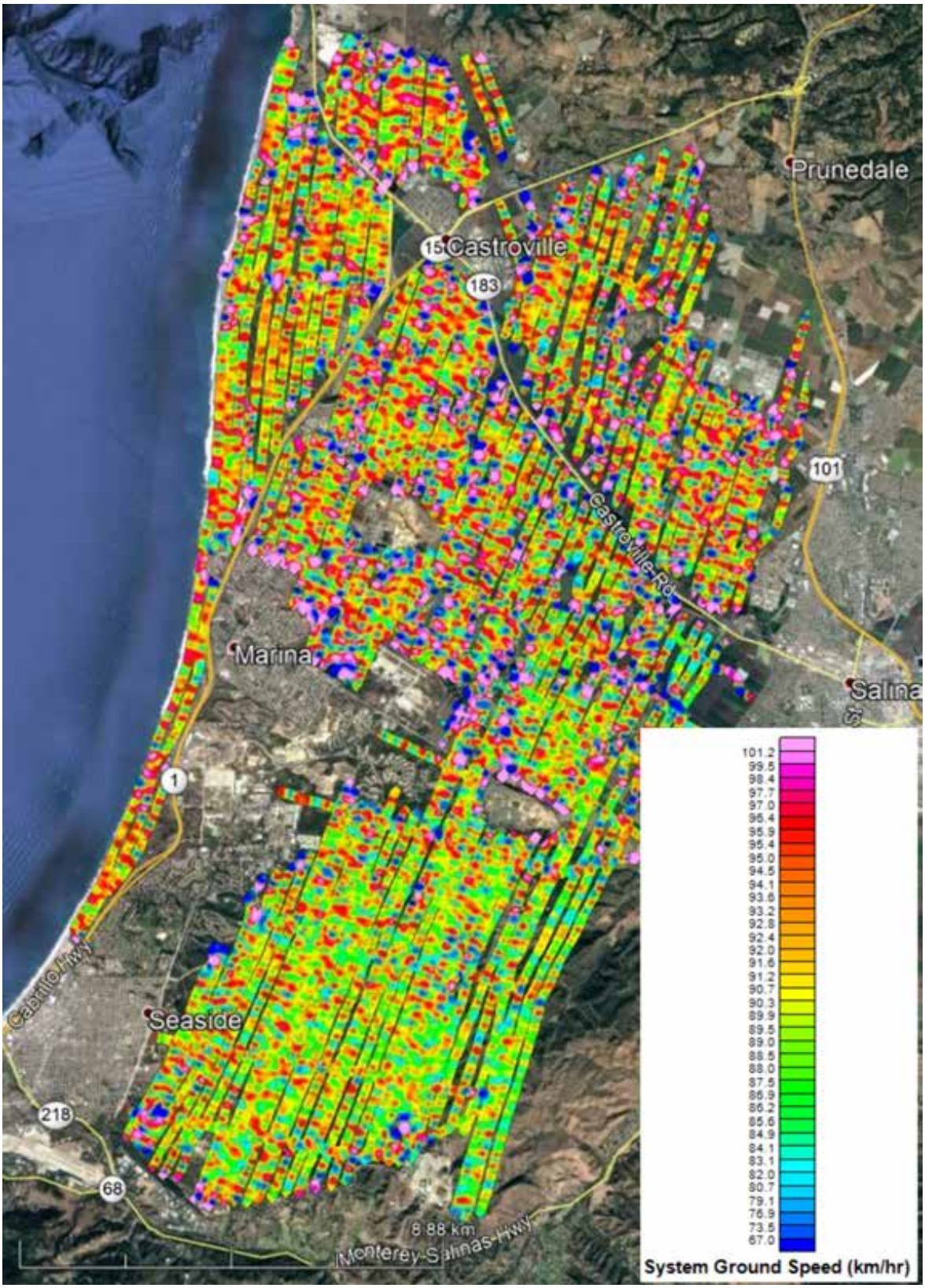

Figure 3-7. Map of the ground speed recorded during the MCWD 2019 survey, as-flown flight lines are indicated as black lines.

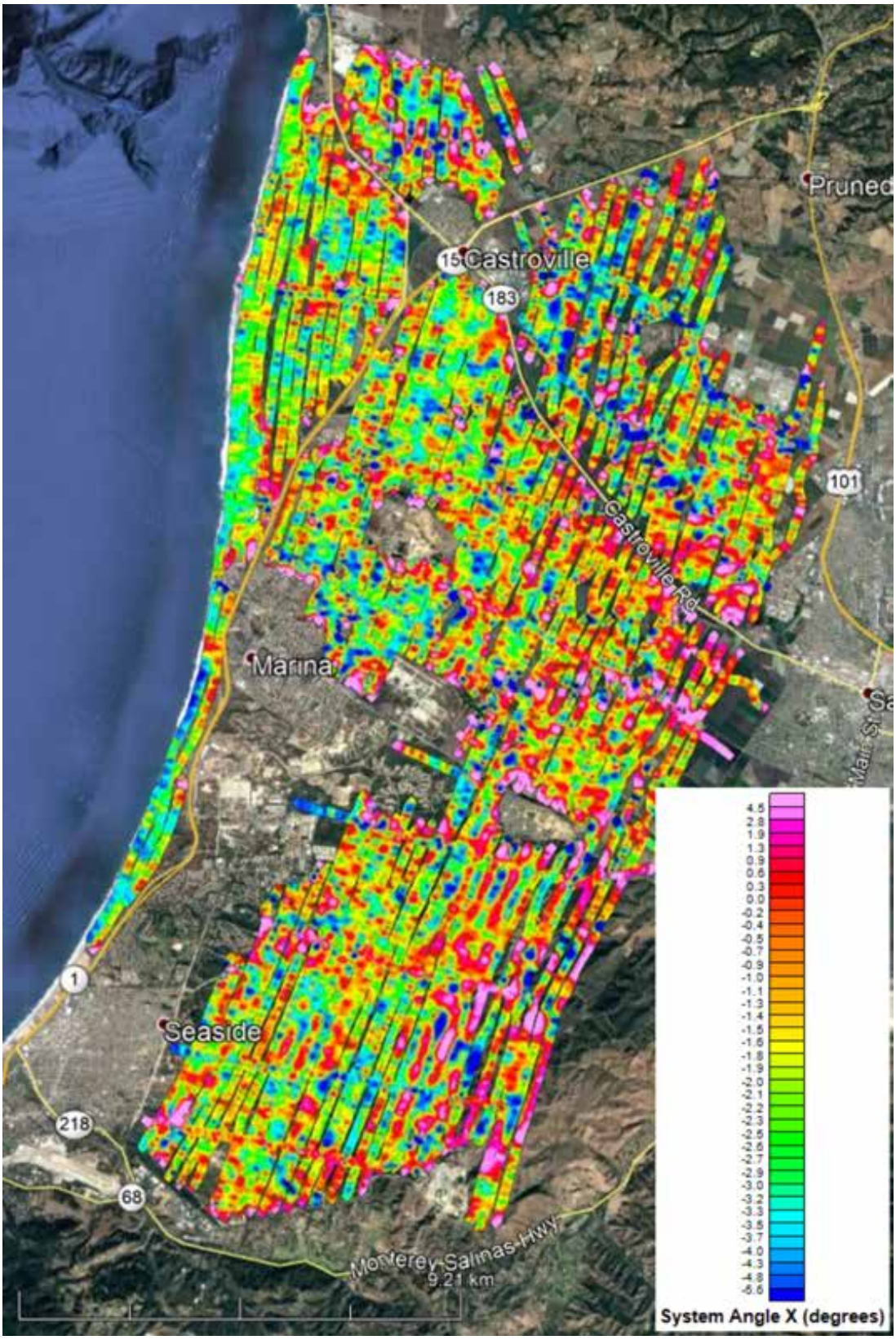

Figure 3-8. Map of the X-angle tilt recorded during the MCWD 2019 survey, as-flown flight lines are indicated as black lines.

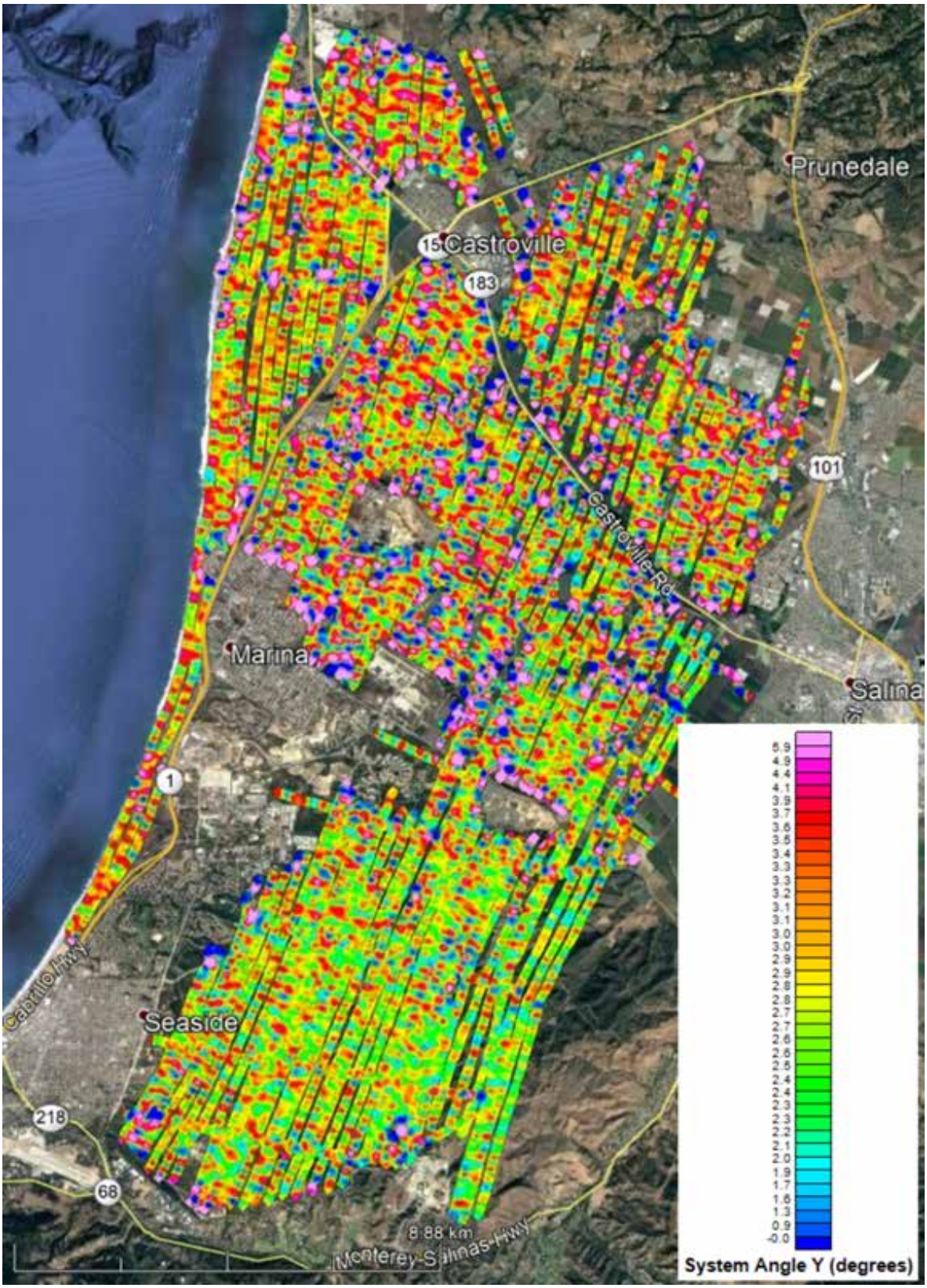

Figure 3-9. Map of the Y-angle tilt recorded during the MCWD 2019 survey, as-flown flight lines are indicated as black lines.

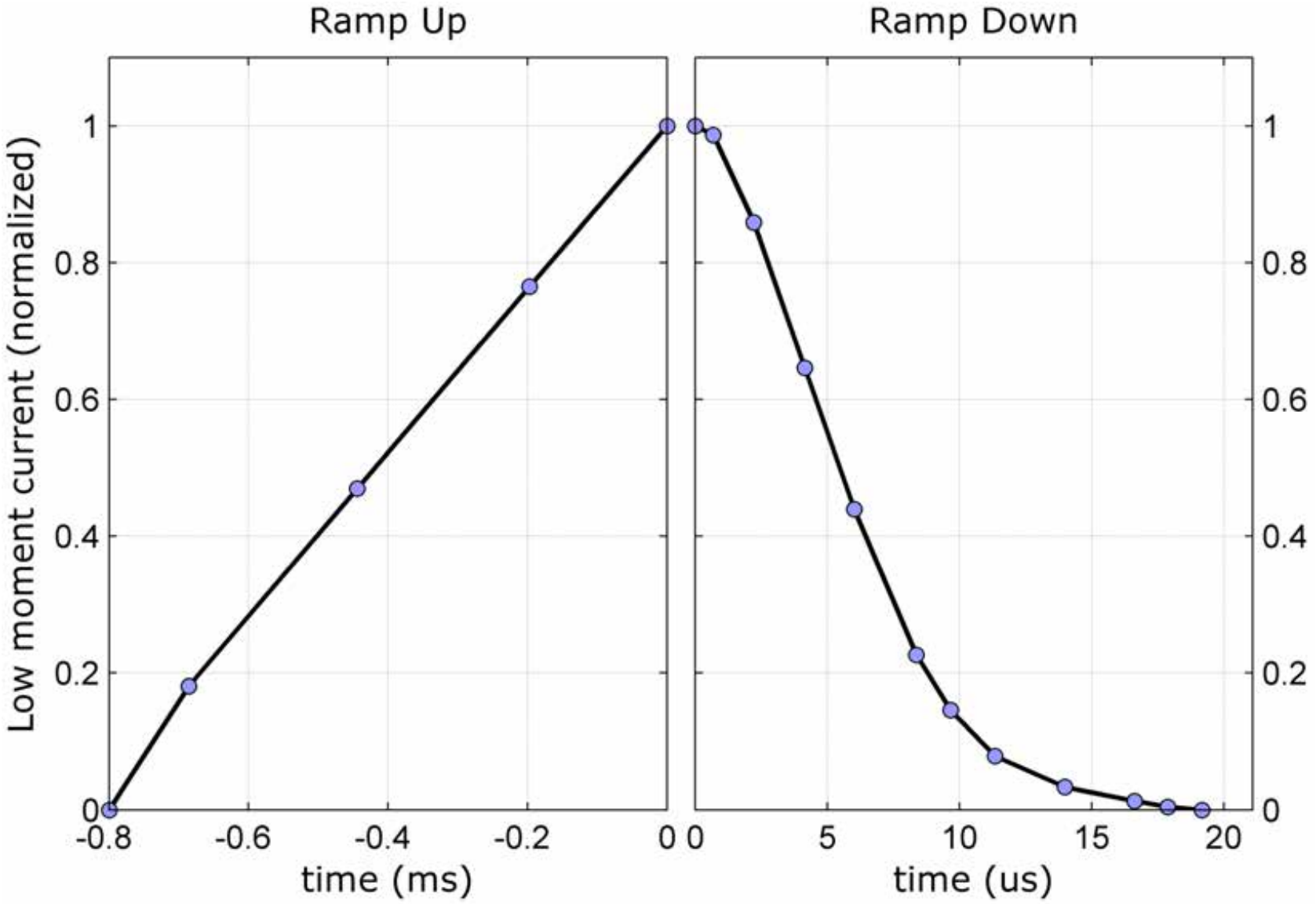

Figure 3-10. Plot of the 210 Hz LM waveform recorded during the MCWD 2019 survey. Current ramp up is on the left and the ramp down to turn off is on the right. Note the different x-axis scales between the left and right sides of the figure.

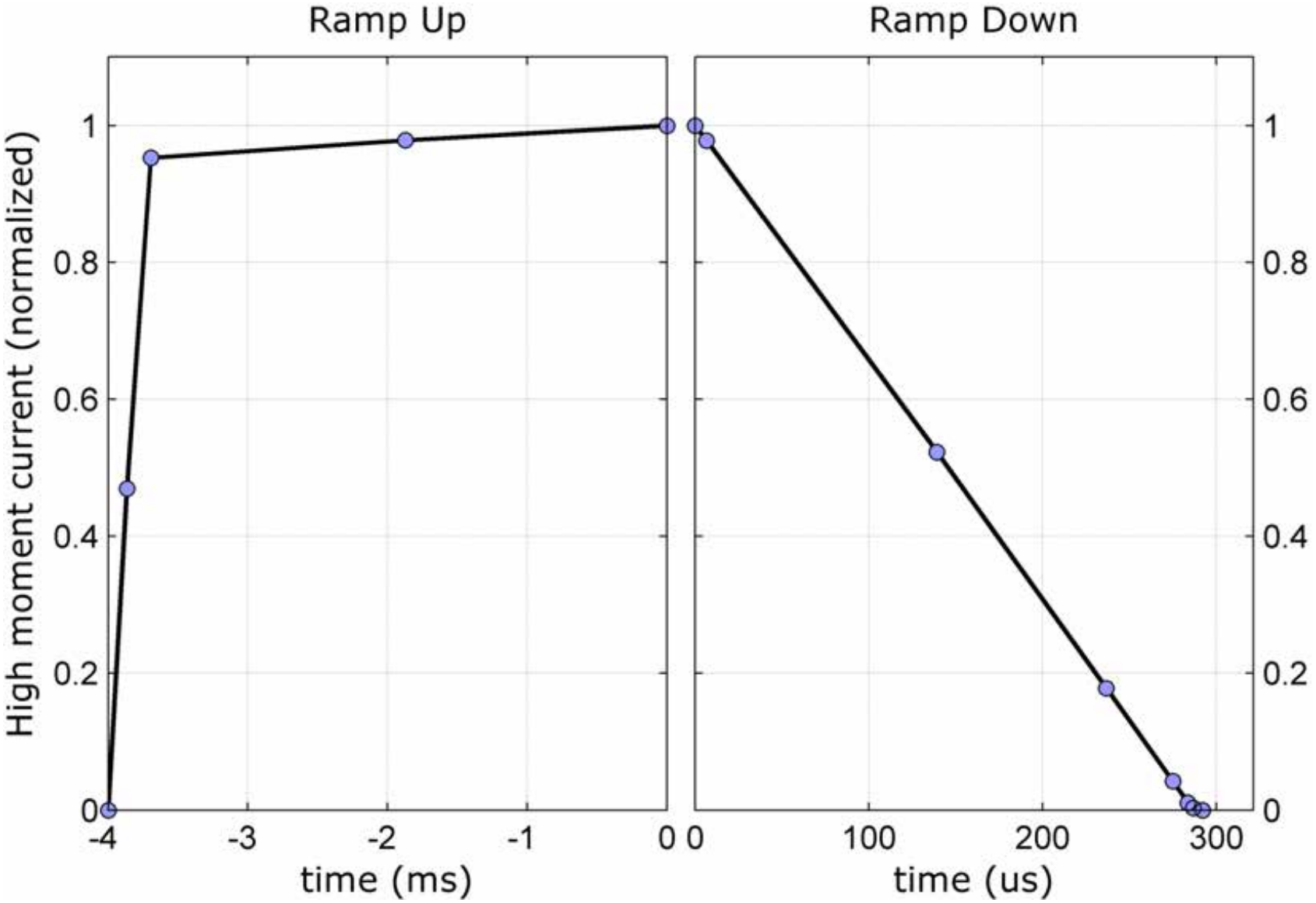

Figure 3-11. Plot of the 30 Hz HM waveform recorded during the MCWD 2019 survey. Ramp up is on the left and ramp down to turn off is on the right. Note the different x-axis scales between the left and right sides of the figure.

3.4.2 Primary Field Compensation

A standard SkyTEM data acquisition procedure involves review of acquired raw data by SkyTEM in Denmark for Primary Field Compensation (PFC) prior to continued data processing by AGF (Schamper et al., 2014). The primary field of the transmitter affects the recorded early time gates, which in the case of the Low Moment, are helpful in resolving the near surface resistivity structure of the ground. The Low Moment uses a saw tooth waveform which is calculated and then used in the PFC correction to correct the early time gates.

3.4.3 Power Line Noise Intensity (PLNI)

The SkyTEM 312 system is configured to provide an estimate of the amplitude of the powerline noise intensity (PLNI) of the 60 Hz signals. The PLNI is produced by performing a spectral frequency content analysis on the raw received Z-component SkyTEM data. For every HM data block, a Fourier Transform (FT) is performed on the latest usable time gate data. The FT is evaluated at the local power line transmission frequency (60 Hz) yielding the amplitude spectral density of the local power line noise. The PLNI map is useful when investigating the impacts of powerlines on the data quality. The 60 Hz powerline signals have little impact on the Rx signal due to time-gating and proper filtering. However, the conductive wires that are used to transmit the power do cause EM coupling impacts on the data and those data need to be removed prior to inversion. The PLNI for the MCWD survey is presented in Figure 3-12.

The MCWD 2019 AEM-flight lines with blue colors representing data retained for inversion and red lines representing 312 data removed due to infrastructure and late time noise are presented in Figure 3-13.

3.4.4 Magnetic Field Data

As part of the SkyTEM 312 system a Total Field magnetometer is included in the data acquisition package (Figure 3-3, Table 3-1). The magnetic field signal is useful for determining deep seated geological contacts and is also extremely valuable for locating intrusive bodies. Neither of those was the target of the survey within MCWD. However, the magnetic field is also sensitive to anthropogenic features that contain ferrous metal and is also used in the electromagnetic decoupling process. A plot of the Total Magnetic Field signal in the area of the MCWD is presented in Figure 3-14. Both geological structure and cultural features can be identified within the survey area.

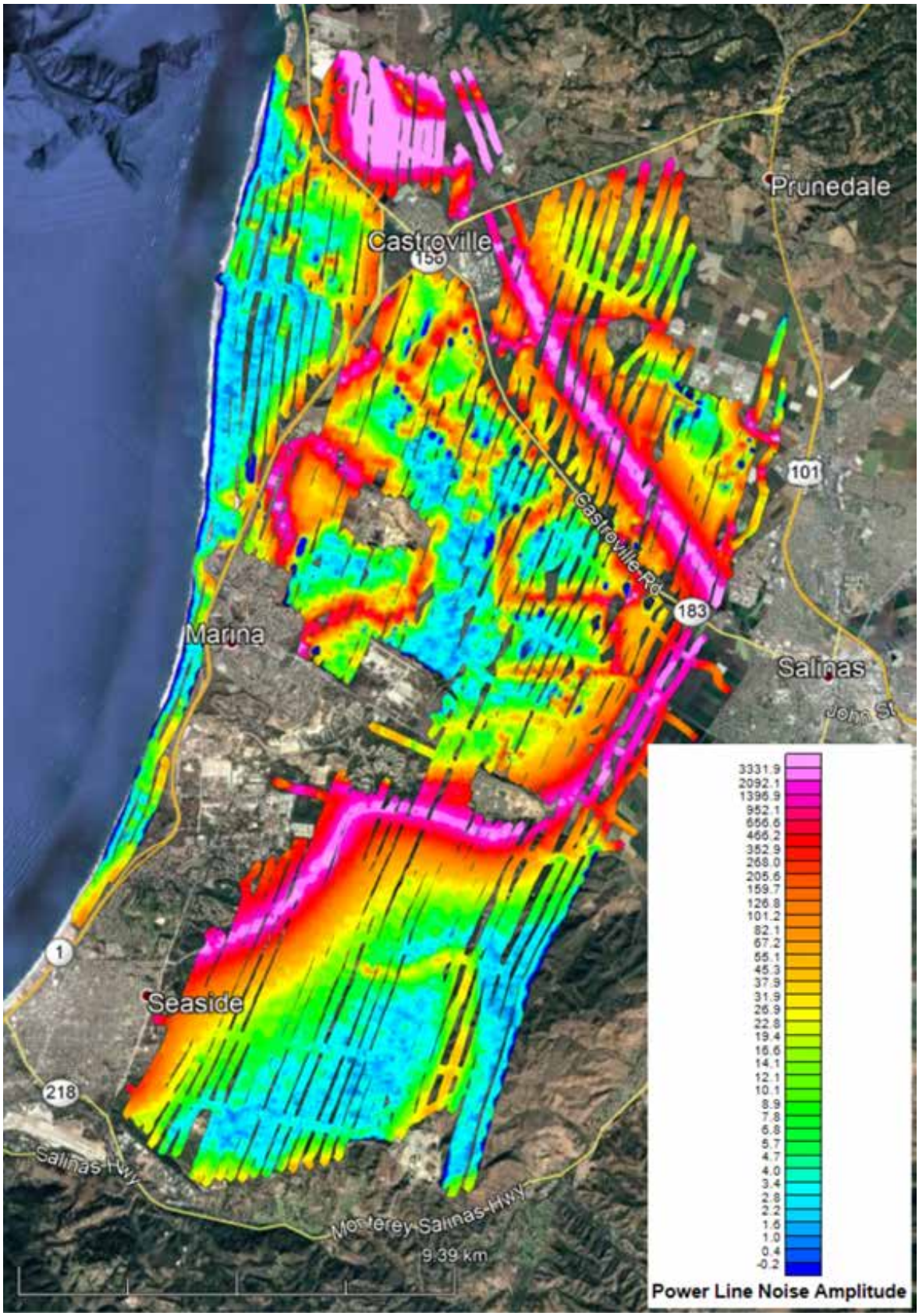

Figure 3-12. Power Line Noise Intensity (PLNI) for the MCWD 2019 AEM survey area.

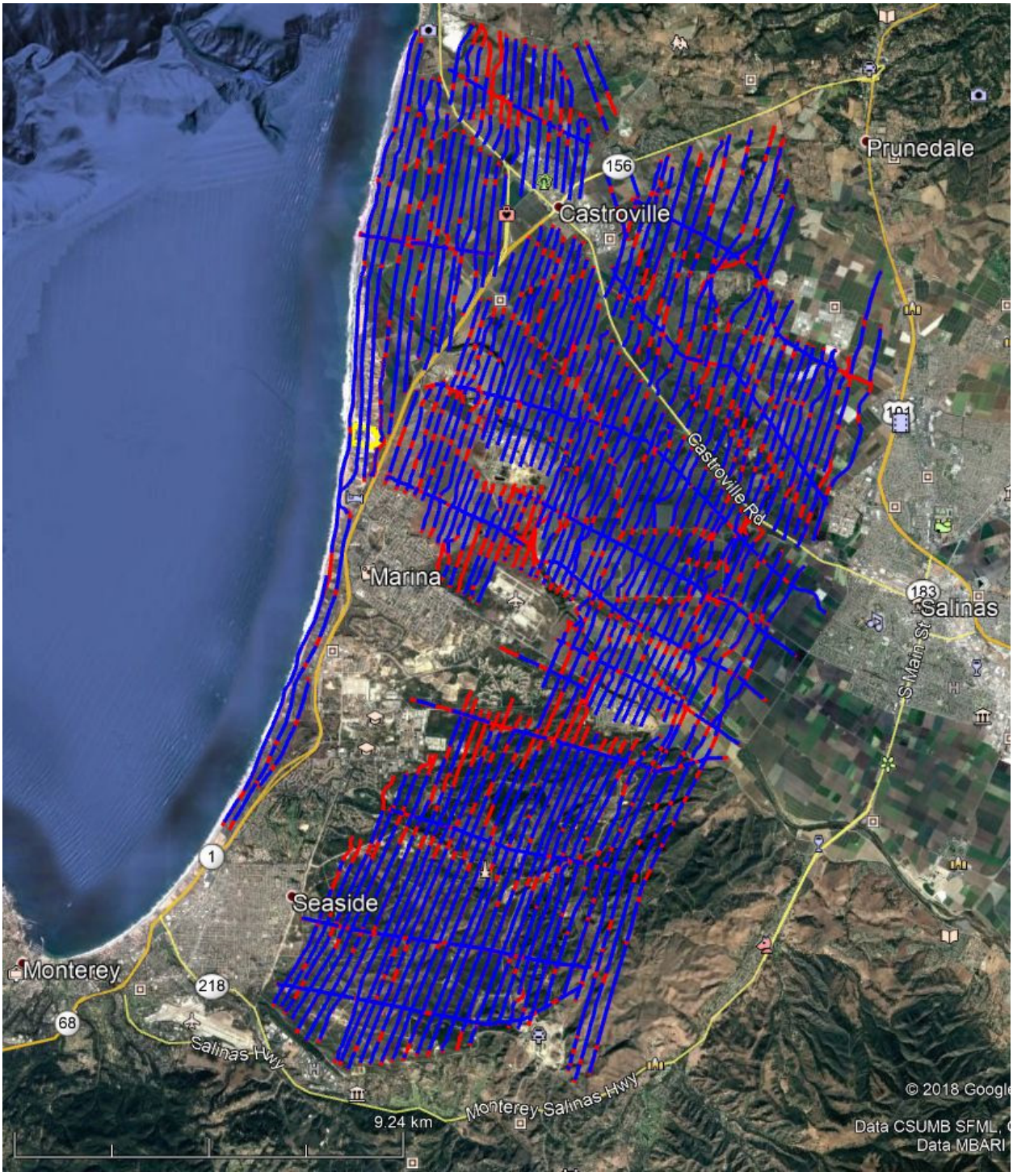

Figure 3-13. Locations of inverted data (blue lines) along the AEM flight lines (red lines) in the MCWD 2019 AEM survey area. Where blue lines are not present indicates decoupled (removed) data. Google Earth kmz's of the inverted data locations as well as the flight lines are included in Appendix 3\KMZ.

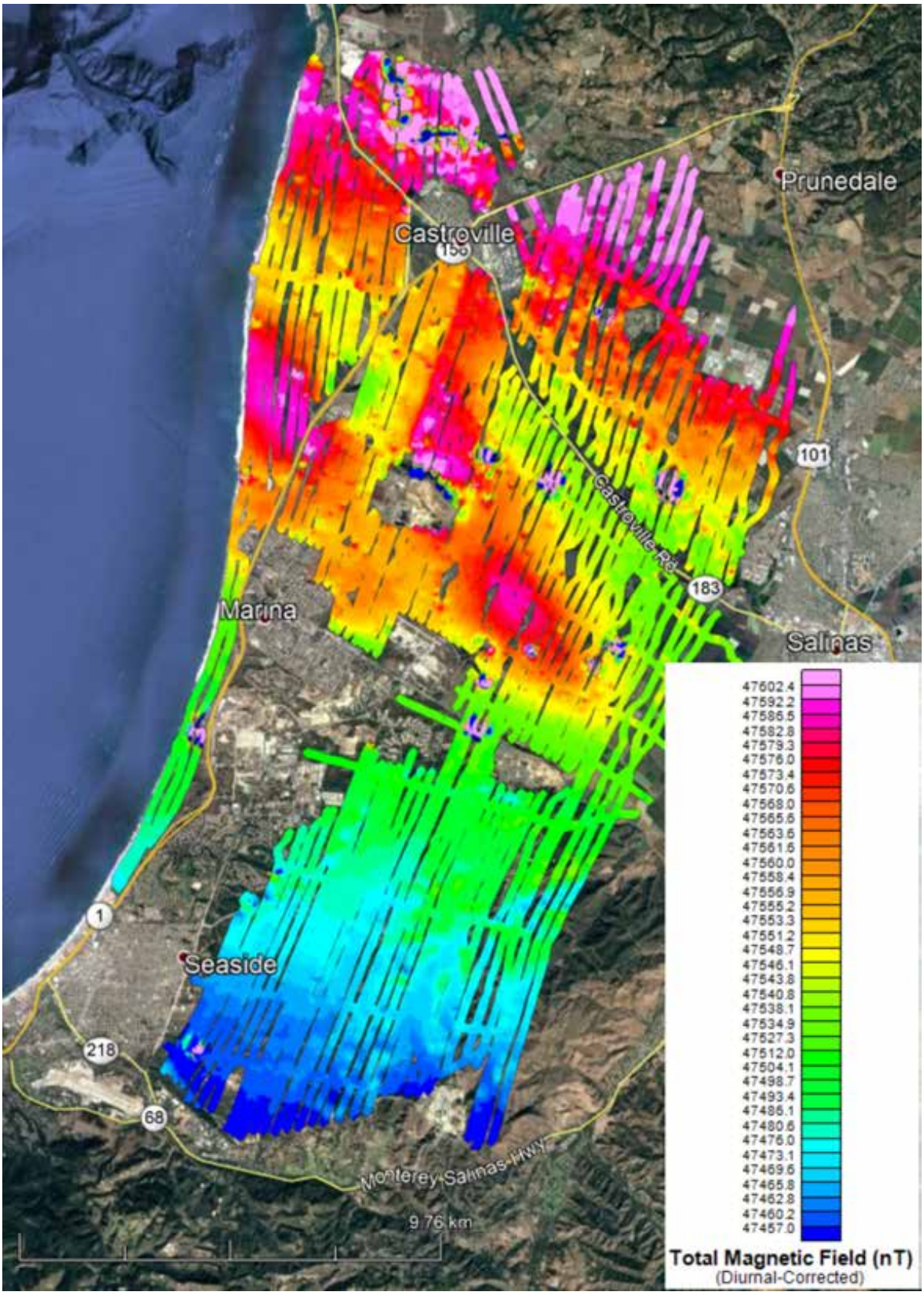

Figure 3-14. Total Magnetic Field (corrected for diurnal drift) for the MCWD 2019 survey area.

3.4.5 Automatic Processing

The AEM data collected by the 312 were processed using Aarhus Workbench version 5.8.3 (Aarhus Geosoftware (https://www.aarhusgeosoftware.dk/)) described in HydroGeophysics Group, Aarhus University (2011).

Automatic processing algorithms provided within the Workbench program are initially applied to the AEM data. DGPS locations were filtered using a stepwise, second-order polynomial filter of nine seconds with a beat time of 0.5 seconds, based on flight acquisition parameters. The AEM data are corrected for tilt deviations from level and so filters were also applied to both of the tilt meter readings with a median filter of three seconds and an average filter of two seconds. The altitude data were corrected using a series of two polynomial filters. The lengths of both eighth-order polynomial filters were set to 15 seconds with shift lengths of six (6) seconds. The lower and upper thresholds were 1 and 100 meters, respectively.

Trapezoidal spatial averaging filters were next applied to the AEM data. The times used to define the trapezoidal filters for the Low Moment were $1.0x10^{-5}$ sec, $1.0x10^{-4}$ sec, and $1.0x10^{-3}$ sec with widths of 4, 7, and 18 seconds. The times used to define the trapezoid for the High Moment were $1.0x10^{-4}$ sec, $1.0x10^{-3}$ sec, and $1.0x10^{-2}$ sec with widths of 10, 20, and 36 seconds. The trapezoid sounding distance was set to 1.0 seconds and the left/right setting, which requires the trapezoid to be complete on both sides, was turned on. The spike factor and minimum number of gates were both set to 25 percent for both soundings. Lastly, the locations of the averaged soundings were synchronized between the two moments.

3.4.6 Manual Processing and Laterally-Constrained Inversions

After the implementation of the automatic filtering, the AEM data were manually examined using a sliding two-minute time window. The data were examined for possible electromagnetic coupling with surface and buried utilities and metal, as well as for late time-gate noise. Data affected by these were removed. Examples of locating areas of EM coupling with pipelines or power lines and recognizing and removing coupled AEM data in Aarhus Workbench are shown in Figure 3-15 and Figure 3-16, respectively. Examples of two inversions, one without EM coupling and the other with EM coupling, are shown in Figure 3-17. Areas were also cut out where the system height was flown greater than 60 m (200 feet) above the ground surface which caused a decrease in the signal level.

The AEM data were then inverted using a Laterally-Constrained Inversion (LCI) algorithm (HydroGeophysics Group Aarhus University, 2011). The profile and depth slices were examined, and any remaining electromagnetic couplings were masked out of the data set.

After final processing, 737.6 line-km (455.3 line-miles) of 312 data were retained for the final inversions for the MCWD 2019 AEM survey area. This amounts to a data retention of 83.7% for the SkyTEM 312 data set. These high rates are the result of careful flight line planning and design.

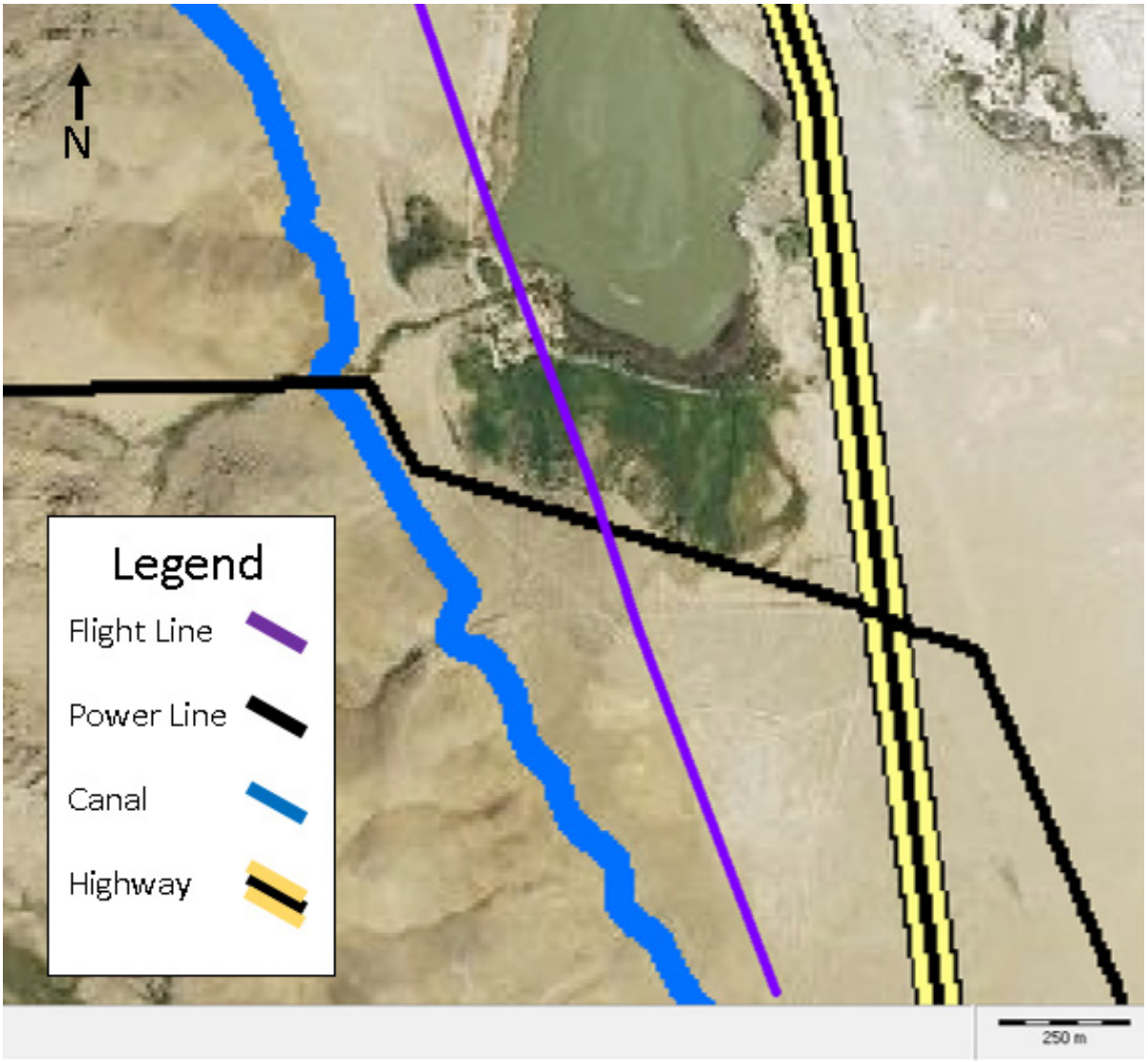

Figure 3-15. Example locations of electromagnetic coupling with pipelines or power lines.

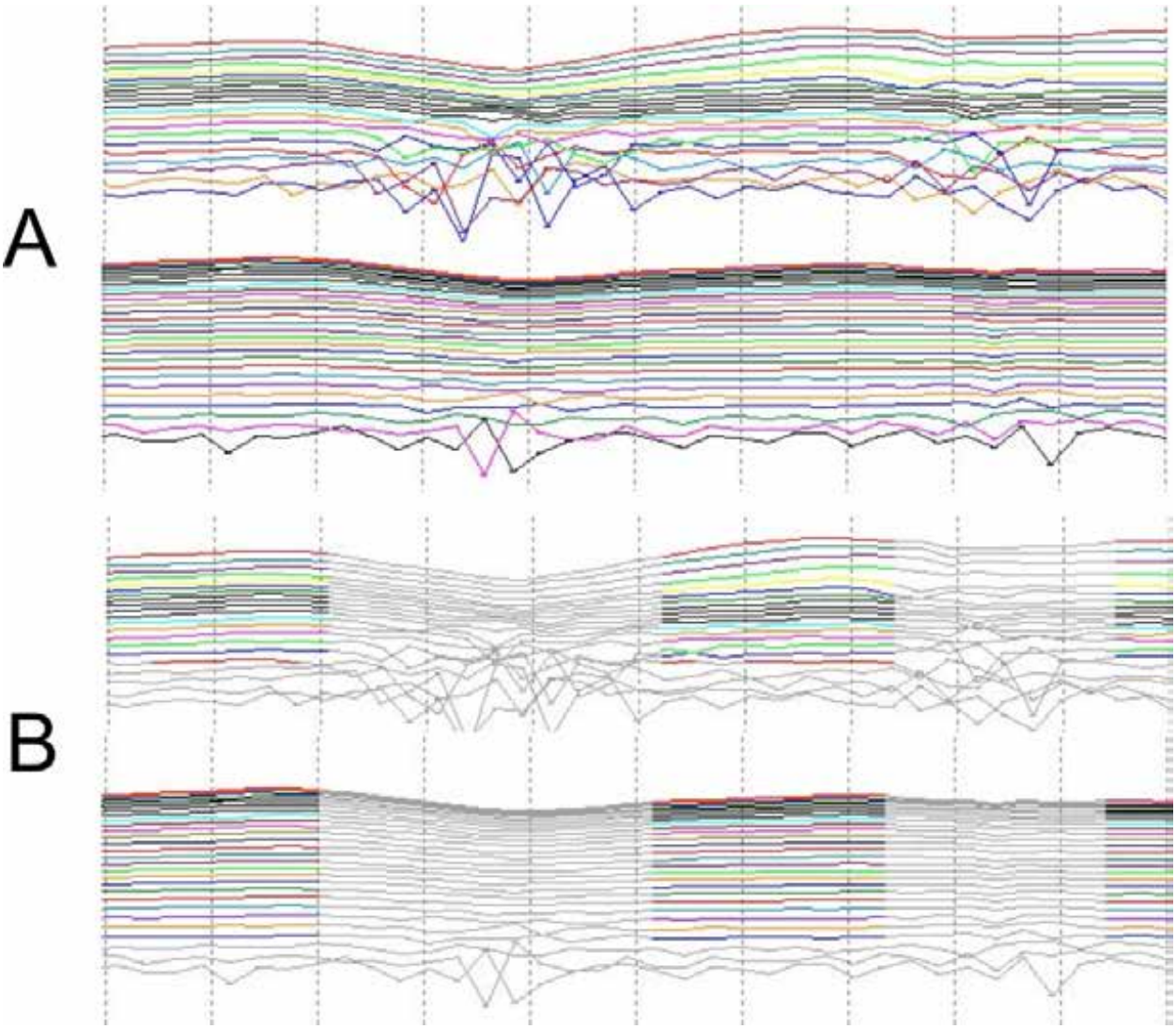

Figure 3-16. A) Example of AEM data affected by electromagnetic coupling in the Aarhus Workbench editor. The top group of lines is the unedited data with the Low Moment on top and the High Moment on the bottom. The bottom group shows the same data after editing.

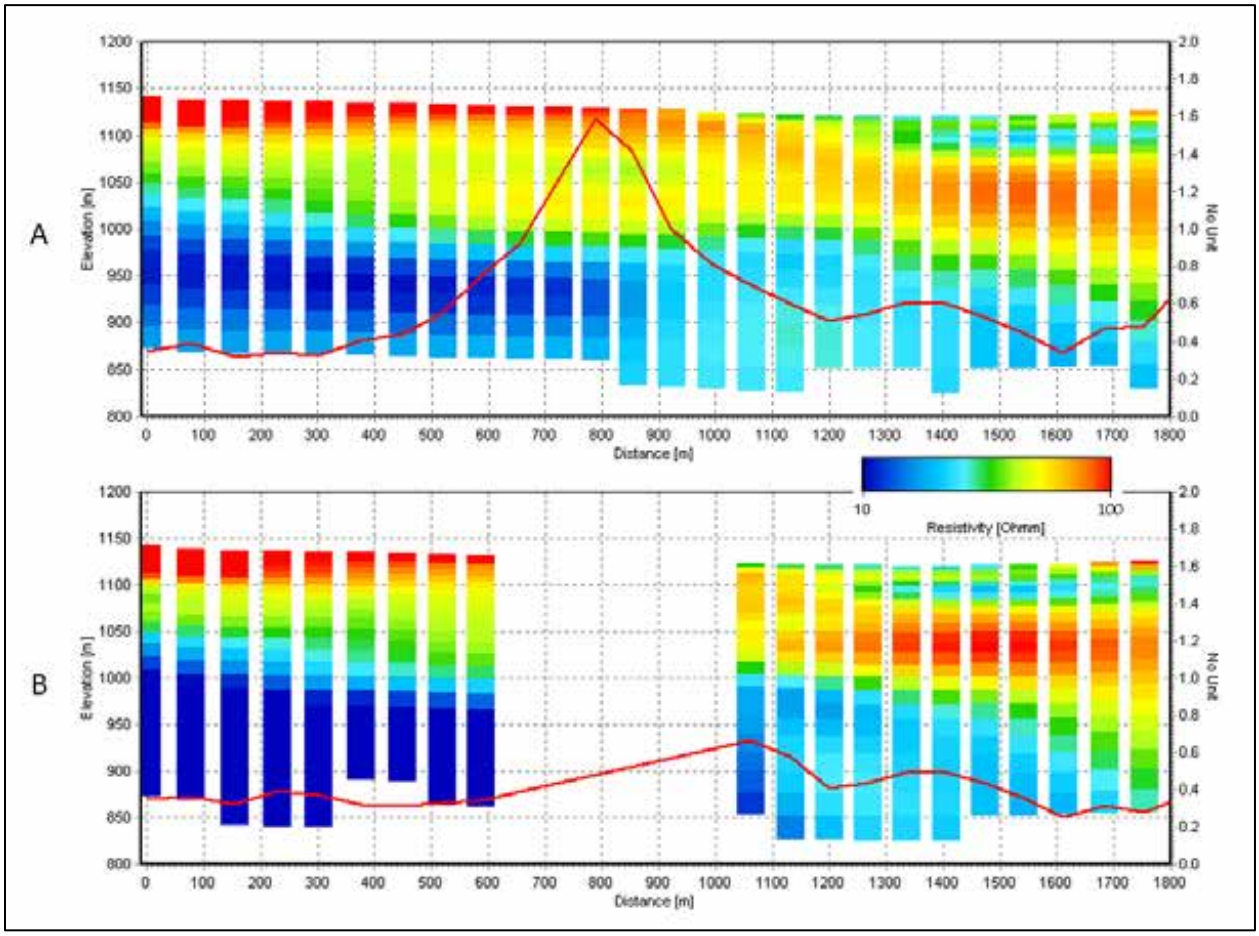

Figure 3-17. A) Example of Laterally-Constrained inversion results where AEM data affected by coupling with pipelines and power lines were not removed. B) Inversion results where AEM data affected by coupling were removed.

3.5 Spatially-Constrained Inversion

Following the initial decoupling and LCI analysis, Spatially-Constrained Inversions (SCI) were performed. SCI's use EM data along, and across, flight lines within user-specified distance criteria (Viezzoli et al., 2008).

The MCWD AEM data were inverted using SCI smooth models with 40 layers, each with a starting resistivity of 10 Ohm-m (equivalent to a 10 ohm-m halfspace). The thicknesses of the inversion models for the 2019 SkyTEM 312 were different from the 2017 SkyTEM 304 because of the different sensing character of the two systems. While the 312 images deeper than the 304 (and needs deeper and thicker layers), the 304M is more sensitive to the near-surface (and so needs finer layering at the surface). Also, the thicknesses of the layers increase with depth as the resolution of the technique decreases (an example of a 30-layer model is presented in Figure 3-18). The thicknesses of the first layer of the 312 models were about 6.6 ft (2 m) (Table 3-5) with the thicknesses of the consecutive layers increasing by a factor of about 1.1. The depth to the bottom of the 39th layer for the 312 were set to 1,639 ft, with maximum thicknesses up to about 130 ft. The spatial reference distance, ***s***, for the constraints were set to 328 ft (100 m) with a power law fall-off of 0.75. The vertical and lateral constraints, ***ResVerSTD*** and ***ResLatStD***, were set to 2.4 and 1.4, respectively, for all layers. The 2017 304 data were inverted with a 30-layer model with the first layer being 9.8 ft (3 m) thick and the bottom layer at a depth of 1023 ft.

In addition to the recovered resistivity models, the SCI's also produce data-model residual error values (single sounding error residuals) and Depth of Investigation (DOI) estimates. The data residuals compare the measured data with the response of the individual inverted models (Christensen et al., 2009). The DOI provides a general estimate of the depth to which the AEM data are sensitive to changes in the resistivity distribution at depth (Christiansen and Auken, 2012). Two DOI's are calculated: an "Upper" DOI at a cumulative sensitivity of 1.2 and a "Lower" DOI set at a cumulative sensitivity of 0.6. Examination of the SCI results will indicate that a much lower cumulative sensitivity, maybe 0.1 to 0.2, would still be sufficient to delineate the MCWD 2019 AEM DOI in various locations throughout the survey area. A more detailed discussion on the DOI can be found in Asch et al. (2015).

Figure 3-19 presents a histogram of the MCWD 2019 SkyTEM 312 SCI inversion data/model residuals. A map of data to model error residuals for the MCWD 2019 AEM study area is presented for the SkyTEM 312 inversion results in Figure 3-20.

Table 3-5: Thickness and depth to bottom for each layer in the 40-layer Spatially Constrained Inversion (SCI) AEM earth models for the MCWD 2019 SkyTEM 312 data. The thickness of the model layers increase with depth as the resolution of the AEM technique decreases.

Layer	Depth to Bottom (ft)	Thickness (ft)	Depth to Bottom (m)	Thickness (m)	Layer	Depth to Bottom (ft)	Thickness (ft)	Depth to Bottom (m)	Thickness (m)
1	6.6	6.6	2.0	2.0	21	337.6	31.5	102.90	9.6
2	13.8	7.2	4.2	2.2	22	371.7	34.1	113.30	10.4
3	21.3	7.5	6.5	2.3	23	408.8	37.1	124.60	11.3
4	29.5	8.2	9.0	2.5	24	448.8	40.0	136.80	12.2
5	38.4	8.9	11.7	2.7	25	492.2	43.3	150.00	13.2
6	48.2	9.8	14.7	3.0	26	539.1	46.9	164.30	14.3
7	58.7	10.5	17.9	3.2	27	589.6	50.5	179.70	15.4
8	70.2	11.5	21.4	3.5	28	644.4	54.8	196.40	16.7
9	82.7	12.5	25.2	3.8	29	703.8	59.4	214.50	18.1
10	96.1	13.5	29.3	4.1	30	767.8	64.0	234.00	19.5
11	110.6	14.4	33.7	4.4	31	837.0	69.2	255.10	21.1
12	126.0	15.4	38.4	4.7	32	912.1	75.1	278.00	22.9
13	142.7	16.7	43.5	5.1	33	993.2	81.0	302.70	24.7
14	161.1	18.4	49.1	5.6	34	1081.1	87.9	329.50	26.8
15	180.8	19.7	55.1	6.0	35	1175.9	94.8	358.40	28.9
16	202.1	21.3	61.6	6.5	36	1278.6	102.7	389.70	31.3
17	225.1	23.0	68.6	7.0	37	1389.8	111.2	423.60	33.9
18	250.0	24.9	76.2	7.6	38	1509.9	120.1	460.20	36.6
19	276.9	26.9	84.4	8.2	39	1639.8	129.9	499.80	39.6
20	306.1	29.2	93.3	8.9					

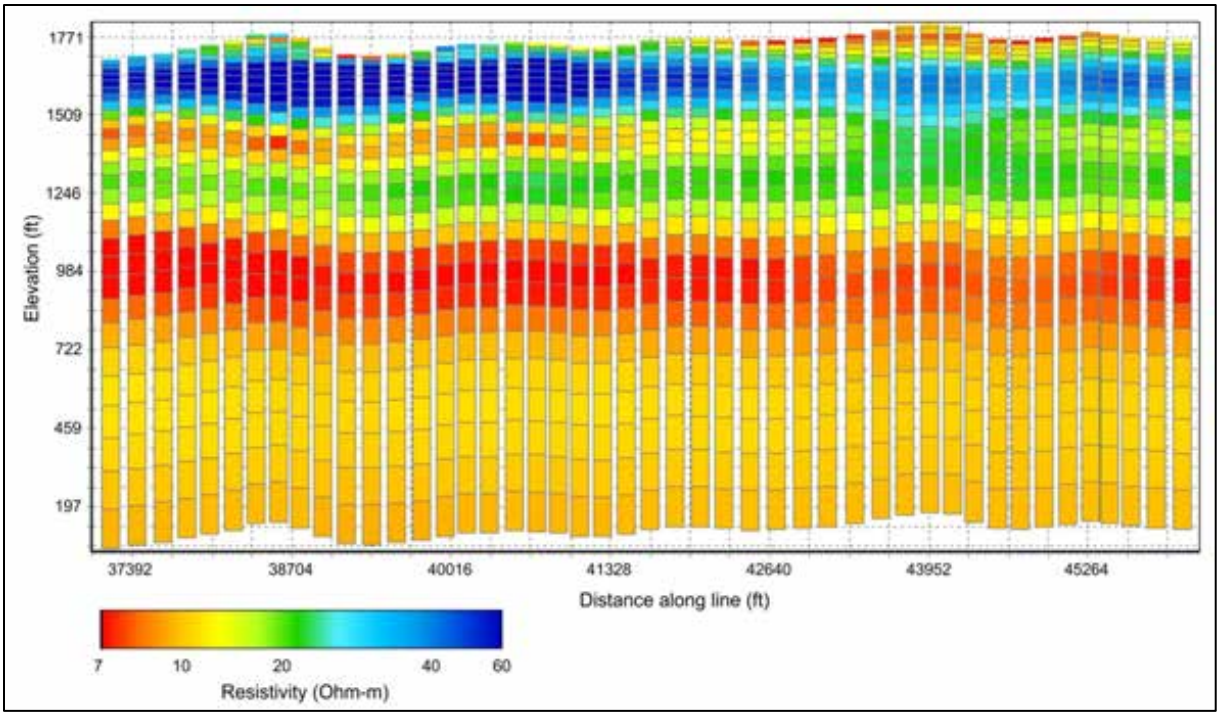

Figure 3-18. An example of an AEM profile illustrating increasing model layer thicknesses with depth. This is a 30-layer model.

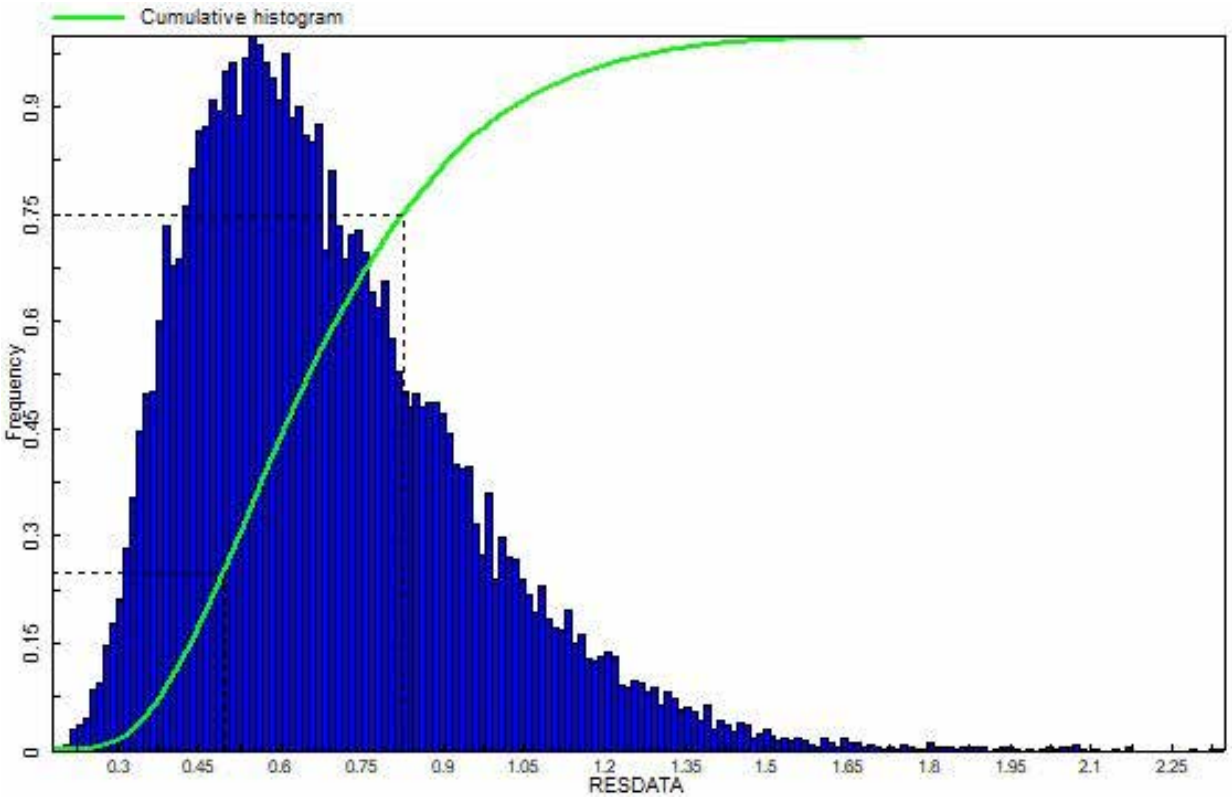

Figure 3-19. Data/model residual histogram for the 2019 MCWD SkyTEM312 SCI inversion results.

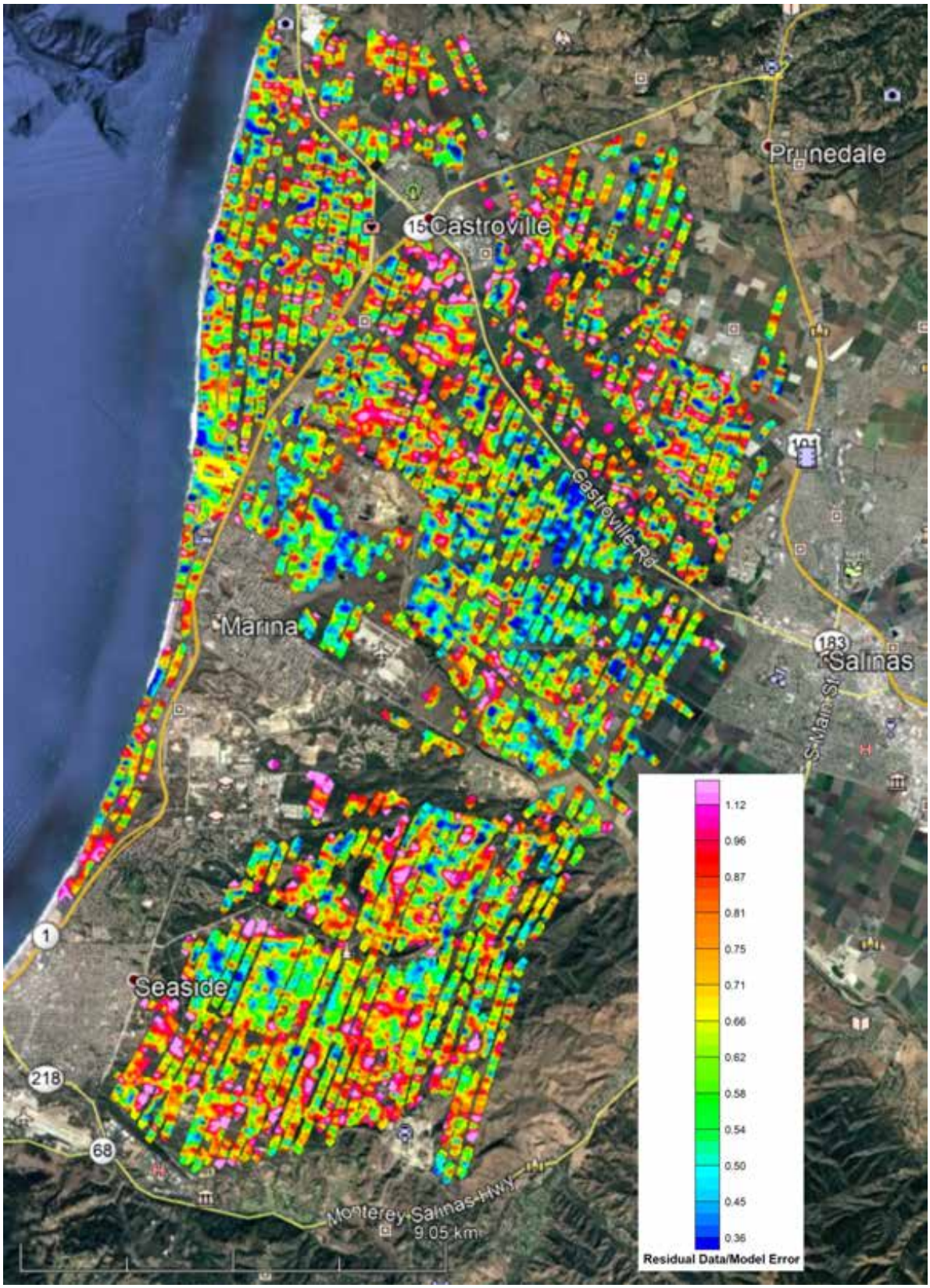

Figure 3-20. Map of data-inversion model residuals for the 2019 MCWD SkyTEM 312 SCI inversion results.

3.6 Merge AEM Flight Lines and Databases from Different Flights

After the inversion process several short lines and databases from different flights were combined to form continuous lines within the survey area. These continuous lines allow for improved viewing and interpretation of the AEM inversions results. Table 3-6 lists the original flown lines and the new combined lines for the MCWD 2019 SkyTEM 312 survey. A map of the merged flight lines is presented in Figure 3-21.

Table 3-6. Combination of SkyTEM 312 flight lines within the MCWD 2019 AEM survey area.

	Original Lines	New Line		Original Lines	New Line
1	200701, 200801	200700	25	207101, 207301	207100
2	200901, 201001	200900	26	207601, 207701, 207702	207600
3	201101, 201201, 201301	201100	27	207901, 208001, 208002	207900
4	201401, 201501, 201601	201400	28	208201, 208202, 208301, 208401	208200
5	201701, 201801, 201901	201700	29	208501, 208502	208500
6	202001, 202101	202000	30	208601, 208701, 208702, 208703	208600
7	202201, 202301, 202401	202200	31	208801, 208901, 208902, 208903	208800
8	202501, 202601, 202701	202500	32	209001, 209101, 209201	209000
9	202801, 202901	202800	33	209201, 209301	209200
10	203001, 203101	203000	34	209401, 209501, 209601	209400
11	203201, 203301	203200	35	209701, 209801, 209802, 209901	209700
12	203401, 203501, 203601	203400	36	210001, 210101, 210201	210000
13	203701, 203801, 203901	203700	37	210501, 210301, 210302,210401	210300
14	204001, 204101, 204201	204000	38	210601, 210602, 210701	210600
15	204301, 204401, 204501	204300	39	210801, 210901, 210902, 211201	210800
16	204701, 204801	204700	40	211001, 211101, 211102	211000
17	205001, 205101	205000	41	211301, 211401, 211501	211300
18	205201, 205301	205200	42	211601, 211701, 211702	211600
19	205501, 205601	205500	43	211801, 211901, 211902	211800
20	205701, 205702, 205801, 205901	205700	44	212001, 300701	212000
21	100603, 206001, 206101	206000	45	212201, 212202, 300801	212200
22	206201, 206301	206200	46	212301, 300901	212300
23	206501, 206601	206500	47	100601, 100602	100600
24	206801, 206901	206800	48	300301, 300302	300300

Figure 3-21. Labeled MCWD 2019 AEM flight line map of merged flight lines.

4 AEM Results and Interpretation

This section provides the details on the process involved in the interpretation of the MCWD 2019 AEM data and inversion results and comparison with the 2017 MCWD AEM investigation.

4.1 Begin Interpretive Process – Develop the Project Digital Elevation Model

To ensure that the elevation used in the project is constant for all the data sources (i.e. AEM and boreholes) a Digital Elevation Model (DEM) was constructed for the MCWD 2019 AEM survey area. The data was downloaded from the U.S. Geological Survey National Elevation Dataset (NED) located on the National Map Website (USGS, 2019) at a spatial resolution of approximately 30 meters. The geographic coordinates are North American Datum of 1983 (NAD 83) and the elevation values are referenced to the North American Vertical Datum of 1988 (NAVD 88) meters. Figure 4-1 is a map of the DEM for the MCWD 2019 AEM survey area having a vertical relief within the flight line coverage of 427 m with a minimum elevation of -0.1 m and a maximum elevation of 281 m. This DEM was used to reference all elevations within the AEM and borehole datasets.

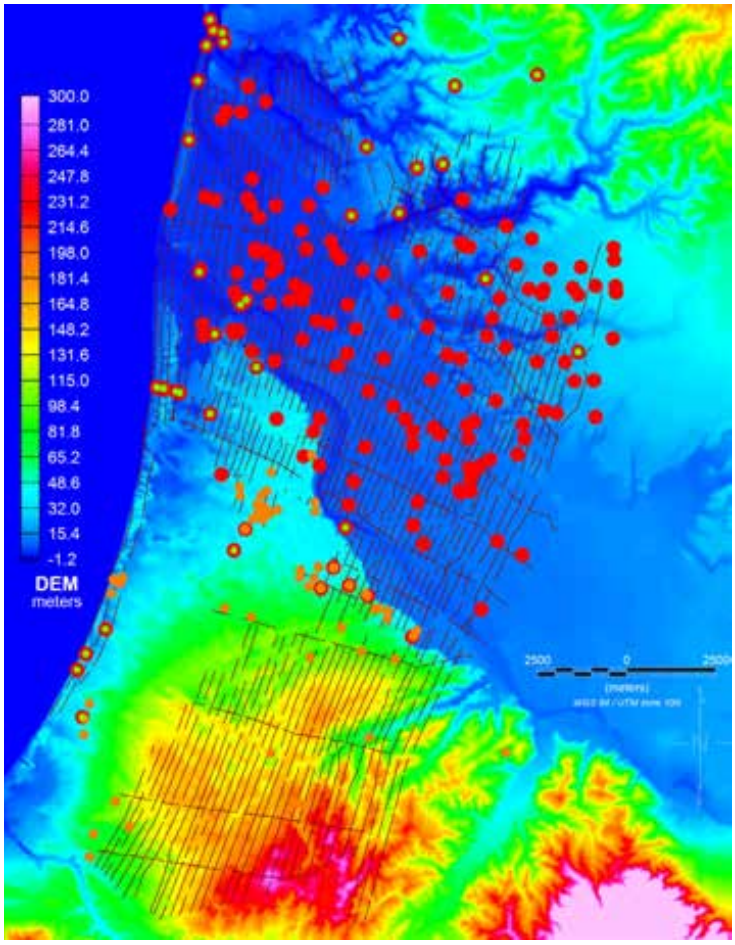

Figure 4-1. Map of the Digital Elevation Model for the MCWD 2019 AEM survey area with boreholes. Data source is the one (1) arc-second National Elevation Dataset (USGS, 2019). Projection is NAD 83, meters, and the elevation values are referenced to NAVD 88, meters.

4.2 Comparison of 2019 Inverted AEM Data with Geophysical Logs

The first step in the analysis was to check how the 2019 AEM compared to the 2017 AEM at the locations of the MPWSP borehole logs. Borehole MW-1 is presented in Figure 4-2, MW-4 in Figure 4-3, MW-5 in Figure 4-4, MW-6 in Figure 4-5, MW-7 in Figure 4-6, MW-8 in Figure 4-7, and MW-9 in Figure 4-8.

Then, after final combination of the AEM data, characterization of the subsurface was performed in cross-section format using Datamine Discover Profile Analyst (DatamineDiscover, 2019). Several examples of the AEM inverted resistivity results are presented below, working from the Monterey Bay inland, along with 16-inch Short Normal (SN) geophysical logs that are within 250 meters of the flight lines. The geophysical logs (the locations indicated by the green dots on the flight maps on each figure) are very useful in validating the AEM survey results.

The first example of the AEM resistivity inversion results for the MCWD 2019 AEM survey is presented in Figure 4-9. This is AEM flight line L200101, a 19 km long profile located along the beach on the Monterey Bay (the red line in the flight map at the top part of the figure). The profile shows an electrically very conductive zone, on the order of 1-2 ohm-m, overlying more resistive material (around 10-15 ohm-m). There are several SN logs along this line that show a good match with the AEM results. The SN logs on the southern end of the profile (left side in the box) show that the AEM inversion results match the delineation between the very conductive material and the more resistive material.

Similar comparison are made along flight lines L200200 (Figure 4-10), L200400 (Figure 4-11), and L201700 (Figure 4-12). The inversion results along L201700, which is located away from the coast, also illustrate the sensitivity of the AEM to the near-surface geology with the delineation of the thin resistive zone (green) above the more conductive (red) zone. Flight line L202500 (Figure 4-13), still further inland from the coast than the flight lines in the previous figures, also shows delineation of both thin resistive and conductive zones.

Flight lines L206800 (Figure 4-14) and L212200 (Figure 4-15) present flight lines, with boreholes for comparison, that extend south of the Salinas River onto Fort Ord. The borehole on the north end of L206800 (Figure 4-14) shows a good match with the resistive material near the surface and conductive material at depth (about 200m-250m, 650 ft – 820 ft). On the southern ends of these two profiles (in the red boxes), in the hills of Fort Ord, present thick beds of both resistive (blue) and conductive (red) material indicating likely zones of fresher water and intruded saline water at depth. All the 2D resistivity profiles of the 2019 MCWD AEM survey are presented in Appendix 1-2D Profiles.

3D fence diagrams of the 2019 inverted AEM survey data are presented in Figure 4-16 (looking east), Figure 4-17 (looking northeast), Figure 4-18 (looking north), and Figure 4-19 (looking west). In the blue boxes in these figures is an area showing likely fresher water (blue colored) overlying much more saline water (red color). The red boxes in these figures show the area of the survey conducted over Fort Ord that delineate the thick interbeds of resistive fresh water overlying the more conductive zones of saline water at depth. Additional 3D fence diagrams can be found in Appendix 2.

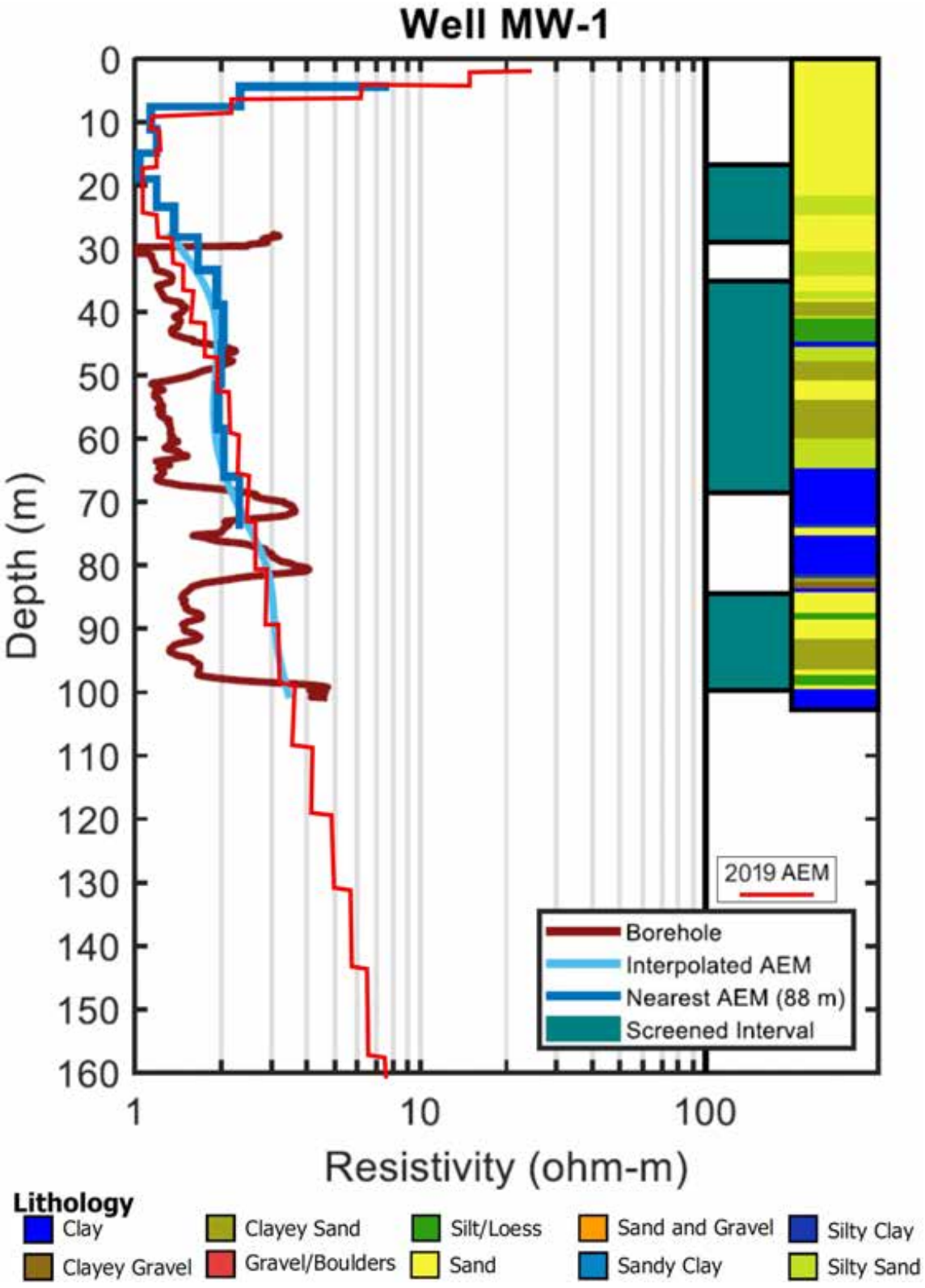

Figure 4-2. Comparison at MW-1 between lithologic and geophysical resistivity data including 2017 (blue lines) and 2019 AEM inversion results (red line) closest to the borehole and the MW-1 geophysical log (modified from Figure 4 from Gottschalk et al., 2018).

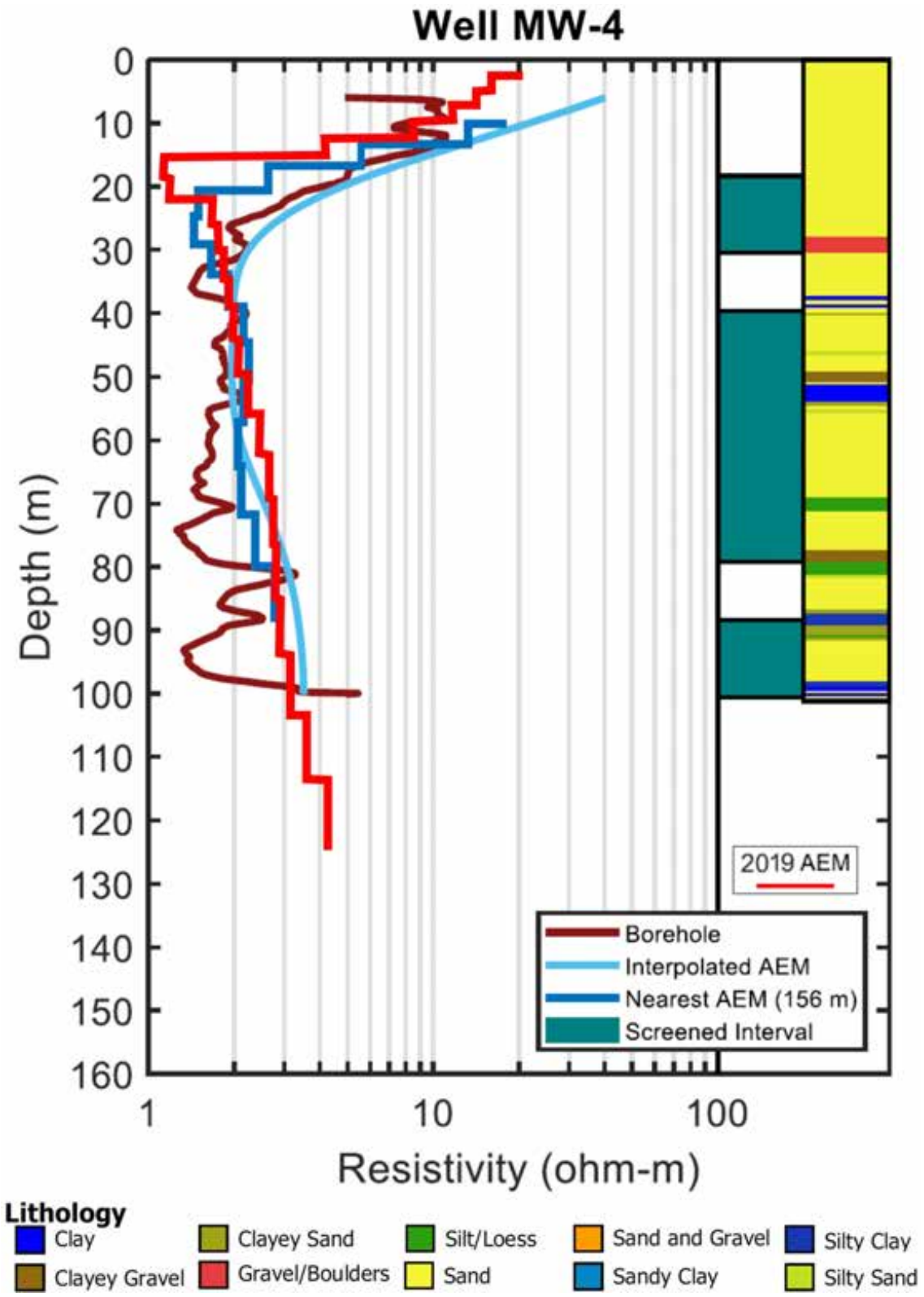

Figure 4-3. Comparison at MW-4 between lithologic and geophysical resistivity data including 2017 (blue lines) and 2019 AEM inversion results (red line) closest to the borehole and the MW-4 geophysical log (modified from Figure 5 from Gottschalk et al., 2018).

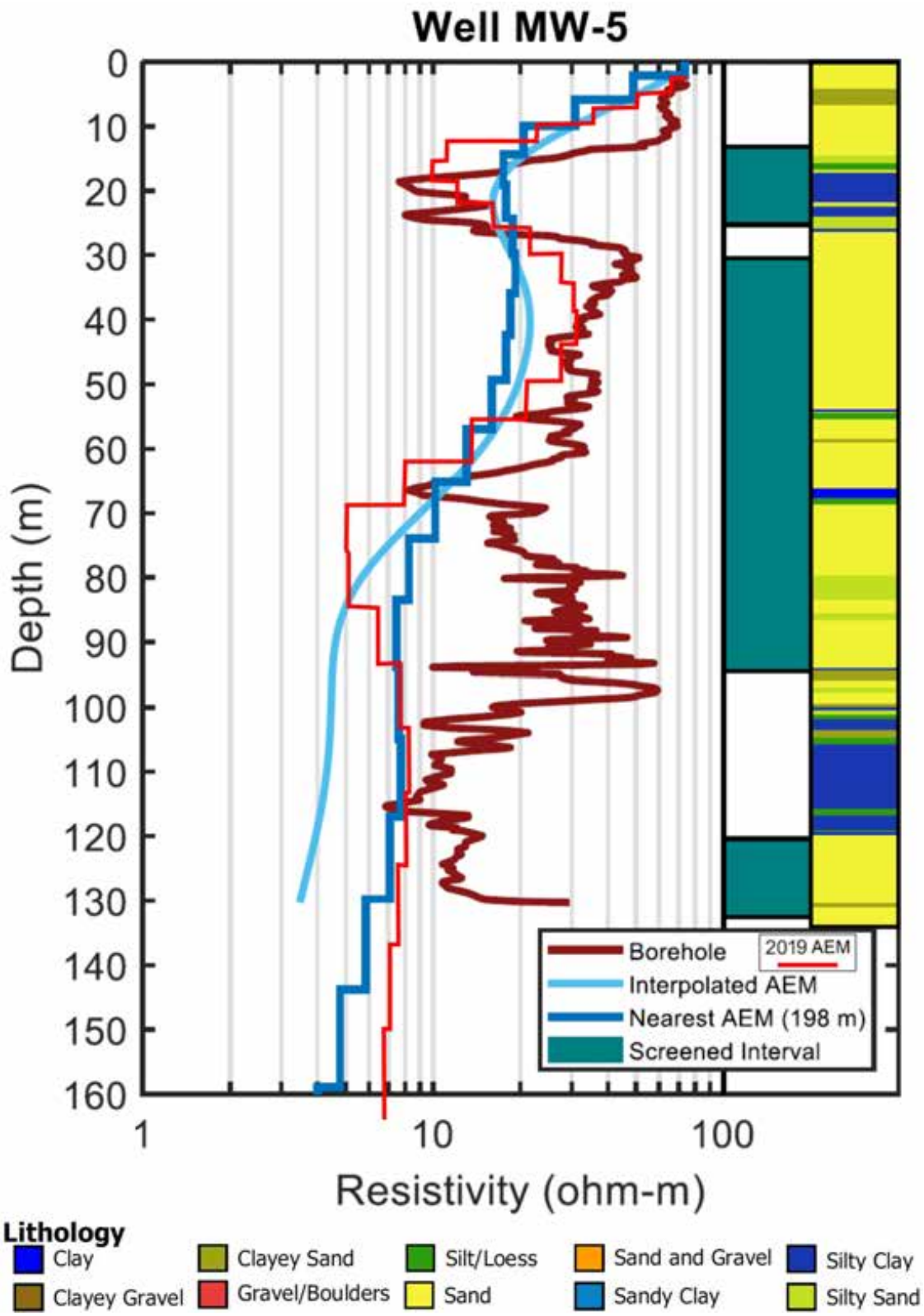

Figure 4-4. Comparison at MW-5 between lithologic and geophysical resistivity data including 2017 (blue lines) and 2019 AEM inversion results (red line) closest to the borehole and the MW-5 geophysical log (modified from Figure 6 from Gottschalk et al., 2018).

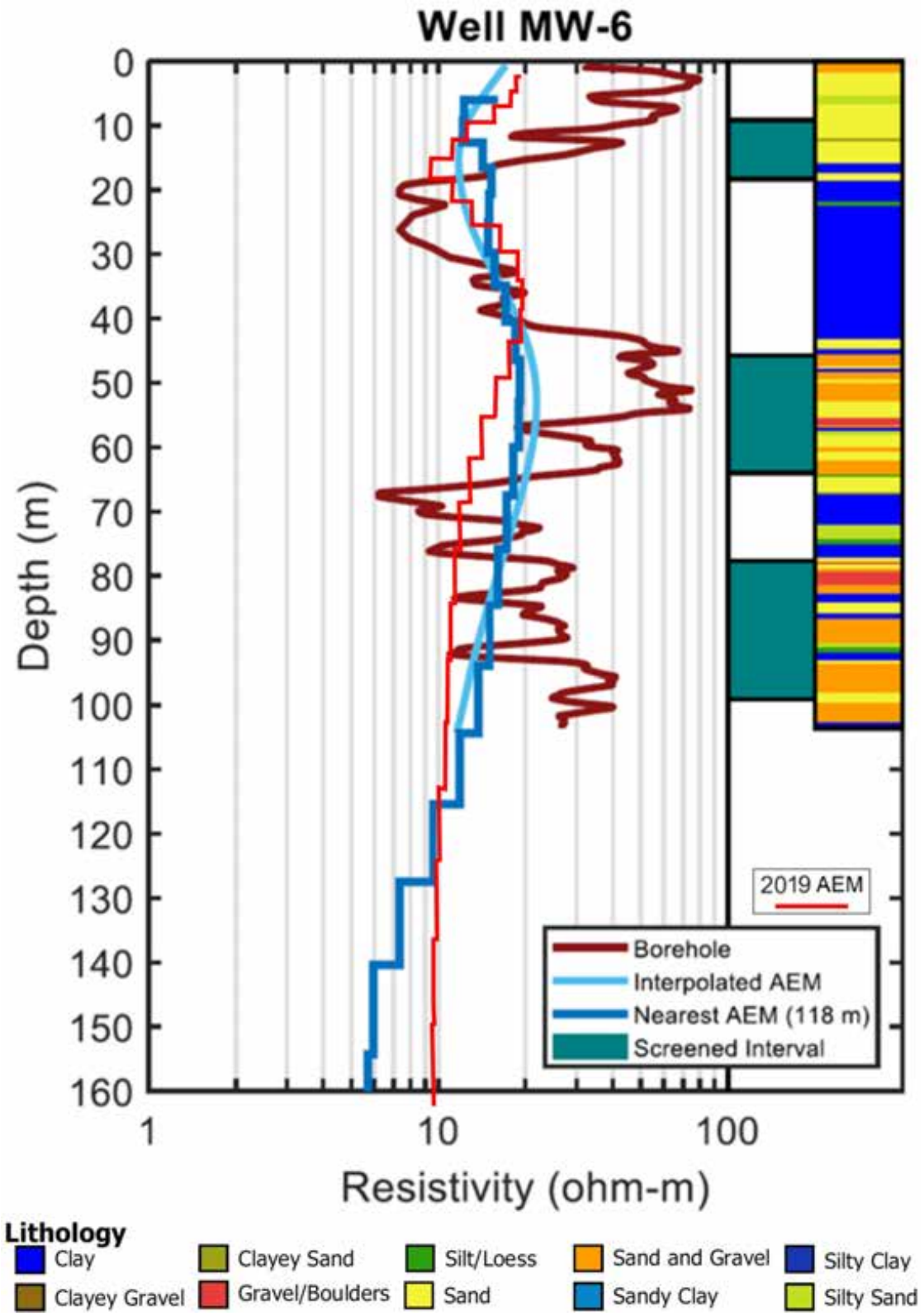

Figure 4-5. Comparison at MW-6 between lithologic and geophysical resistivity data including 2017 (blue lines) and 2019 AEM inversion results (red line) closest to the borehole and the MW-6 geophysical log (modified from Figure 7 from Gottschalk et al., 2018).

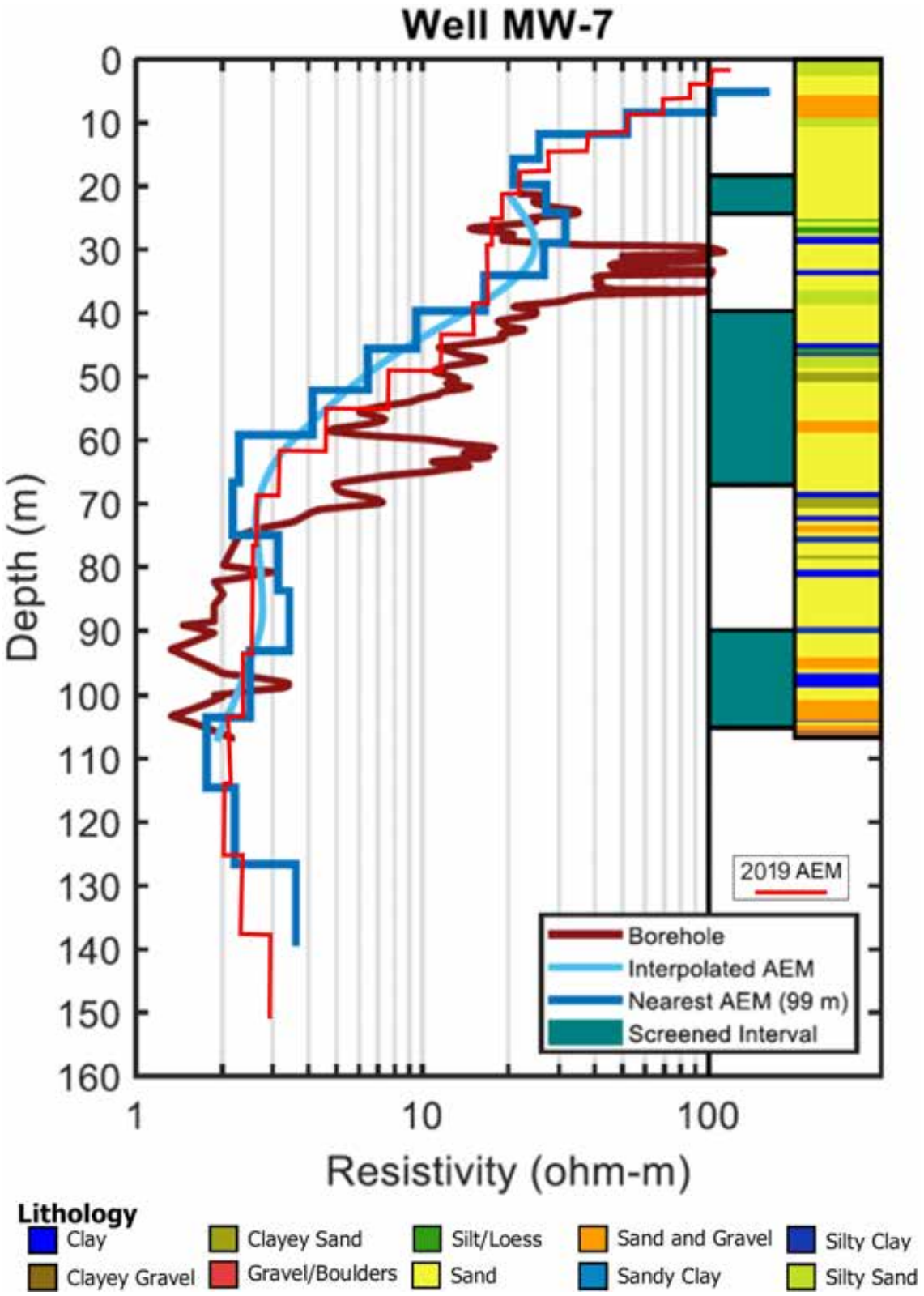

Figure 4-6. Comparison at MW-7 between lithologic and geophysical resistivity data including 2017 and 2019 AEM inversion results closest to the borehole and the MW-7 geophysical log (modified from Figure 8 from Gottschalk et al., 2018).

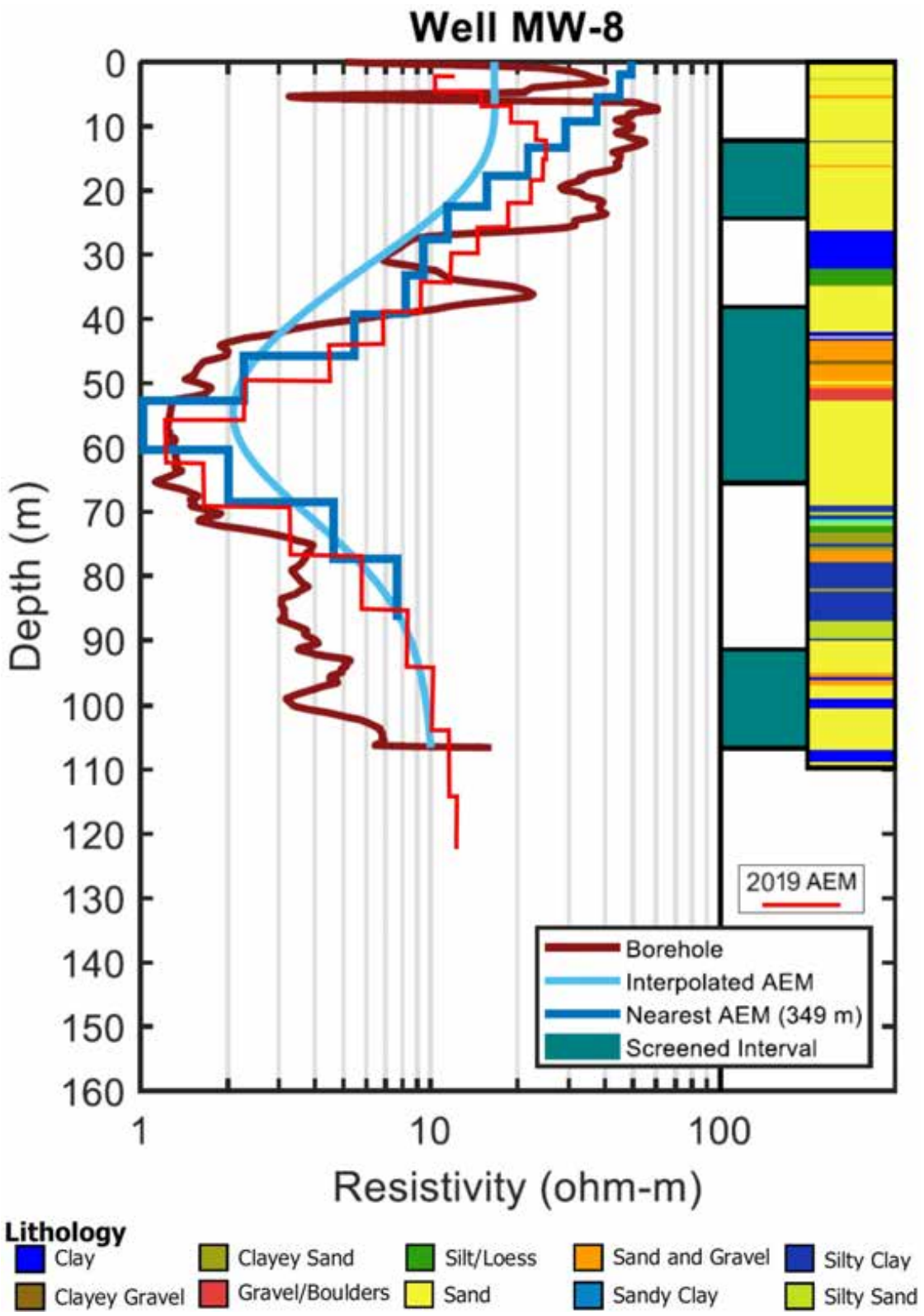

Figure 4-7. Comparison at MW-8 between lithologic and geophysical resistivity data including 2017 (blue lines) and 2019 AEM inversion results (red line) closest to the borehole and the MW-8 geophysical log (modified from Figure 9 from Gottschalk et al., 2018).

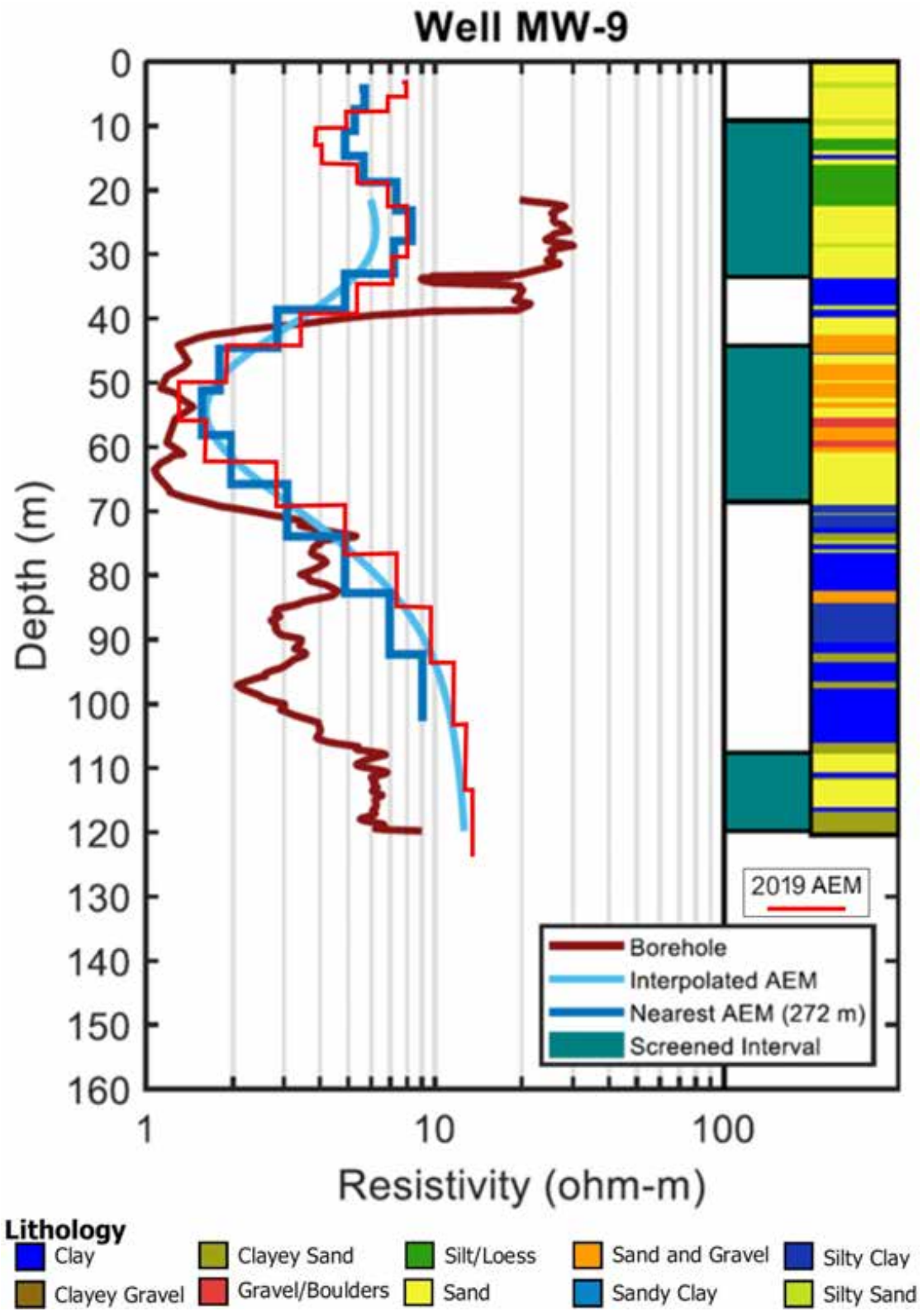

Figure 4-8. Comparison at MW-9 between lithologic and geophysical resistivity data including 2017 (blue lines) and 2019 AEM inversion results (red line) closest to the borehole and the MW-9 geophysical log (modified from Figure 10 from Gottschalk et al., 2018).

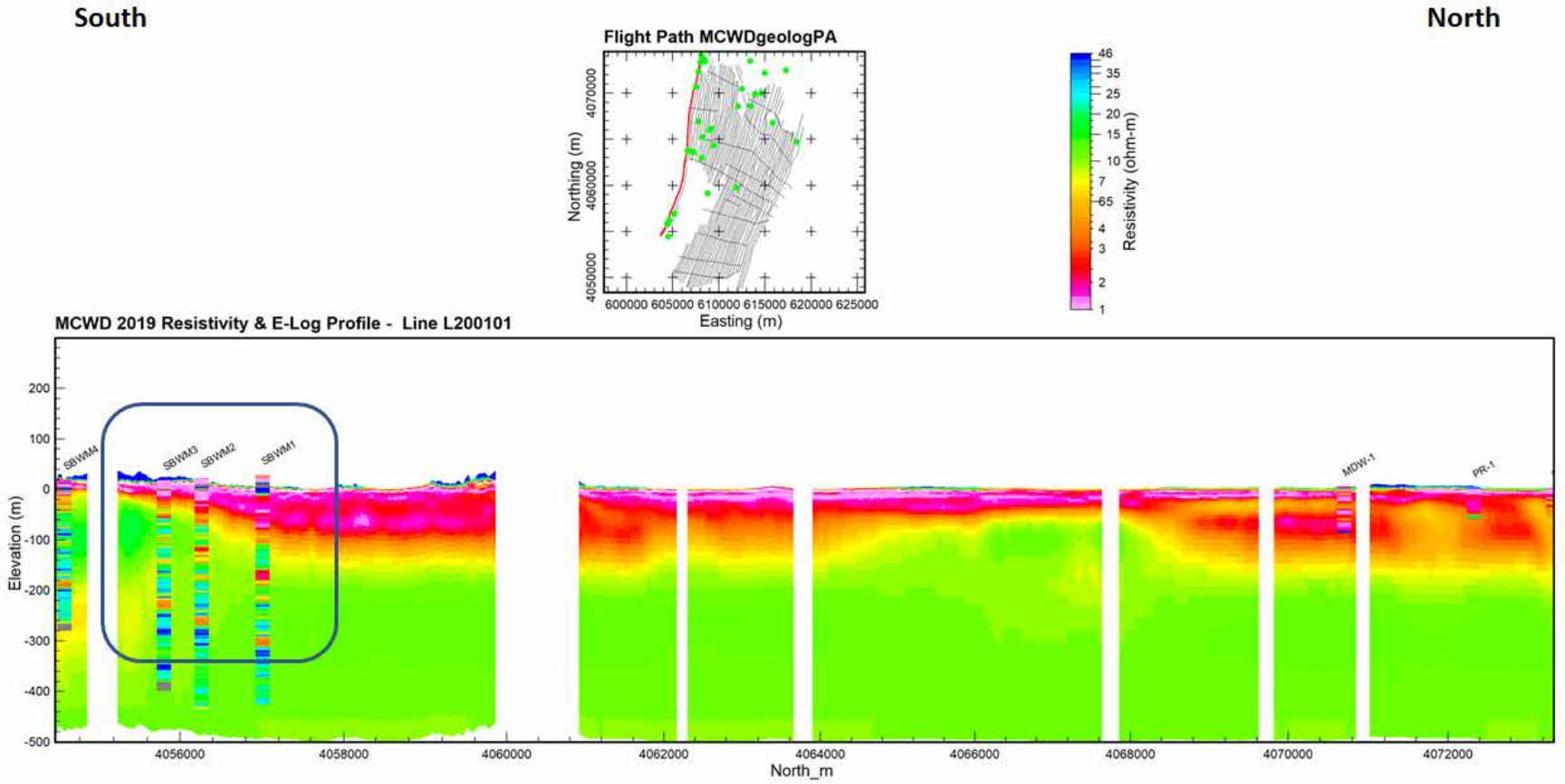

Figure 4-9. Inverted AEM resistivity profile of MCWD 2019 AEM survey line L200101, a north-south flight line near the beach approximately 19 km long, with geophysical 16-inch Short Normal electrical logs (green dots on map) for comparison at the same scale. The projection is NAD83, UTM 10N, meters and elevation values are referenced to NAVD88, meters.

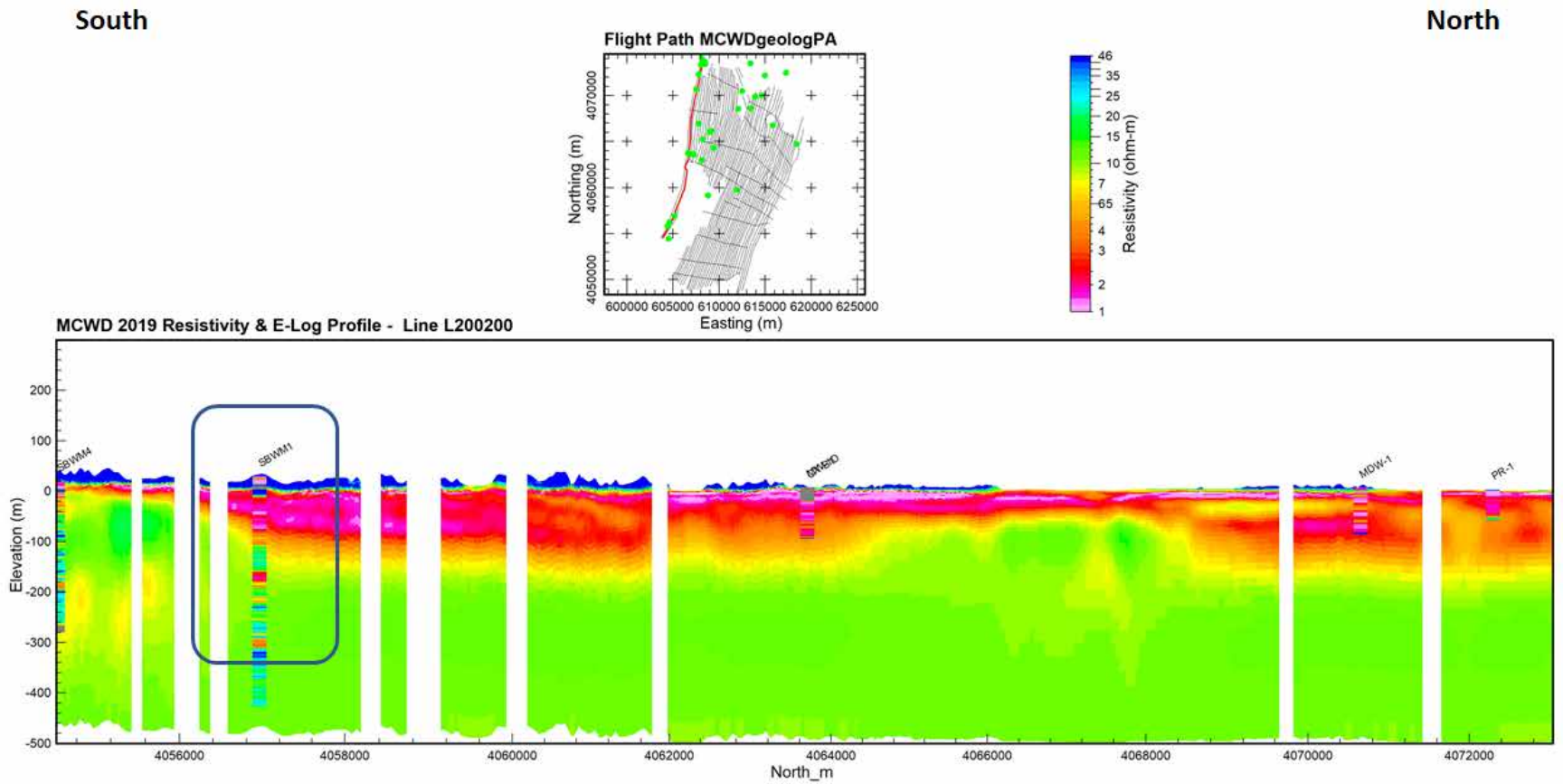

Figure 4-10. Inverted AEM resistivity profile of MCWD 2019 AEM survey line L200200, a north-south flight line near the beach approximately 19 km long, with geophysical 16-inch Short Normal electrical logs (green dots on map) for comparison at the same scale. The projection is NAD83, UTM 10N, meters and elevation values are referenced to NAVD88, meters.

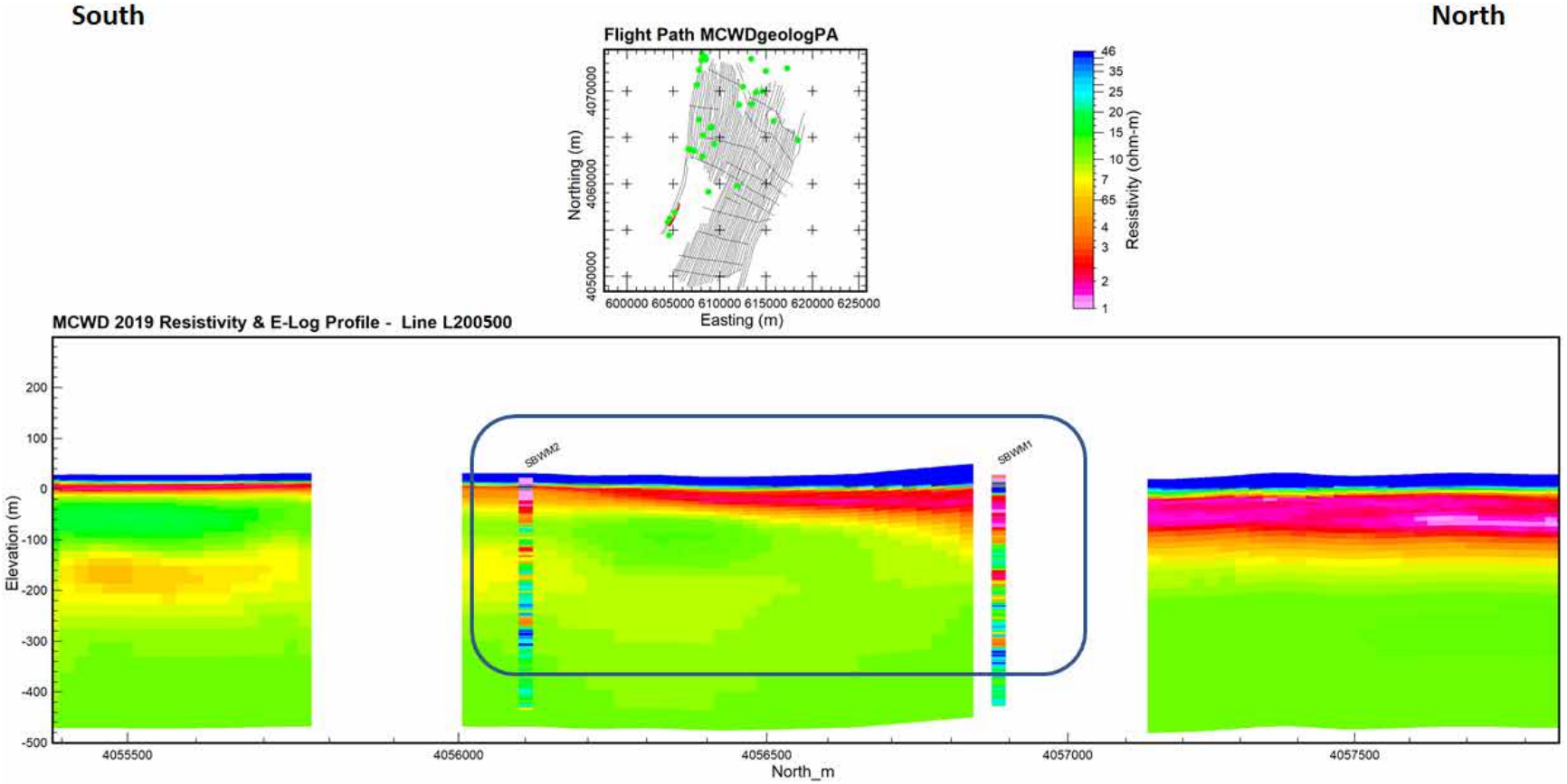

Figure 4-11. Inverted AEM resistivity profile of MCWD 2019 AEM survey line L200500, a north-south flight line near the beach at the southern end of the survey area approximately 2.5 km long, with geophysical 16-inch Short Normal electrical logs (green dots on map) for comparison at the same scale. The projection is NAD83, UTM 10N, meters and elevation values are referenced to NAVD88, meters.

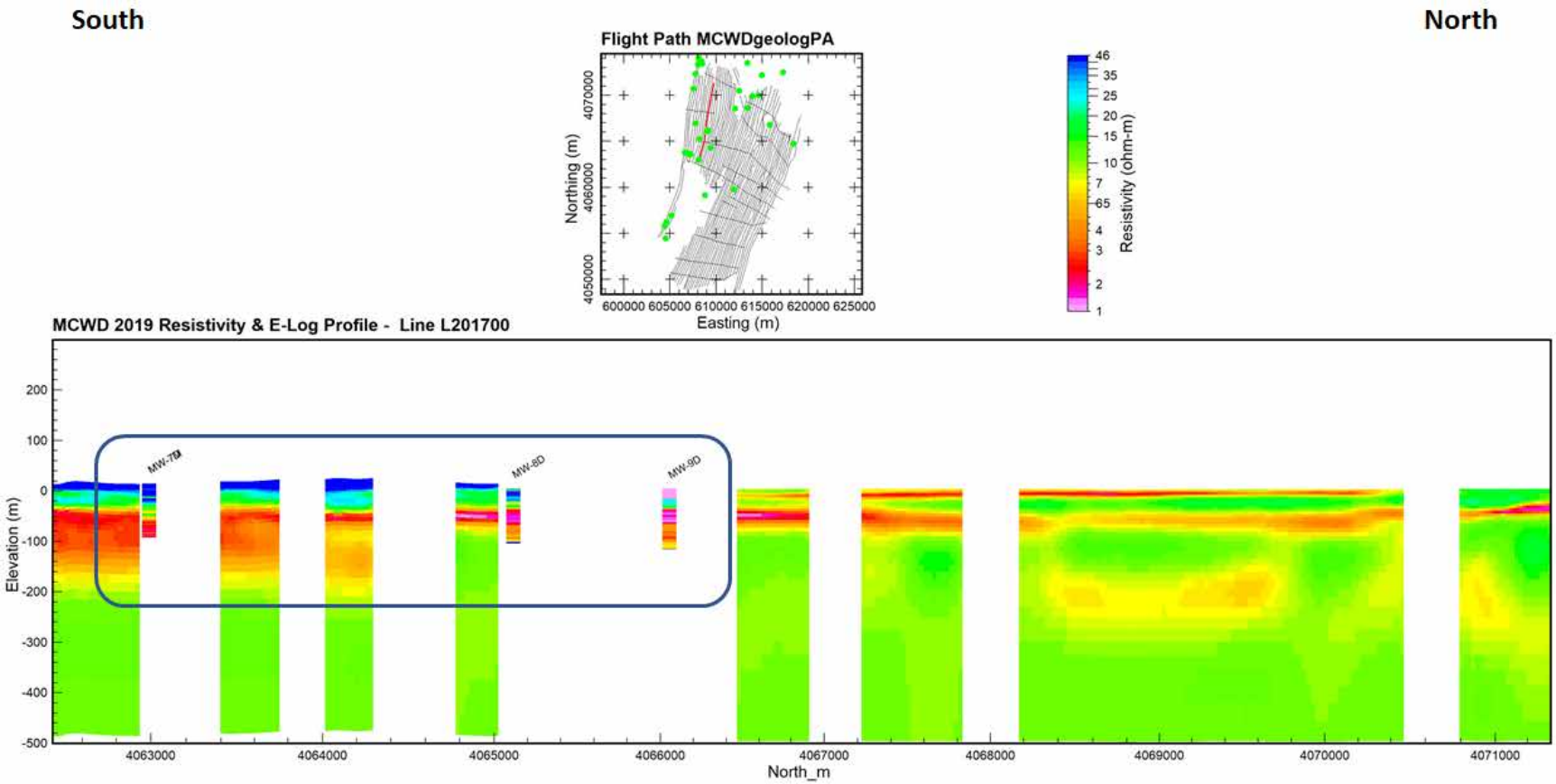

Figure 4-12. Inverted AEM resistivity profile of MCWD 2019 AEM survey line L201700, a north-south flight line inland from the coast approximately 9 km long, with geophysical 16-inch Short Normal electrical logs (green dots on map) for comparison at the same scale. The projection is NAD83, UTM 10N, meters and elevation values are referenced to NAVD88, meters.

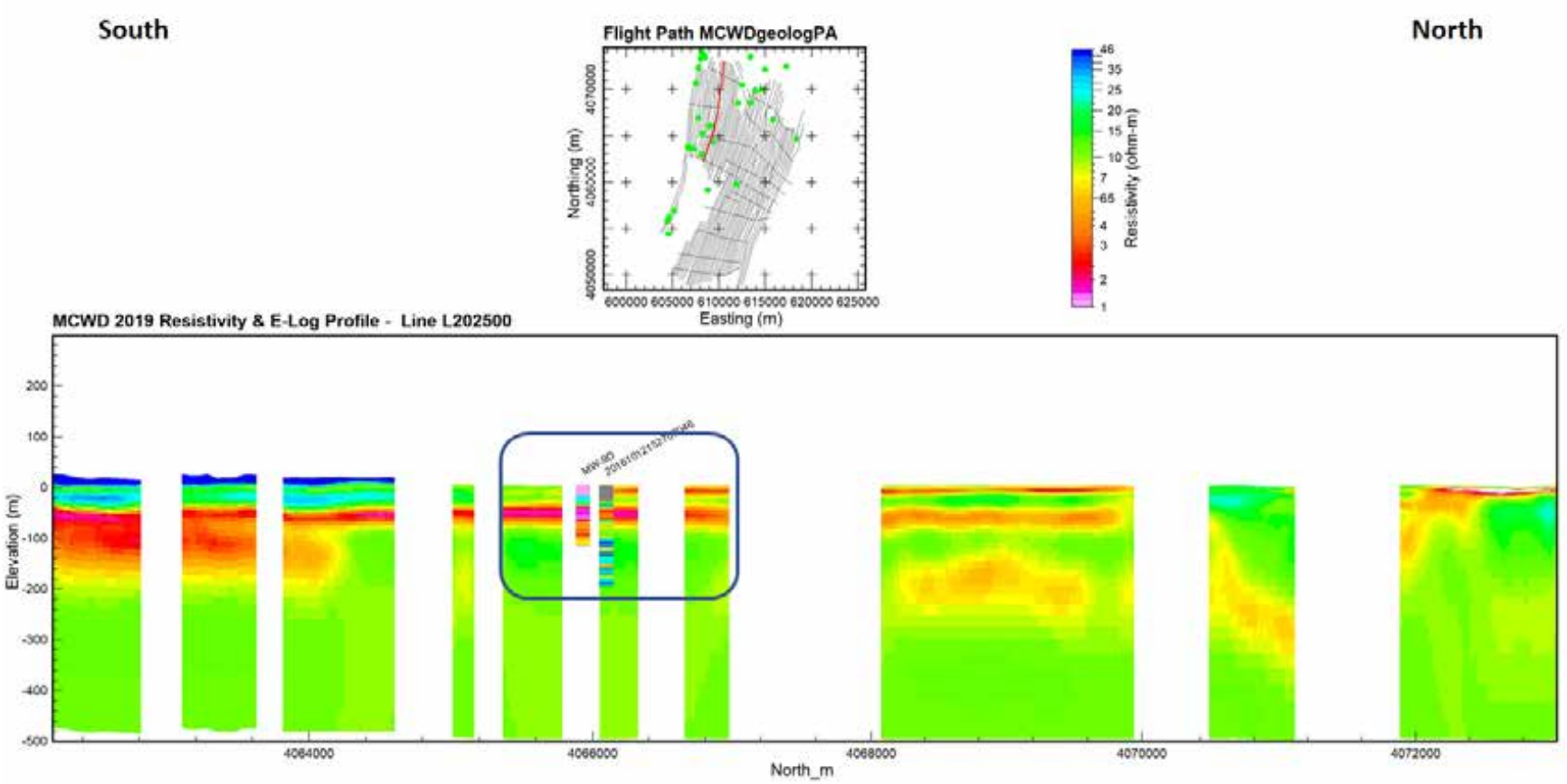

Figure 4-13. Inverted AEM resistivity profile of MCWD 2019 AEM survey line L202500, a north-south flight line further inland approximately 10 km long, with geophysical 16-inch Short Normal electrical logs (green dots on map) for comparison at the same scale. The projection is NAD83, UTM 10N, meters and elevation values are referenced to NAVD88, meters.

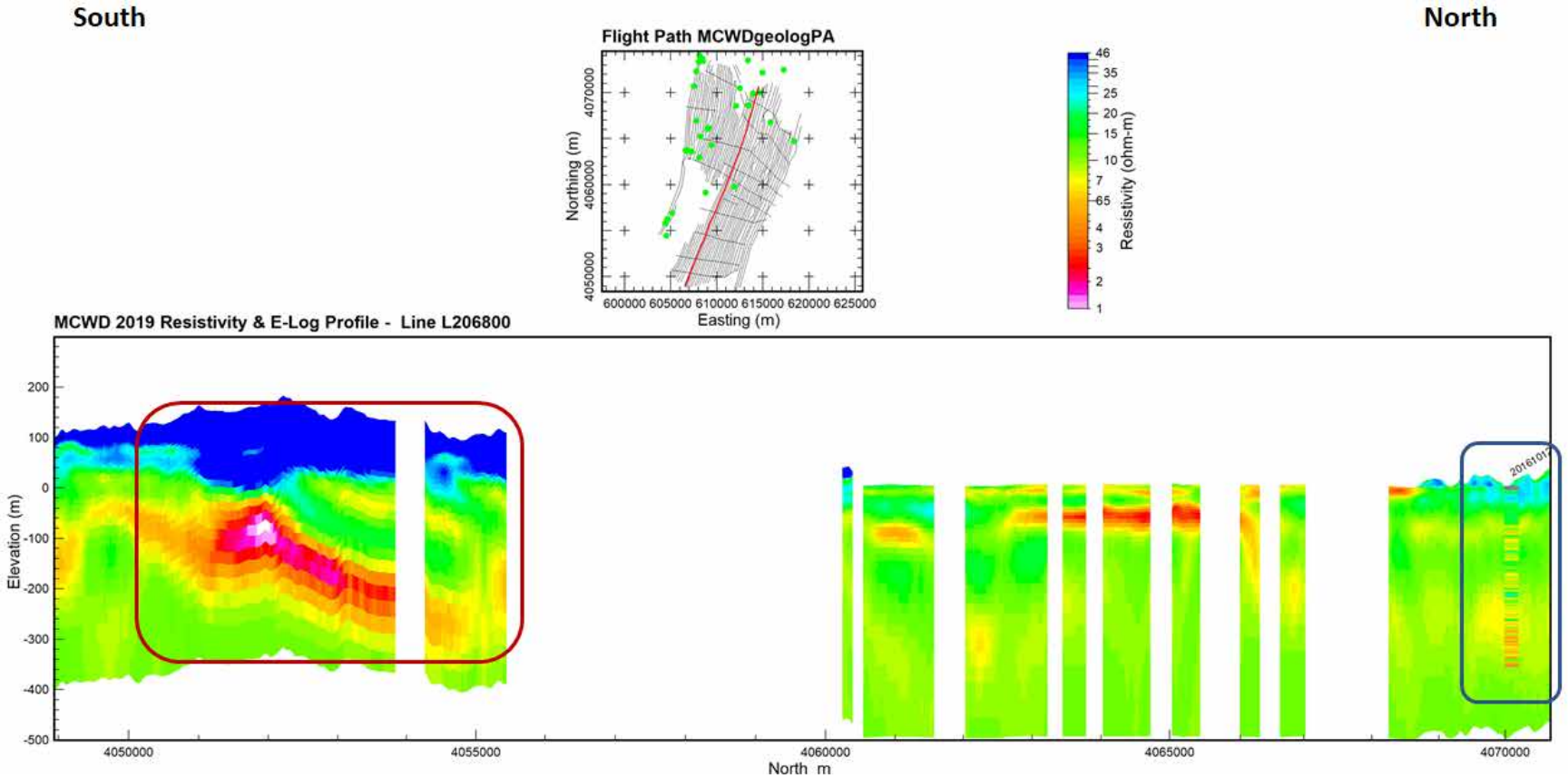

Figure 4-14. Inverted AEM resistivity profile of MCWD 2019 AEM survey line L206800, a north-south flight line, approximately 22 km long, further inland that extended the survey south onto Fort Ord, with geophysical 16-inch Short Normal electrical logs (green dots on map) for comparison at the same scale. The projection is NAD83, UTM 10N, meters and elevation values are referenced to NAVD88, meters.

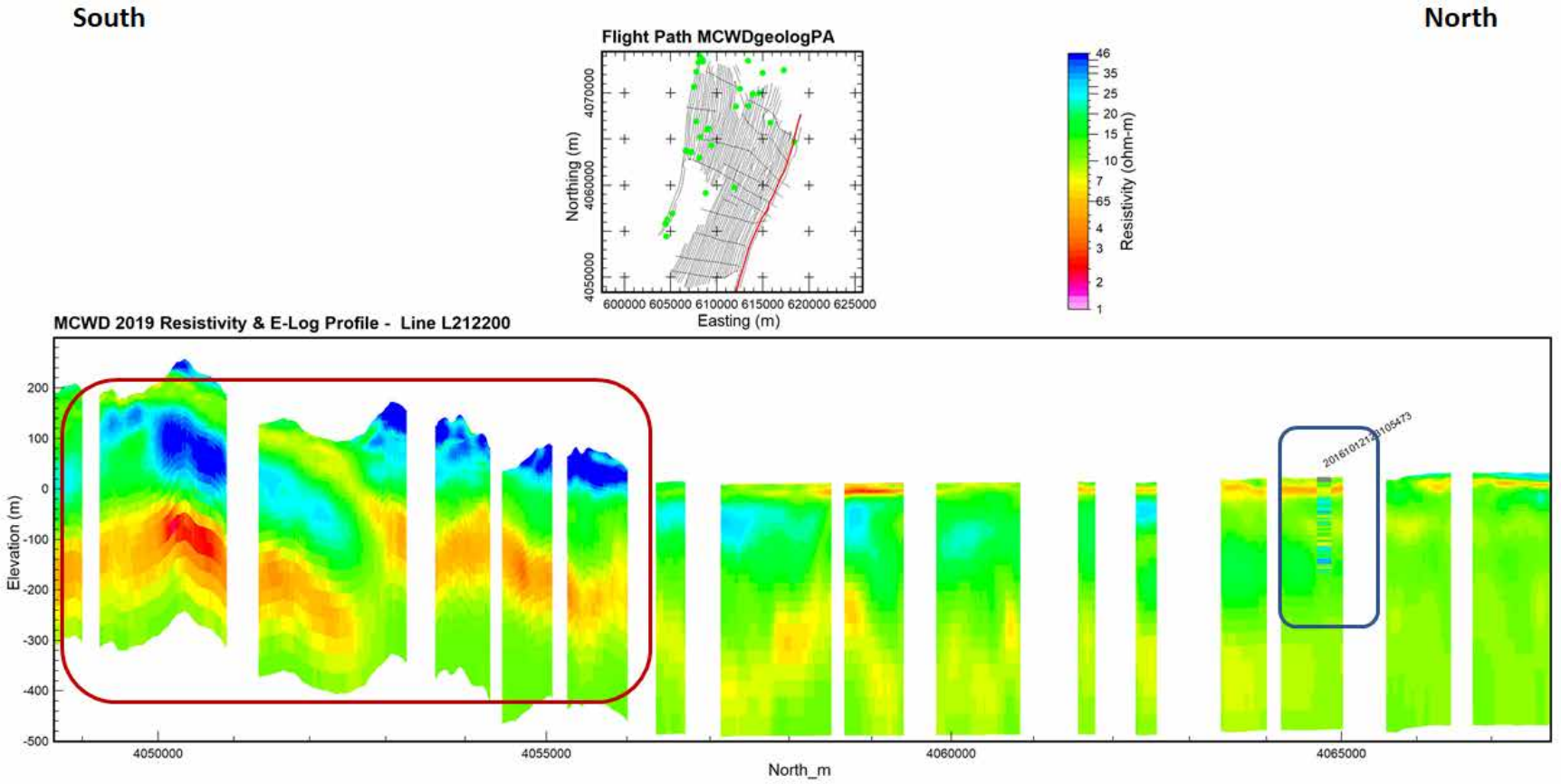

Figure 4-15. Inverted AEM resistivity profile of MCWD 2019 AEM survey line L212200, a north-south flight line near the beach approximately 19 km long, with geophysical 16-inch Short Normal electrical logs (green dots on map) for comparison at the same scale. The projection is NAD83, UTM 10N, meters and elevation values are referenced to NAVD88, meters.

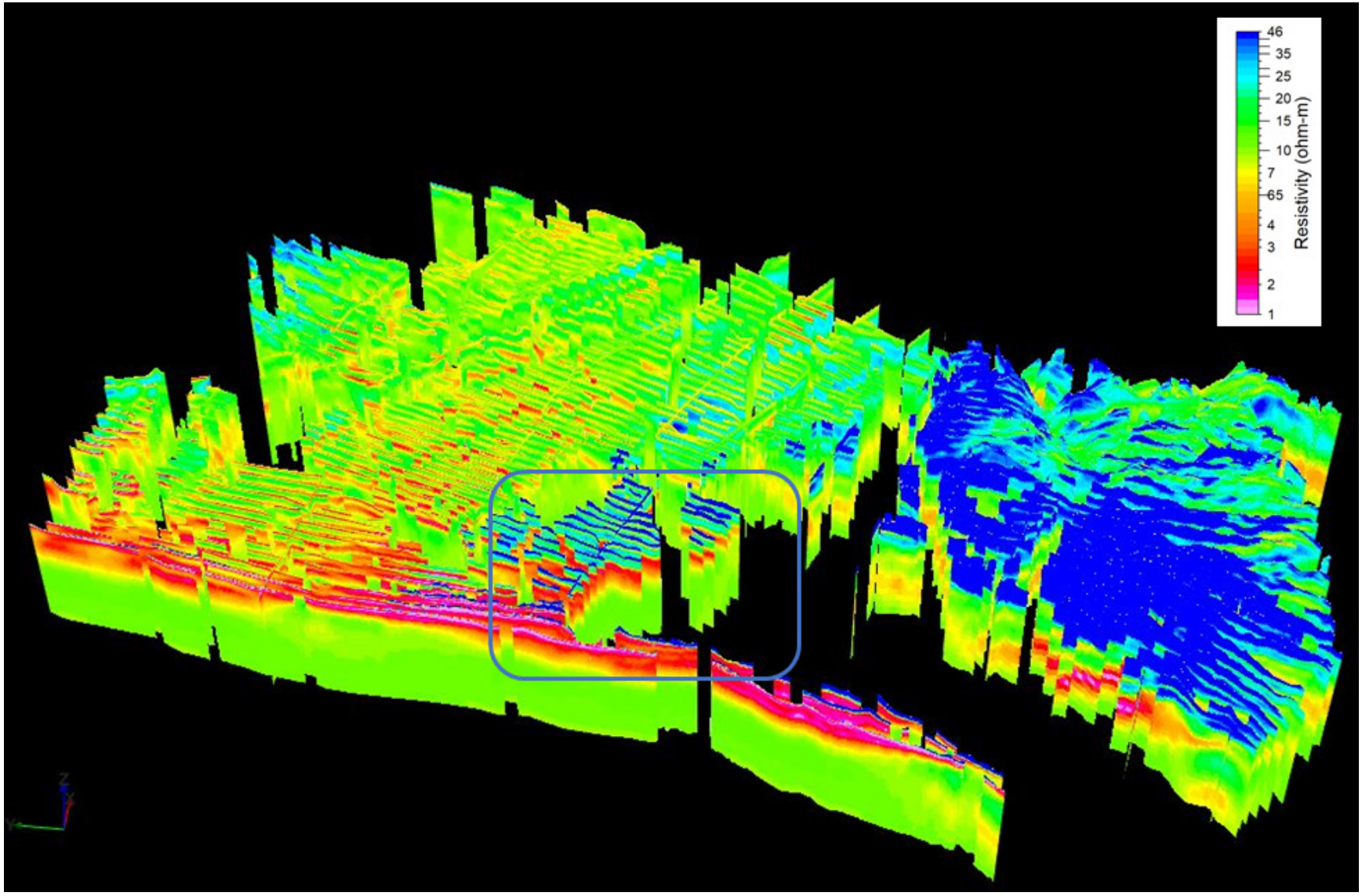

Figure 4-16. 3D fence diagram of the inverted resistivities of the MCWD 2019 AEM survey data, looking to the east. V.E.=10x.

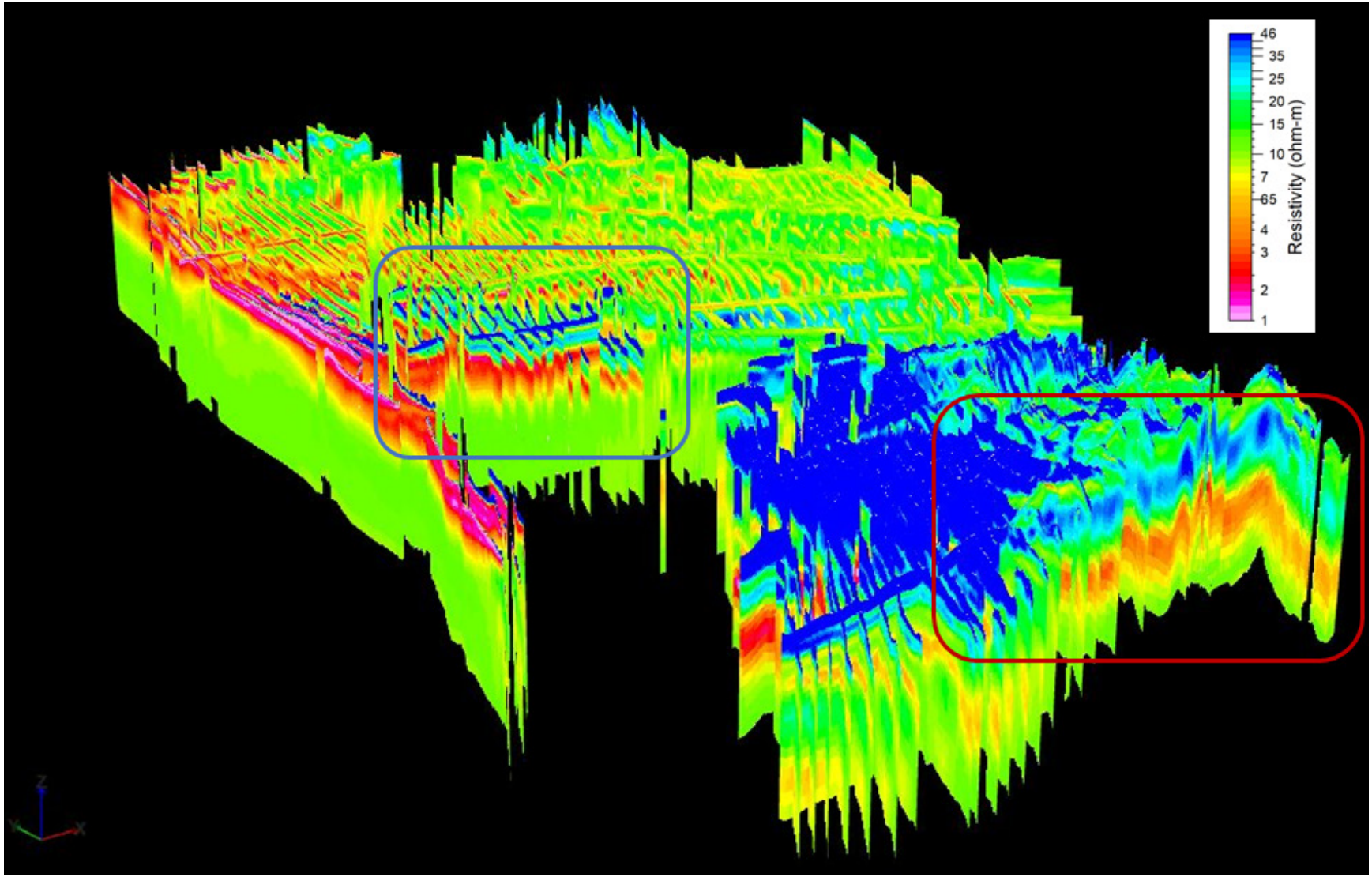

Figure 4-17. 3D fence diagram of the inverted resistivities of the MCWD 2019 AEM survey data, looking to the northeast. V.E.=10x.

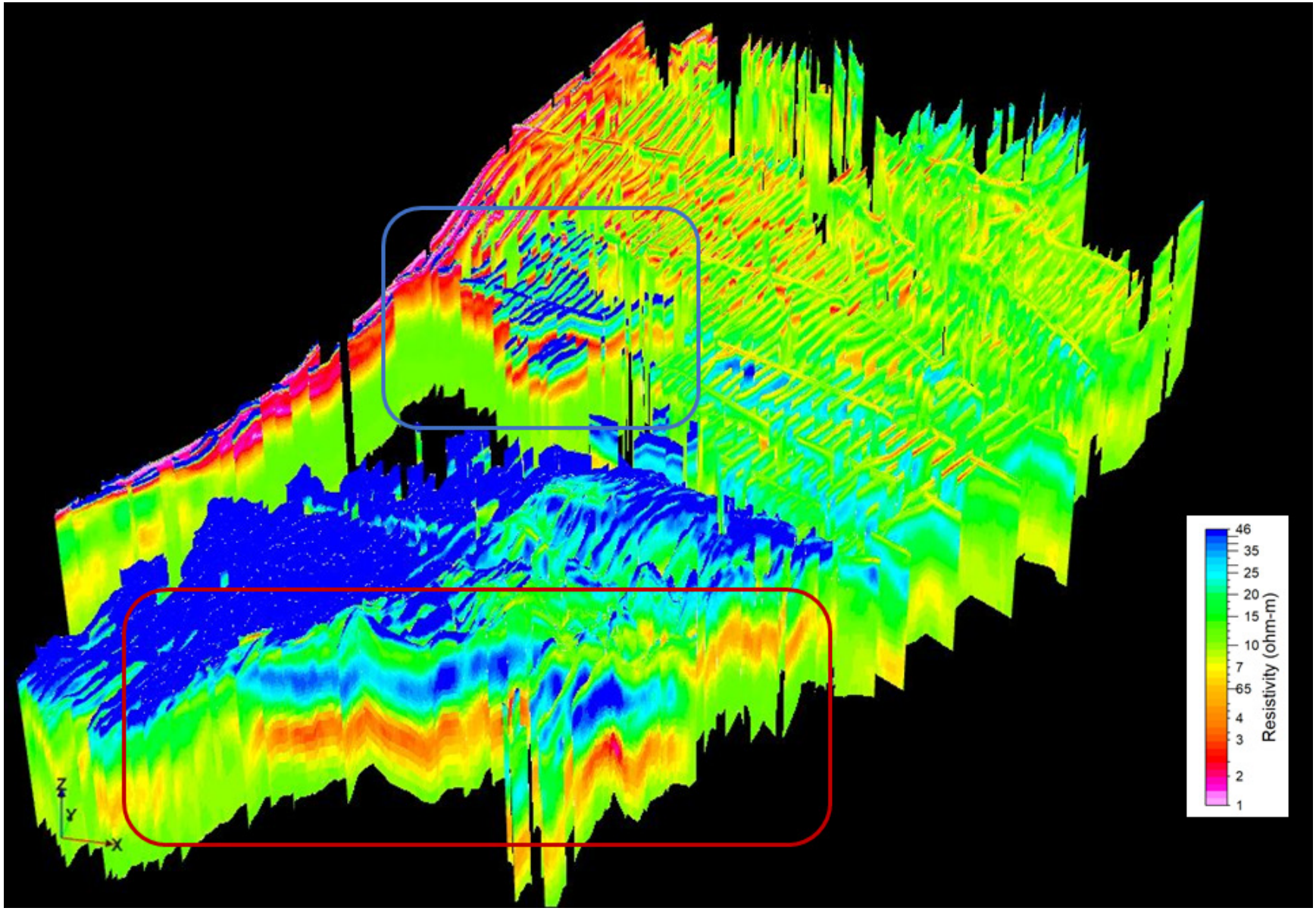

Figure 4-18. 3D fence diagram of the inverted resistivities of the MCWD 2019 AEM survey data, looking to the north. V.E.=10x.

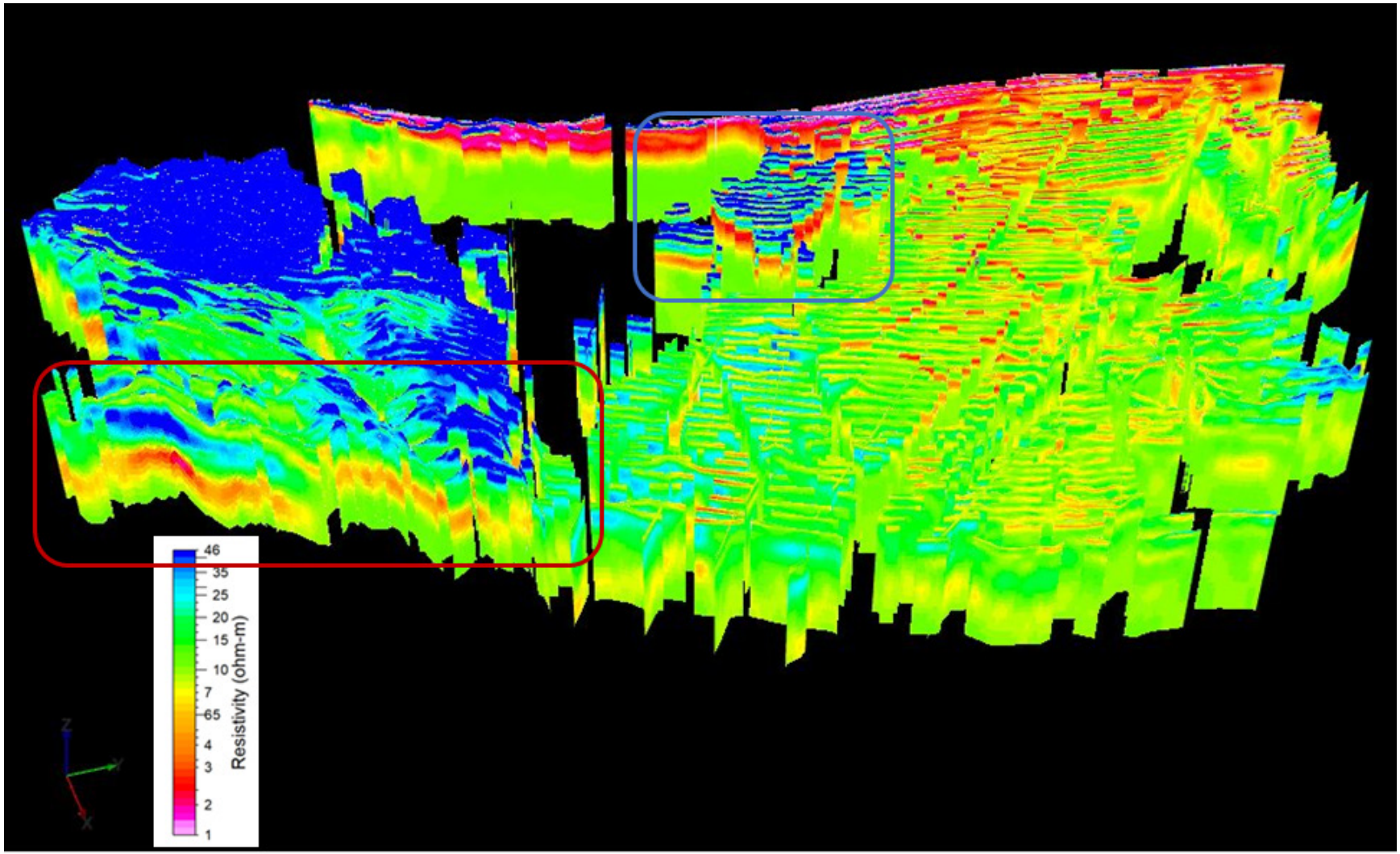

Figure 4-19. 3D fence diagram of the inverted resistivities of the MCWD 2019 AEM survey data, looking to the west. V.E.=10x.

4.3 Comparison of 2017 and 2019 AEM Resistivity Inversion Results

This section presents comparisons of the AEM inverted resistivity results for the 2017 SkyTEM 304M and the 2019 SkyTEM 312 surveys. Note that the SkyTEM 312 is a more powerful system (as a result of its higher electromagnetic moment) than the SkyTEM 304M system, providing deeper resolution. The locations of the flight lines presented, again working from the coast inland, are indicated by the red lines on the flight path maps at the top of the figures. The AEM inversion results from 2017 are depicted in the top 2D profile and those from 2019 are shown in the bottom profile. Borehole lithological logs, from wells within 250 m of a flight line, are projected onto the 2D profiles. The color-depicted lithological units in the boreholes are defined by the lithology legend included on each figure. The resistivity color scale in the presented figures ranges, as before, from 1 ohm-m to 50 ohm-m.

Flight lines L200101 (Figure 4-20) and L200202 (2017)/200200 (2019) (Figure 4-21), which are closest to the coast, both show similar results for both 2017 and 2019– a very electrically conductive zone (red) overlying more resistive material (green to blue). These results indicate that it is likely that the 180-Foot Aquifer is mostly saturated with saline water.

The comparison of the 2017 AEM and 2019 AEM along flight line L200301 (Figure 4-22), still near the coast, shows that they are quite similar except for a slight difference at a northing of 4067500 N (blue box). Flight line L200501 (top-2017)/L200500 (bottom-2019) (Figure 4-23), about 400 m inland from L200301, shows a greater difference between the 2017 results and the 2019 results between a northing of 4067800 and 4068600. Otherwise the results along L200501 are quite similar for the two surveys. The difference is still greater along flight line L201201/L201100 in this area (Figure 4-24).

Flight lines L204001 (top-2017) and L204000 (bottom-2019) are much further inland (Figure 4-25). L204001(top) shows a much greater concentration of conductive material at depth in the 400-Foot Aquifer (near northing 4068000) that is not observed in the 2019 data (L204000-bottom). However, note that at the southern end of these two profiles, that resistive (blue) material (indicated by the "Likely Fresh Water" boxes) overlies the very conductive (red) material that may be characterizing the 180-Foot Aquifer.

L204701 (top - Figure 4-26) also shows similar conductive material (near northing 4068000) and also more conductive material between northings 4065000 and 4066000 (blue box) that is not observed in the 2019 results (L204700 – bottom in Figure 4-26). Also note in Figure 4-26 that there are further indications at the southern ends of the flight lines of resistive material (likely fresher water) overlying the conductive material (likely saline water) at northing 4062000 in both the 2017 and 2019 AEM inversion results.

Figure 4-27 presents flight lines L206801 (2017) and L206800 (2019) which show similar results to the previous examples between northings 4062000 and 4069000. In addition, these profiles have a red dashed line (highlighted in the red ellipses at the southern end of the profiles) that indicates the 75 ohm-m cutoff that was determined in the analysis of the 2017 AEM survey to represent the top of the water table (Gottschalk et al., 2018). See Figure 4-28 for full spatial coverage of the <75 ohm-m water table. These images indicate fresh water (blue zones) sitting on more saline water (red zones).

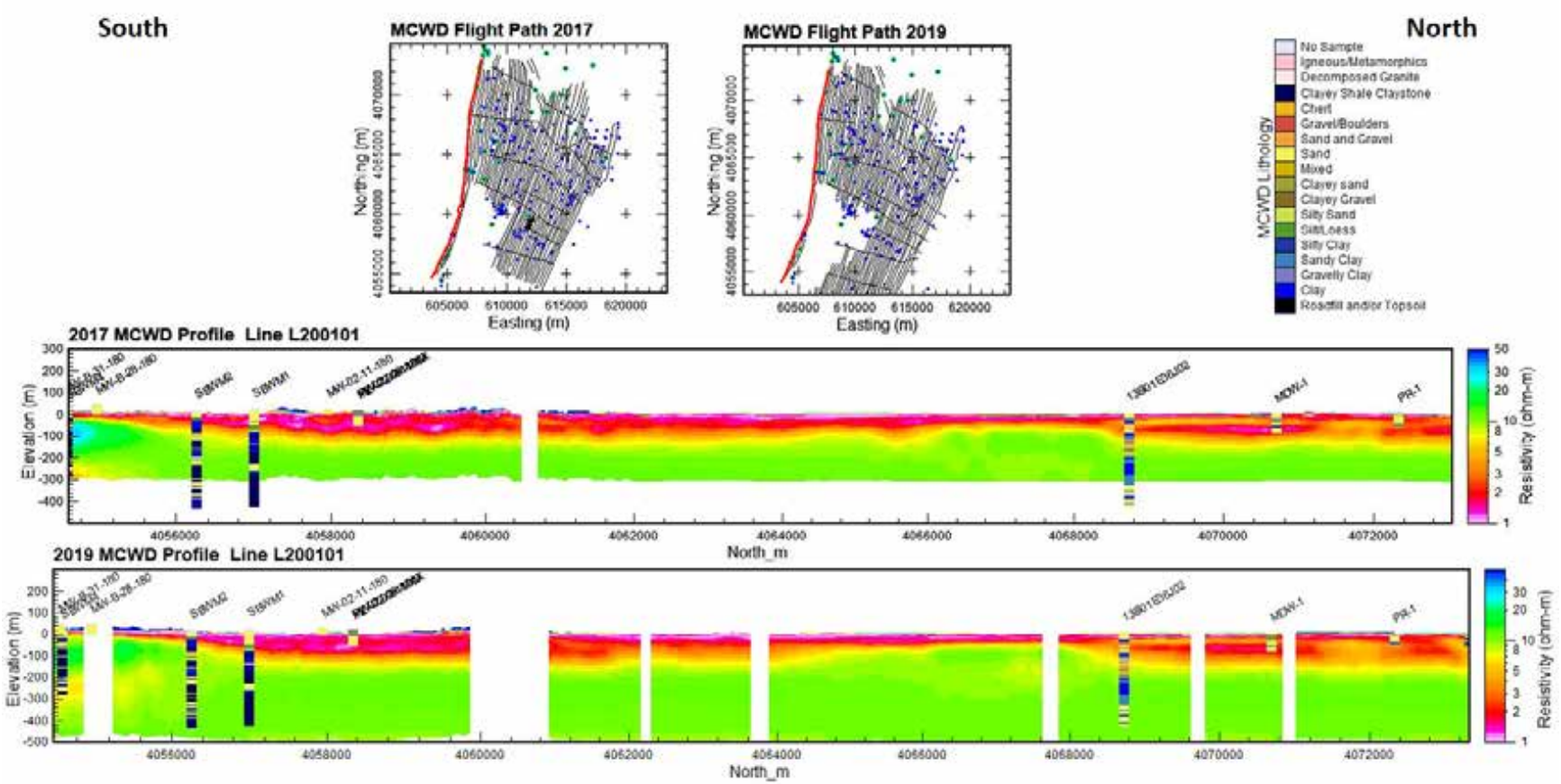

Figure 4-20. Comparison in 2D Profile format of the AEM resistivity inversion results for MCWD 2017 (top) and 2019 (bottom) data along flight line 200101 (red lines in flight map), along the beach. The two sections look quite similar, indication little change in the water quality along this flight line. On the flight map, blue dots are lithology logs and green dots are geophysical logs. V.E.=10x. The projection is NAD83, UTM 10N, meters and elevation values are referenced to NAVD88, meters.

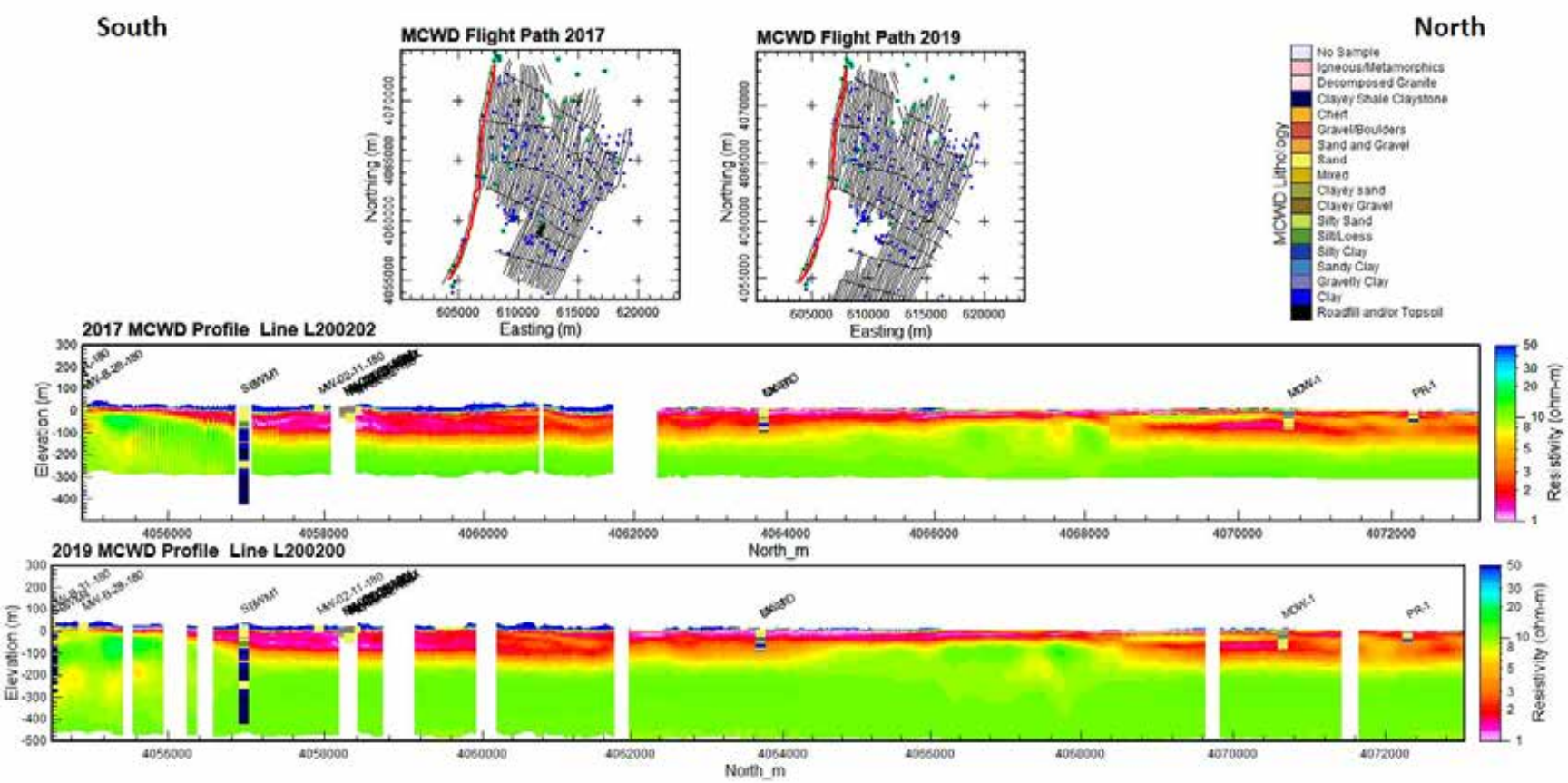

Figure 4-21. Comparison in 2D Profile format of the AEM resistivity inversion results for MCWD 2017 (top) and 2019 (bottom) data along flight line 200202/200200 (red lines in flight map), along the beach. Similar to Figure 4-13, there is little difference between the inversion results for 2017 and 2019 along this flight line. On the flight map, blue dots are lithology logs and green dots are geophysical logs. V.E.=10x. The projection is NAD83, UTM 10N, meters and elevation values are referenced to NAVD88, meters.

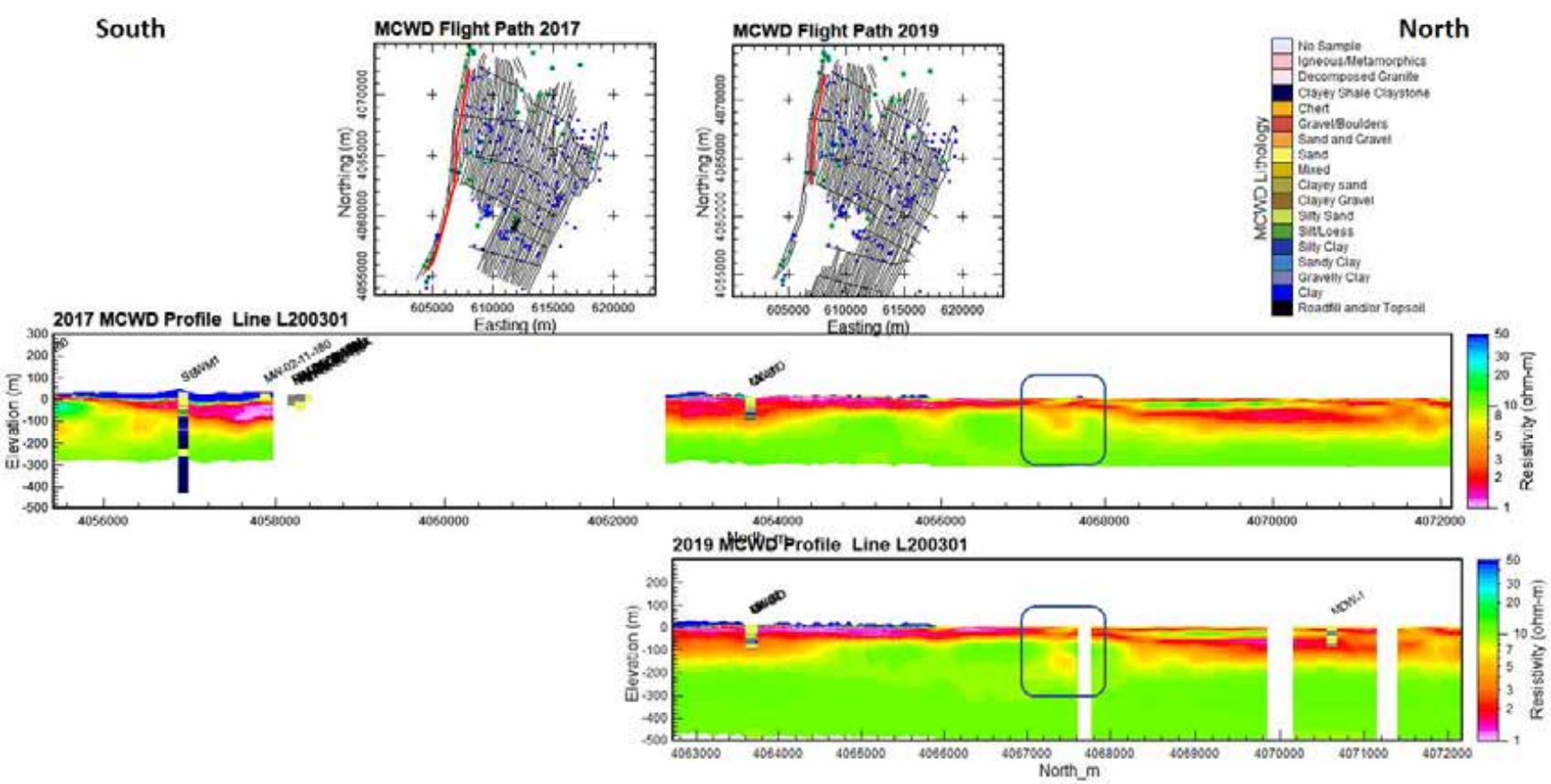

Figure 4-22. Comparison in 2D Profile format of the AEM resistivity inversion results for MCWD 2017 (top) and 2019 (bottom) data along flight line 200301 (red lines in flight map), along the beach. Note the slight difference in the resistivity distribution in the blue boxes. On the flight map, blue dots are lithology logs and green dots are geophysical logs. V.E.=10x. The projection is NAD83, UTM 10N, meters and elevation values are referenced to NAVD88, meters.

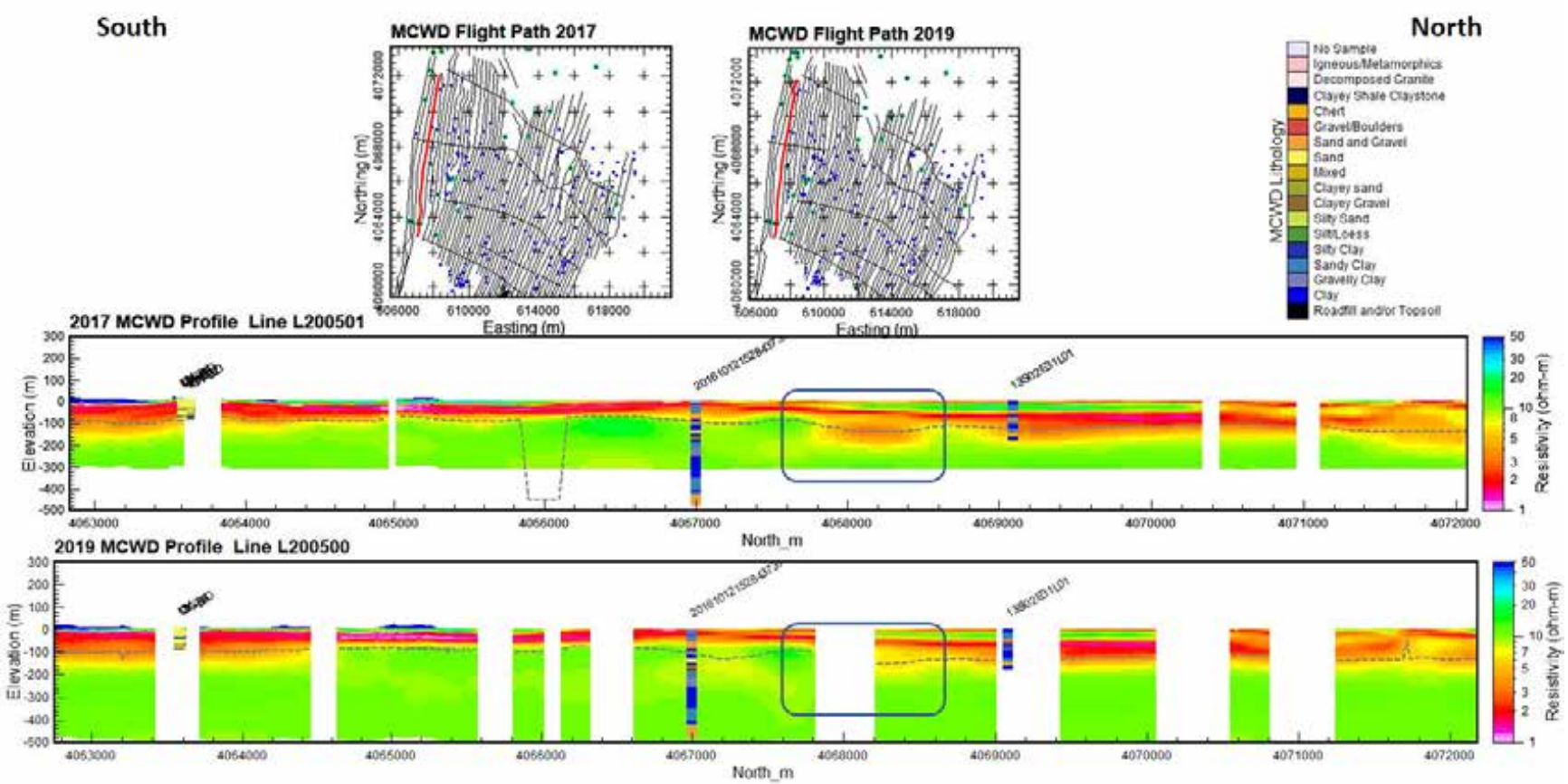

Figure 4-23. Comparison in 2D Profile format of the AEM resistivity inversion results for MCWD 2017 (top) and 2019 (bottom) data along flight line 200501 (red lines in flight map), which is a little further inland. Note the difference in the resistivity distribution within the blue boxes. On the flight map, blue dots are lithology logs and green dots are geophysical logs. V.E.=10x. The projection is NAD83, UTM 10N, meters and elevation values are referenced to NAVD88, meters.

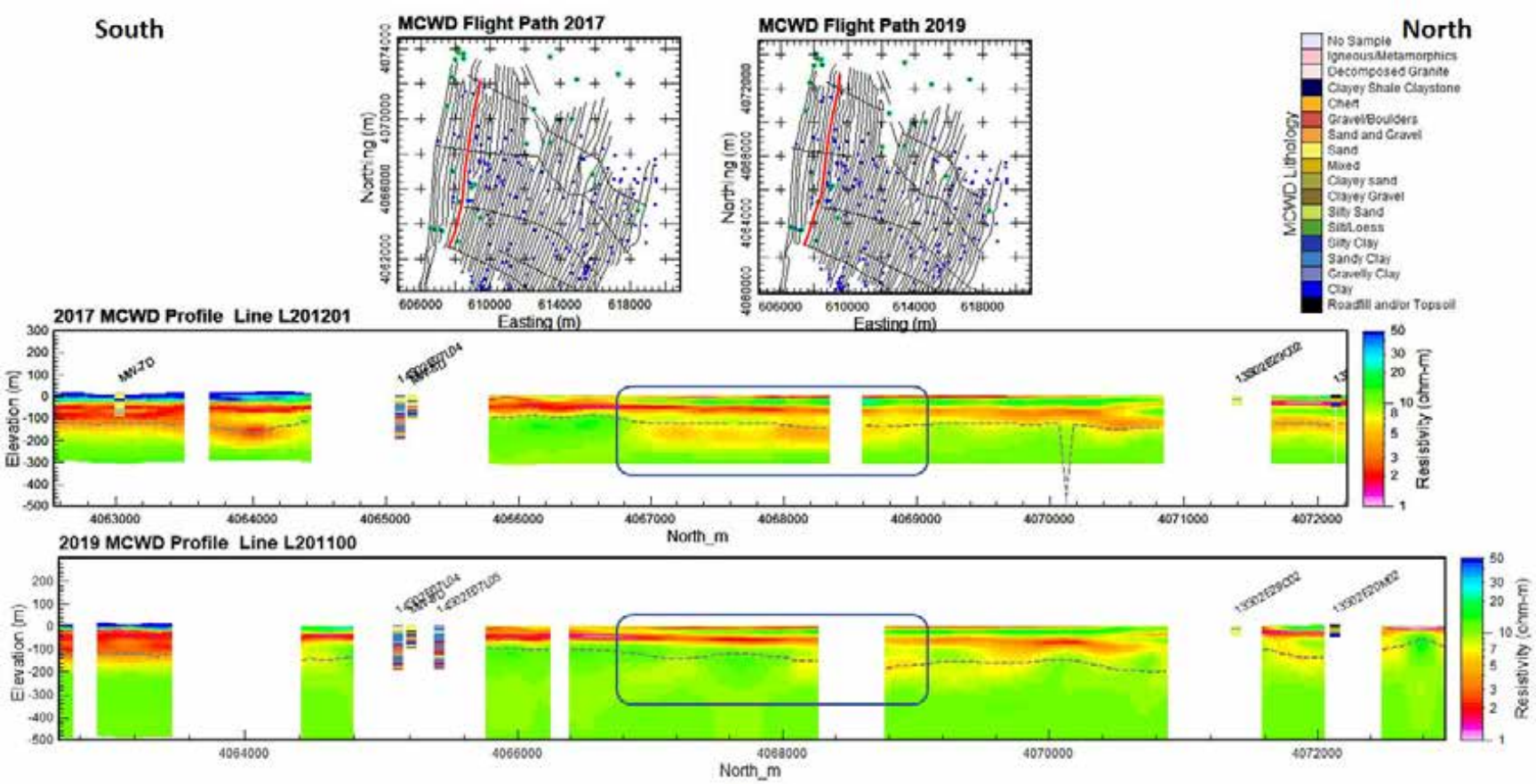

Figure 4-24. Comparison in 2D Profile format of the AEM resistivity inversion results for MCWD 2017 (top) and 2019 (bottom) data along flight line 201201/201100 (red lines in flight map). Note the difference in the resistivity distribution within the blue boxes. On the flight map, blue dots are lithology logs and green dots are geophysical logs. V.E.=10x. The projection is NAD83, UTM 10N, meters and elevation values are referenced to NAVD88, meters.

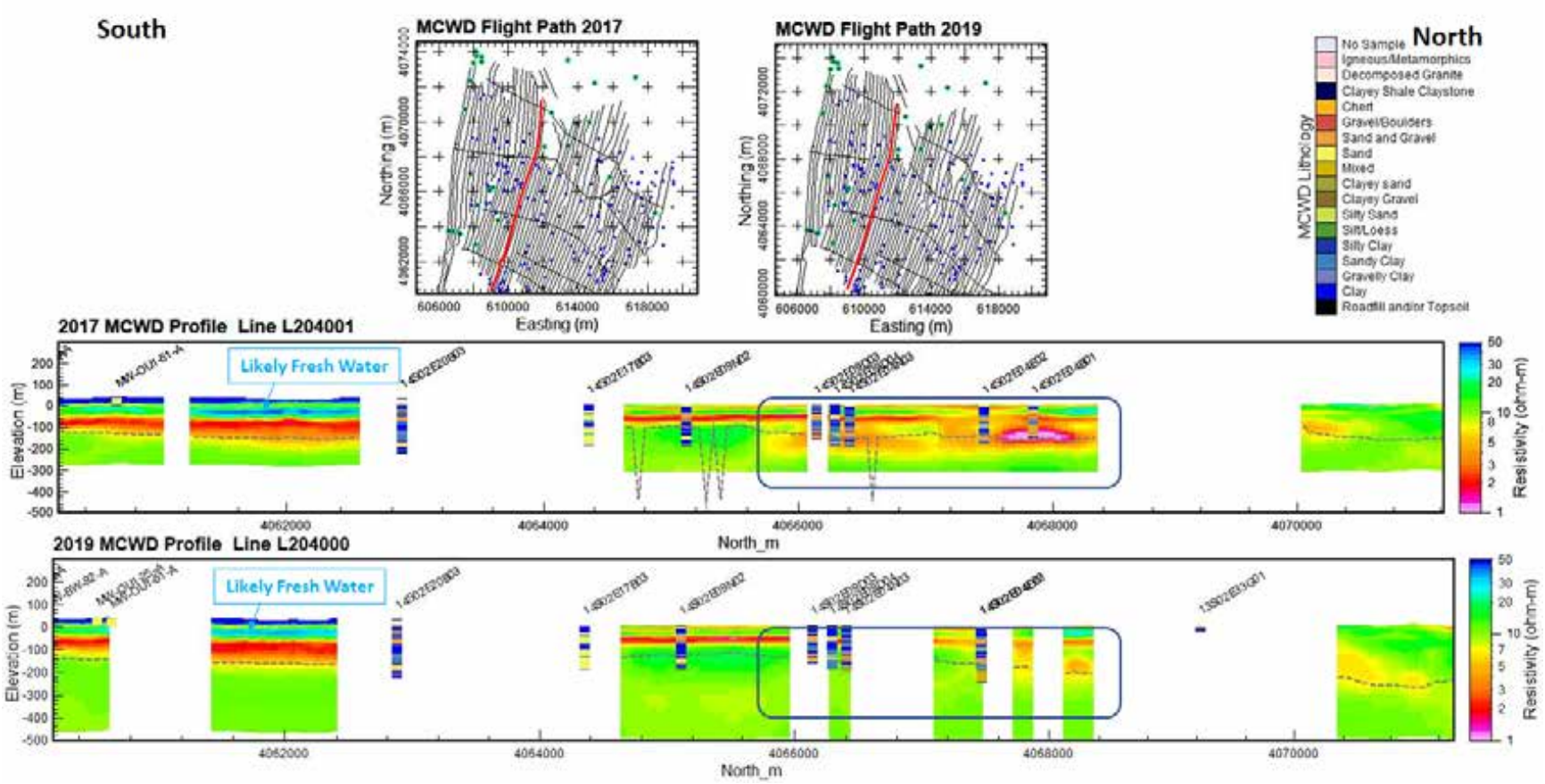

Figure 4-25. Comparison in 2D Profile format of the AEM resistivity inversion results for MCWD 2017 (top) and 2019 (bottom) data along flight line 204001/204000 (red lines in flight map). Note the difference in the resistivity distribution within the blue boxes. On the flight map, blue dots are lithology logs and green dots are geophysical logs. V.E.=10x. The projection is NAD83, UTM 10N, meters and elevation values are referenced to NAVD88, meters.

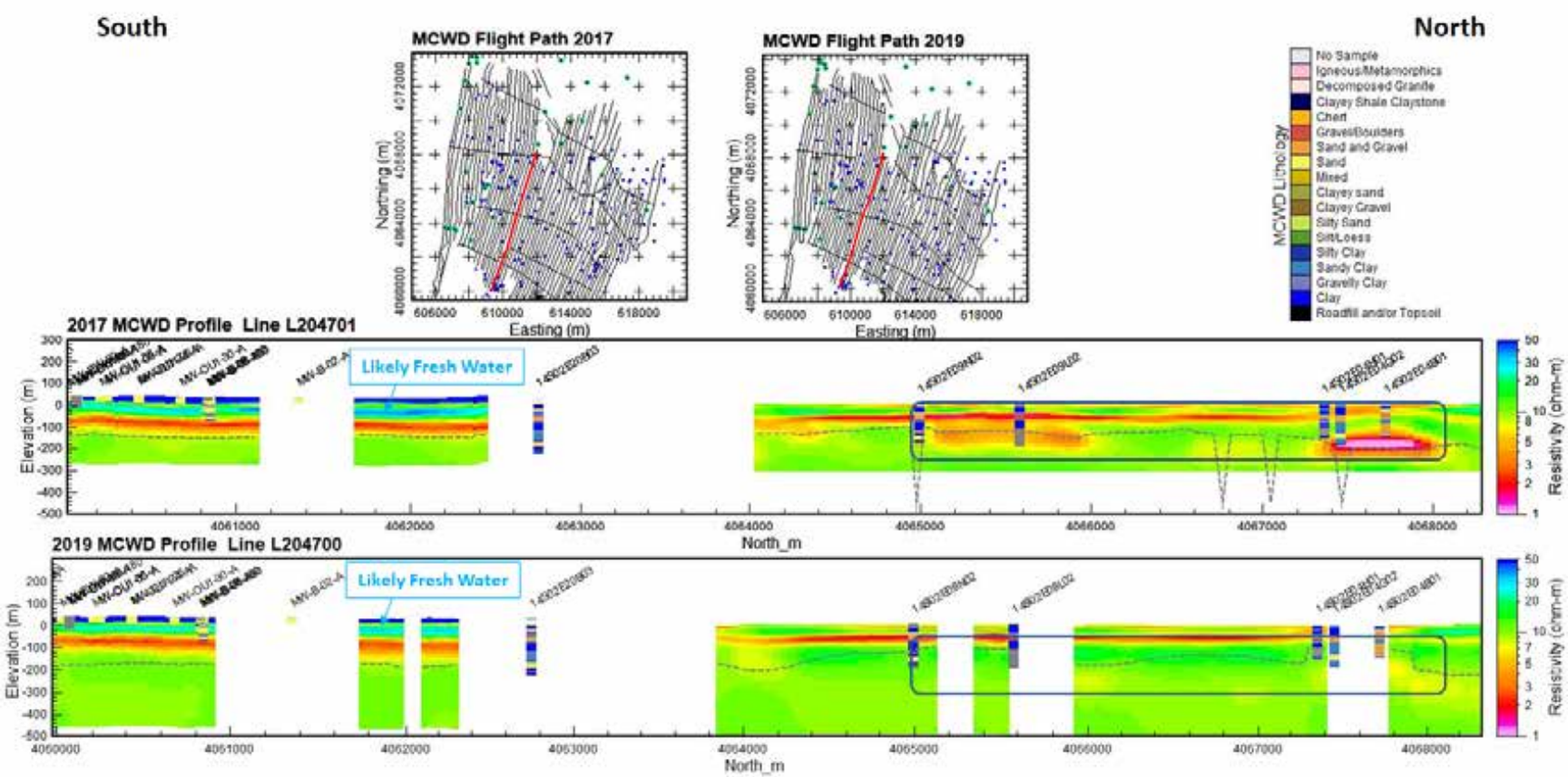

Figure 4-26. Comparison in 2D Profile format of the AEM resistivity inversion results for MCWD 2017 (top) and 2019 (bottom) data along flight line 204701/204700 (red lines in flight map). Note the difference in the resistivity distribution within the 400-ft aquifer in the blue boxes. Also note the zone of likely fresh water on the southern end of the line. On the flight map, blue dots are lithology logs and green dots are geophysical logs. V.E.=10x. The projection is NAD83, UTM 10N, meters and elevation values are referenced to NAVD88, meters.

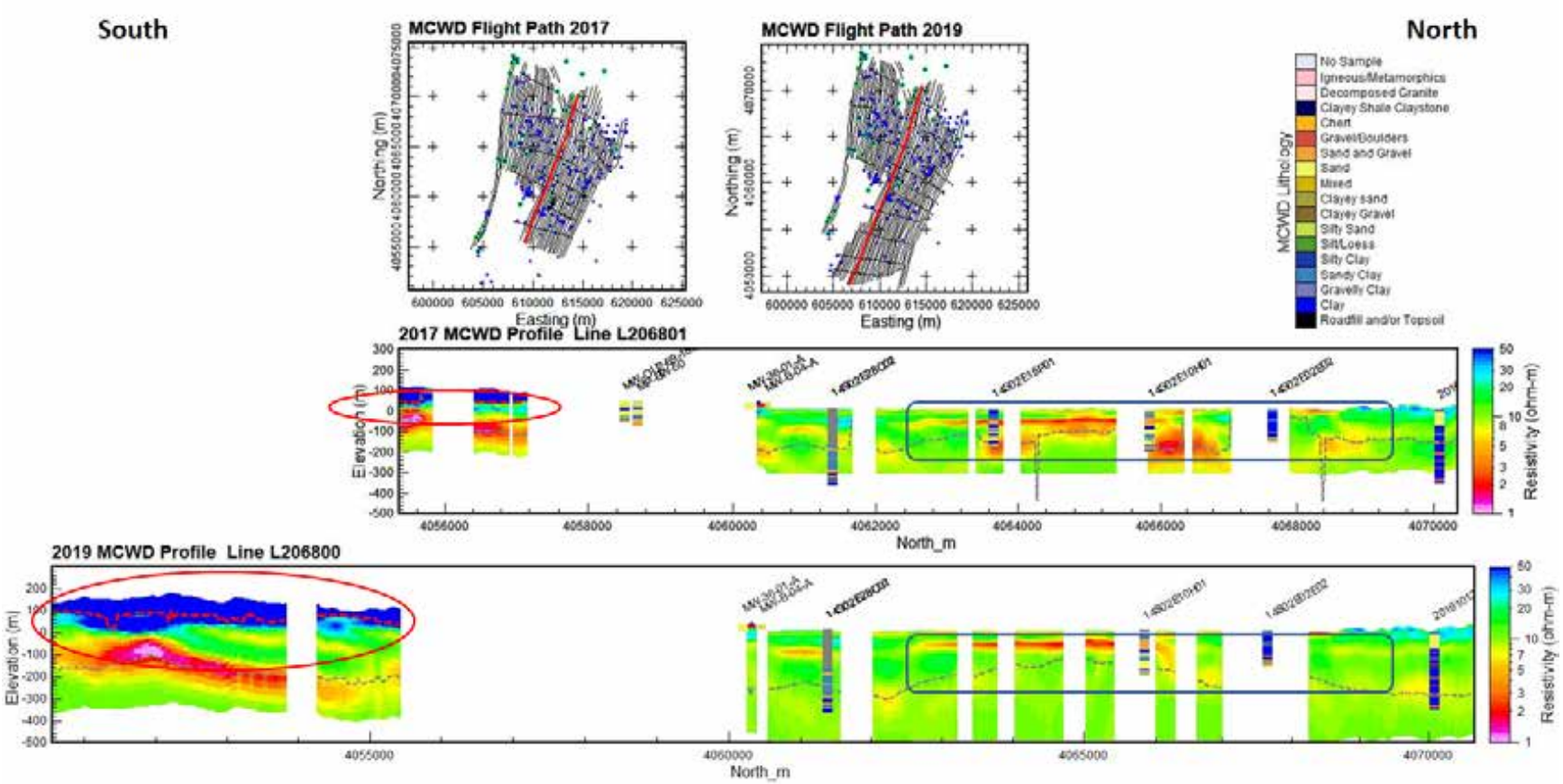

Figure 4-27. Comparison in 2D Profile format of the AEM resistivity inversion results for MCWD 2017 (top) and 2019 (bottom) data along flight line 206801/204800 (red lines in flight map). Note the difference in the resistivity distribution within the 400-ft aquifer in the blue boxes. On the flight map, blue dots are lithology logs and green dots are geophysical logs. The dashed red line on the southern end of the profile indicates the 75 ohm-m demarcation as the top of the groundwater table. See Figure 4-28 for a map of the water table elevation based on locations where resistivities above 75 ohm-m. The projection is NAD83, UTM 10N, meters and elevation values are referenced to NAVD88, meters. V.E.=10x.

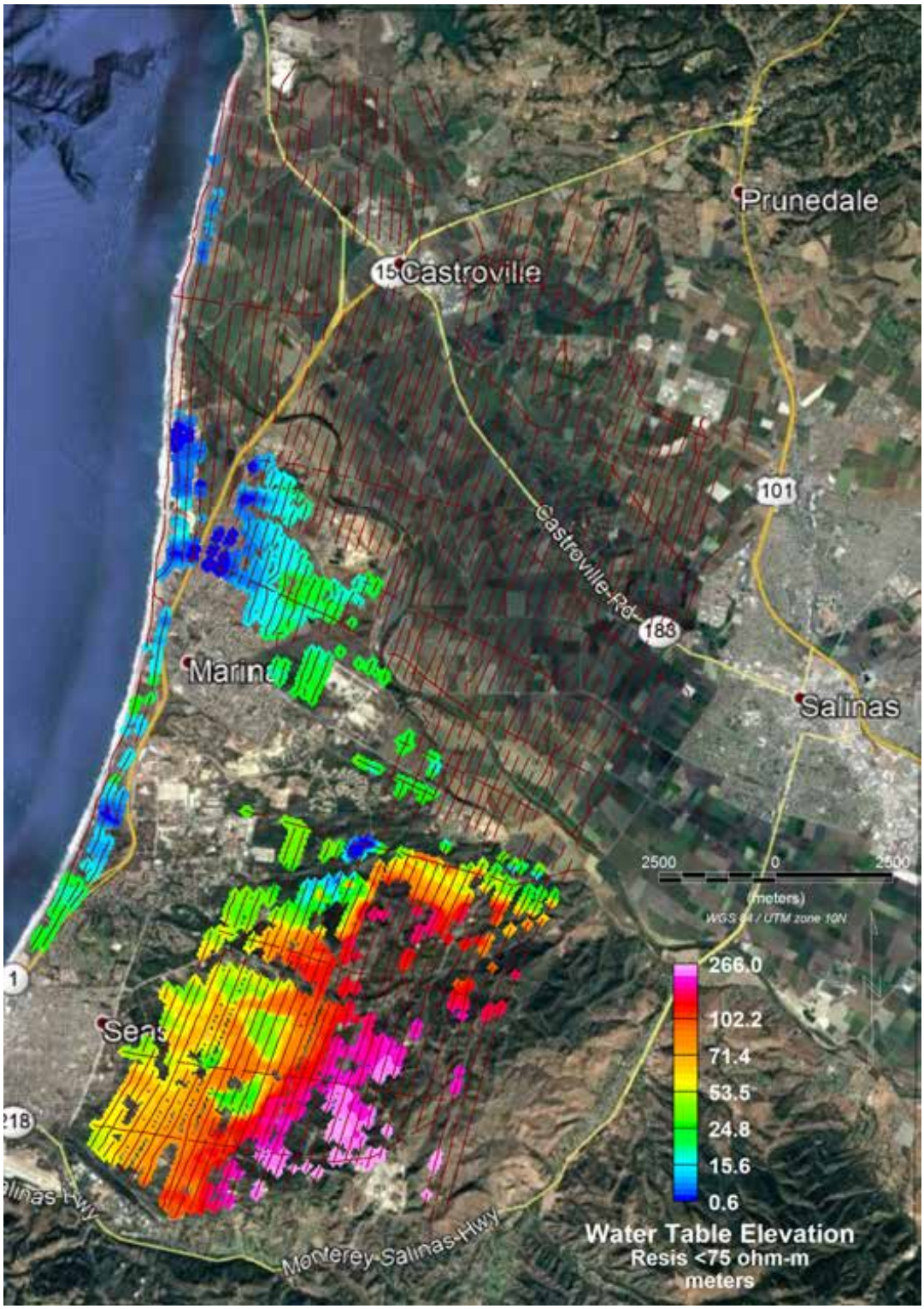

Figure 4-28. Map showing spatial coverage of water table elevation determined by locations where resistivities are greater than 75 ohm-m and elevation of 75 ohm-m material is top of the groundwater table (Gottschalk et al., 2018). Where there is no data indicates an area with resistivities <75 ohm-m.

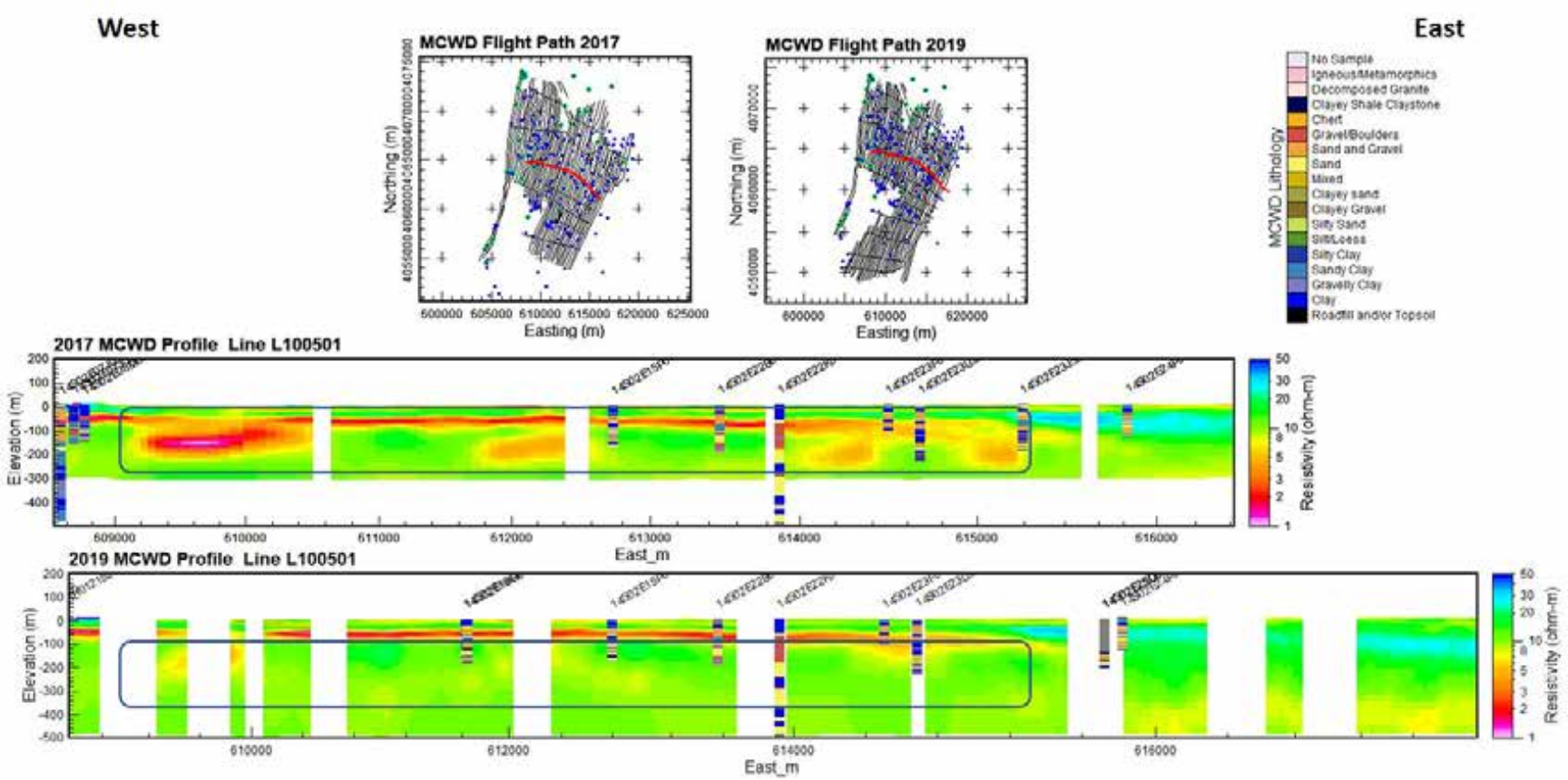

Figure 4-29. Comparison in 2D Profile format of the AEM resistivity inversion results for MCWD 2017 (top) and 2019 (bottom) data along flight line 100501 (red lines in flight map). Note the difference in the resistivity distribution within the 400 ft aquifer in the blue boxes. On the flight map, blue dots are lithology logs and green dots are geophysical logs. V.E.=10x. The projection is NAD83, UTM 10N, meters and elevation values are referenced to NAVD88, meters.

Figure 4-29 presents an approximate east-west "tie" line, L100501, showing similar results of more conductive material identified in the 2017 AEM survey, likely in the 400-Foot Aquifer, that is, predominantly, not present in the 2019 AEM investigation.

Additional comparisons of the inverted resistivity results from the 2017 and 2019 MCWD AEM surveys can be located in Appendix 1 – 2D Profiles.

4.4 Basis of MCWD Chloride Concentration Estimations

The AEM resistivities are "bulk" or "formation" resistivities that include the rock, groundwater, and everything within the given volume that the current is passing through. In order to convert these bulk resistivities to ground water TDS concentrations, some conversions are necessary. First from bulk resistivity to groundwater resistivity and then to groundwater conductivity, and, secondly, from groundwater conductivity to electrical conductance (EC) to groundwater salinity and TDS concentrations.

In order to make these conversions, a comparison table and regression analysis is carefully developed consisting of sampled groundwater conductivities and TDS's and AEM resistivities at the same locations and depths, if possible.

In previous analyses of the 2017 MCWD AEM investigation results (AGF, 2018; AGF, 2019) in response to comments by the Hydrologic Working Group (HWG) and their contractors, a rationale was presented, based on availability and knowledge of its stability, for using salinity to electrical conductance (EC) to AEM resistivity relationships from studies conducted in southern Florida (Fitterman and Prinos, 2011). Since some data from the Marina area is now available online at the MPWSP website (https://www.watersupplyproject.org/test-well), an analysis of local chloride concentration, TDS, and EC compared to the 2019 AEM inverted resistivities has been conducted. The following presents some of the analysis and results of this study.

The MCWD 2019 AEM survey took place between April 24, 2019 and April 26, 2019. It therefore seemed appropriate to find EC and salinity concentrations at locations across the survey area from that timeframe to compare with the inverted AEM resistivities. However, the only data publicly available online were scanned data lists from the April 10, 2019 to May 15, 2019 MPWSP well data monitoring report number 160 (MPWSP, 2019). The report contains varying versions of monitoring data from each of the MPWSP monitoring wells (MW-1 to MW-9, there is no MW-2 in the area). Notably at the end of the report is a graph presenting a relationship between TDS and EC in the MPWSP monitoring wells. This graph is reproduced in Figure 4-30.

A table (Table 4-2) was constructed of the available monitoring data acquired during the same time period as when the AEM survey was performed. In this case, data from April 24, 2019 at 12:00 PM was selected as nominally representing the nature of the water quality during the AEM survey. It would have been nice to have used all the data from the AEM acquisition period. However, the data was not in a format amenable to that option. The data in Table 4-2 lists MPWSP monitoring well data including the well names, the locations of the wells, sampling screen intervals in feet, measured specific conductance

and TDS and salinity concentrations from April 24, 2019 at 12PM, the mean AEM inverted resistivity at the approximate screen interval depths (indicated by the AEM layer numbers used), and the distance (in meters) from the closest AEM sounding to the monitoring well. Note that there is no MW-2 data in the table and also no MW-5S, MS-5M, and MW-7M monitoring data in MPWSP monitoring report No. 160 (MPWSP, 2019). Going back to the equation in Figure 4-30 and inserting a value of EC = 294.9 μS, which is the listed value from borehole MW-9D retrieved from MPWSP monitoring report No. 160 (MPWSP, 2019), results in a calculated TDS of -94.36 mg/L, a negative value. The actual TDS value reported is 404.5 mg/L, a 498 mg/L difference.

One observation of interest in Table 4-2 is that for the MW-1 wells (S, M, D), the EC's are 50221 μS, 51263 μS, and 42,936 μS and the mean AEM resistivities are 8.8, 8.7, and 12.1 ohm-m. What is interesting is that you would think that the resistivities for EC's on the order of 50,000 μS would be lower than that for 43,000 μS. But that isn't the case for MW-1. Keep in mind that the AEM inverted resistivities matched both the lithological and geophysical logs very well, which provides confidence in their distribution over the survey area.

Figure 4-31 presents the regression relationship between Salinity (mg/L) and the Measured Specific Conductance (μS) monitoring data from April 24, 2019 at 12PM. In this case, the relation has an R^2 = 0.97 (the closer to 1.0, the better). There are a few things to note in this figure. First is the regression relationship (Salinity = (0.6653 x EC) + 119.54). If EC = 100 μS, Salinity = 186.07 mg/L which is a positive number and so could exist, unlike the relationship from the MPWSP report No. 160 (MPWP, 2019) in Figure 4-30 which resulted in a negative value.

The next item of note in Figure 4-31 is the binary distribution of the EC vs Salinity values. Either they are very high (above 40,000 μS) or low (less than 8,000 μS) with nothing in between.

Finally, in Figure 4-31, note the point labeled "MW-4M" is far off the trend line which directly affects the relationship between Salinity and EC. Note also that all the high EC/Salinity values are not on the trend line, probably because of the MW-4M data point. This suggests that there might be some values with low confidence in the data listed in Table 4-1 coming from the MPWSP monitoring well reports.

The next step in the analysis is to develop a stable relationship between the groundwater EC or resistivity and the AEM or formation resistivity. A comparison between the AEM resistivities and the measured EC from April 24, 2019 is presented in Figure 4-32. The calculated R^2 = 0.53 which is low and indicates a somewhat poor relationship. This is likely because the distribution of EC is above 40,000 μS and below 8,000 μS while the range of AEM resistivities is between 1 and 30 ohm-m. It is better if the ranges of values compared are of the same order of magnitude in amplitude.

One way to normalize the data so that they are of the same order of magnitude is to take a natural log (*Ln*) or one or both of the data sets. Taking the natural log of the measured EC and then repeating the regression analysis results in Figure 4-33 where the R^2 = 0.66. Better than 0.53, but still not great. One possible reason for the low R^2 coefficient is the large spread of the data across the plot which means that all the data far away from the trend line do not have a good or coherent relationship suggesting

that either one set of data or both are not of good quality with high confidence. In order to investigate if this spread is lithology -related, the recorded lithologies in each screen interval were compiled. This is presented in Table 4-2 and plotted up in Figure 4-34.

Looking back at Section 4.2 which showed a very good correlation of the AEM inversion results with the borehole short normal (SN) geophysical logs as well as the lithology logs, it is suggested that it is not the AEM data that has issues with quality, noise, and/or calibration..

The way then to approach this issue with low confidence EC values is to iteratively remove EC values that are located the most distant from the trend line in Figure 4-33 and re-run the regression analysis. The result of this iterative analysis is presented in Figure 4-35 where the $R^2 = 0.96$, which indicates a very good relationship. To get this value six (6) EC data had to be removed from the analysis. The retained data set are indicated in Table 4-3 which lists the MPWSP monitoring well name, the screen intervals and the average recorded lithology over that screen interval, the measured electrical conductance (EC), the natural log of the measured EC, the measured TDS and Salinity concentration values, and the mean AEM inverted resistivities as described in the discussion on Table 4-1 above. The last two columns list the results of applying the relationship shown in Figure 4-35 to the mean AEM resistivities. Compare the natural log of the measured specific conductance to the predicted natural log of the specific conductance as well as the measured and predicted specific conductance data.

The result of the regression analysis of the local MPWSP monitoring well data suggests that several of the TDS, Salinity, and EC data are questionable or non-existent (in the case of MW-5S, MW-5M, and MW-7M). As mentioned above, besides the missing data, this is likely due to measurement quality, noise in the system, and/or calibration of the borehole measuring tools.

4.4.1 Southern Florida Chloride Concentration – AEM Relationship

In order to make a reasonable approximation of the Salinity to EC to AEM resistivities was to search and examine published literature for a similar analysis at a similar site. This search resulted in finding a USGS Open-File Report published by Fitterman and Prinos (2011) describing a similar time-domain geophysical electromagnetic investigation over salt water intruding into the Everglades in southern Florida. The results of the Fitterman and Prinos (2011) study are presented in Figure 4-36.

We recognize that there will be a difference in the character of the electrical conductivity of the saline water in southern Florida and in the Monterey Bay and the intruded coastal geologic materials. We are using the Florida relationships only to produce an approximation for this analysis.

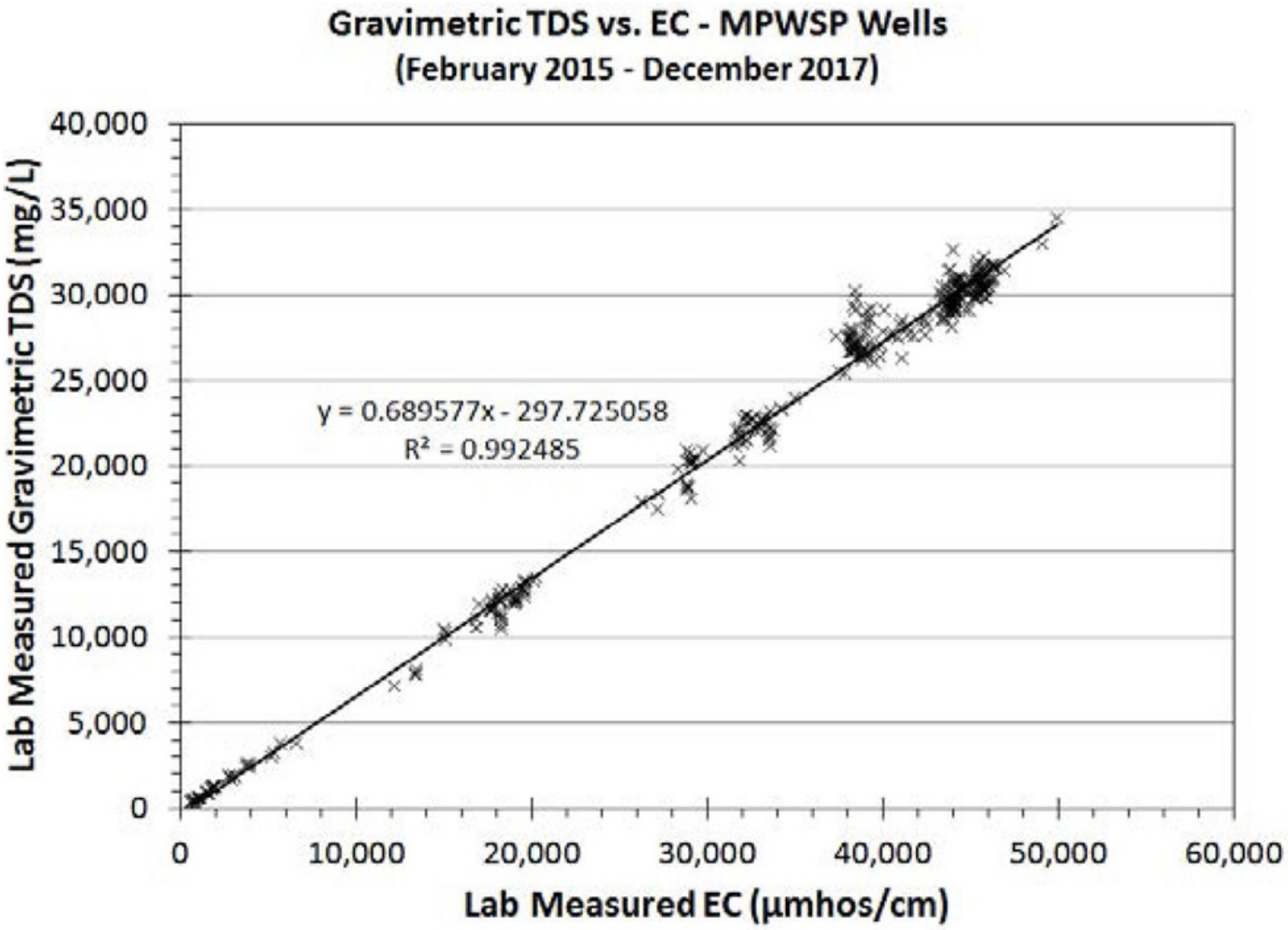

Figure 4-30. MPWSP published relationship between Total Dissolved Solids (TDS) and Electrical Conductance (EC) in the MPWSP wells. From page 605 of the April 10, 2019 to May 15, 2019 MPWSP monitoring well report No. 160 (MPWSP, 2019).

Table 4-1. MPWSP monitoring well data including well name, location in California State Plane Zone 4 feet and UTM zone 10 N meters, screen intervals in feet and meters, measured specific conductance and TDS and salinity concentrations from April 24, 2019 at 12PM, the mean AEM inverted resistivity at the approximate screen interval depths (indicated by the AEM layer numbers used), and the distance (meters) from the closest AEM sounding to the monitoring well. Note that there is no MW-2 data and no MW-5S, MS-5M, and MW-7M monitoring data.

HoleID	E CASP4 ft	N CASP4 ft	E UTM 10N m	N UTM 10N m	Screen Top ft	Screen Bot ft	Screen Top m	Screen Bot m	Meas. Spec. Cond. µS 4/24/2019 12PM	TDS Conc mg/L	Salinity mg/L	AEM Mean Rho Ohm_m	AEM Lyr #	Dist (m) AEM to MW
MW-1S	5739356	2154745	606648	4063716	55	95	17	29	50221.2	34150	32900	1.2	7-9	96
MW-1M	5739348	2154752	606646	4063718	115	225	35	69	51263.2	34900	33700	1.8	11-16	
MW-1D	5739338	2154754	606643	4063718	277	327	84	100	42935.8	29200	27900	3.0	19-20	
MW-3S	5739977	2154600	606839	4063679	50	90	15	27	40351.7	27400	25900	1.4	6-9	91
MW-3M	5739989	2154593	606843	4063677	105	215	32	66	43256.6	29400	28000	1.9	10-16	
MW-3D	5739999	2154590	606846	4063677	285	330	87	101	46802	31800	30700	2.9	19-20	
MW-4S	5741428	2154171	607286	4063567	60	100	18	30	2037.4	1400	1100	4.6	7-10	148
MW-4M	5741417	2154173	607283	4063568	130	260	40	79	34844.9	23700	33200	2.0	12-18	
MW-4D	5741406	2154174	607280	4063568	290	330	88	101	40847.5	27800	26400	2.6	19-20	
MW-5S	5748567	2156239	609434	4064288	43	83	13	25	NA	NA	NA	11.0	6-8	58
MW-5M	5748564	2156230	609433	4064285	100	310	30	94	NA	NA	NA	18.1	11-19	
MW-5D	5748561	2156221	609432	4064282	395	435	120	133	6449.7	4400	3600	8.1	22-24	
MW-6S	5756164	2141143	611939	4059787	30	60	9	18	2239.6	1500	1200	13.6	4-6	111
MW-6M	5756154	2141138	611936	4059786	150	210	46	64	1411.6	1000	710	13.4	13-16	
MW-6D	5756145	2141133	611933	4059784	255	325	78	99	1833.2	3300	2600	9.2	18-20	
MW-7S	5744148	2152099	608141	4062971	60	80	18	24	1477.8	1000	800	24.9	7-8	108
MW-7M	5744146	2152110	608140	4062974	130	220	40	67	NA	NA	NA	9.5	12-16	
MW-7D	5744144	2152121	608140	4062977	295	345	90	105	40179.5	27300	25900	2.3	19-20	
MW-8S	5744872	2159440	608268	4065215	40	80	12	24	761.5	500	400	19.9	5-8	376
MW-8M	5744866	2159431	608266	4065212	125	215	38	66	49993.3	34000	32900	3.3	12-16	
MW-8D	5744861	2159421	608265	4065209	300	350	91	107	1375.1	900	700	9.5	20-21	
MW-9S	5747345	2162011	608988	4066029	30	110	9	34	4804.9	3300	2600	5.8	4-10	292
MW-9M	5747354	2162017	608991	4066031	145	225	44	69	43606.7	29700	28300	2.0	13-16	
MW-9D	5747362	2162023	608994	4066033	353	393	108	120	294.9	404.5	300	12.1	21-22	

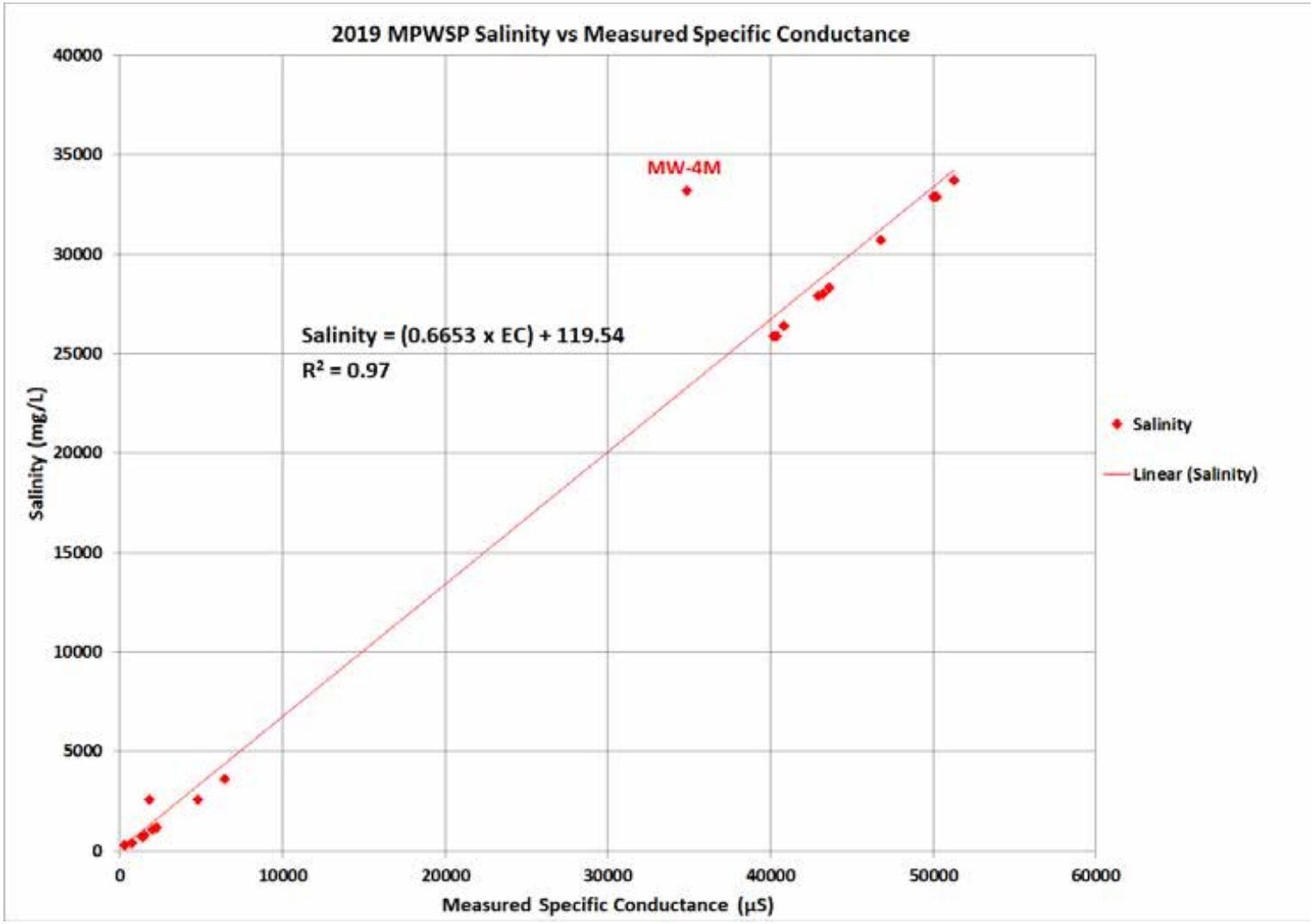

Figure 4-31. The regression relationship for monitoring data from April 24, 2019 at 12PM. In this case, the relation between Salinity (mg/L) and the Measured Specific Conductance (µS) has an R^2 = 0.97 (the closer to 1.0, the better). Compare this relationship to that presented in Figure 4-30. Note that the value for MW-4M is far off the trend line. Also note the concentration of values only above 40000 µS and only below 8000 µS.

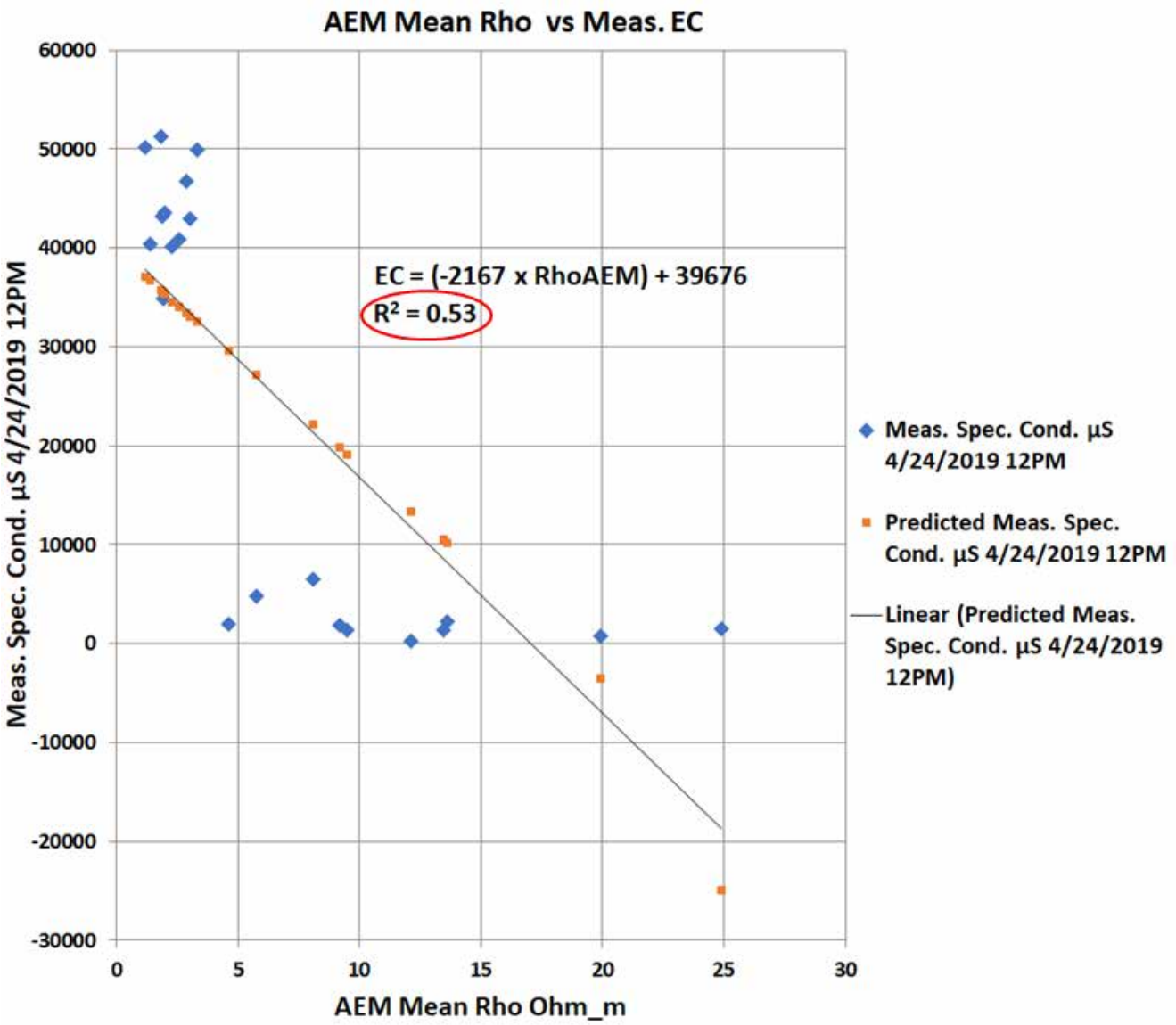

Figure 4-32. Regression relationship between the mean inverted AEM resistivity and the measured electrical conductance (EC) using all the data in Table 4-2 in their natural units. The R^2 is 0.53.

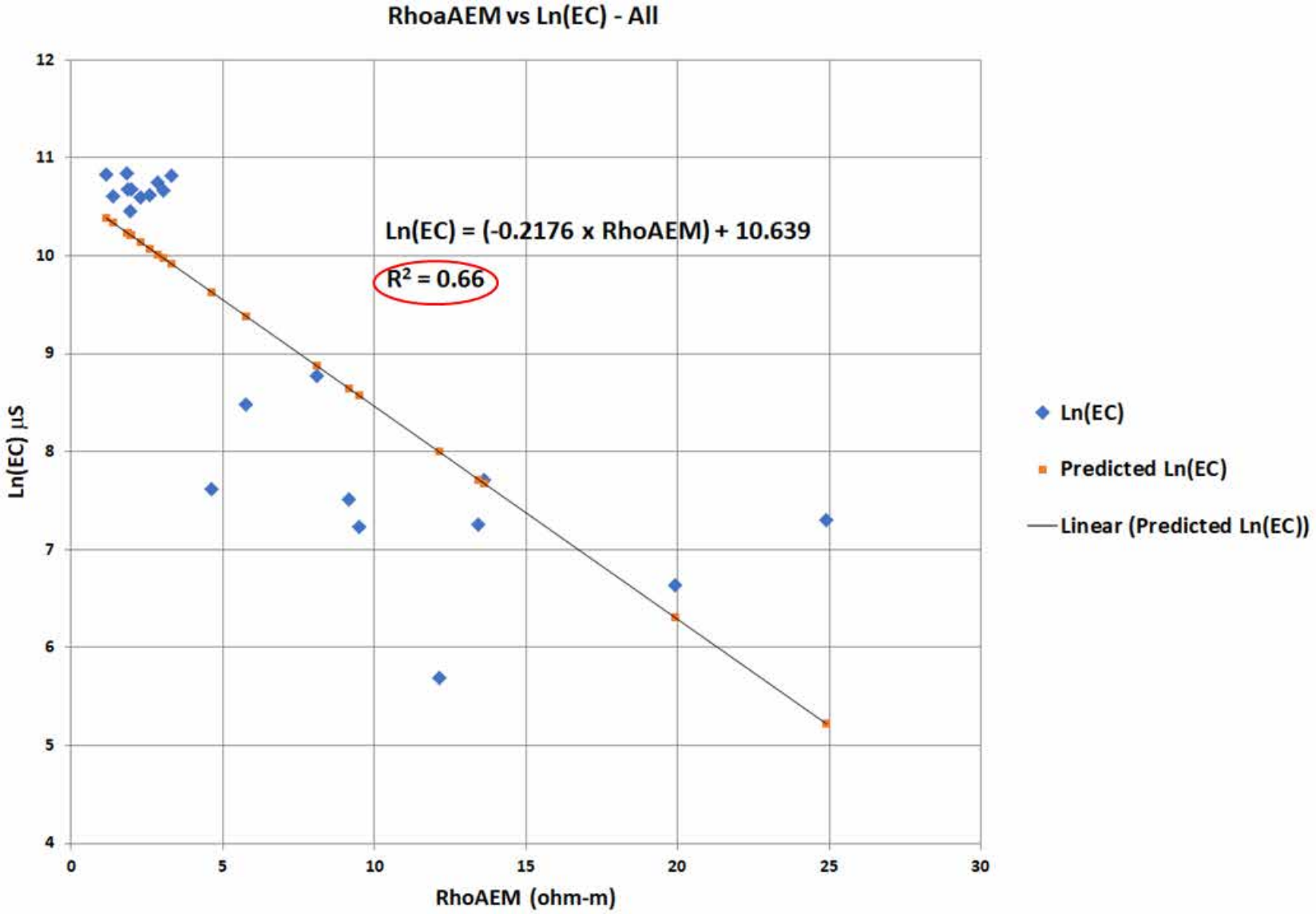

Figure 4-33. Regression relationship between the mean inverted AEM resistivity and the natural log (Ln) of all of the measured electrical conductance (EC) data in Table 4-2. The R^2 is 0.65. The natural log was calculated to put both data sets at the same order of magnitude.

Table 4-2. MPWSP monitoring well data including well name, screen intervals in feet and meters, the average lithology within the specific screen intervals, measured specific conductance and its natural log from April 24, 2019 at 12PM, and the mean AEM inverted resistivity at the approximate screen interval depths.

HoleID	Screen Top ft	Screen Bot ft	Screen Top m	Screen Bot m	Screen Interval Lithology	Meas. Spec. Cond. µS 4/24/2019 12PM	Ln(EC)	AEM Mean Rho Ohm_m
MW-1S	55	95	17	29	Sand	50221	10.824	1.2
MW-1M	115	225	35	69	Clayey Sand	51263	10.845	1.8
MW-1D	277	327	84	100	Clayey Sand	42936	10.667	3.0
MW-3S	50	90	15	27	Sand	40352	10.605	1.4
MW-3M	105	215	32	66	Clayey Sand	43257	10.675	1.9
MW-3D	285	330	87	101	Sand	46802	10.754	2.9
MW-4S	60	100	18	30	Sand	2037	7.619	4.6
MW-4M	130	260	40	79	Clayey Sand	34845	10.459	2.0
MW-4D	290	330	88	101	Clayey Sand	40848	10.618	2.6
MW-5S	43	83	13	25	Silty Clay, Sand			11.0
MW-5M	100	310	30	94	Sand			18.1
MW-5D	395	435	120	133	Sand	6450	8.772	8.1
MW-6S	30	60	9	18	Sand	2240	7.714	13.6
MW-6M	150	210	46	64	Sand	1412	7.252	13.4
MW-6D	255	325	78	99	Sand	1833	7.514	9.2
MW-7S	60	80	18	24	Sand	1478	7.298	24.9
MW-7M	130	220	40	67	Clayey Sand, Clay			9.5
MW-7D	295	345	90	105	Sand	40180	10.601	2.3
MW-8S	40	80	12	24	Sand	762	6.635	19.9
MW-8M	125	215	38	66	Sand	49993	10.820	3.3
MW-8D	300	350	91	107	Sand	1375	7.226	9.5
MW-9S	30	110	9	34	Silty Sand	4805	8.477	5.8
MW-9M	145	225	44	69	Sand	43607	10.683	2.0
MW-9D	353	393	108	120	Clayey Sand	295	5.687	12.1

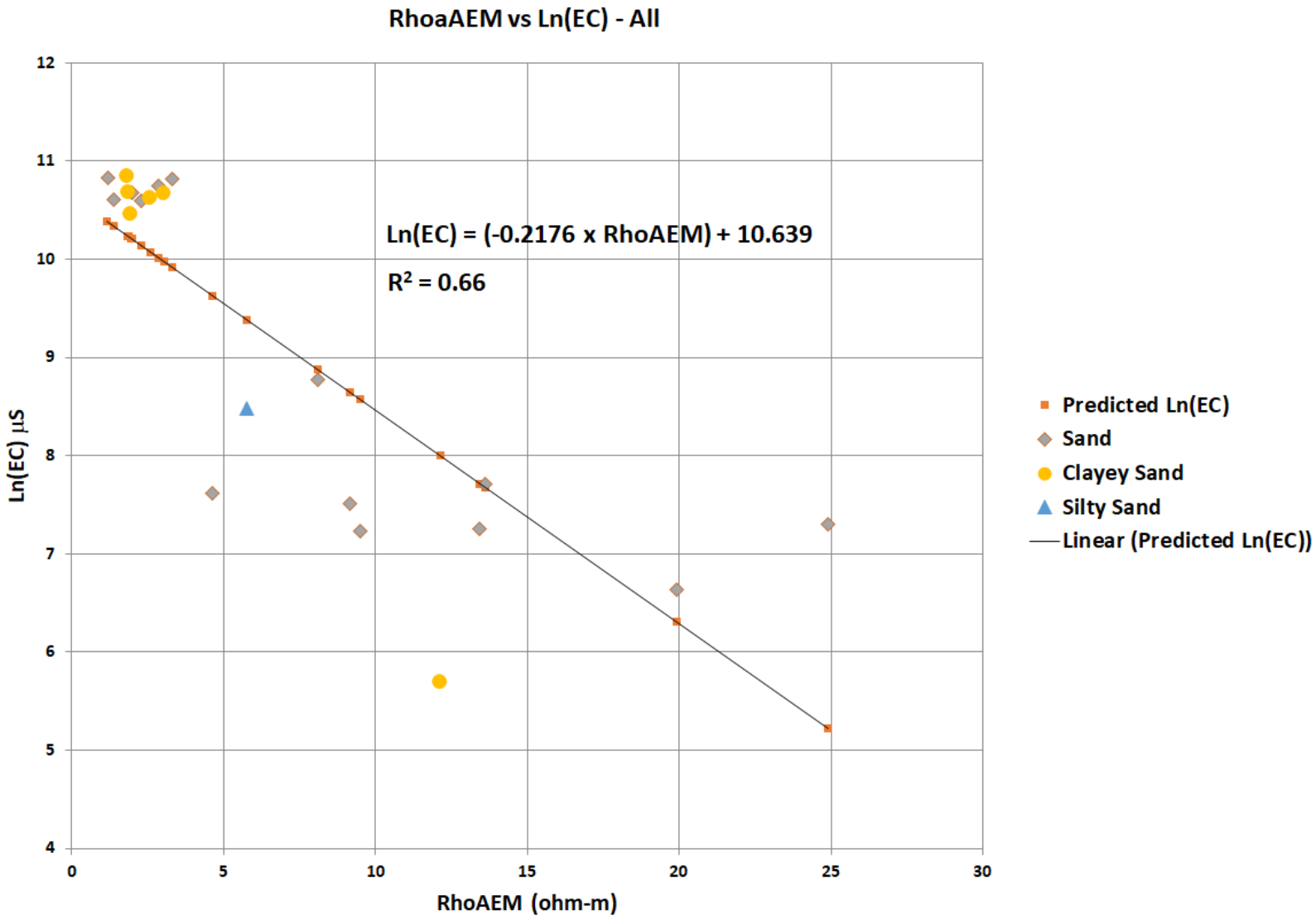

Figure 4-34. This is the same plot as in Figure 4-33 with the change being that the individual data points are represented by the average recorded lithology at the specific screen intervals. Brown diamonds – Sand, yellow circles – clayey sand, and blue triangle – silty sand. The idea is to query if there is a certain lithology group that plots far away from the trend line. But that doesn't appear to be any clear pattern.

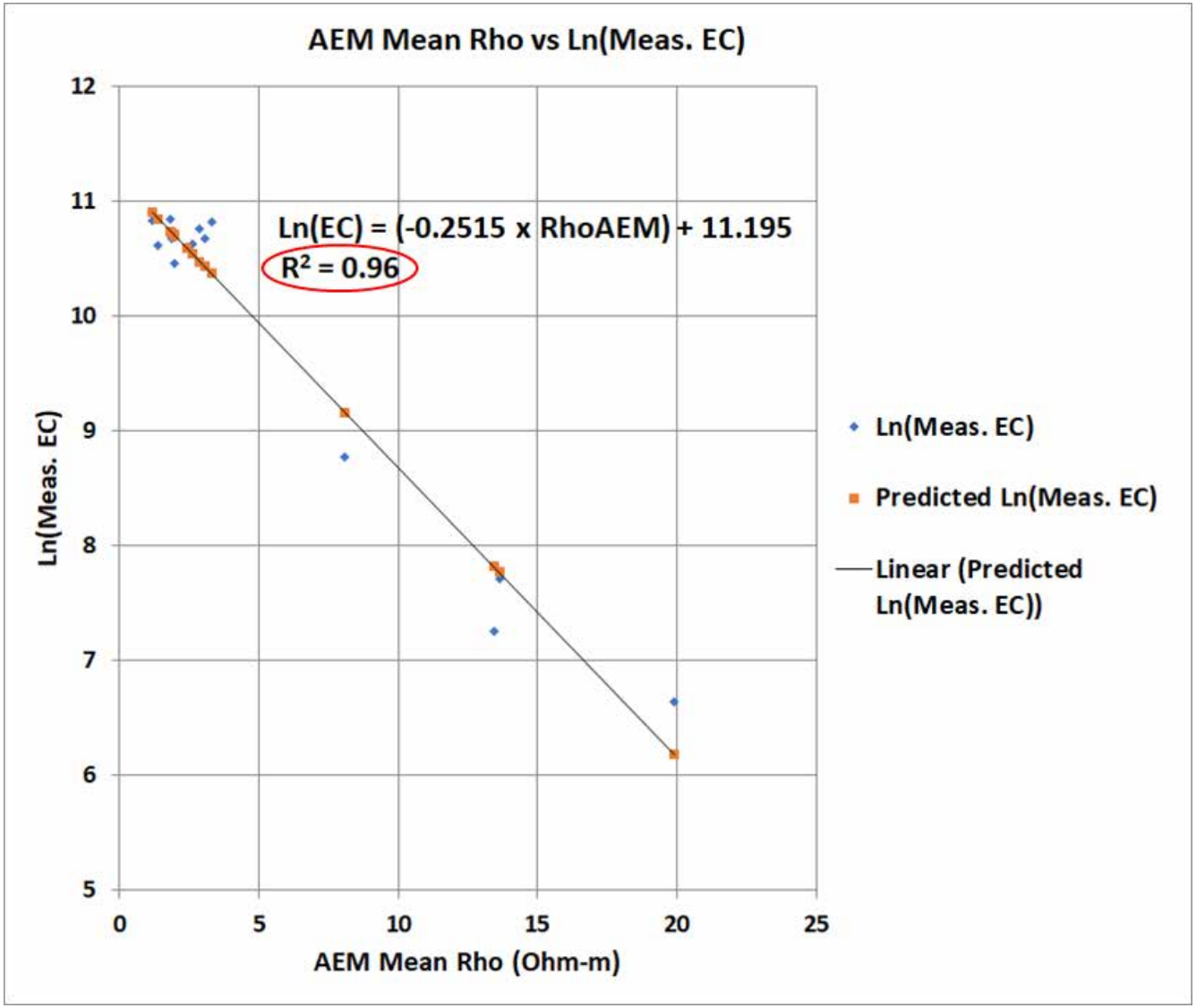

Figure 4-35. Regression relationship between the mean inverted AEM resistivity and the natural log (Ln) of the 12 measured electrical conductance (EC) data retained in Table 4-4. The R^2 is 0.96. The natural log was calculated to put both data sets at the same order of magnitude.

Table 4-3. This table indicates in the last column the final list of borehole data far from the trendline in Figure 4-33 that needed to be cut in order to produce an $R^2 = 0.96$. The last two columns list the results of applying the relationship shown in Figure 4-35 to the mean AEM resistivities. Compare the natural log of the measured EC to the predicted EC as well as the calculated specific conductance.

HoleID	Screen Top ft	Screen Bot ft	Screen Top m	Screen Bot m	Screen Interval Lithology	Meas. Spec. Cond. µS 4/24/2019 12PM	Ln(EC)	TDS Conc mg/L	Salinity mg/L	AEM Mean Rho Ohm_m	CUT	Pred. Ln(Meas. EC)	Pred. EC
MW-1S	55	95	17	29	Sand	50221	10.8	34150	32900	1.2		10.898	54053
MW-1M	115	225	35	69	Clayey Sand	51263	10.8	34900	33700	1.8		10.732	45821
MW-1D	277	327	84	100	Clayey Sand	42936	10.7	29200	27900	3.0		10.432	33922
MW-3S	50	90	15	27	Sand	40352	10.6	27400	25900	1.4		10.845	51298
MW-3M	105	215	32	66	Clayey Sand	43257	10.7	29400	28000	1.9		10.725	45465
MW-3D	285	330	87	101	Sand	46802	10.8	31800	30700	2.9		10.471	35266
MW-4S	60	100	18	30	Sand	2037	7.6	1400	1100	4.6	x	10.028	22653
MW-4M	130	260	40	79	Clayey Sand	34845	10.5	23700	33200	2.0		10.705	44559
MW-4D	290	330	88	101	Clayey Sand	40848	10.6	27800	26400	2.6		10.544	37934
MW-5S	43	83	13	25	x	NA	NA	NA	NA	11.0		8.434	4599
MW-5M	100	310	30	94	x	NA	NA	NA	NA	18.1		6.653	775
MW-5D	395	435	120	133	Sand	6450	8.8	4400	3600	8.1		9.158	9489
MW-6S	30	60	9	18	Sand	2240	7.7	1500	1200	13.6		7.770	2367
MW-6M	150	210	46	64	Sand	1412	7.3	1000	710	13.4		7.815	2477
MW-6D	255	325	78	99	Sand	1833	7.5	3300	2600	9.2	x	8.886	7232
MW-7S	60	80	18	24	Sand	1478	7.3	1000	800	24.9	x	4.933	139
MW-7M	130	220	40	67	x	NA	NA	NA	NA	9.5		8.813	6723
MW-7D	295	345	90	105	Sand	40180	10.6	27300	25900	2.3		10.617	40805
MW-8S	40	80	12	24	Sand	762	6.6	500	400	19.9		6.185	485
MW-8M	125	215	38	66	Sand	49993	10.8	34000	32900	3.3		10.365	31731
MW-8D	300	350	91	107	Sand	1375	7.2	900	700	9.5	x	8.806	6673
MW-9S	30	110	9	34	Silty Sand	4805	8.5	3300	2600	5.8	x	9.741	17006
MW-9M	145	225	44	69	Sand	43607	10.7	29700	28300	2.0		10.695	44113
MW-9D	353	393	108	120	Clayey Sand	295	5.7	405	300	12.1	x	8.144	3444

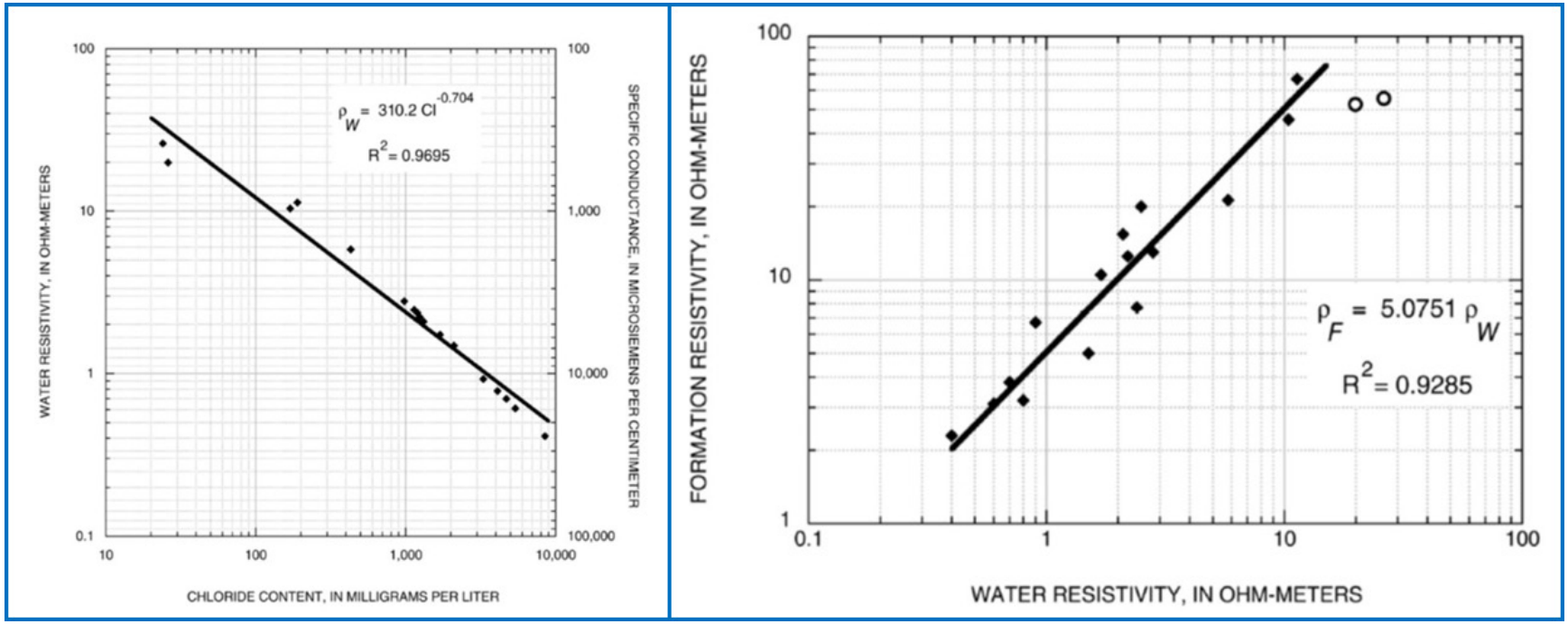

Figure 4-36. Regression relationships between chloride concentration and water resistivity on the left and between water resistivity and inverted bulk resistivity on the right (from Fitterman and Prinos, 2011).

4.5 2019 MCWD AEM Resistivity and Chloride Concentration 2D Profiles

In this section and the sections that follow comparisons are made, initially, between the MCWD 2019 AEM inverted resistivities and the chloride concentration distribution as calculated per the Fitterman and Prinos (2011) relations and then between the MCWD 2017 and 2019 results.

It is important to note that when one examines the AEM resistivity earth-model profiles, and the corresponding chloride concentration profiles, the examiner must keep in mind that they are looking at geologic materials, most containing water, that are being represented as chloride concentrations. For example, unsaturated alluvium on the surface, having a higher electrical resistivity because of the dry material, converts to a low equivalent "chloride concentration". Unsaturated dry surface material, having a high resistivity converts to a low chloride concentration even though it has nothing to do with water quality. Thus, the reader must keep the nature of the basic geology in the area (Dune Sand material, 180 ft aquifer, 180ft/400ft aquitard, 400 ft aquifer) in mind when examining the 2D profiles, 3D fence diagrams, depth slices, and 3D voxels of chloride concentrations.

The displayed chloride concentration range is presented in Figure 4-37.

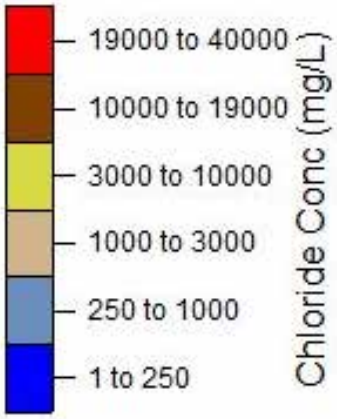

Figure 4-37. Presented chloride concentration distribution.

The same 2D profiles as were presented in Section 4.2 showing just the inverted AEM resistivities in comparison with the geophysical logs are now presented again in comparison with 2D profiles of the calculated chloride concentrations. Figure 4-38 presents flight line L200101, Figure 4-39 presents flight line L200200, Figure 4-40 presents flight line L200400, Figure 4-41 presents flight line L201700, Figure 4-42 presents flight line L202500, Figure 4-43 presents flight line L206800, and Figure 4-44 presents flight line L212200, 3D fence diagrams of the MCWD 2019 interpreted chloride concentrations are presented looking to the east (Figure 4-45), to the northeast (Figure 4-46), to the north (Figure 4-47), and looking to the south (Figure 4-48).

All the 2D profile comparisons of the MCWD 2019 AEM resistivities and chloride concentrations can be found in Appendix 1-2D Profiles and the 3D Fence Diagram views in Appendix 2 – 3D Images.

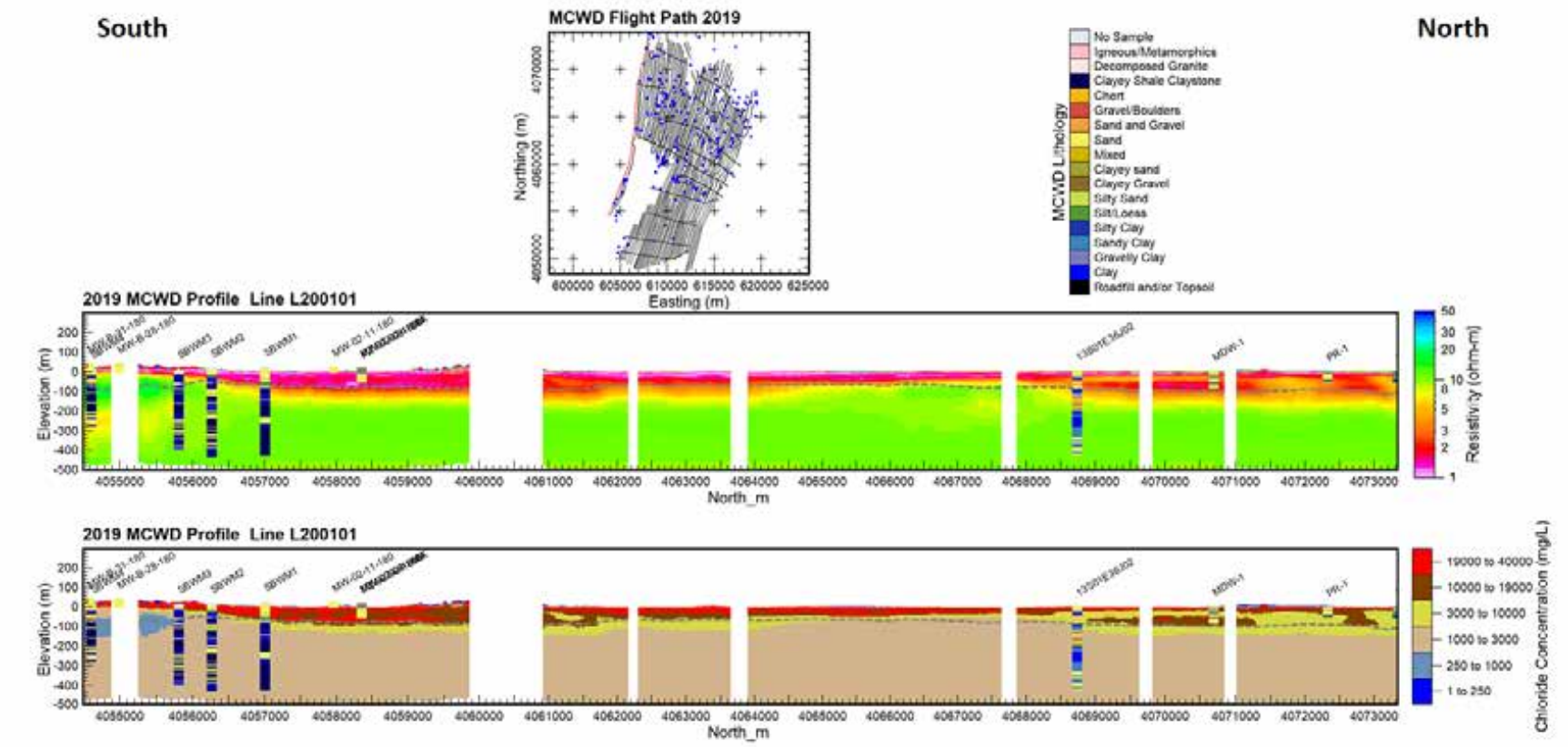

Figure 4-38. Inverted AEM resistivity and calculated chloride concentration profiles of MCWD 2019 AEM survey line L200101 with lithological and geophysical 16-inch Short Normal electrical logs (green dots on map) using the same resistivity scale. The projection is NAD83 UTM Zone 10N (meters) and the elevation values are referenced to NAVD 88 (meters).

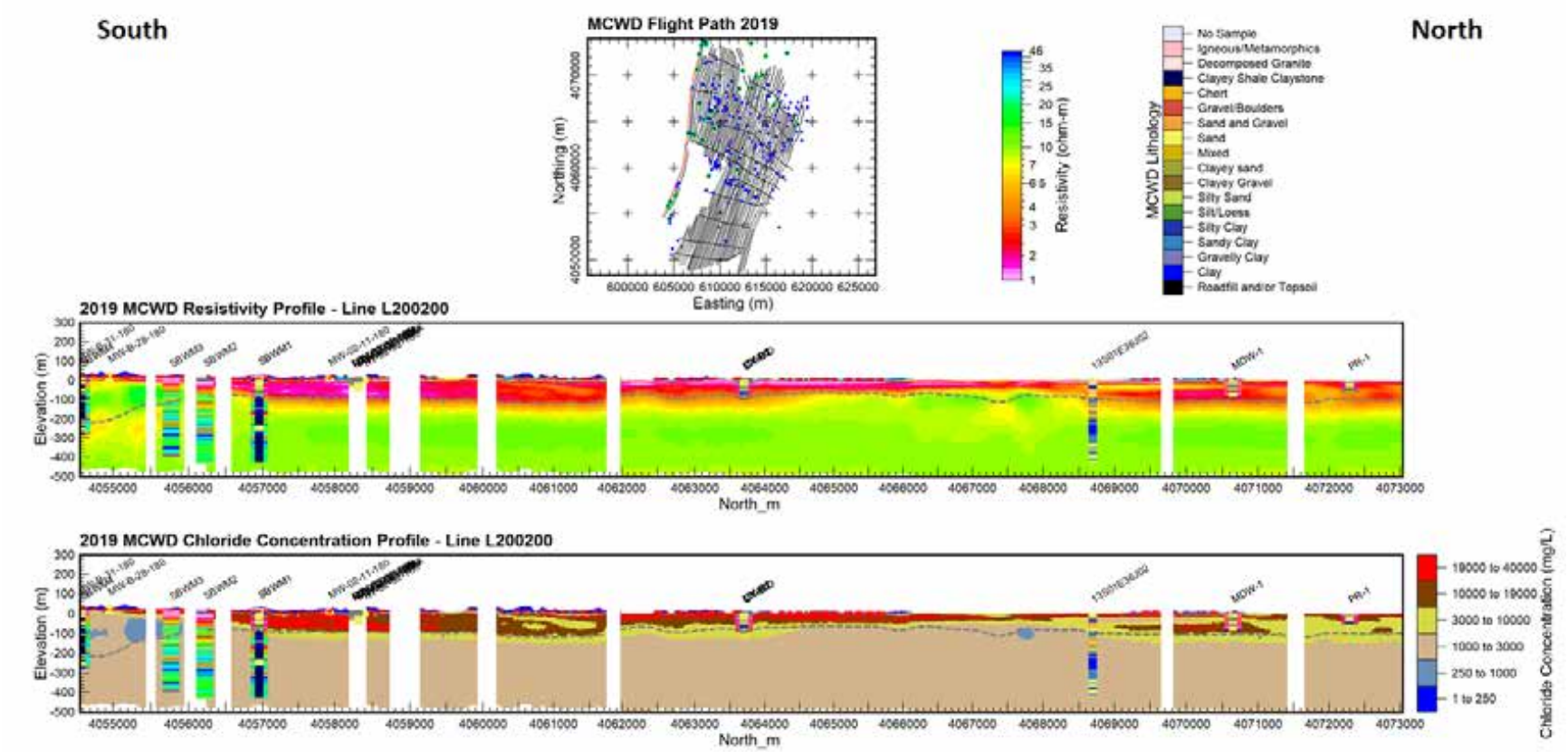

Figure 4-39. Inverted AEM resistivity and calculated chloride concentration profiles of MCWD 2019 AEM survey line L200200 with lithological and geophysical 16-inch Short Normal electrical logs (green dots on map) using the same resistivity scale. The projection is NAD83 UTM Zone 10N (meters) and the elevation values are referenced to NAVD 88 (meters).

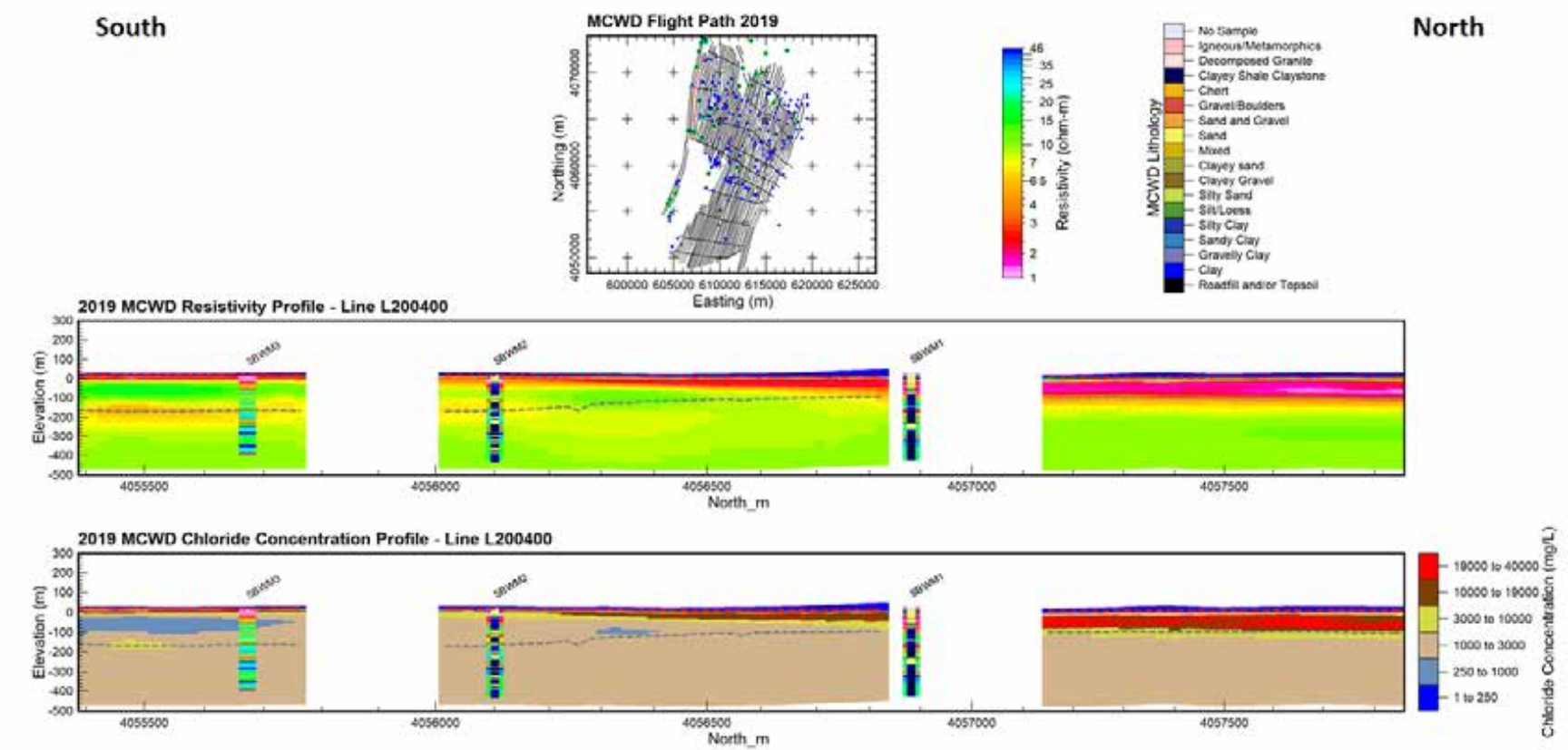

Figure 4-40. Inverted AEM resistivity and calculated chloride concentration profiles of MCWD 2019 AEM survey line L200400 with lithological and geophysical 16-inch Short Normal electrical logs (green dots on map) using the same resistivity scale. The projection is NAD83 UTM Zone 10N (meters) and the elevation values are referenced to NAVD 88 (meters).

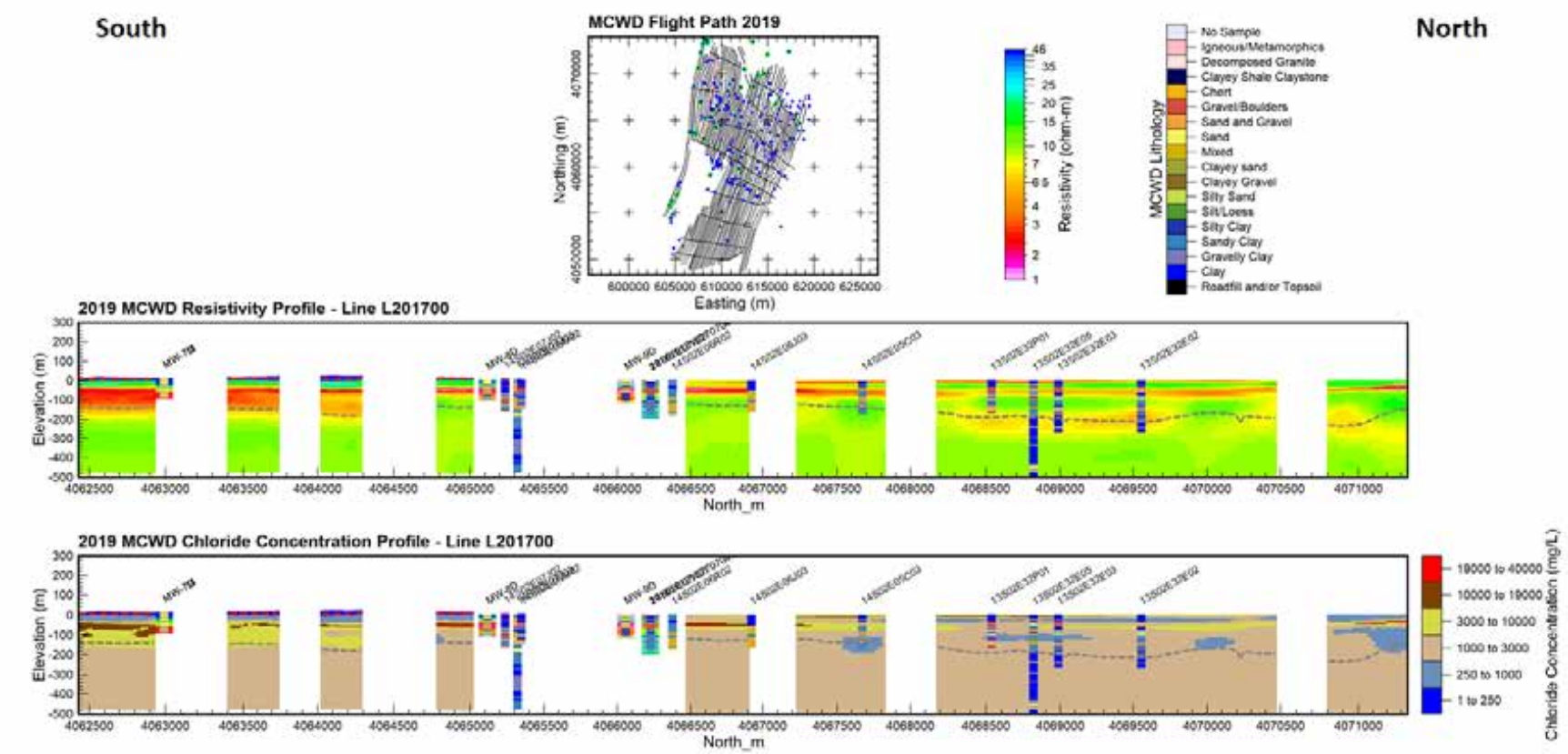

Figure 4-41. Inverted AEM resistivity and calculated chloride concentration profiles of MCWD 2019 AEM survey line L201700 with lithological and geophysical 16-inch Short Normal electrical logs (green dots on map) using the same resistivity scale. The projection is NAD83 UTM Zone 10N (meters) and the elevation values are referenced to NAVD 88 (meters).

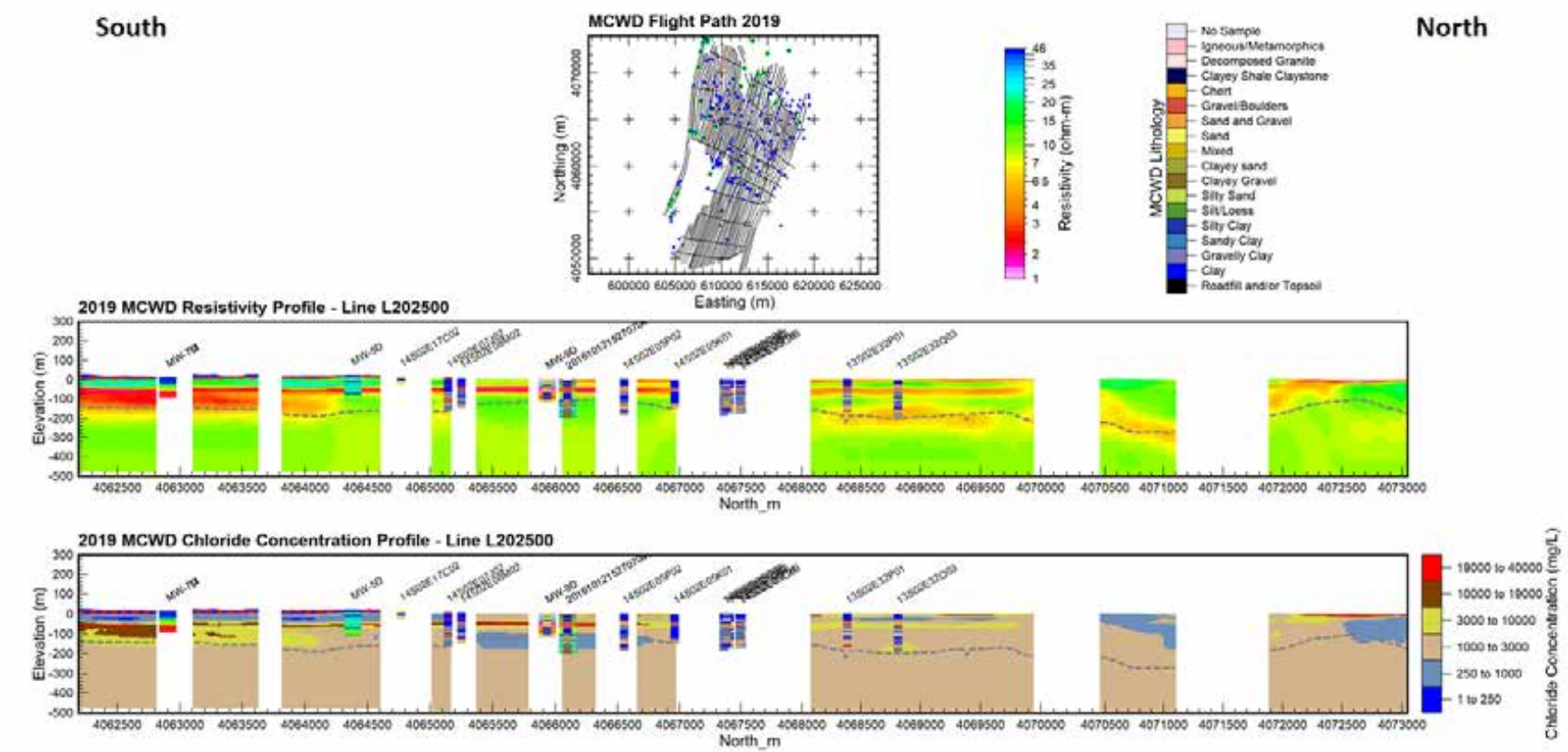

Figure 4-42. Inverted AEM resistivity and calculated chloride concentration profiles of MCWD 2019 AEM survey line L202500 with lithological and geophysical 16-inch Short Normal electrical logs (green dots on map) using the same resistivity scale. The projection is NAD83 UTM Zone 10N (meters) and the elevation values are referenced to NAVD 88 (meters).

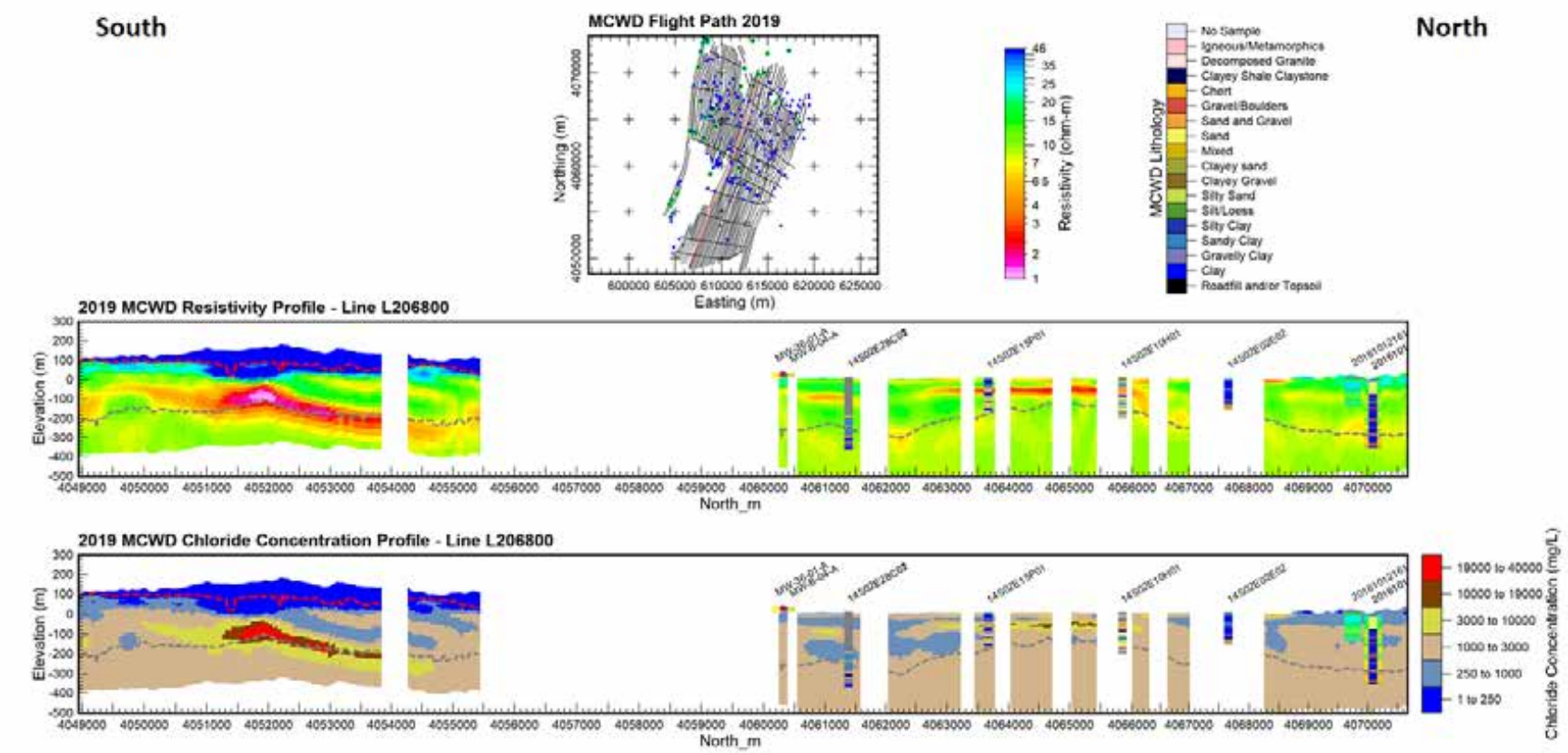

Figure 4-43. Inverted AEM resistivity and calculated chloride concentration profiles of MCWD 2019 AEM survey line L206800 with lithological and geophysical 16-inch Short Normal electrical logs (green dots on map) using the same resistivity scale. The projection is NAD83 UTM Zone 10N (meters) and the elevation values are referenced to NAVD 88 (meters).

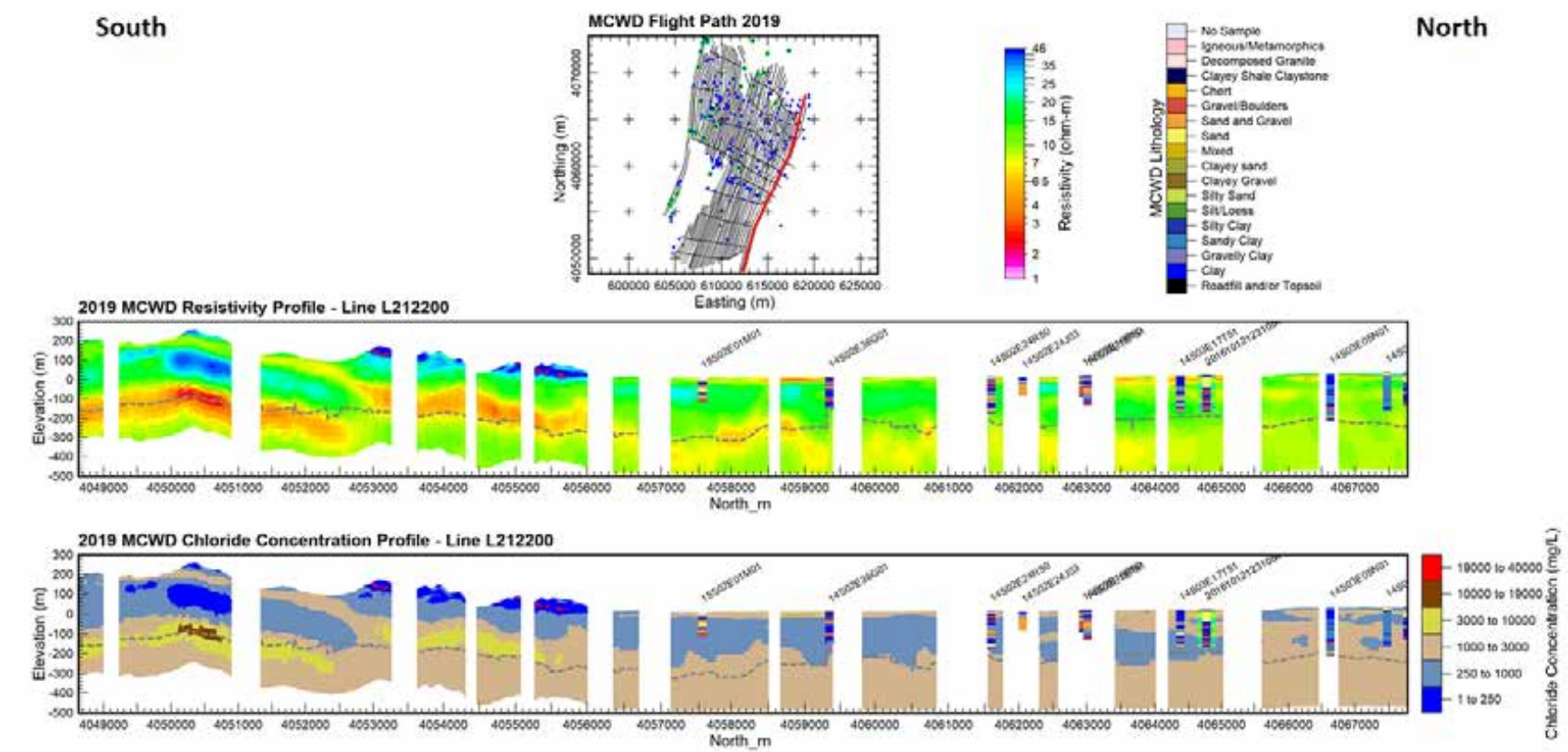

Figure 4-44. Inverted AEM resistivity and calculated chloride concentration profiles of MCWD 2019 AEM survey line L212200 with lithological and geophysical 16-inch Short Normal electrical logs (green dots on map) using the same resistivity scale. The projection is NAD83 UTM Zone 10N (meters) and the elevation values are referenced to NAVD 88 (meters).

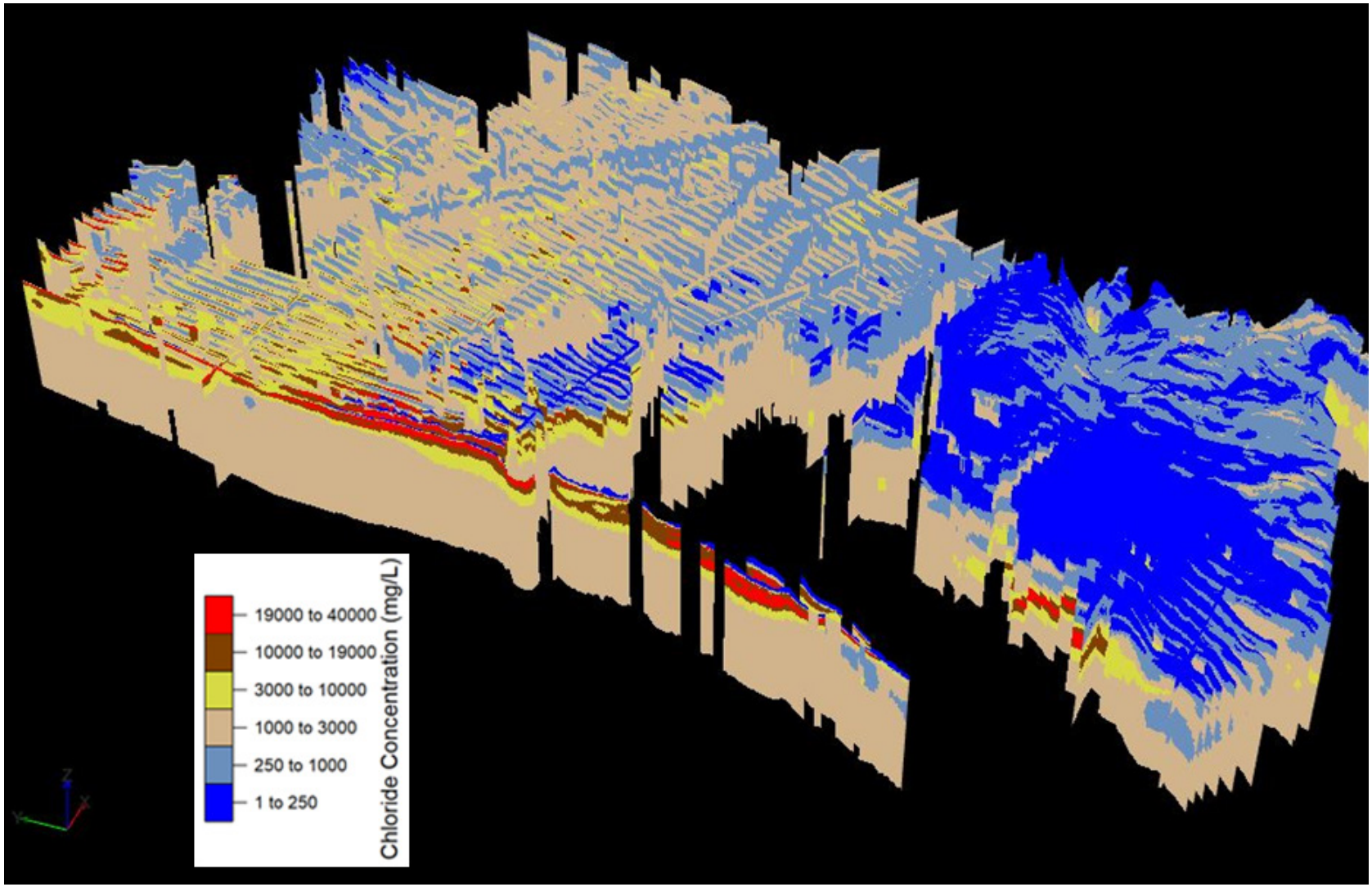

Figure 4-45. 3D fence diagram of MCWD 2019 inverted AEM resistivity and calculated chloride concentrations, looking to the east. V.E.=x10.

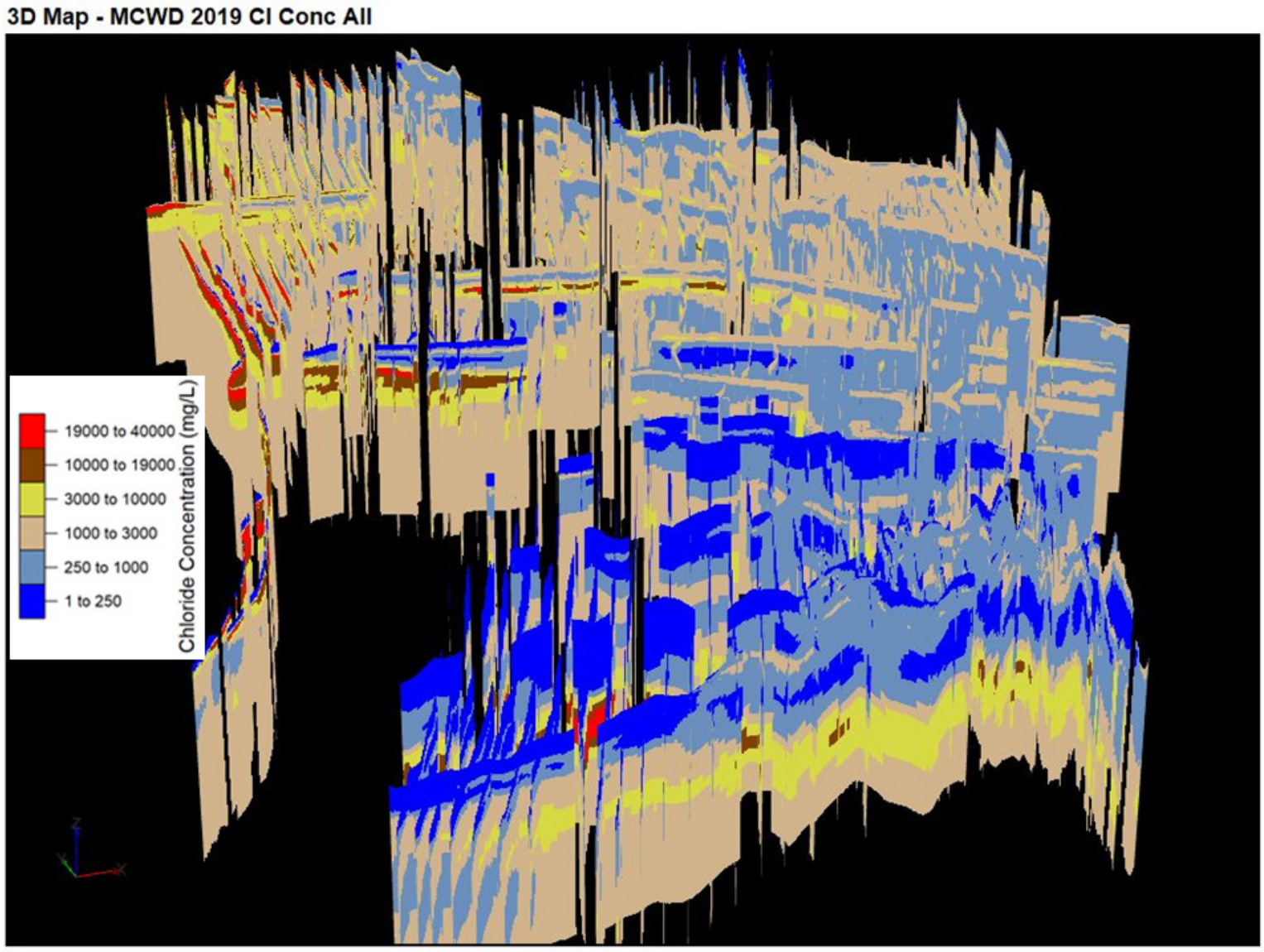

Figure 4-46. 3D fence diagram of MCWD 2019 inverted AEM resistivity and calculated chloride concentrations, looking to the northeast. V.E.=x10.

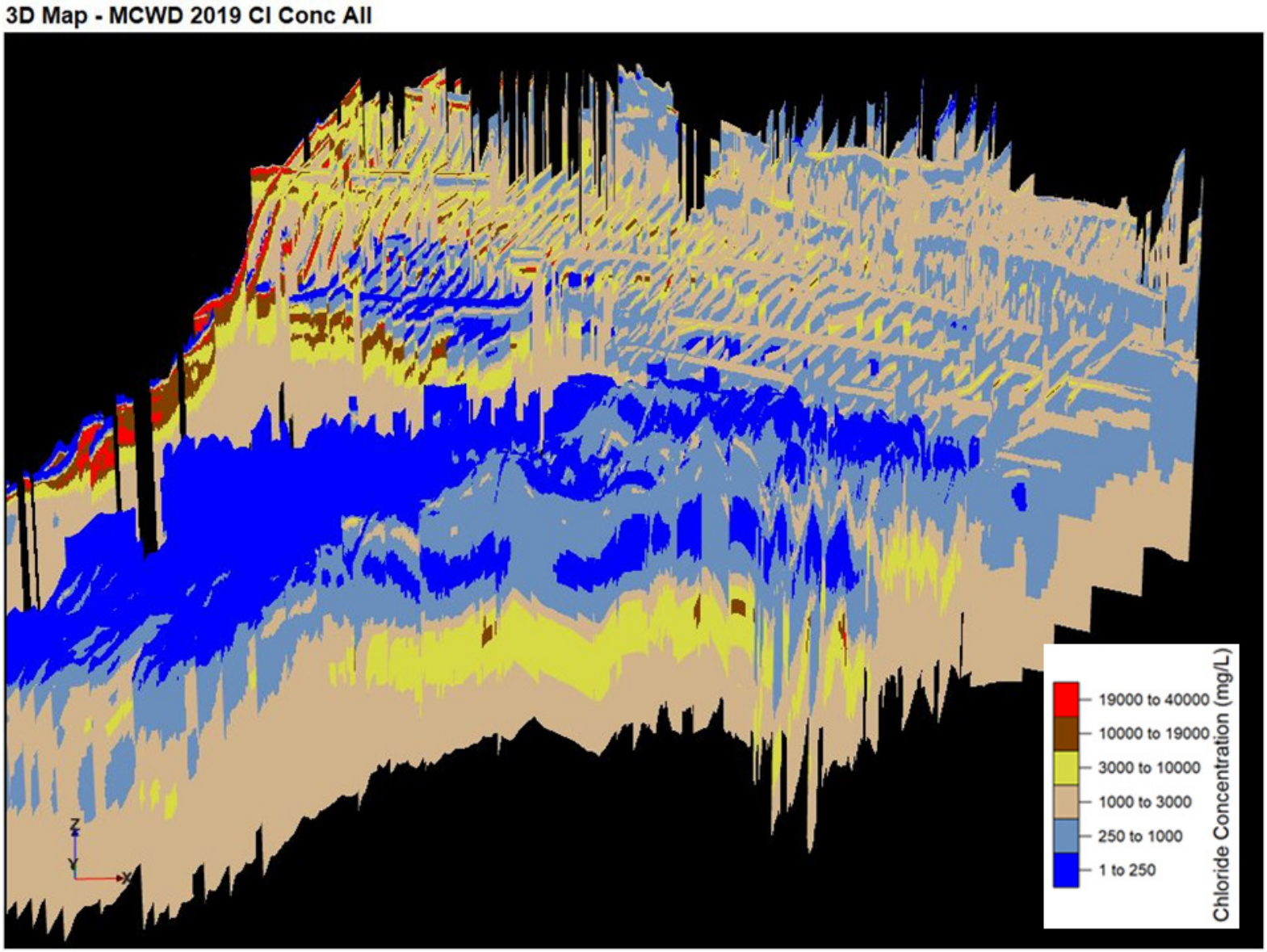

Figure 4-47. 3D fence diagram of MCWD 2019 inverted AEM resistivity and calculated chloride concentrations, looking to the north. V.E.=x10.

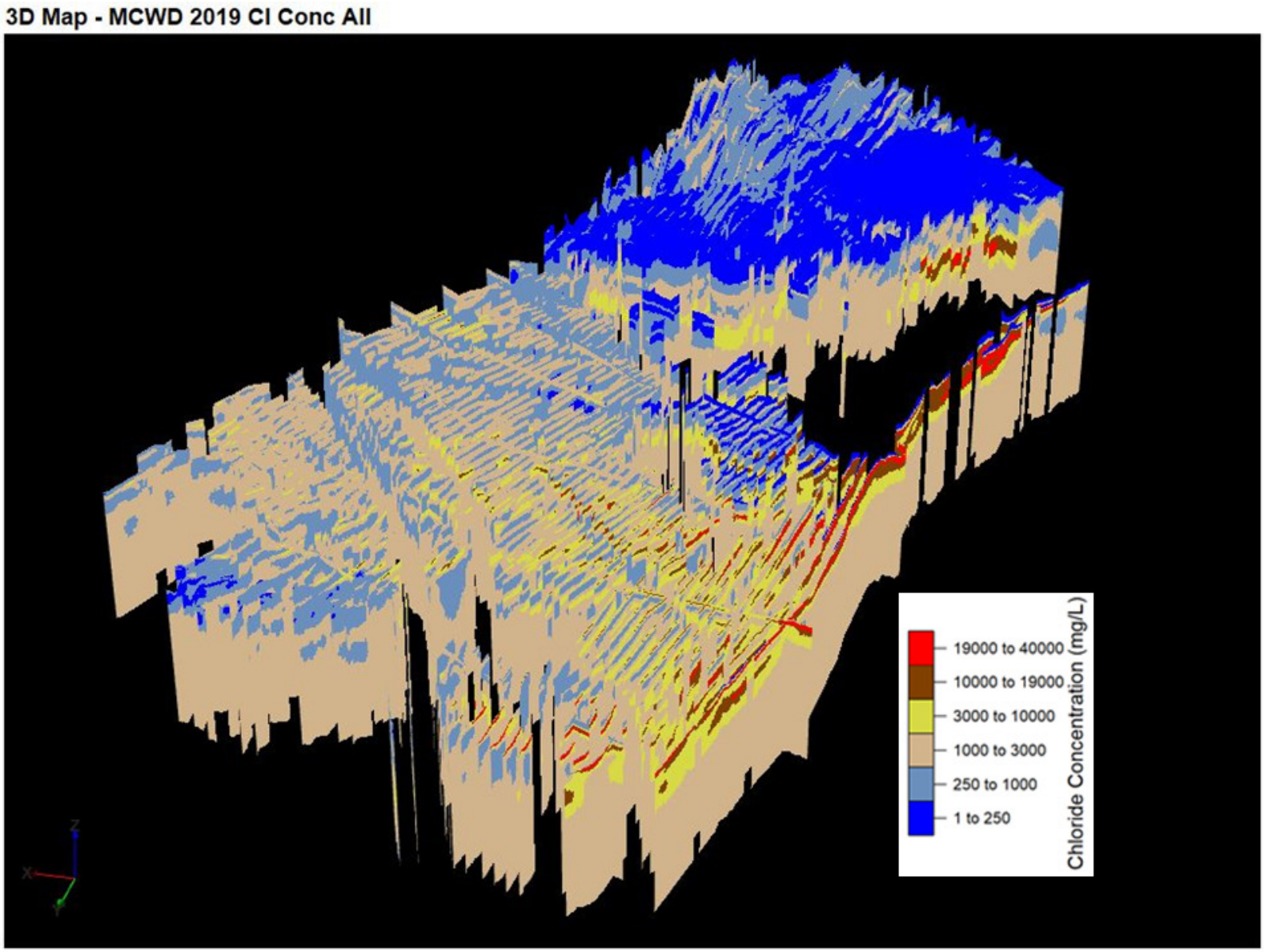

Figure 4-48. 3D fence diagram of MCWD 2019 inverted AEM resistivity and calculated chloride concentrations, looking to the south. V.E.=x10.

4.6 Comparison of MCWD 2017 and 2019 AEM Chloride Concentration Distributions – 2D Profiles, Depth Slices, Northing Slices, Easting Slices

Comparison 2019-2017 CLconc 2D profiles

Comparison 2019-2017 Depth Slices

Comparison 2019-2017 Northing Slices

Comparison 2019-2017 Easting Slices

Comparison 2019-2017 Voxel slices.

Comparison 2019-2017 Voxel Ranges BelowRho75om-m_1-500_10000-40000

Included in this section are comparisons of the MCWD 2017 AEM survey results and the 2019 AEM survey results via the calculated chloride concentrations. The comparisons are presented in multiple formats. First as 2D profiles: L200101-Figure 4-49, L200202-Figure 4-50, L200501-Figure 4-51, L201201-Figure 4-52, L204001-Figure 4-53, L204701-Figure 4-54, L206801-Figure 4-55, L100501-Figure 4-56.

Next, the comparisons are made using 3D voxels. An example of the full 3D voxel of the MCWD 2019 AEM-calculated estimated chloride concentrations is presented in Figure 4-57.

The 3D voxel can be cut into depth slices and the 2017 and 2019 results compared: -4 m/-13 ft – Figure 4-58, -23 m/-75 ft – Figure 4-59, -47 m/-154 ft – Figure 4-60, -56 m/-184 ft – Figure 4-61, -80 m/-263 ft – Figure 4-62, -100 m/-328 ft – Figure 4-63, -133 m/-436 ft – Figure 4-64.

Examples of the voxels being cut along UTM eastings and northings (in meters) are presented in Figure 4-65 (at Easting 611450), Figure 4-66 (at Easting 615450), and Figure 4-67 (at Northing 4062400).

Finally, the display of the 3D voxels can be “thresholded” to show only certain chloride concentration ranges. This allows for visual comparisons between different chloride concentration ranges of interest. Figure 4-68 shows what appears to be a single 3D voxel. Actually, it is composed of six (6) ranges with all ranges displayed. Figure 4-69 presents the same 3D voxel with the 1,000 mg/L to 3,000 mg/L (1k-3k) display turned off and only ranges 1-500 mg/L and 3,000-40,000 mg/L (10k-40k) displayed. Figure 4-70 presents a comparison of the estimated chloride concentrations from the MCWD 2017 and 2019 investigations displaying only estimated chloride concentration ranges 1-500 mg/L and 10k-40k mg/L (no 1k-3k mg/L and 3k to 10k mg/L ranges) with a view looking to the east. Figure 4-71 shows the same ranges as Figure 4-70 but the view is to the north.

All the 2D profile comparisons can be found in Appendix 1 – 2D Profiles. Additional 3D voxel images can be found in Appendix 2 – 3D Images. In addition, a 3D voxel Datamine Discover PA session (Datamine Discover, 2019) has been developed that can be opened in a Datamine Discover PA viewer program (the setup and data files are in Appendix 3-Deliverables/Voxel/PA). Figure 4-72 presents a screen capture of the Datamine Discover PA Viewer (Datamine Discover PA, 2019) session. The operator can change views of the 2019 inverted resistivity and estimated chloride concentrations as well as change which ranges are displayed for the MCWD 2017 and 2019 AEM investigations.

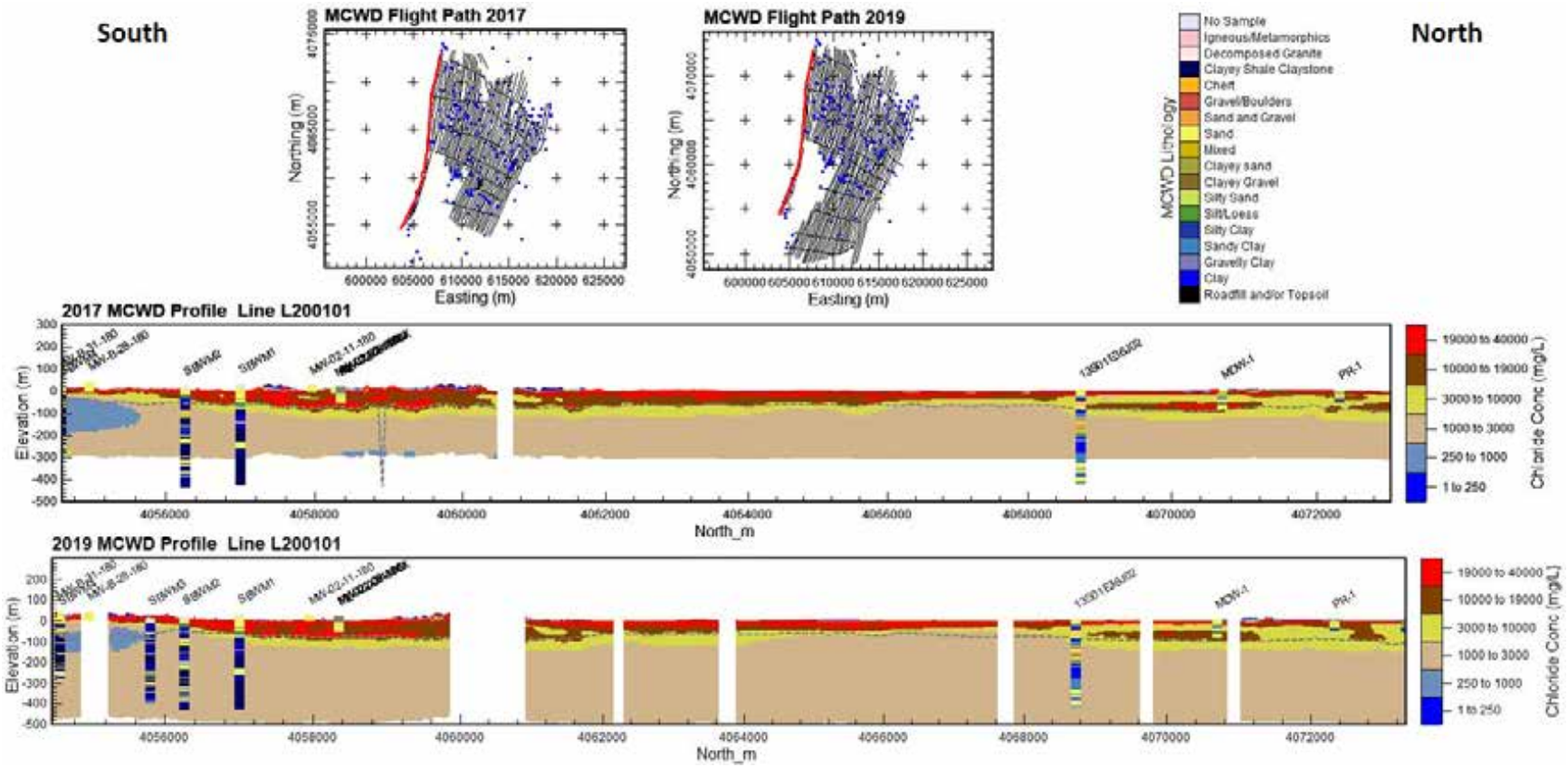

Figure 4-49. Comparison of MCWD 2017 (top) and 2019 (bottom) calculated chloride concentrations along flight line L200101 with lithology logs within 250 m of the flight line. The projection is NAD83, UTM 10N, meters, and the elevation values are referenced to NAVD 88, meters.

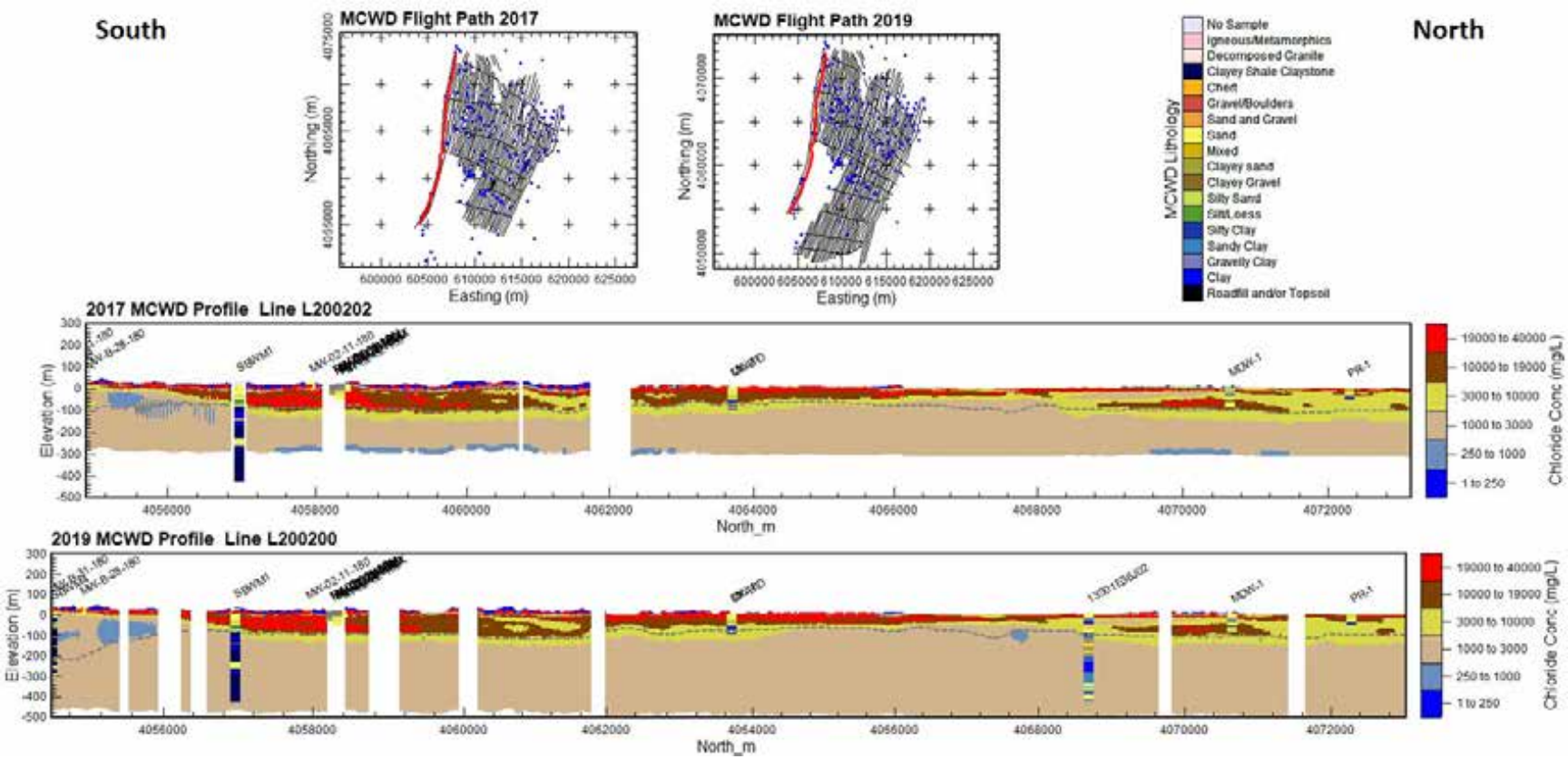

Figure 4-50. Comparison of MCWD 2017 (top) and 2019 (bottom) calculated chloride concentrations along flight line L200202/L200200 with lithology logs within 250 m of the flight line. The projection is NAD83, UTM 10N, meters, and the elevation values are referenced to NAVD 88, meters.

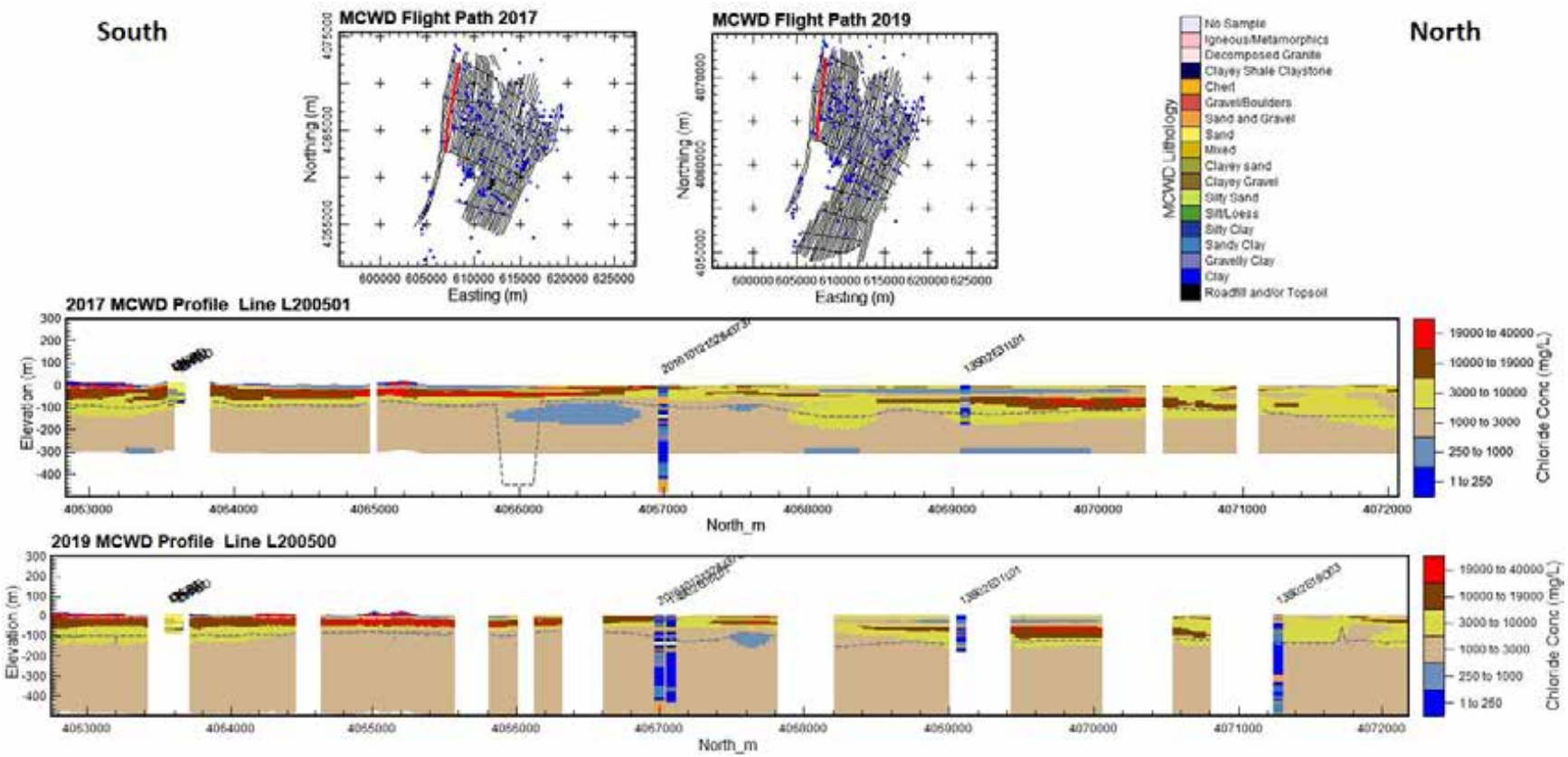

Figure 4-51. Comparison of MCWD 2017 (top) and 2019 (bottom) calculated chloride concentrations along flight line L200501/L200500 with lithology logs within 250 m of the flight line. The projection is NAD83, UTM 10N, meters, and the elevation values are referenced to NAVD 88, meters.

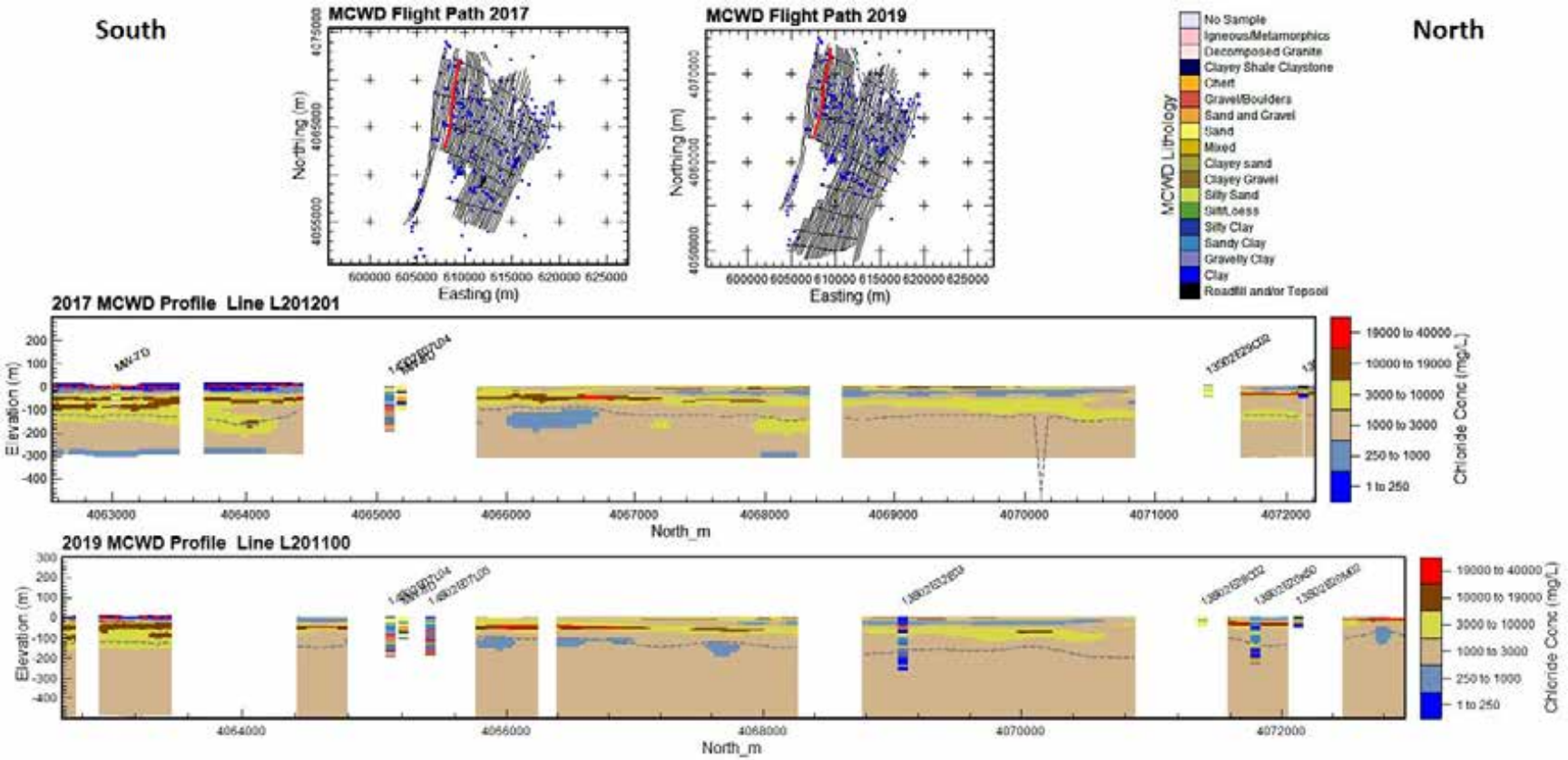

Figure 4-52. Comparison of MCWD 2017 (top) and 2019 (bottom) calculated chloride concentrations along flight line L201201 with lithology logs within 250 m of the flight line. The projection is NAD83, UTM 10N, meters, and the elevation values are referenced to NAVD 88, meters.

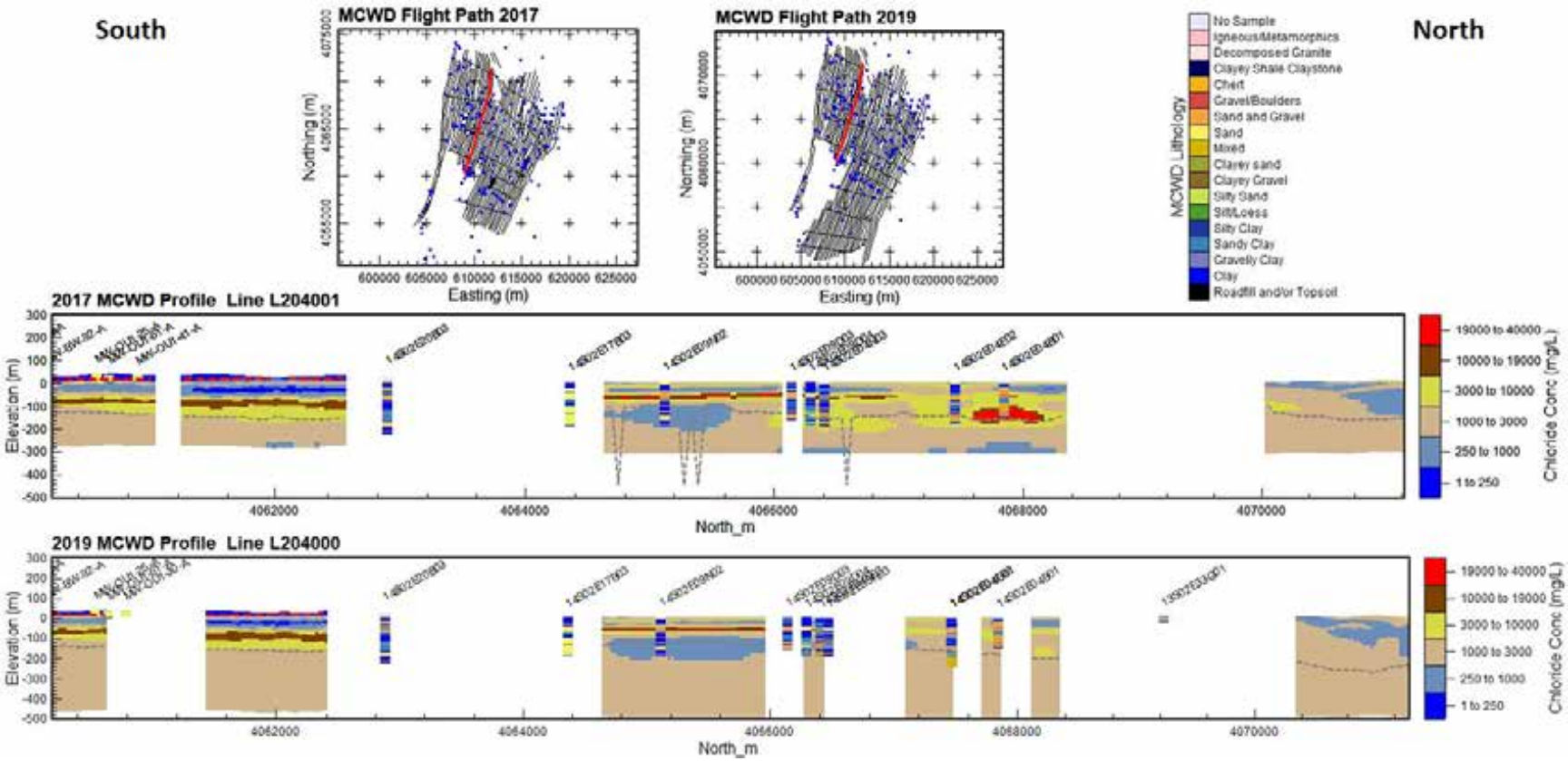

Figure 4-53. Comparison of MCWD 2017 (top) and 2019 (bottom) calculated chloride concentrations along flight line L204001/L204000 with lithology logs within 250 m of the flight line. The projection is NAD83, UTM 10N, meters, and the elevation values are referenced to NAVD 88, meters.

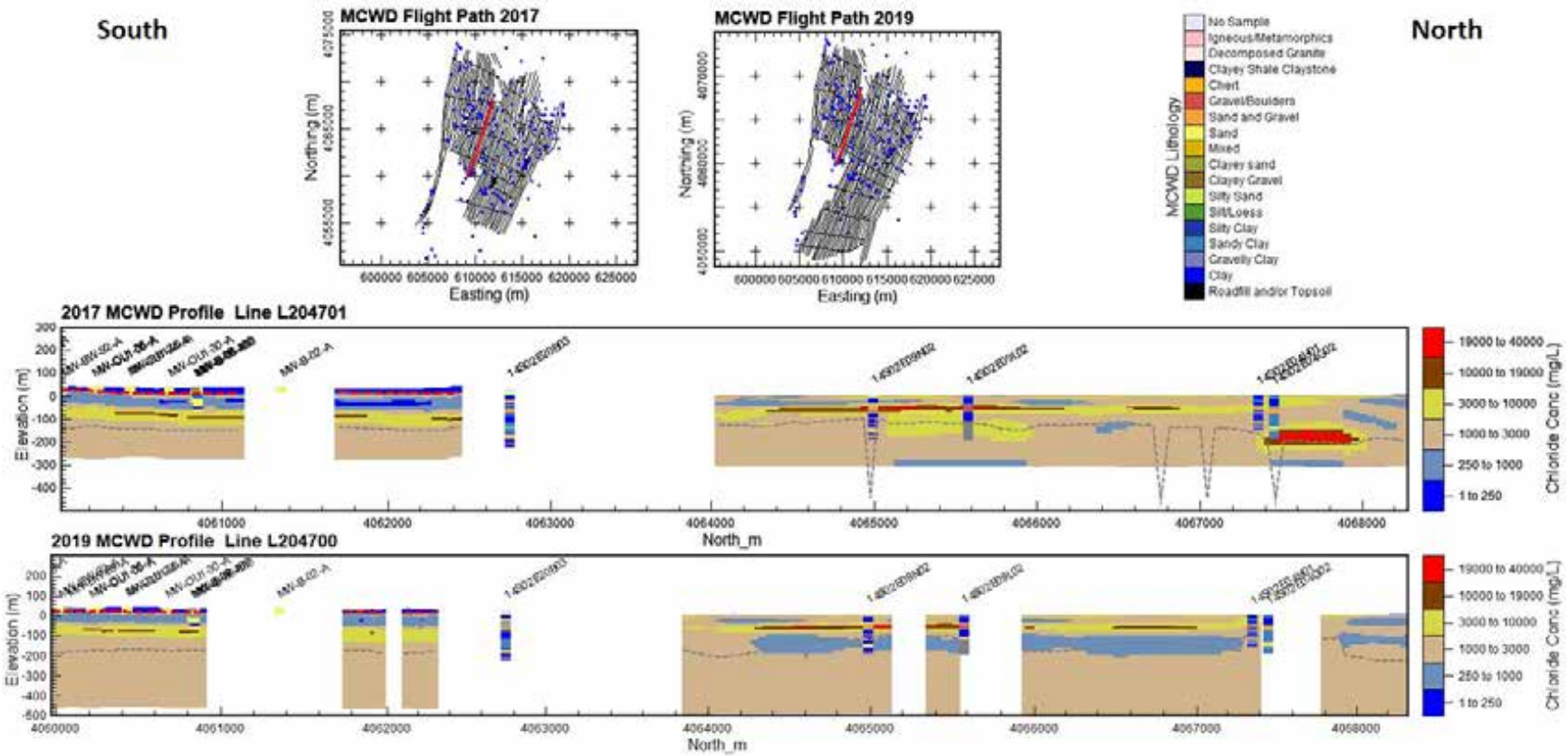

Figure 4-54. Comparison of MCWD 2017 (top) and 2019 (bottom) calculated chloride concentrations along flight line L204701/L204700 with lithology logs within 250 m of the flight line. The projection is NAD83, UTM 10N, meters, and the elevation values are referenced to NAVD 88, meters.

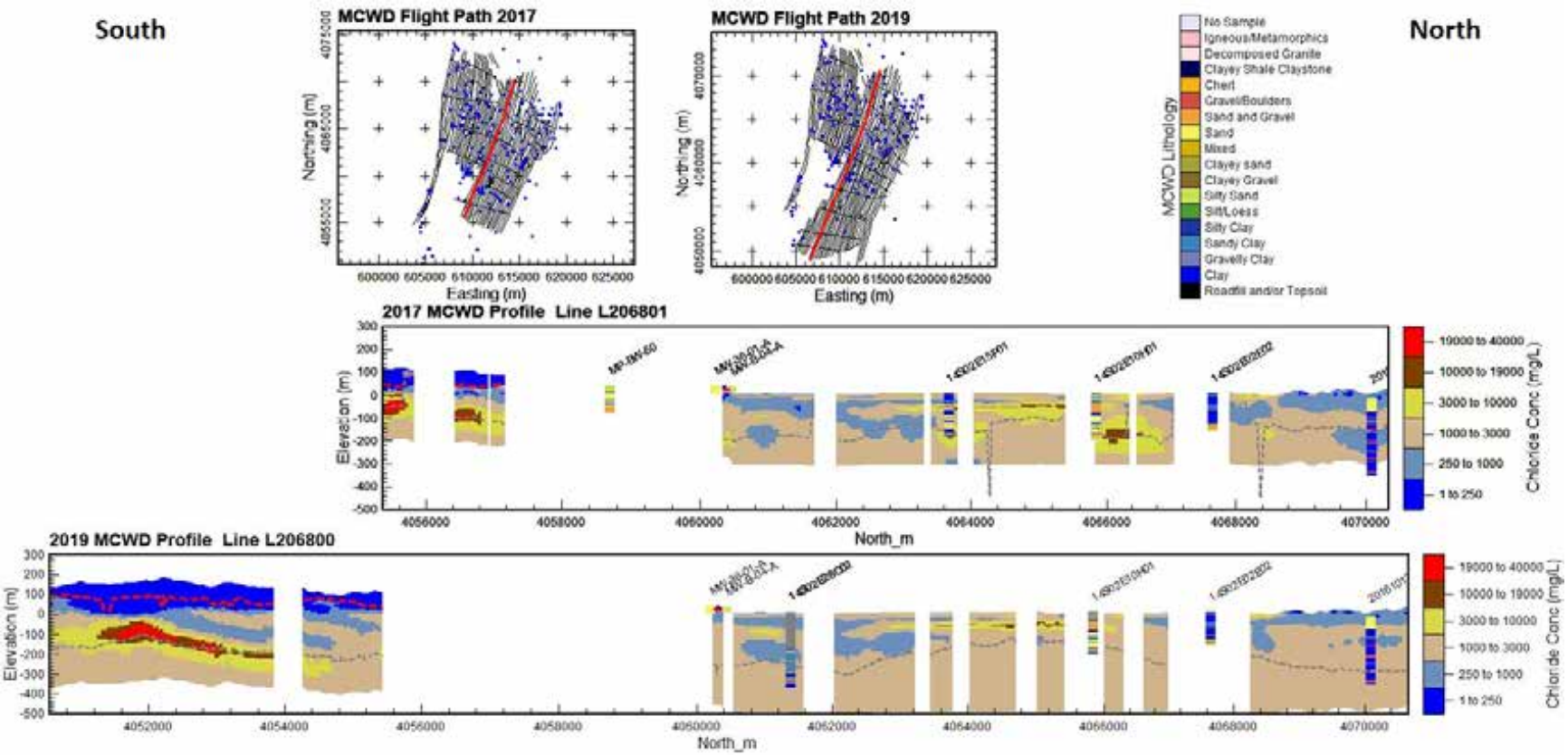

Figure 4-55. Comparison of MCWD 2017 (top) and 2019 (bottom) calculated chloride concentrations along flight line L206801/L206800 with lithology logs within 250 m of the flight line. The projection is NAD83, UTM 10N, meters, NAVD88 me and the elevation values are referenced to NAVD 88, meters.

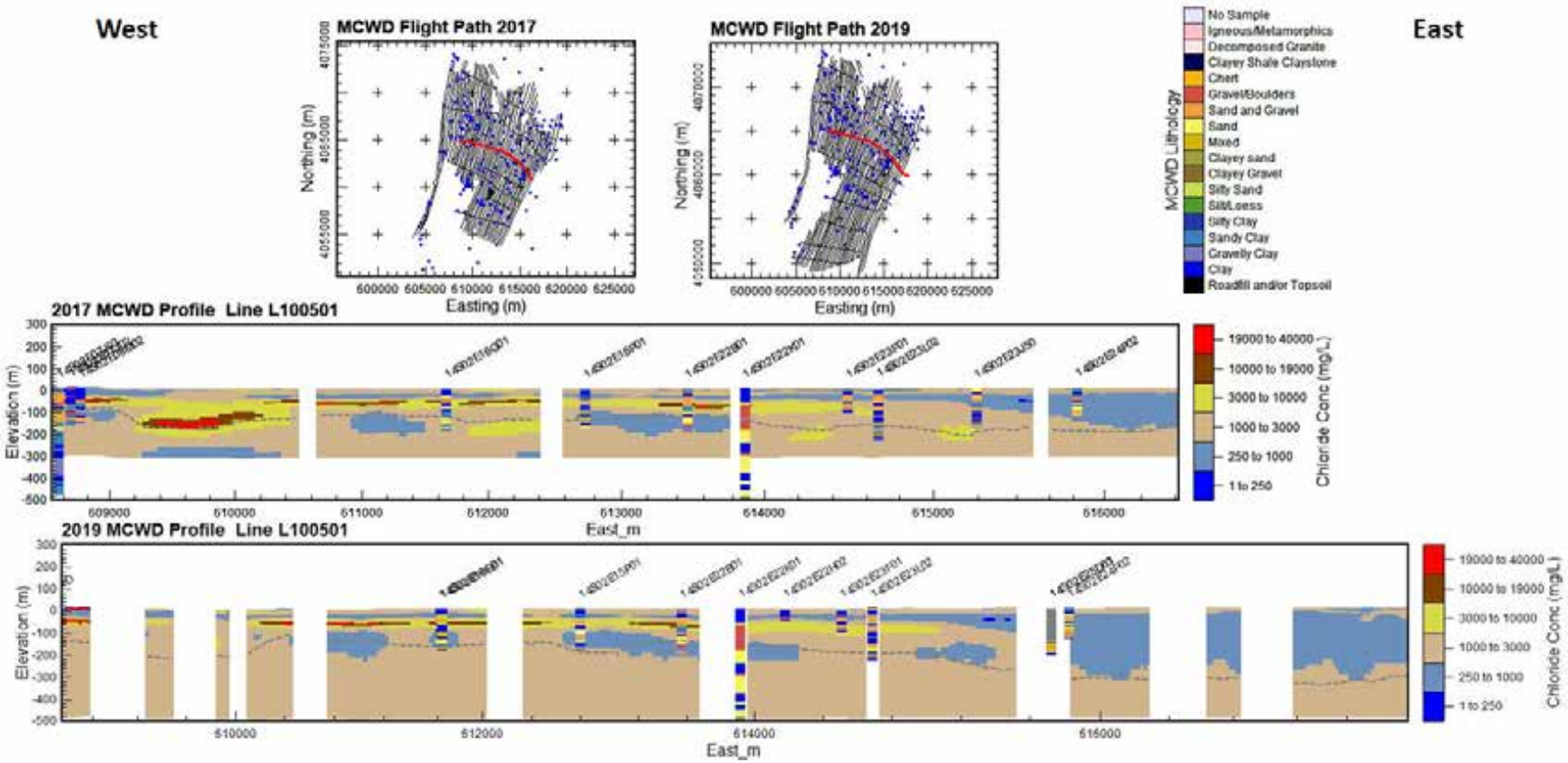

Figure 4-56. Comparison of MCWD 2017 (top) and 2019 (bottom) calculated chloride concentrations along flight line L100501 with lithology logs within 250 m of the flight line. The projection is NAD83, UTM 10N, meters, and the elevation values are referenced to NAVD 88, meters.

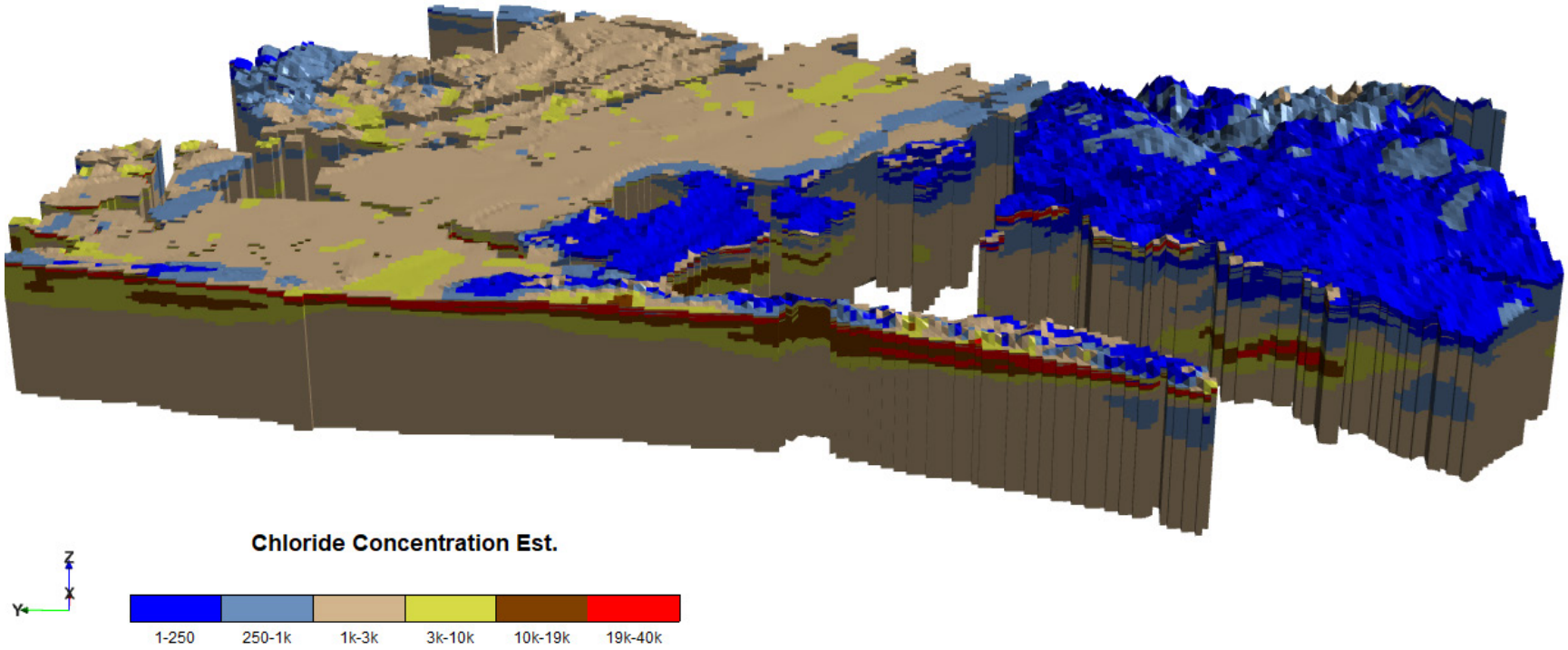

Figure 4-57. 3D voxel of the MCWD 2019 AEM-derived estimated chloride concentrations with a view to the east. V.E.=x5.

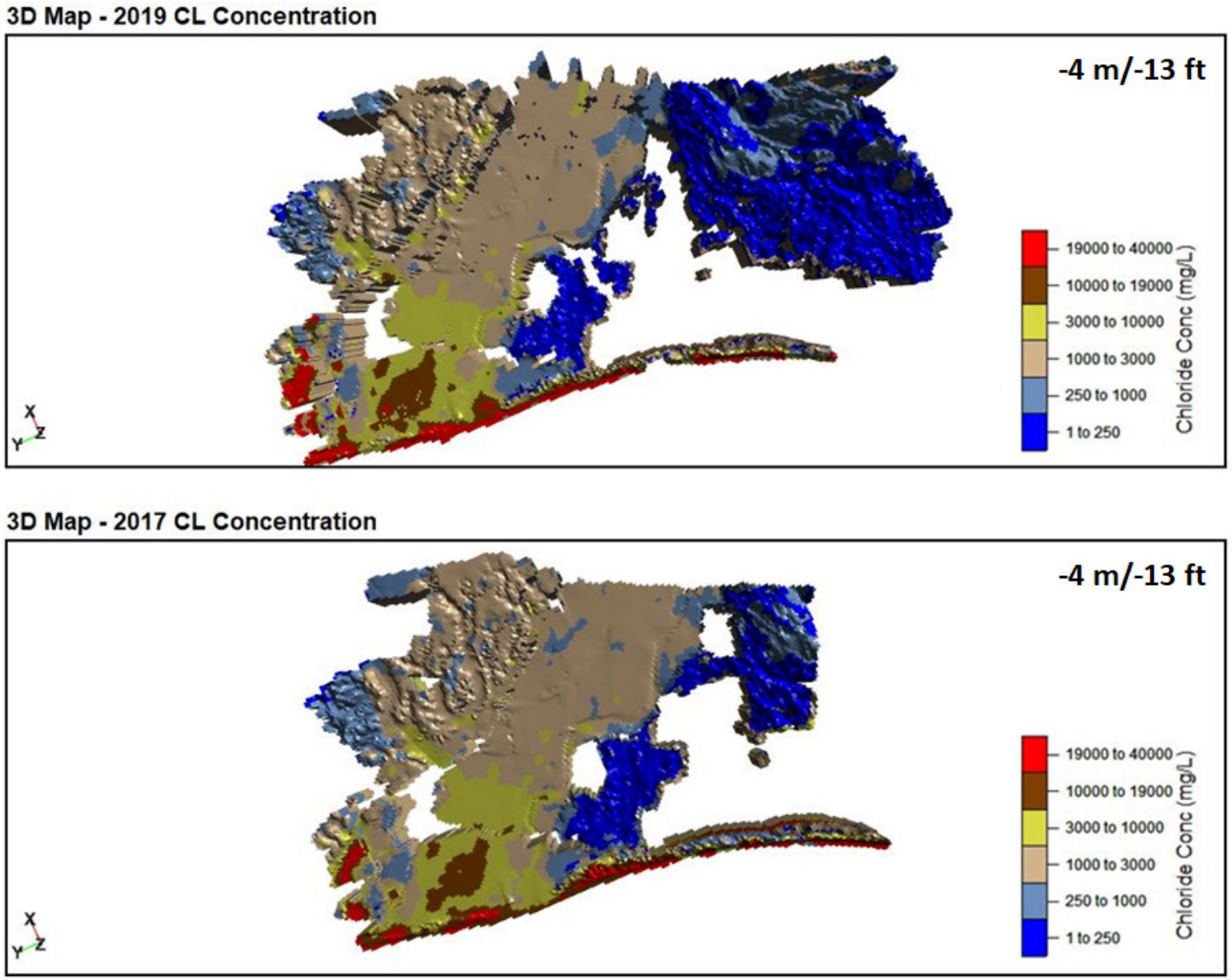

Figure 4-58. Depth slice comparison at -4 m/-13 ft of MCWD 2017 and 2019 AEM investigations via calculated chloride concentrations.

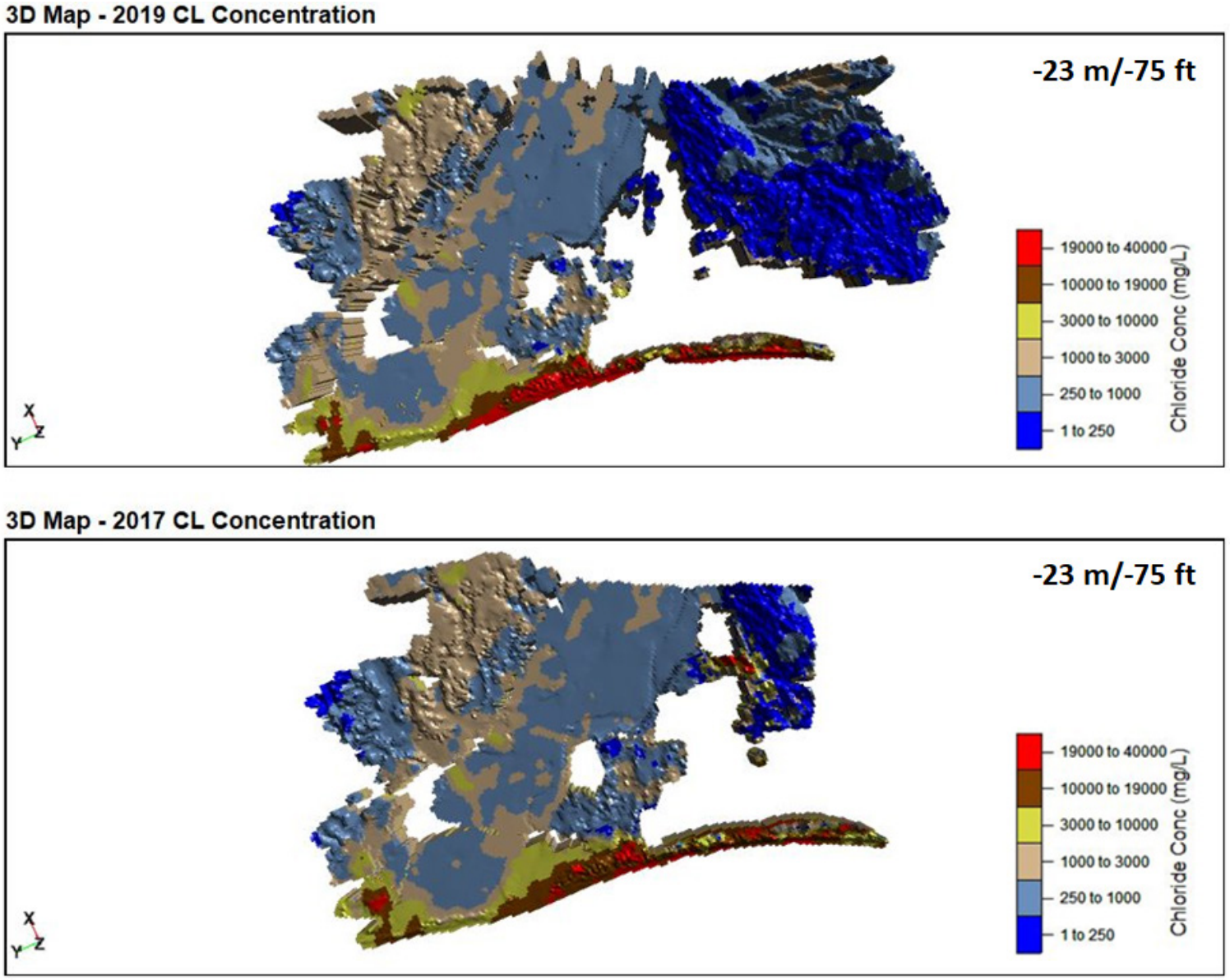

Figure 4-59. Depth slice comparison at -23 m/-75 ft of MCWD 2017 and 2019 AEM investigations via calculated chloride concentrations.

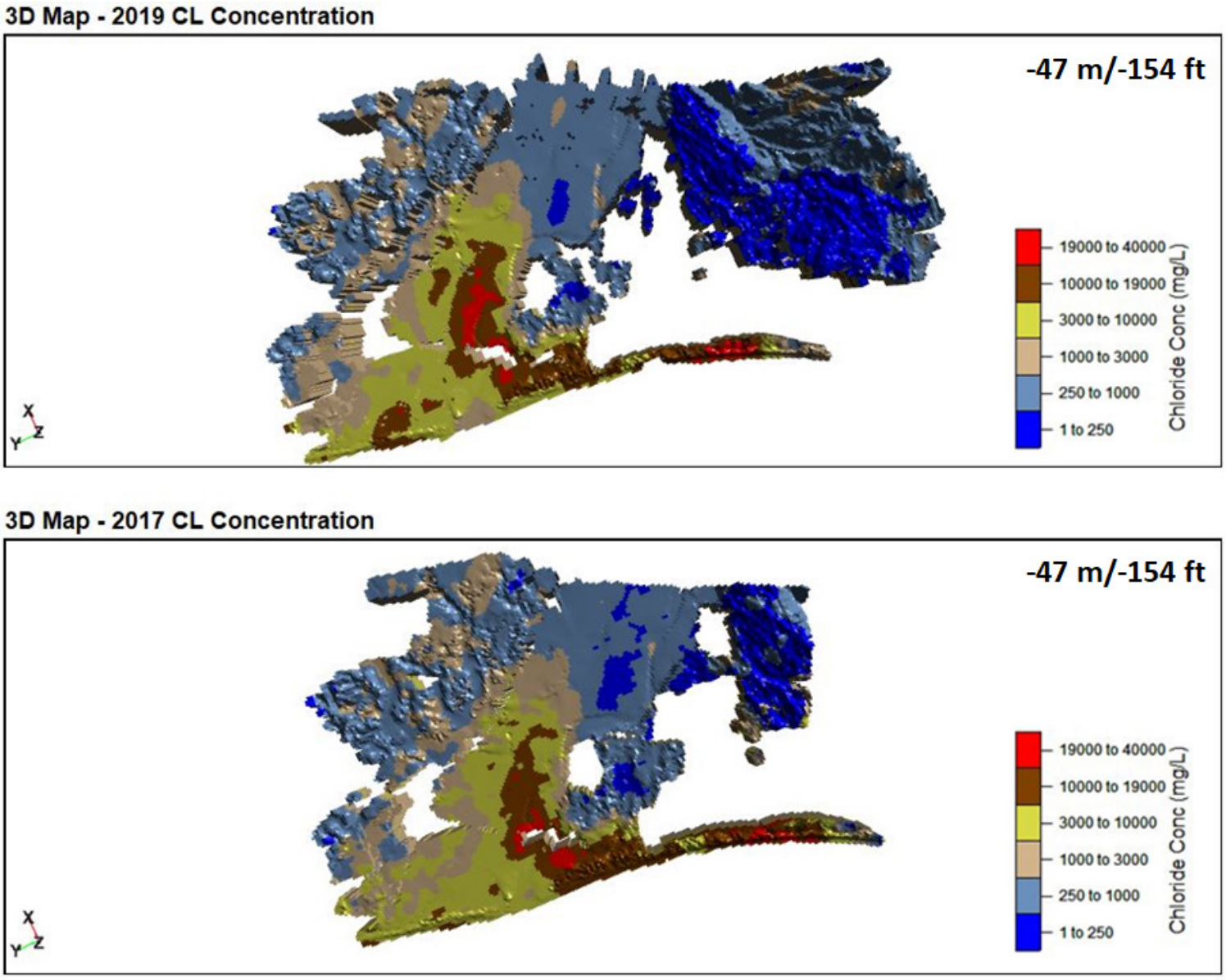

Figure 4-60. Depth slice comparison at -47 m/-154 ft of MCWD 2017 and 2019 AEM investigations via calculated chloride concentrations.

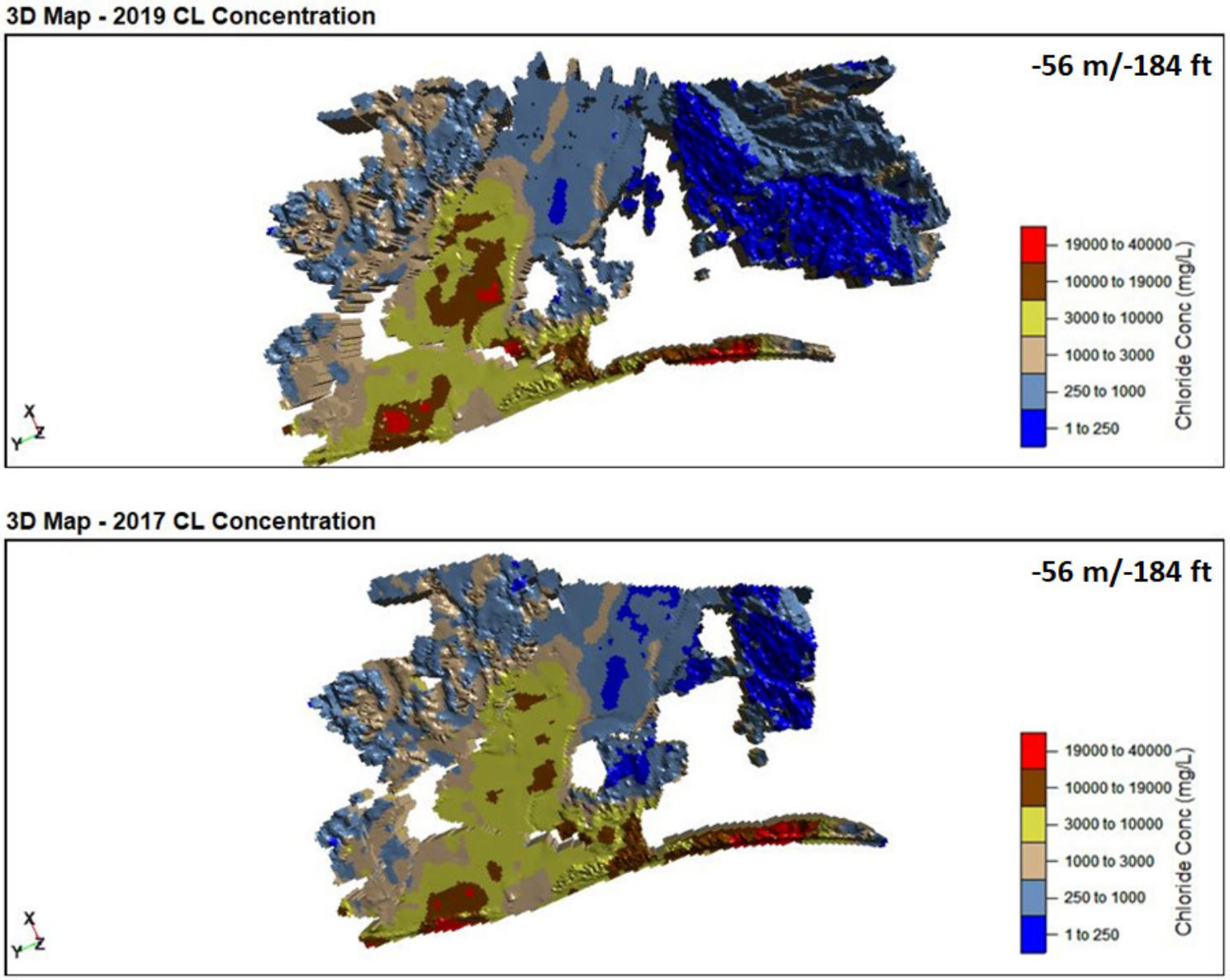

Figure 4-61. Depth slice comparison at -56 m/-184 ft of MCWD 2017 and 2019 AEM investigations via calculated chloride concentrations.

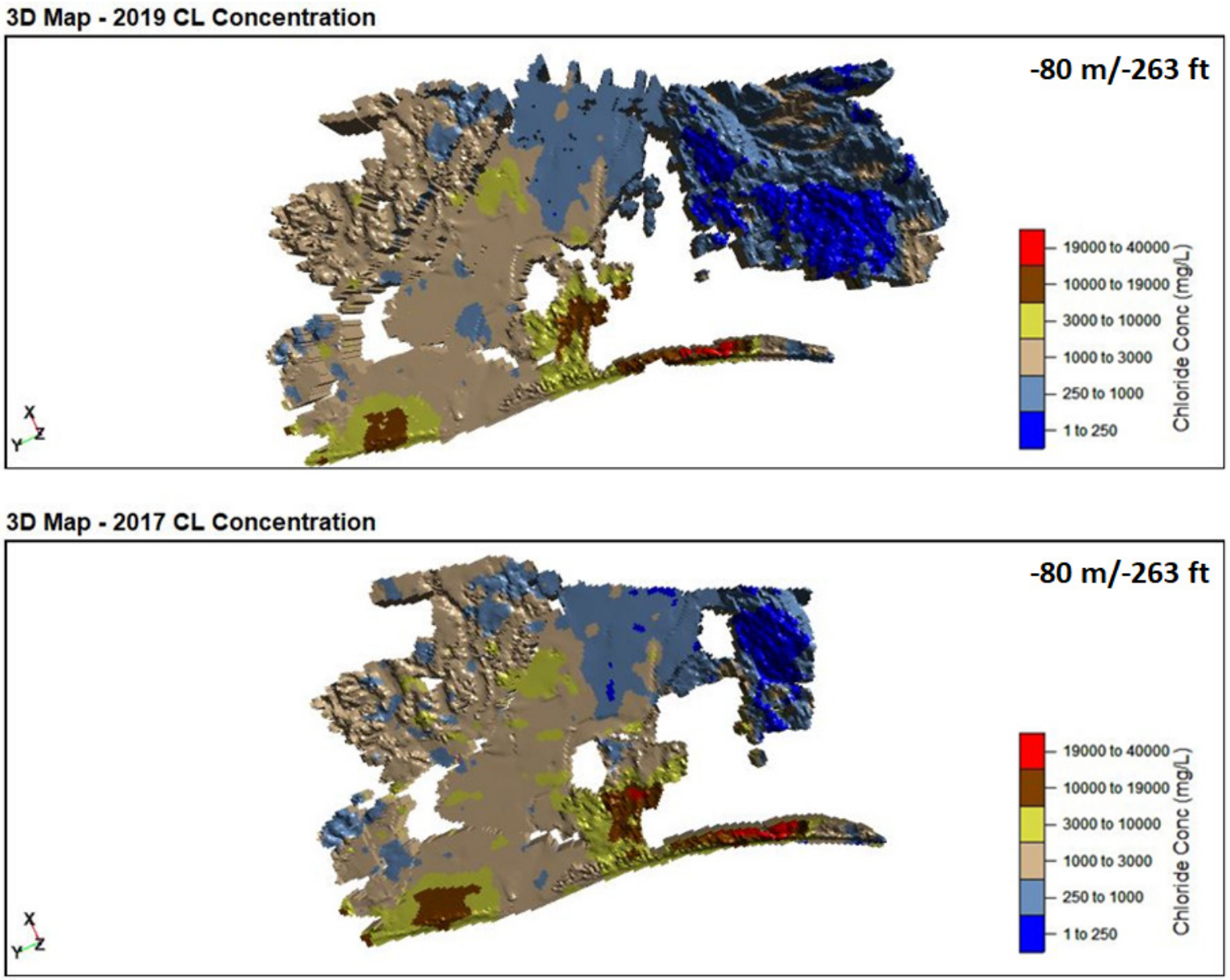

Figure 4-62. Depth slice comparison at -80 m/-263 ft of MCWD 2017 and 2019 AEM investigations via calculated chloride concentrations.

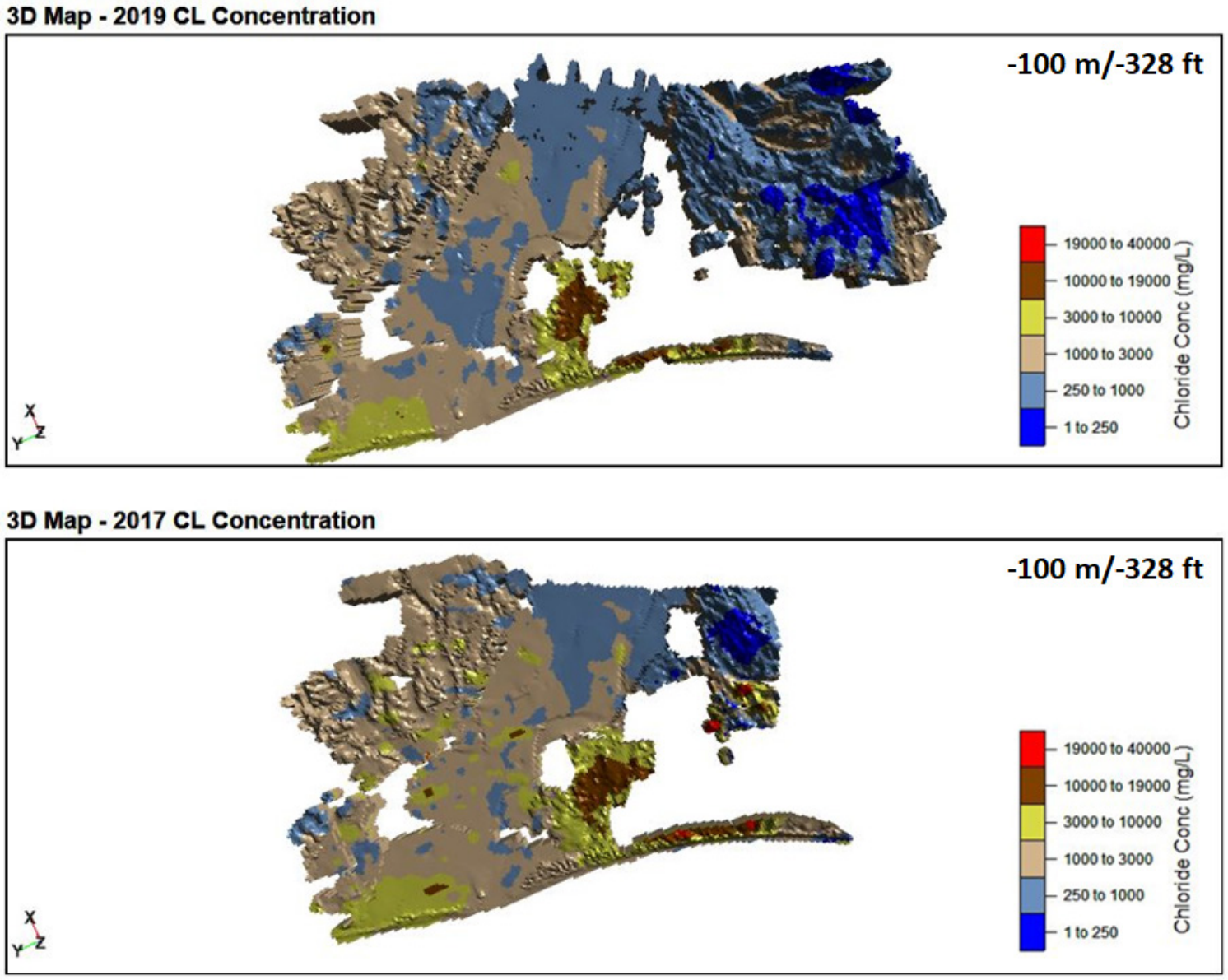

Figure 4-63. Depth slice comparison at -100 m/-328 ft of MCWD 2017 and 2019 AEM investigations via calculated chloride concentrations.

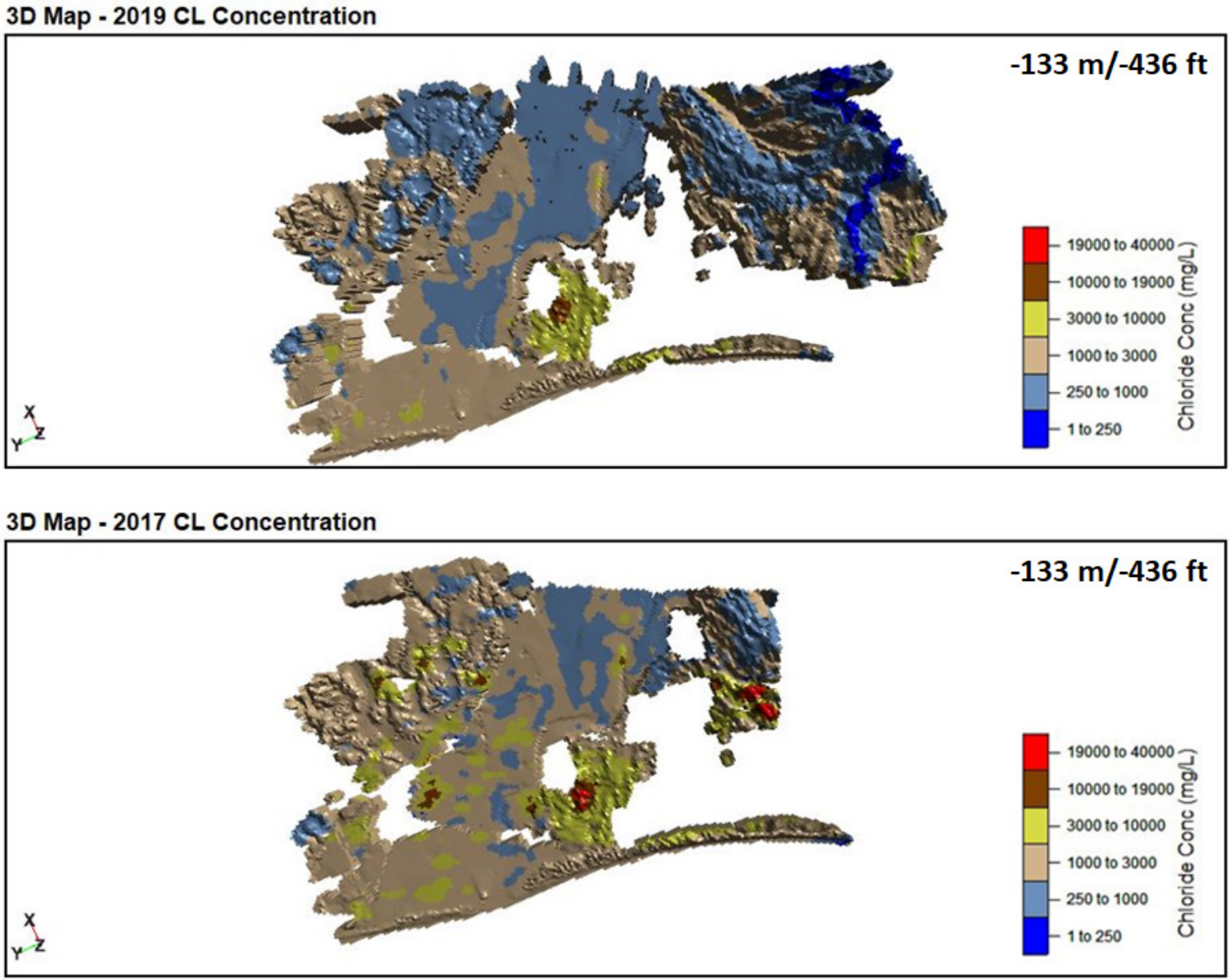

Figure 4-64. Depth slice comparison at -133 m/-436 ft of MCWD 2017 and 2019 AEM investigations via calculated chloride concentrations.

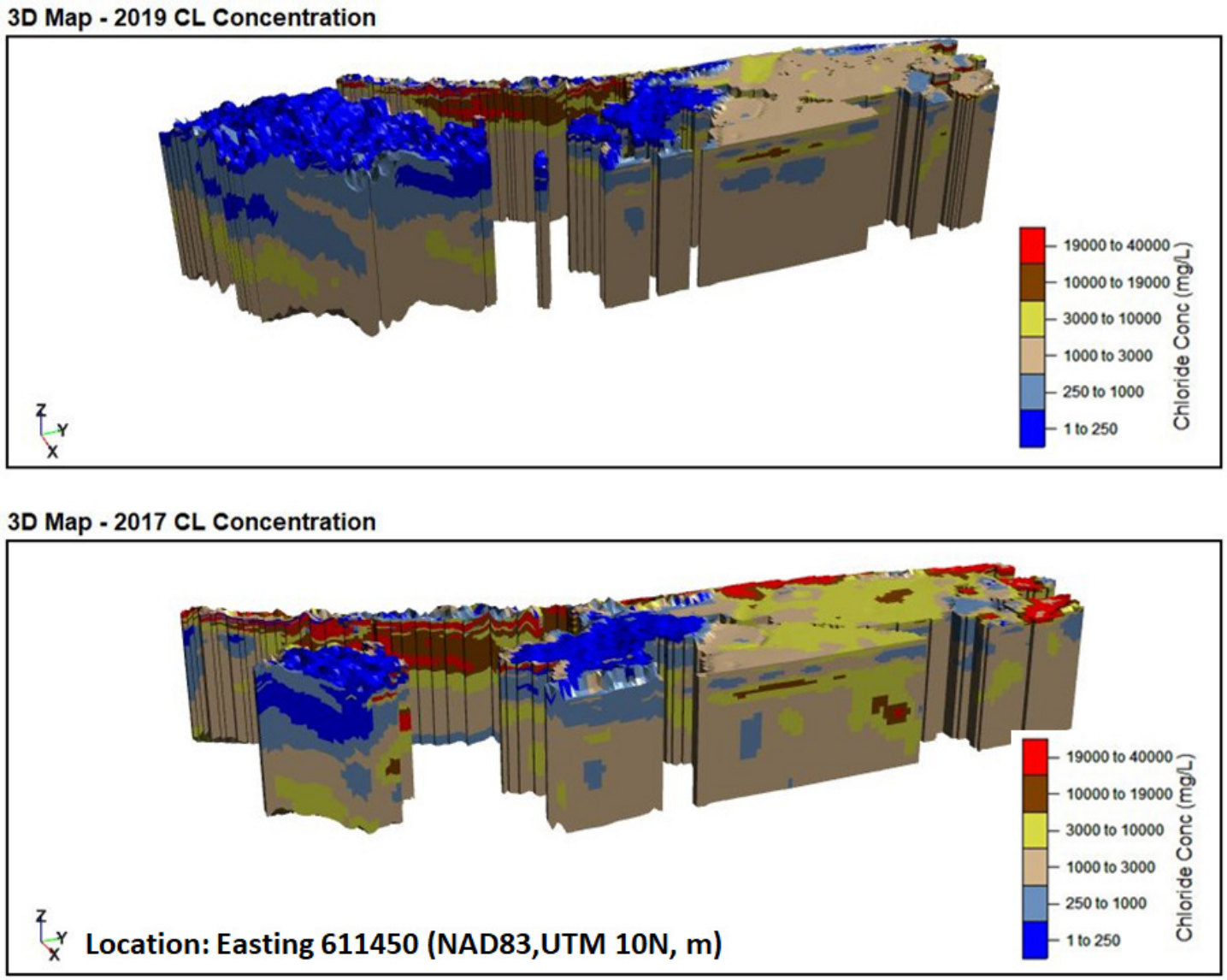

Figure 4-65. Example slice along UTM 10N Easting 611450 (m) of 3D voxels for 2017 (bottom) and 2019 (top) AEM-derived calculated chloride concentrations.

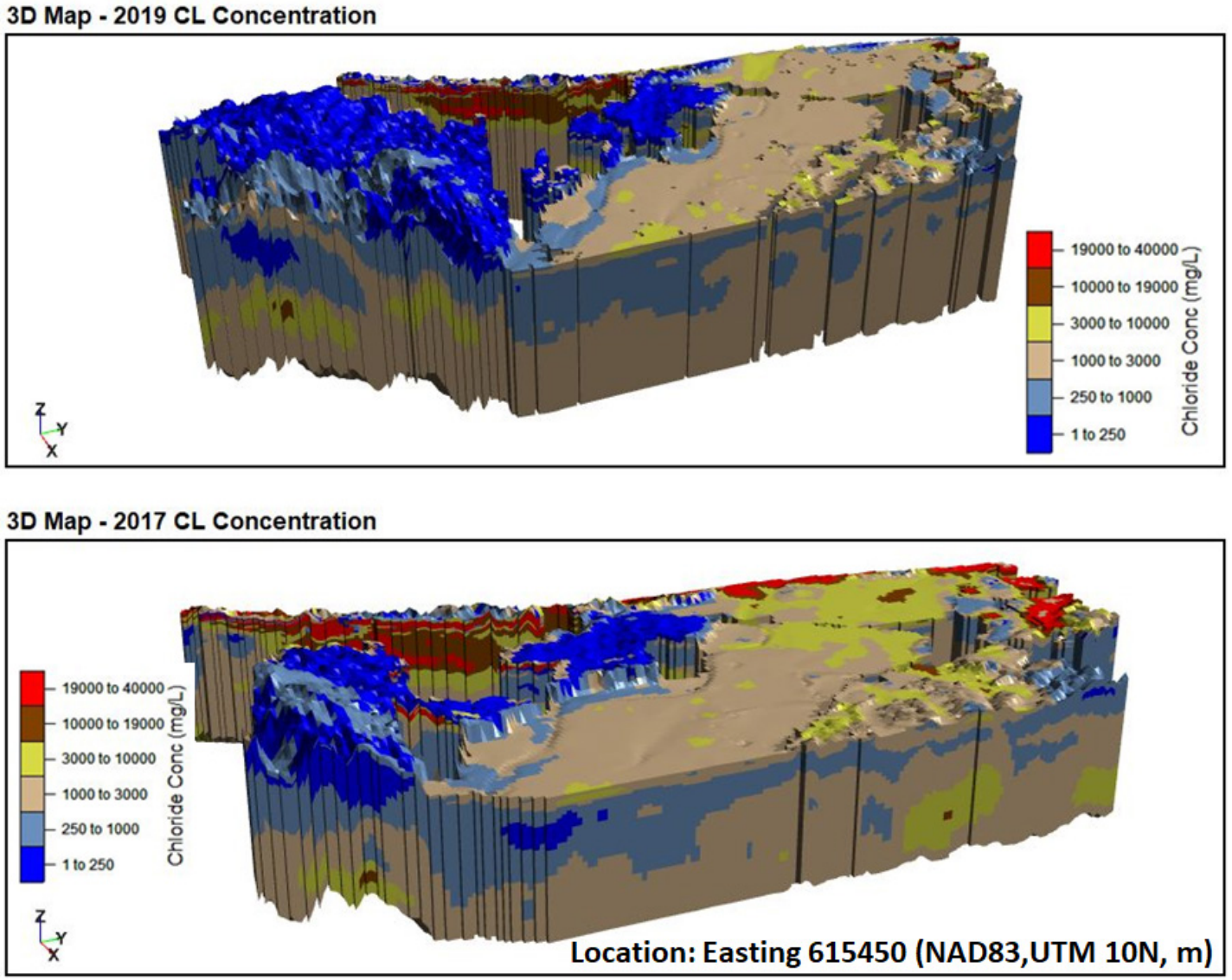

Figure 4-66. Example slice along UTM 10N Easting 615450 (m) of 3D voxels for 2017 (bottom) and 2019 (top) AEM-derived calculated chloride concentrations.

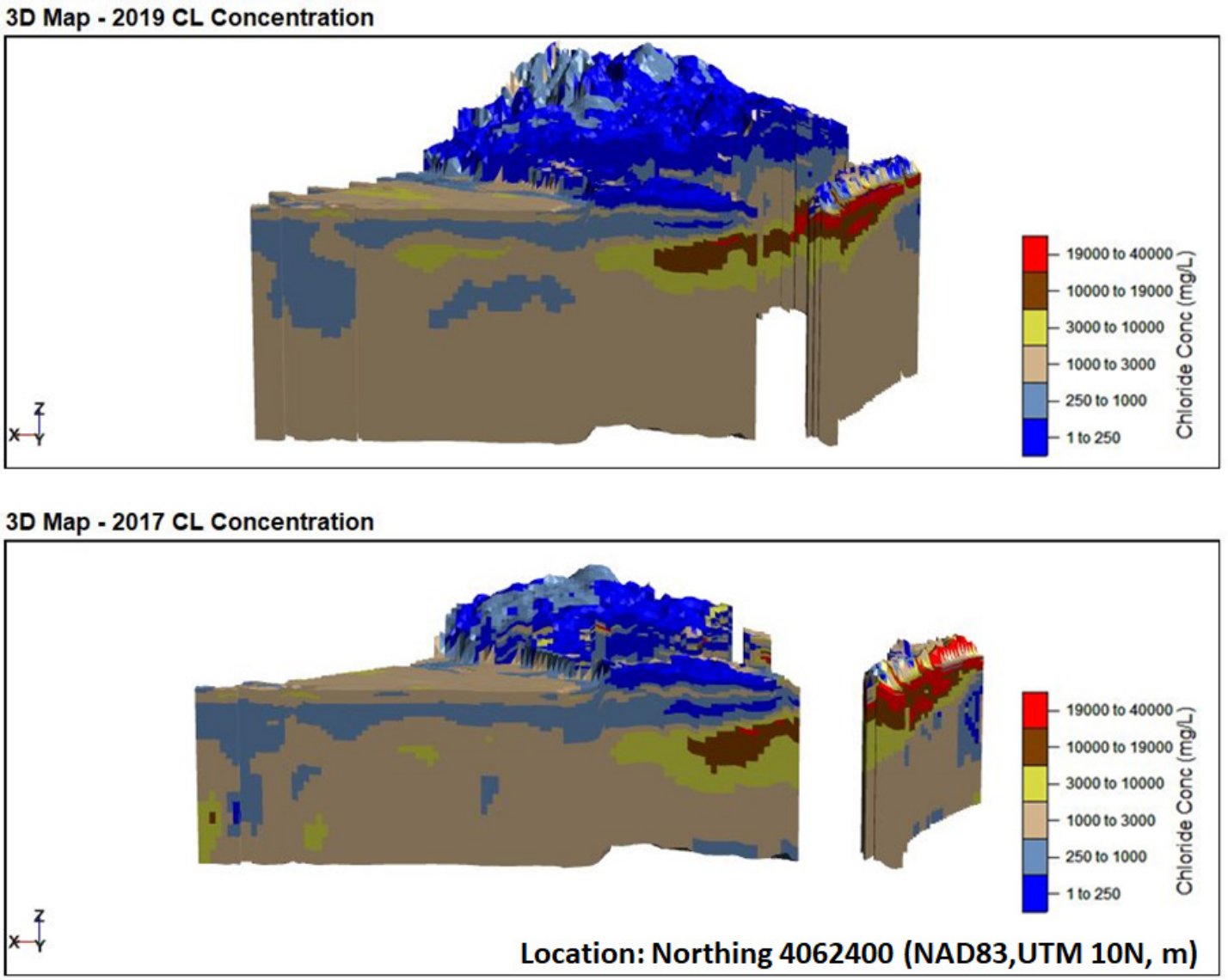

Figure 4-67. Example slice along UTM 10N Northing 4062400 (m) of 3D voxels for 2017 (bottom) and 2019 (top) AEM-derived calculated chloride concentrations.

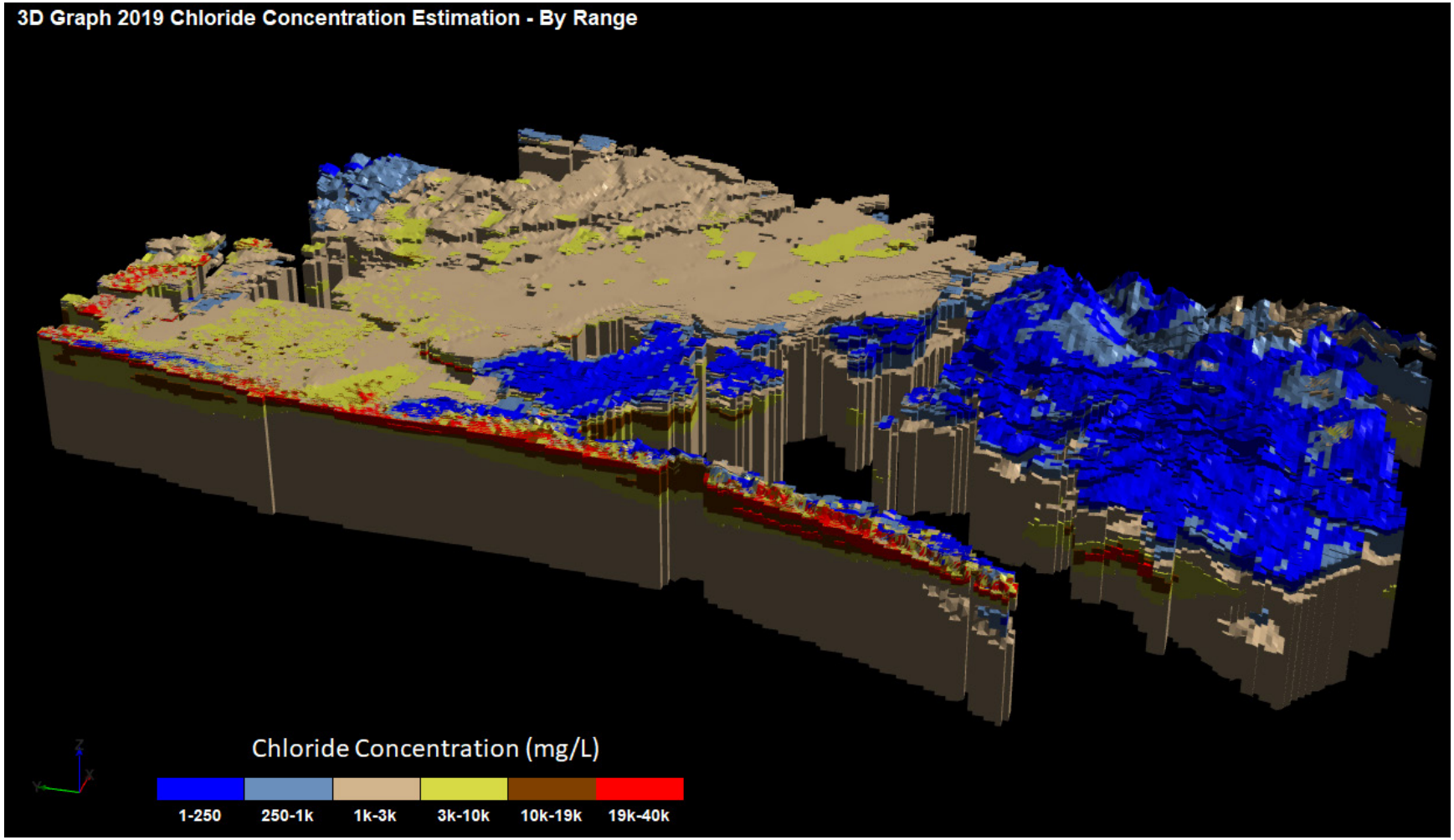

Figure 4-68. 3D voxel of the MCWD 2019 AEM-derived estimated chloride concentrations with a view to the east. While this image is similar to Figure 4-48, it is different in that it is actually five (5) voxels, each representing a different range of estimated chloride concentrations. V.E.=x5.

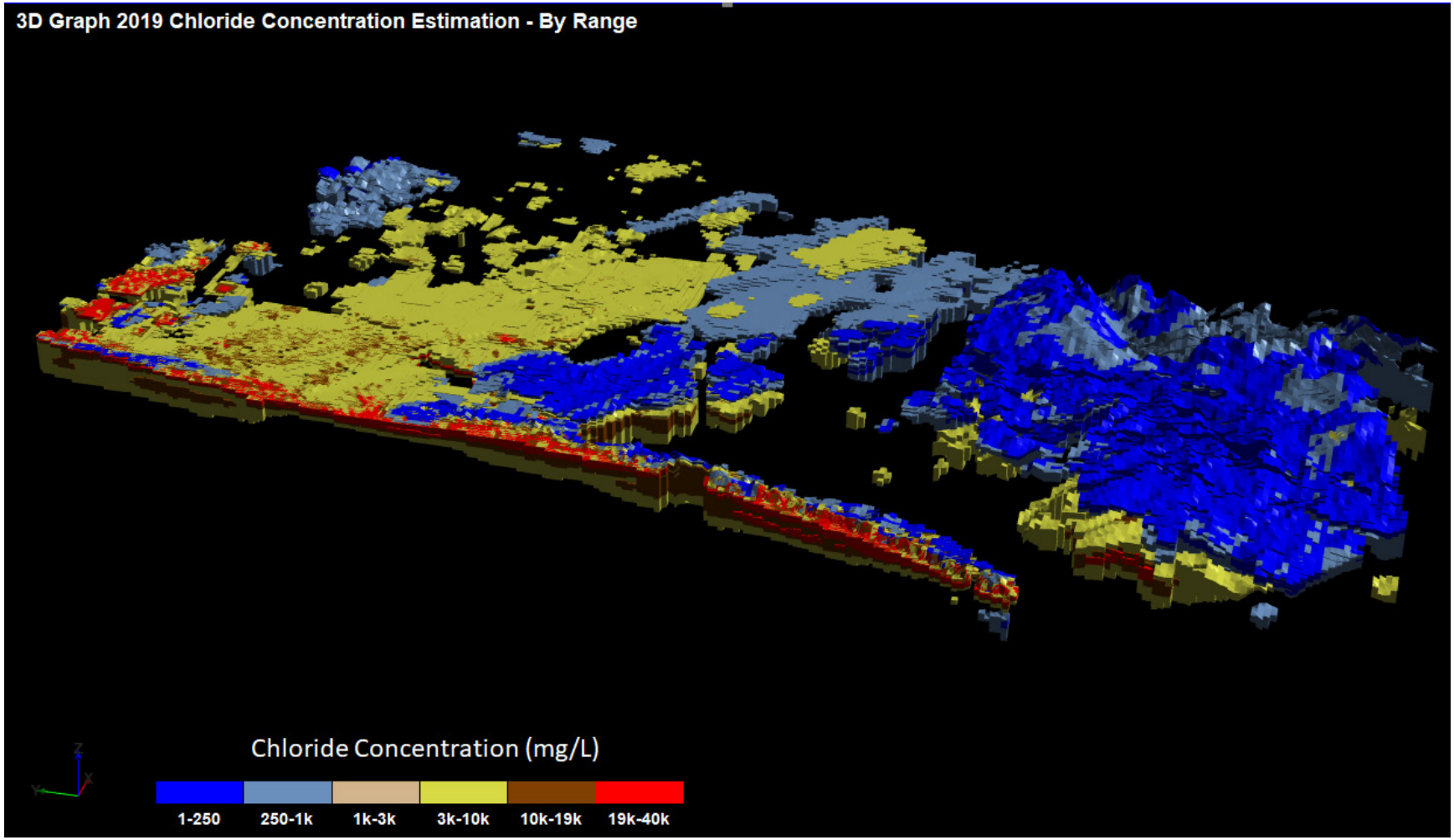

Figure 4-69. This is the same 3D voxel as in Figure 4-68 except that the display of the 1k-3k chloride concentration range has been turned off in order to see the relationships of the other chloride concentration ranges. V.E.=x5.

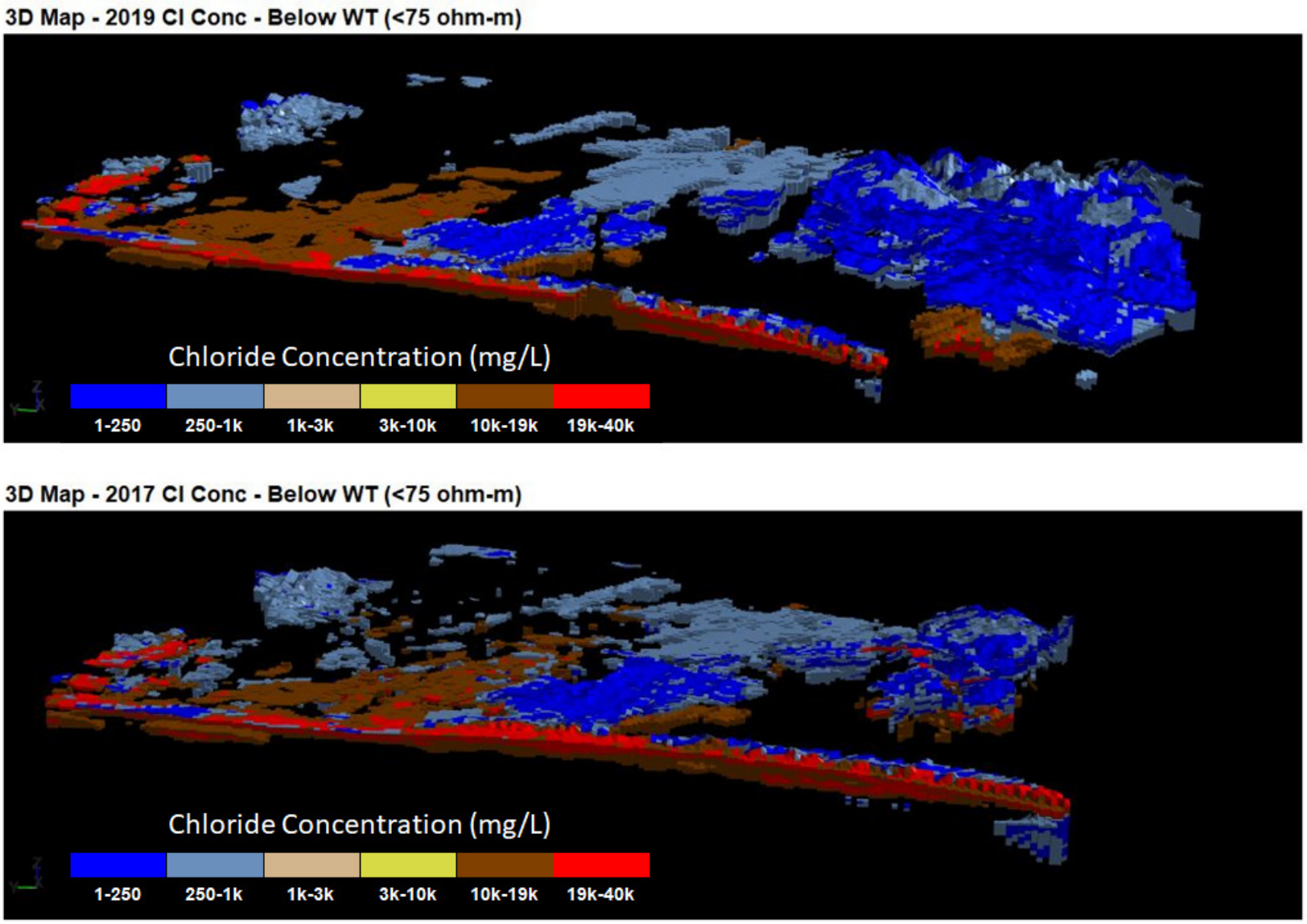

Figure 4-70. Example comparison of 3D voxels of MCWD 2017 and 2019 estimated chloride concentration ranges 1-500 mg/L (blue to bluish-grey colors) and 10k-40k (brown to red colors). The view is to the east. V.E.=x5.

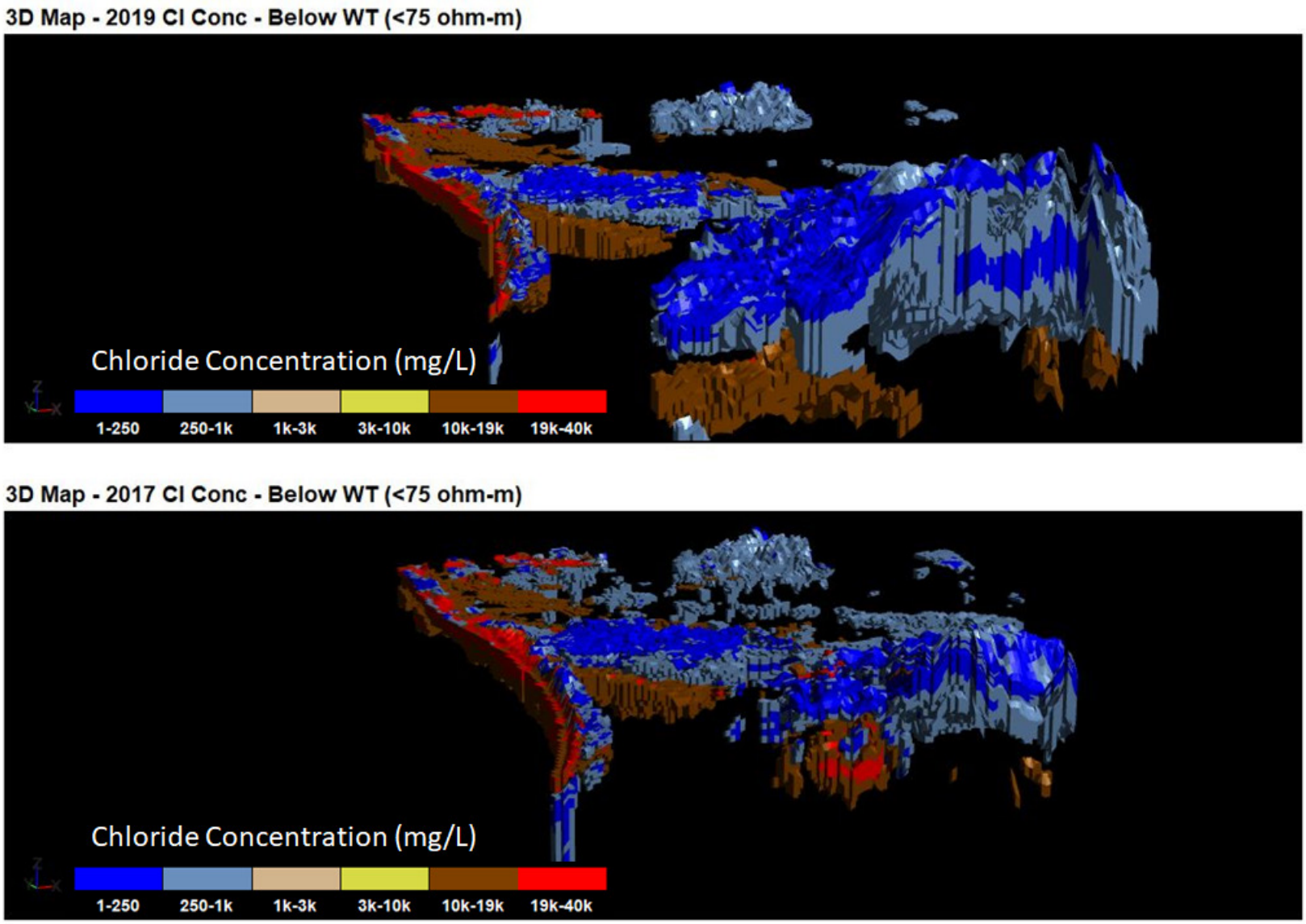

Figure 4-71. Same example comparison of 3D voxels of MCWD 2017 and 2019 estimated chloride concentration ranges 1-500 mg/L (blue to bluish-grey colors) and 10k-40k (brown to red colors) as in Figure 4-70, except the view is now to the northeast. V.E.=x5.

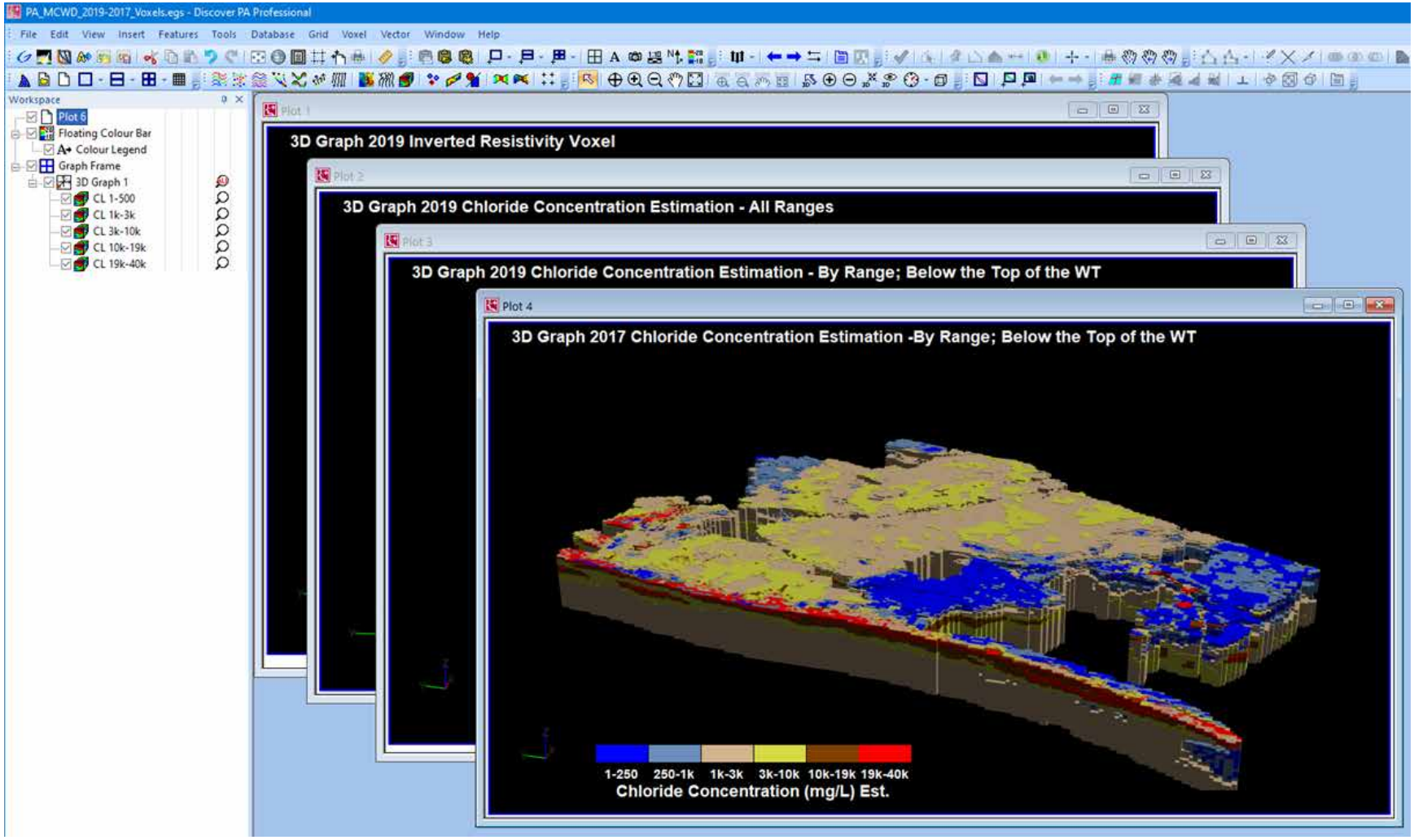

Figure 4-72. Screen capture of the Datamine Discover PA Viewer (Datamine Discover PA, 2019) session which is part of the project deliverables. This session allows the operator to change views of the 2019 inverted resistivity and estimated chloride concentrations as well as change which ranges are displayed for the MCWD 2017 and 2019 AEM investigations.

4.7 Key AEM Findings and Recommendations

The Key Findings and Recommendations provided to the MCWD in this section are based on the interpretation and understanding gained from the addition of the AEM data to existing information and from discussions with the MCWD about their management challenges.

4.7.1 2019 AEM Investigation

The MCWD 2019 AEM investigation successfully, and accurately per borehole correlations, mapped the subsurface resistivity distribution and provided an estimation of the chloride concentration within the AEM survey boundary. Besides mapping the known locations of fresher water, additional fresher water is indicated under the hills south of the Salinas River on Fort Ord of which some is likely flowing downhill towards the Salinas Valley. Below this zone of fresher water on Fort Ord is a clear very conductive zone that is likely more saline water.

4.7.2 Comparison of MCWD 2017 and 2019 AEM Investigations

A comparison between the MCWD AEM investigations from May 2017 and April 2019 has been conducted via 2D profiles and 3D voxels. The main differences between the two survey periods is that the 2019 electrical resistivity at a depth near the coast, primarily north of the Salinas River, and continuing inland, that is likely the 400-Foot Aquifer, does not indicate the very low resistivities observed in the 2017 AEM investigation that are interpreted to be saline water, likely sea water. While there are some local variations, the resistivity mapping of the 180-Foot Aquifer generally does not show much difference between 2017 and 2019.

If MCWD believes that there have been substantial changes in the subsurface over the 2019 investigation area due to variations in local environmental conditions, then it is recommended that MCWD consider an additional AEM mapping campaign or part or all of the 2019 AEM survey area.

4.7.3 Need Additional Water Table and Water Quality Data Across the Salinas River Valley

It was observed during analysis of the AEM inversion results when applying the available water table elevation and water quality data, that there isn't a lot of this information publicly available. The only available water quality information was from the MPWSP monitoring well reports and those were not consistent in their reporting or possibly accuracy and calibration. Additional compilation and integration of water level measurement locations and accurate water quality data would improve local water table and water quality maps and help in the analysis and interpretation of the previously acquired, and any future, AEM data.

5 Description of Data Delivered

5.1 Tables Describing Included Data Files

Table 5-1 describes the raw data files included in Appendix 3_Deliverables \Raw_Data. As discussed above, six (6) 312 flights were required to acquire the 2019 MCWD AEM data (Figure 3-5). Grouped by flight date, there are four (4) data flies included in Appendix 3\Raw_Data for each flight. These files have extensions of "*.sps" and "*.skb". The "*.sps" files include navigation and DGPS location data and the "*.skb" files include the raw AEM data that have been PFC-corrections (discussed in Section 3.4.2). Two additional sets of files are used for all the flights. These are the system description and specifications file (with the extension "*.gex") in the GEO subdirectory and the 'mask' file (with the extension "*.lin"), in the MASK subdirectory, which correlates the flight dates, flight numbers, and assigned line numbers.

Table 5-2 describes the data columns in the ASCII *.xyz file 20190606_EM_MAG_AUX_PLNI_Monterey.xyz. This file contains the electromagnetic data, plus the magnetic and navigational data, as supplied directly from SkyTEM.

The result of the SCI is included in MCWD2019_AEM_SCI_Inv_v1.xyz and the data columns of these databases are described in Table 5-3.

The borehole data used to assist in the interpretation of the SCI inversion results are included in the files listed in Table 5-4. Each type of borehole information has both a collar file containing the location of each of the wells, and a second file containing the borehole data for the individual wells. The data column descriptions for the collar files are listed in Table 5-5. Table 5-6 describes the channels in the lithology borehole data files and Table 5-7 describes the channels in the geophysical borehole data files.

The various interpretation results are included in the data file MCWD2019_Interp_v2.xyz in ASCII format. Table 5-8 describes the data columns of those files.

ESRI Arc View Binary Grids of the surfaces that were used in the interpretation (DEM, water table) and derived from the interpretation (top of geological units) of the AEM and borehole are listed in Table 5-9 and stored in Appendix 3_Deliverables\Grids.

In summary, the following are included as deliverables:

- Raw EM Mag data as ASCII *.xyz
- SCI inversion as ASCII *.xyz
- Borehole databases as ASCII *.xyz
- Interpretations as ASCII *.xyz
- Raw Data Files - SkyTEM files *.geo, *skb, *.lin
- ESRI ArcView grid files – surface, topo, etc.
- 3D fence diagrams of the lithologic interpretation

KMZs for AsFlown, Retained data

Table 5-1. Raw SkyTEM data files

Folder	File Name	Description
Data	..NavSys.sps, …PaPc.sps, ...RawData_PFC.skb, …DPGS.sps	Raw data files included for each flight used in importing to Aarhus Workbench
Geo	20190603_312_Monterey_DualWaveform_60Hz_skb.gex 20190603_312_Monterey_DualWaveform_60Hz_skb_SR2.gex 20190603_312_Monterey_DualWaveform_60Hz_skb_SR2.sr2	312 System Description
Mask	20190426_Production.lin	Production file listing dates, flights, and assigned line numbers

Table 5-2. Channel name, description, and units for 20190606_EM_MAG_AUX_PLNI_Monterey.xyz with EM, magnetic, DGPS, Inclinometer, altitude, and associated data.

Parameter	Description	Unit
Fid	Unique Fiducial Number	
Line	Line Number	
Flight	Name of Flight	yyyymmdd.ff
DateTime	DateTime Format	Decimal days
Date	DateTime Format	yyyymmdd
Time	Time UTC	hhmmss.sss
AngleX	Angle (in flight direction)	Degrees
AngleY	Angle (perpendicular to flight direction)	Degrees
Height	Filtered Height Measurement	Meters [m]
Lon	Longitude, WGS84	Decimal Degrees
Lat	Latitude, WGS84	Decimal Degrees
E_UTM10N_m	Easting, NAD83 UTM Zone 10N	Meters [m]
N_UTM10N m	Northing, NAD83 UTM Zone 10N	Meters [m]
DEM_m	Digital Elevation	Meters [m]
Alt	DGPS Altitude above sea level	Meters [m]
GDSpeedL	Ground Speed	Kilometers/hour [km/h]
Curr_LM	Current, Low Moment	Amps [A]
Curr_HM	Current, High Moment	Amps [A]
LMZ_G01	Normalized (PFC-Corrected) Low Moment Z-RxCoil values array	$pV/(m^4*A)$
HMZ_G01	Normalized (PFC-Corrected) High Moment Z-RxCoil values array	$pV/(m^4*A)$
HMX_G01	Normalized (PFC-Corrected) High Moment X-RxCoil values array	$pV/(m^4*A)$
PLNI	Power Line Noise Intensity monitor	V/m^2
Bmag_Raw	Raw Base Station Mag Data filtered	nanoTesla [nT]
Diurnal	Diurnal Mag Data	nanoTesla [nT]
MAG_Raw	Raw Mag Data	nanoTesla [nT]
Mag_Cor	Mag Data Corrected for Diurnal Drift	nanoTesla [nT]
RMF	Residual Magnetic Field	nanoTesla [nT]
TMI	Total Magnetic Intensity	nanoTesla [nT]

Table 5-3. Channel name, description, and units for MCWD2019_AEM_SCI_Inv_v1.xyz with EM inversion results.

Parameter	Description	Unit
LINE	Line Number	
East_m	Easting NAD83, UTM Zone 10	Meters [m]
North_m	Northing NAD83, UTM Zone 10	Meters [m]
DEM_m	DEM from 30 m grid NED NAVD88	Meters [m]
FID	Unique Fiducial Number	
TIME	Date Time Format	Decimal days
ALT_M	Altitude of system above ground	Meters [m]
INVALT	Inverted Altitude of system above ground	Meters [m]
INVALTSTD	Inverted Altitude Standard Deviation of system above ground	Meters [m]
DELTAALT	Change in Altitude of system above ground	Meters [m]
RESDATA	Residual of individual sounding	
RESTOTAL	Total residual for inverted section	
DOI_CONSERVATIVE_M	More conservative estimate of DOI, bgs	Meters [m]
DOI_STANDARD_M	Less conservative estimate of DOI, bgs	Meters [m]
RHO_0 THROUGH RHO_38	Inverted resistivity of each later	Ohm-m
RHO_STD_0 THROUGH RHO_STD_38	Inverted resistivity error per layer	
SIGMA_I_0 THROUGH SIGMA_I_38	Conductivity	S/m
DEP_TOP_M_0 THRU DEP_TOP_M_38	Depth to the top of individual layers	Meters [m]
DEP_BOT_M_0 THRU DEP_BOT_M_38	Depth to the bottom of individual layers	Meters [m]
THK_M_0 THROUGH THK_M_38	Thickness of individual layers	Meters [m]

Table 5-4. Files containing borehole information.

Database (*.xyz)	Description
MCWDELogs_Collar.xyz	Geophysical Short Normal Resistivity Elogs
MCWDELogs_Data.xyz	
FortOrdLith_Collar.xyz	Lithology logs
FortOrdLith_Data.xyz	
MCWDLith_Collar.xyz	
MCWDLith_Data.xyz	

Table 5-5: Channel name, description, and units for collar files.

Parameter	Description	Unit
DH_Hole	Name of individual boreholes	
DH_East	Easting of boreholes, NAD83, UTM Zone 10	Meters (m)
DH_North	Northing of boreholes, NAD83, UTM Zone 10	Meters (m)
DH_RL	Elevation of top of borehole	Meters (m)
DH_Dip	Dip of borehole	Degrees
DH_Azimuth	Azimuth of borehole	Degrees
DH_Top	Depth to top of borehole	Meters (m)
DH_Bottom	Depth to bottom of borehole	Meters (m)

Table 5-6. Channel name description and units for Lithology borehole data.

Parameter	Description	Unit
DH_Hole	Name of Borehole	
DH_East	Easting of boreholes, NAD83, UTM Zone 10	Meters (m)
DH_North	Northing of boreholes, NAD83, UTM Zone 10	Meters (m)
DH_RL	Elevation of top of borehole	Meters (m)
DH_From	End of interval	Meters (m)
DH_To	Start of interval	Meters (m)
Lithcode	Lithology description associated with 30 categories	
DH_Description	Description of lithology material	

Table 5-7. Channel name description and units for E-Logs borehole data.

Parameter	Description	Unit	Type of Log
DH_Hole	Name of Borehole		
DH_East	Easting of boreholes, WGS84, UTM Zone 10	Meters (m)	
DH_North	Northing of boreholes, WGS84, UTM Zone 10	Meters (m)	
DH_RL	Elevation of borehole data point	Meters (m)	
DH_Depth	Depth	Meters (m)	
SN	Short Normal Resistivity 16in	Ohm-m	GP
LN	Long Normal Resistivity 64in	Meters (m)	GP

Table 5-8: Channel name, description, and units for the interpretation results file MCWD2019_Interp_v1.xyz.

Parameter	Description	Unit
LINE	Line Number	
Easting	Easting NAD83, UTM Zone 10	Meters (m)
Northing	Northing NAD83, UTM Zone 10	Meters (m)
DEM_m	Topography at 30m sampling (NAVD 1988)	Meters (m)
East_CASP4ft	Easting, California State Plane, Zone 4	Feet (ft)
North_CASP4ft	Northing, California State Plane, Zone 4	Feet (ft)
RHO[0] through RHO[38]	Array of Inverted model resistivities of each later	Ohm-m
RESDATA	Inversion model residuals of each individual sounding	
RhoLT75[0] through RHOLT75[38]	Array of inverted model resistivities <75 ohm-m	Ohm-m
CLconcFitt	Array of Chloride concentrations via Fitterman relationship	mg/L
EC_MPWSP	Electrical Conductance calculated using derived MPWSP relation	µS
Salinity_MPWSP	Salinity calculated using derived MPWSP relation	mg/L
TDS_MPWSP	TDS calculated using derived MPWSP relation	mg/L
WT75	Water Table for resistivities <75 ohm-m	Meters (m)
DEP_TOP[0] through DEP_TOP[38]	Depth to the top of individual layers	Meters (m)
DEP_BOT[0] through DEP_BOT[38]	Depth to the bottom of individual layers	Meters (m)
DEM_DepTop[0] thru DEM_DepTop[38]	Array of elevations of top of each model layer	Meters (m)
DOI_Conservative	More conservative estimate of DOI from Workbench	Meters (m)
DOI_Standard	Less conservative estimate of DOI from Workbench	Meters (m)

Table 5-9. Channel name, description, and units for Voxel files: a) MCWD2017_CLconc_LT75_Voxel.xyz; b) MCWD2019_CLconc_All_Voxel.xyz; c) MCWD2019_CLconc_LT75_Voxel.xyz; d) MCWD2019_Resistivity_Voxel

Parameter	Description	Unit
X	Easting UTM 10N	Meters (m)
Y	Northing UTM 10N	Meters (m)
Z	Depth of Voxel Node	Meters (m)
Resistivity	Voxel cell resistivity value	Ohm-m
CLconc	Chloride concentration	mg/L

6 References

AGF, 2018, Technical Memorandum dated 16 April 2018 presented to the Marina Coast Water District on *Review of Geophysical Discussion in Response to Comments in CAL-AM Monterey Peninsula Water Supply Project Final Environmental Impact Report/Environmental Impact Statement SCH#2006101004, March 28, 2018*, Aqua Geo Frameworks, LLC., 30 p.

AGF, 2019, Technical Memorandum dated 11 February 2019 presented to the Marina Coast Water District on *Response to Comments on Aqua Geo Frameworks (AGF) Technical Memo to MCWD dated April 16, 2018 in HWG COMMENTS ON TECHNICAL APPENDICES/ATTACHMENTS TO LETTERS SUBMITTED BY MCWD AND CITY OF MARINA TO THE CPUC AND MBNMS ON APRIL 19, 20018, Dated August 15, 2018*: 27pp.

Asch, T.H., Abraham, J.D., and Irons, T., 2015, A discussion on depth of investigation in geophysics and AEM inversion results, Presented at the Society of Exploration Geophysicists Annual Meeting, New Orleans.

Asch, T.H., Gottschalk, I., Knight, R., Abraham, J.D., Cannia, J.C., Van Der Maaten, K., 2018, An airborne electromagnetic investigation of the Marina, CA hydrogeologic framework: presented at the Symposium on the Application of Geophysics to Environmental and Engineering Problems, Nashville, Tennessee, 27 March 2018.

Carney, C.P., Abraham, J.D., Cannia, J.C., and Steele, G.V., 2015, Airborne Electromagnetic Geophysical Surveys and Hydrogeologic Framework Development for Selected Sites in the Lower Elkhorn Natural Resources District: prepared for the Lower Elkhorn Natural Resources District by Exploration Resources International Geophysics LLC, Vicksburg, MS. .http://www.enwra.org/LENRD2014AEMDataDownload.html (accessed December 31, 2018)

Christensen, N. B., J. E. Reid, and M. Halkjaer, 2009, "Fast, laterally smooth inversion of airborne time-domain elecromagnetic data." *Near Surface Geophysics* 599-612.

Christiansen, A. V. and E. Auken, 2012, "A global measure for depth of investigation." *Geophysics,Vol. 77, No. 4* WB171-177.

DatamineDiscover, 2019, Datamine Discover Profile Analyst, available on the world-wide web at: https://www.dataminesoftware.com/discover/.(accessed September 30, 2019)

Fitterman, D.V., and Prinos, S.T., 2011, Results of time-domain electromagnetic soundings in Miami-Dade and southern Broward Counties, Florida: U.S. Geological Survey Open-File Report 2011–1299, 289 p. https://pubs.usgs.gov/of/2011/1299/

Foged, N., Auken, E., Christiansen, A.V., and Sorensen, K.I., 2013, Test-site calibration and validation of airborne and ground based TEM systems: Geophysics, V.78, No.2, E95-E106.

Gottschalk, I., Knight, R., Asch, T., Abraham, J., and Cannia, J., 2018, Interpretation of Hydrostratigraphy and Water Quality from AEM Data Collected in the Northern Salinas Valley, CA: Stanford University, 15 March 2018, 69pp. https://mcwd.org/docs/gsa/Stanford_AEM_Data_Report_Final.pdf

HydroGeophysics Group, Aarhus University, 2010, "Validation of the SkyTEM system at the extended TEM test site." Aarhus, Denmark.

HydroGeophysics Group, Aarhus University, 2011, "Guide for processing and inversion of SkyTEM data in Aarhus Workbench", Version 2.0."

Knight, R., E. Grunewald, T. Irons, K. Dlubac, Y. Song, H. N. Bachman, B. Grau, D. Walsh, J. D. Abraham, and J. Cannia, 2012, Field experiment provides ground truth for surface nuclear magnetic resonance measurement: Geophysical Research Letters, v.39, no. 3, 7p, accessed April 27, 2019 at https://agupubs.onlinelibrary.wiley.com/doi/10.1029/2011GL050167.

Ley-Cooper, Y. and Davis, A., 2010. Can a borehole conductivity log discredit a whole AEM survey?: *in* Extended abstracts of the Australian Society of Exploration Geophysicists Annual meeting Aug 20-24, Sydney, Australia.

MPWSP, 2019, Monterey Peninsula Water Supply Project, Test Slant Well Long Term Pumping Monitoring Report No. 160, 10-April-19 - 15-May-19: Geoscience Support Services, Inc., published May 21, 2019, 606pp. https://www.watersupplyproject.org/test-well (accessed September 10, 2019).

Schamper, C., Auken, E., and Sorensen, K., 2014, Coil response inversion for very early time modelling of helicopter-borne time-domain electromagnetic data and mapping of near-surface Geologic Layers. European Association of Geoscientistis & Engineers, Geophysical Prospecting.

SkyTem Airborne Surveys Worldwide, 2019, SkyTEM312, https://skytem.com/tem-systems/ (accessed May 28, 2019)

U.S. Geological Survey (USGS), 2019, The National Map, 2018, 3DEP products and services: The National Map, 3D Elevation Program Web page, http://nationalmap.gov/3DEP/3dep_prodserv.html (accessed April 1, 2019)

Viezzoli, A., A. V. Christiansen, E. Auken, and K. Sorensen, 2008, "Quasi-3D modeling of airborne TEM data by spatially constrainted inversion." *Geophysics Vol. 73 No. 3* F105-F11